University of Alberta

Numerical and Field Studies of River Ice Jam Dynamics

by

Yuntong She

A thesis submitted to the Faculty of Graduate Studies and Research
in partial fulfillment of the requirements for the degree of

Doctor of Philosophy

in

Water Resources Engineering

Department of Civil and Environmental Engineering

Edmonton, Alberta
Fall 2008

Your file Votre référence
ISBN: 978-0-494-46423-6
Our file Notre référence
ISBN: 978-0-494-46423-6

Abstract

In many Canadian communities, river ice jams pose a significant flood threat each spring. The occurrence of ice jam formation and release events is typically rapid and highly unpredictable; thus making their observation and measurement difficult and dangerous. Consequently, knowledge has been limited by the scarcity of reliable data pertaining to these highly dynamic and complicated processes. Furthermore, the capability of forecasting ice jam related floods has been limited to relatively simple conditions.

In this study, numerical models were developed for the purpose of real-time prediction of flood level caused by river ice jam events. Models of varying levels of complexity were built on an open-channel hydrodynamic model: *River1-D*. Given our limited understanding of these phenomena, ice effects were first included into *River1-D* in a simplified manner, to investigate the extent of ice complexity necessary to successfully simulate flood waves produced by ice jam release events. Full ice effects were then considered in a more complex version of the model, to provide a more comprehensive description of ice dynamics and ice-water interactions during both jam formation and release processes. Applications of the proposed models to hypothetical, experimental, and actual ice jam events provide detailed time-series information of water level, discharge, ice thickness and velocity, thus provided valuable complementary data to the limited available field measurements, and offer a more complete view of river ice jam processes. Field observations were carried out annually during river breakup from 2005 to 2008, for the purpose of obtaining qualitative and quantitative data; these have contributed to our

understanding of jam processes and have aided the validation of the proposed numerical models.

The work presented in this thesis includes the first numerical assessment of ice effects based on actual ice jam release events; the first attempt to numerically simulate how an ice jam breaks through a downstream ice cover; and the first attempt to investigate how an ice accumulation responds to applied forces based on experimental data. This research contributes to an advancement of understanding the ice and water components of ice jam processes, and is a step further towards the ultimate goal: to be able to accurately forecast water level variations due to ice movements during river breakup.

Acknowledgement

The author would like to thank the external examiner, Dr. Hung Tao Shen of Clarkson University and the other committee members Drs. Herbert Yang, Oy Leuangthong, and Mark Loewen, for committing their time and effort in reviewing this thesis.

Financial support to the author was provided by: the FS Chia PhD Scholarship; the Izaak Walton Killam Memorial Scholarship; the R. (Larry) Gerard Memorial Scholarship in Ice Engineering; the Dissertation Fellowship; and various research and teaching assistantships provided by the University of Alberta. Additional funding for this research was provided through grants from the NSERC and the Alberta Ingenuity Centre for Water Research received by author's supervisor. All are gratefully acknowledged.

The author would like to express special gratitude to her supervisor, Dr. Faye Hicks, for her excellent guidance, generous encouragement, and inspiring scientific discussions throughout the author's work. Her passion for research has greatly influenced the author and has led to the accomplishment of this thesis work. The opportunities of field work and attending conferences were much appreciated. The author is also grateful to her co-supervisor, Dr. Peter Steffler, for his insightful advice on many numerical questions the author had. His patience is greatly appreciated. His keen interest of the topic and broad knowledge on a variety of topics greatly helped the project progress smoothly and efficiently, even with all the complications involved.

The author acknowledges the support provided by Alberta Environment for the Athabasca River field study, with particular thanks to Dr. Chandra Mahabir, Evan

Friesenhan, Claudine Robichaud, and Larry Garner. Gratitude is expressed to Dr. Brian Morse of the Université Laval and Dr. Edward Stander of the State University of New York at Cobleskill, for their support and collaboration on the breakup monitoring program. Thanks also to the Regional Municipality of Wood Buffalo for their support and assistance with the field study.

The author would like to express sincere gratitude to Dr. Dan Healy, University of Alberta and AMEC Earth & Environment, Dr. Hung Tao Shen, Clarkson University, Dr. Spyros Beltaos, National Water Research Institute, and Mr. Brian Burrell, New Brunswick Department of the Environment and Local Government, for the data and invaluable advices they contributed to this study.

Thanks also to Perry Fedun for providing field work assistance and computer support, and to Nicolas Abarca, Robyn Andrishak, Carlos Godoy, Brett Howard, David Keller, Chris Krath, and Agata Wojtowicz, for their assistance with field data collection and/or data processing. For their assistance with field work, Simon Nolin and François Nzokou Tanekou of the Université Laval are also acknowledged.

On a more personal note, I would like to thank Yang, for always being there with me, especially for the hours of frustration. Thanks to my parents for their unconditional love and support. Great thanks also to my grandparents. Their great expectations on me have motivated my every effort in producing this thesis.

Table of Contents

List of Figures

List of Tables

List of Symbols

A	channel cross sectional area perpendicular to flow
A_i	ice volume within the upper ice layer per unit length
A_i'	non-dimensional ice volume within the upper ice layer per unit length
A_w	cross sectional area of the lower water layer perpendicular to flow
A_0	area scale
α	dispersion parameter in ice continuity equation
α_H	ratio of the water flow area affected by ice friction to that affected by bed friction
B	channel width
β	parameter determining the behaviour of breaking front
β_b	bank-to-ice friction coefficient
C_*	non-dimensional Chezy coefficient
C_i	coefficient for cohesion in an ice jam
C_o	coefficient for the internal strength of an ice jam
c_b	celerity of a breaking front formed when ice jam breaking through ice cover
$\dot{\varepsilon}$	strain rate of an ice accumulation

$\dot{\varepsilon}_c$ a small value of strain rate of an ice accumulation

F Froude number

f_i Darcy-Weisbach friction factor of the bottom of an ice accumulation

f_o composite Darcy-Weisbach friction factor

ϕ internal friction angle of an ice jam

g acceleration due to gravity

γ_e effective unit weight of an ice jam used in the jam stability equation

H elevation of water surface above channel bed

H' non-dimensional elevation of water surface above channel bed

H_w depth of the lower water layer

η viscosity of ice accumulation used in Hibler's constitutive model

$\eta_{\max}$ a large bounding viscosity of ice accumulation used in Hibler's constitutive model

j constant in the proposed constitutive model

K_p passive pressure coefficient of an ice jam

K_{xy} lateral thrust coefficient of an ice jam

k_b roughness height of channel bed

k_i roughness height of the bottom of an ice accumulation

k_o composite roughness height

L length scale

λ seepage coefficient

λ_1 empirical resistance parameter used in the model with simplified ice effects

λ_2 dispersion parameter

m power law coefficient used in the proposed constitutive model

μ coefficient describing the internal strength of an ice jam

N surface ice concentration

N_{max} maximum allowable surface ice concentration

n_b Manning's roughness coefficient of channel bed

n_i Manning's roughness coefficient of the bottom of an ice accumulation

n_{io} Manning's roughness coefficient of the bottom of single layer ice

P pressure term

p porosity of an ice accumulation

Q total discharge of ice layer and water layer

Q_i ice discharge in the upper ice layer

Q_i' non-dimensional ice discharge in the upper ice layer

Q_u water discharge in the upper ice layer

Q_w water discharge in the lower water layer

Q_0 discharge scale

q_w water discharge in the lower water layer per unit width

ρ density of water

ρ_i density of ice

R composite hydraulic radius of the lower layer flow

R_b hydraulic radius of the bed-influenced portion of the flow

R_i hydraulic radius of the ice-influenced portion of the flow

R_i' non-dimensional hydraulic radius of the ice-influenced portion of the flow

S_o channel slope

S_f friction slope

S_w water surface slope

s_i specific gravity of ice

σ internal resistance stress of an ice accumulation

σ' non-dimensional internal resistance stress of an ice accumulation

T time scale

t temporal coordinate

t' non-dimensional temporal coordinate

t_{eq} equilibrium ice jam thickness

t_i ice thickness

t_i' non-dimensional ice thickness

t_{io} single layer ice thickness

τ_b shear stress on the flow from channel bed

τ_i shear stress under the ice resulting from the flow

V_i ice velocity

V_i' non-dimensional ice velocity

V_s seepage flow velocity in the upper ice layer

V_w mean flow velocity in the lower water layer

V_w' non-dimensional mean flow velocity in the lower water layer

V_0 velocity scale representing the velocity of unperturbed flow

x longitudinal coordinate

x' non-dimensional longitudinal coordinate

x_j distance from the head of an ice jam

Y_0 depth scale representing the normal depth of unperturbed flow

z depth coordinate

1 Introduction

River ice jams often cause very unpredictable floods in many cold regions of the world. Ice jams can occur at freeze-up, or as a result of a mid-winter thaw, but the most serious ice jam flood events generally happen with the onset of warm weather in the spring. In this period, a frozen river may experience a rapid increase in flow, due to significant snowmelt runoff, that can mechanically break the ice cover and carry the ice downstream in an ice run. Jamming of the broken ice can occur when the ice run encounters an obstruction (e.g. intact ice covers, sharp bends, bridges, bars and islands). Backwater effects resulting from ice jams can cause upstream flooding. Also, an ice jam can fail suddenly, causing a flash flood downstream as the combined water and ice waves rush through the river channel.

In Canada, ice jam floods have been documented for more than a century, and have frequently set records as the most extreme and destructive flood events. The City of Fort McMurray in the Athabasca River basin, Alberta is a place where possible flooding caused by ice jams is an annual worry. Nine ice jam flood events were reported at this site from 1875 to 1964 (Blench 1964), and additional two major ones occurred in 1977 and 1997. The 1875 event was the most extreme one and was reported in the archives of the Hudson's Bay Company. The following quotation from the archives vividly describes the rapid and destructive nature of ice jam events.

"... The winter of 1874-1875 was a bitter one, with deep snow and never a thaw until April. On the 2nd or 3rd of that month, however, a further heavy fall of snow was followed by a sudden rise in temperature. The change of weather and the weight of

melting snow caused the ice for the 85 miles stretch of rapids above the fort [Fort McMurray] to breakup, and it came down at the post it blocked the river and drove the ice 2 miles up the Clearwater [a major tributary] in piles 40 to 50 feet high. In less than an hour the water rose 57 feet, flooding the whole flat and mowing down trees, some 3 ft in diameter, like grass..."

Fort McMurray is not the only place facing frequent ice jam flood problems. For example, in Atlantic Canada, over two thirds of total provincial flood damages are due to ice jams (Environment Canada: Freshwater website). The 1936 event on the Saint John River, New Brunswick, involved the occurrence of twenty-two ice jams. Fifteen bridges were partially or completely damaged; many roads and railways were flooded; homes and businesses were destroyed. Damage costs totaled $1.9 million (about $33.9 million in 1998 dollars) for this single flood event (Environment Canada: Freshwater website). Beltaos (1995) provides a summary of these and numerous other significant events across Canada. More recent events can be found in many related publications. The latest major ice jam flood event occurred in the City of Hay River, Northwest Territories, in May 2008 (observed by River Ice Research Group, University of Alberta, 2008). Although the damages are still being assessed, this event is believed to be comparable to the last big flood event that occurred on this river in 1963, which caused millions of dollars in damages.

River ice jams are also responsible for other impacts on the economy and the environment. Impedance of navigation is often a direct result of ice jams. Shipping can be seriously threatened by the big waves and violent ice runs released by ice jam failure. For example, in the 2008 flood, huge barges at Hay River were floated right up onto the dock

and fishing boats were pushed off their moorings by rising water. Hydropower generation is often severely restrained for the purpose of preventing ice jam formation. The high-speed flow and ice runs resulting from an ice jam release can also lead to severe erosion of river bed and banks, and can damage water quality and aquatic habitat. Climatic variability and the global warming trend may increase the frequency and severity of ice jam events, potentially resulting in much greater impacts on property and life. Proof and details on these impacts can be found in related publications (e.g. Beltaos 1995, Prowse 2000, Beltaos and Prowse 2001, Morse and Hicks 2005, and White et al. 2007).

Despite their significance in northern regions around the world, scientific knowledge of river ice jam events is still quite limited. The rapid and dangerous nature of river ice jams often prevents safe access, making the measurement of such events a very difficult task. Therefore, very little is known about the physics behind ice jam formation and release events, thus limiting our ability to predict such events. Limited prediction ability in turn prevents us from obtaining enough scientific data, since we often do not know where to be and when to be there, to see and to measure ice jam events.

It is the objective of the work embodied by this thesis to improve our knowledge about the dynamics of river ice jam events through data collection and analysis of actual events in the field, as well as numerical model development and application. What follows in this chapter is a background of river breakup scenarios and ice jam processes. Also included is a review of previous research relevant to the work presented in this thesis, illustrated in accordance with the ice jam formation and the ice jam release respectively. Finally the primary objectives of this study are presented in detail and the structure of the thesis is outlined.

1.1 Background

River ice jams may occur when discrete ice floes accumulate near narrow passages or other obstructions. Bridges, sharp river bends, geometry constrictions, and intact ice covers are typical sites prone to formation of ice jams. Under different flow, geometric, meteorological, and ice conditions, ice jams may vary in shape and size as they may develop through various evolution processes.

Figure 1-1 shows a sketch of the initiation and evolution process of an ice jam. Once ice floes arrest to initiate an ice jam, the movement of subsequent ice floes arriving at the upstream end (or the leading edge) of the ice accumulation will be controlled by the hydraulic conditions there. When the buoyant forces can withstand the downward forces and the overturning moments, the incoming ice floes will stop against the leading edge, simply lengthening the ice accumulation by juxtaposition.

When the downward forces and the overturning moments are big enough to overcome buoyancy effects, the individual ice floes will under-turn or slide to the underside of the accumulation. These submerged ice floes may then be deposited under the ice accumulation, causing the accumulation to thicken. This process is called *hydraulic thickening*. It is a local phenomenon, as shown in Figure 1-1e, which is believed to be localized near the upstream end of the accumulation (Beltaos 1995). Healy and Hicks (2006) consistently observed this to occur over a length of 1-1.5 channel widths from the leading edge of the ice accumulation, during 40 experiments conducted in a laboratory flume under varying flow conditions.

As the ice accumulation grows in the upstream direction by juxtaposition and/or hydraulic thickening, the down-slope component of ice weight and the shear load exerted by the water flow on the underside of the ice both increase. These increasing external forces are resisted by the internal strength of the ice accumulation, which primarily increases with the increase of its thickness. Once the internal resistance of the ice accumulation and the bank friction are exceeded, the jam will *collapse and shove* to a much shorter and thicker shape (Figure 1-1f) to resume a new force balance.

Ice jams can occur during freeze-up and mid-winter thaws, but tend to be most severe during the spring breakup period. Owing to the relatively high flows coming from snowmelt runoff and (typically) the lack of freezing between the ice floes, breakup ice jams are almost exclusively formed by consolidation (i.e. by collapsing and shoving). This kind of jam can often attain an aggregate thickness of several meters, with an extremely rough bottom surface resulting from the randomly oriented ice floes. These combine to obstruct and resist the flow, lowering flow velocities and increasing flow depth in response. The associated high backwater is often responsible for the annual peak water level of most northern rivers.

Many factors, such as: sufficient water levels built up upstream, the arrival of a large increase in discharge, or an impacting ice run, can lead to sudden failure of an ice jam. Similar to a smaller-scale dam break event, the release of a major ice jam can produce rapidly rising water levels, together with a dramatic ice run, leading to extremely dangerous flash flood events. The ice run released from an ice jam can again be stopped somewhere downstream by solid ice cover, geometry constrictions, sharp bends, or man-made obstacles, reforming as a new jam. Therefore, dynamic river breakup often involves

a series of ice jam formation and release events, resulting in quite unpredictable floods in terms of both locations and timing of occurrences.

1.2 Current Knowledge of Ice Jam Formation

The formation of an ice jam often produces much higher water levels than those associated with same flow under open-water conditions. Research needs have been focusing on evaluating the flood potential of an ice jam that has already formed; and more recently, on predicting the jam occurrence.

1.2.1 *Ice Jam Stability Theory*

Ice jam stability theory is the most fundamental assumption in predicting the jam-related flood potential. It considers an ice jam as granular material between two parallel walls; and its strength is just enough to resist the applied gravitational and hydraulic forces. A number of similar relationships governing ice jam stability were developed by applying a force balance to the jam (e.g. Pariset et al. 1966, Uzuner and Kennedy 1976). Ashton (1986) presented the following equation as the typical formulation of the ice jam stability relationships.

$$[1\text{-}1] \quad t_i \frac{\partial t_i}{\partial x} = a + bt_i + ct_i^2$$

in which:

$$a = \frac{\tau_i}{2K_p\gamma_e};\ b = \frac{\rho_i g S_w - 2C_i/B}{2K_p\gamma_e};\ c = \frac{-C_o}{K_p B}$$

where:

γ_e is the effective unit weight of the ice, and is defined as:

$$\gamma_e = \frac{\rho_i g}{2}(1-p)\left(1-\frac{\rho_i}{\rho}\right);$$

t_i is the thickness of the ice jam;

τ_i is shear stress exerted by the water flow on the bottom of the ice jam;

K_p is the passive pressure coefficient as in Rankine's earth pressure theory, and is usually taken as $\tan^2(\pi/4 + \phi/2)$;

ϕ is the internal friction angle of the ice jam;

C_o is an internal strength coefficient ($C_o = \tan\phi$);

C_i is the cohesion coefficient of the ice jam, usually taken as zero for breakup ice jams;

ρ_i and ρ are the density of ice and water respectively;

S_w is the slope of water surface;

B is the width of the ice jam;

p is the porosity of the ice jam;

g is the gravitational acceleration.

When the ice supply is sufficient, an ice jam would achieve a section of uniform thickness, defined as *equilibrium thickness* t_{eq}. Further supply of ice would merely lengthen the jam without thickening it. The equilibrium section is important since it

produces the maximum water level within the ice jam profile. The *equilibrium thickness* t_{eq} can be calculated by setting $t_i(\partial t_i/\partial x)=0$ in equation [1-1]. A non-dimensional relationship between the maximum water depth and equilibrium ice thickness was also developed from this equation by Beltaos (1983).

It can be seen in equation [1-1] that term *a* represents the water drag applied to the bottom of the jam. Term *b* is the down-slope component of the weight of the jam. Term *c* and the term on the left hand side describe the internal forces within the jam resisting the applied forces. The well-known Rankine's and Mohr-Coulomb failure criteria in soil mechanics theories were used to formulate the internal strength of the ice jam. Ice jam stability theory has been adapted into many computational tools in conjunction with steady flow hydrodynamics, providing estimation of the thickness and associated water levels along breakup jams.

1.2.2 *Experimental Investigations*

1.2.2.1 Experiments under Steady Flow Conditions

Most experimental investigations to date have been conducted under steady flow conditions. Also, many have been case specific, rather than generic process models. For example, Saade and Sarraf (1996) formed a series of stable ice jams using model ice of different sizes and materials. Steady-state water surface profiles along these jams were measured and showed similar tendencies of spatial variations. The phreatic water surface varies linearly and gradually for the upstream approximately 90% jam length, while varies rapidly and non-linearly for the downstream 10% jam length.

Kawai et al. (1997) investigated the development of a jam initiated by an ice cover around bridge piers. The forces that ice jam and ice cover received were considered to be supported by piers. A range of critical Froude number for an individual ice floe to submerge and deposit under the ice cover was determined, which provided the condition under which ice jams are generated. They also observed the jam formation process and found that the jam thickness increased with time initially, until a maximum thickness was reached. After that, ice jams merely extend both upstream and downstream of the location where the ice jams initially formed.

Wang et al. (2006) conducted experiments to study jam formation in a curved channel, since channel bends are locations highly prone to jamming. They observed the longitudinal and transverse velocity distributions under artificial ice covers in a semi-circular section of the experimental flume, and found that the maximum velocity zone shifts down and tends to approach the inner perimeter of the channel as compared to the velocity distribution under open-water conditions. Irregularities of ice jam thickness in the curved section were observed. A critical Froude number equal to 0.14 was proposed for determining whether an ice jam will grow in upstream or downstream direction.

1.2.2.2 Experiments under Unsteady Flow Conditions

Unsteady ice jam consolidation experiments were carried out by Zufelt (e.g. 1990, 1992), and Zufelt and Ettema (1997). They conducted a series of experiments using both real and plastic model ice to explore the unsteadiness and ice momentum effects in ice jam formation processes. Two jam failure modes were identified as: progressive failure, caused by relative discharge increase less than 50%, in which a shoving front was

observed to smoothly move to the downstream end, followed by a thickening front moving back upstream; and complete failure, caused by relative discharge increases over 50%, in which the entire jam moved downstream en masse. They found that the thickness of the final stable jam is underestimated, especially for the complete failure mode, by the ice jam stability theory. Also, they pointed out that the shoving and thickening processes take quite a significant length of time to occur, unlike in the jam stability theory, which treats shoving and thickening as instantaneous processes. Their findings suggest that the ice momentum should be taken into account when estimating jam thickness. Unfortunately, the variations in water level and ice thickness during ice jam consolidation events were documented only qualitatively in their experiments.

Healy and Hicks (e.g. 1999, 2001, 2006, 2007) conducted 80 experimental tests to obtain continuous time-series data of many key parameters (e.g. discharge, water levels, ice jam thickness, flow velocities, and ice cover progression) describing the ice jam formation process, along with the profiles of final stable ice jams. Two scenarios representing two extreme carrier discharge conditions that may be encountered in natural rivers were explored: the scenario of ice jams formed under a constant carrier discharge; and the scenario of ice jams destabilized by a rapid increase in discharge. In the latter scenario, an initial ice jam is failed and shoved to form a new thicker and shorter stable jam. They observed that the process of ice jam formation is highly dynamic, even under a constant carrier discharge. An interesting finding is that the measured thickness and associated water levels within the ice jams, either formed under constant carrier discharge, or consolidated by a highly dynamic flow, agreed reasonably well with the estimation from the ice jam stability formulation in conjunction with a steady flow approximation. The

authors indicated that the question about the applicability of steady-state stationary jam tools still remains, for the scenario in between of the two extremes they had tested. That is, to examine the ice jam consolidation caused by a less dynamic wave, which passes through the ice jam over a duration comparable to that of the consolidation event. Their research data provide valuable quantitative data for validating dynamic ice jam numerical models.

1.2.3 *Field Investigations*

Experiments are sometimes limited by physical scales, ice and flow conditions, and meteorological condition that can be achieved in the laboratory, thus it is essential to get information from the actual events. Field observations have been widely carried out to obtain both quantitative and qualitative data describing thickness and associated water levels caused by ice jams, and their hydraulic characteristics. Variable locations and sudden release of spring breakup jams limit access, thus making the measurement a very difficult task.

1.2.3.1 Measurements of Ice Jam Thickness and Water Levels

To date, only limited data of ice jam thickness and associated water levels have been collected in the field. Many of the documented thickness data were estimated from the thickness of shear walls left behind by a released ice jam (e.g. Beltaos and Burrell 1990), or by tree scars resulting from ice impacts (e.g. Tuthill et al. 2005). Aircraft and oblique air photographs have also been utilized to approximate water and ice top level profiles in inaccessible reaches. Photos are taken of the ice jam level against the river banks and used later when safe access is available for identification and survey (e.g. Beltaos 1983,

Andres and Rickert 1985). More reliable water level surveys can be obtained when road access was available (e.g. Doyle and Andres 1979, Beltaos et al. 1996a). A remote thickness-profiling device named the "Ice Jam Profiler" (IJP) was tested for measuring ice jam thickness on various rivers (Beltaos et al. 1996b). Beltaos et al. (2001) presented detailed ice thickness data collected during several ice jam events using this device. However, each unit cost several thousand dollars to construct and approximately one in two are lost operationally. Ice jam profile data can also be found in a scatter of publications (e.g. Doyle and Andres 1978, Beltaos and Moody 1986, Gerard and Stanley 1988, Malcovish et al. 1988, Beltaos et al. 1994, Andres 1996).

All the above ice jam profile data were collected after a stable ice jam had formed, representing steady state conditions. Morse et al. (2003) developed an upward looking Acoustic Doppler Current Profiler (ADCP) which facilitated measurements of time-series ice thickness, water level, and water and ice velocity at a fixed point. Comprehensive data sets were obtained for brash ice on the Saint Lawrence River, Quebec. A similar setup, known as the Shallow Water Ice Profiling Sonar (SWIPS), has also been utilized to collect continuous ice measurements on the Peace River, northern British Columbia and Alberta, during the ice season in the last three years (Jasek et al. 2005). A wealth of information was achieved for the freeze-up consolidation process during the formation of the winter ice cover, and for the thermal erosion during the entire winter. Unfortunately, no data about break-up jams has been obtained. A key disadvantage of this kind of approach is that measurements were only obtained at a single point in each case. Also, the ice profilers are highly subject to damage or loss during ice jam events. More data

describing the dynamic formation process are still highly desirable and would further advance the understanding of the ice jam events.

1.2.3.2 Other Ice-Jam Characteristics

Understanding the hydraulic characteristics of breakup ice jams has also been achieved with the aid of field observations. For example, the ice jam thickness profiles obtained using the ISP provided sufficient details for estimating and quantifying the roughness of the bottom of ice jams (Beltaos 2001). He found that the absolute roughness increases linearly with average thickness for up to 3 m thick ice accumulation. He suggested that more data are required to assess the roughness for the underside of jams thicker than 3 m. The seepage-flow characteristic of breakup jams has also been evaluated by means of field measurements. Beltaos (1999) analyzed 3-year-measurements of water level profiles and discharges associated with breakup jams initiated by an ice-retention structure in the Credit River at Erindale Park (Mississauga, Ontario), and deduced consistent value for the flow velocity through the voids of jams. These two characteristics, roughness and seepage, are both very important parameters for numerical model calibration and validation.

1.2.4 *Numerical Investigations*

Most of the currently available numerical models for determining ice jam profiles and associated water levels, such as ICEJAM (Flato and Gerard 1986), RIVJAM (Beltaos and Wong 1986), U.S. Army Corps of Engineers' HEC-RAS (Daly and Vuyovich 2003), and the proprietary model, ICESIM (Carson and Groeneveld 1997), are based on the ice jam stability theory and a steady flow approximation. These models have been widely used

for more than two decades, to aid in the estimation of flood levels that may be expected to occur under ice jam conditions. However, both experimental and field investigations have suggested that river ice jamming processes are inherently unsteady. Flow varies greatly during breakup, owing to snowmelt or possible release of upstream ice jams. Even if the carrier discharge is constant, significant unsteadiness can be expected during the jamming processes (Healy and Hicks 2006). Therefore, whether or not a steady flow assumption is reasonable for estimating the thickness and water level profiles related to ice jams remains a question. Moreover, there is no way for steady flow models to predict when and where an ice jam would form, since ice motion is not considered. These issues instigated the development of more advanced computational models.

The first numerical model for the dynamic transport of river ice was proposed by Shen et al. (1990). This model provides a theoretical framework for analyzing the process of ice jam evolution, which cannot be described by the static ice jam stability theory. The ice transport was simulated using a Lagrangian-Eulerian scheme; while the conservation equations of mass and momentum for under-ice flow were solved using the four-point implicit finite difference method with Newton-Raphson scheme. Considering the ice as a granular continuum, they formulated plausible constitutive relationships for internal ice stresses and bank shear for rapid flow regime (low ice concentration, interactions between ice floes are dominant by binary collisions) and slow flow regime (high ice concentration, interactions between ice floes are mainly prolonged contacts). Shen et al. (1990) indicated that the constitutive relationships were based on limited state of knowledge at that time, thus further improvement are required.

Zufelt and Ettema (1997, 2000) developed a one-dimensional dynamic model to simulate ice jam formation under unsteady flow conditions. Ice momentum is included explicitly; and the conservation equations of mass and momentum for both water and ice are solved simultaneously in the model using the box-finite-difference (BFD) method. Following the conventional stability theory, the ice jam is considered as floating granular mass that obeys the Rankine and Mohr-Coulomb failure criterion. Applications of their model suggested that ice momentum presents a significant effect on the final jam thickness profile. They found that the modeled thickness was greater than the equilibrium thickness obtained using ice jam stability theory. Zufelt and Ettema (1997, 2000) also used this model to explore the effects of unsteady inflow hydrographs on ice jam profiles in a series of hypothetical situations. The channel considered in these situations was assumed to be fully covered by ice.

DynaRICE (e.g. Liu and Shen 2000, Shen et al. 2000) is a two-dimensional ice dynamic model to simulate dynamic transport and jamming of surface ice in rivers. Ice momentum is considered explicitly and deterministically. The conservation equations of water and ice are solved in an uncoupled sequence, because Lal and Shen (1992) showed that the speed of a shallow water wave is independent of the speed of the stress wave in an ice layer. The hydrodynamic component of DynaRICE model employs an Eulerian finite element method, while the ice dynamic component employs the Lagrangian method of smoothed particle hydrodynamics (SPH). A unique aspect of this model is that it utilizes a viscous-plastic constitutive model (widely used in sea ice models, adapted with changes) to relate the internal resistance of the moving surface ice to strain rates. In this manner, time-dependent forces and stresses can be handled. Their model was validated with an

analytical solution (a hypothetical ice jam formation driven by water drag only) in a straight uniform rectangular channel. They also utilized the model to simulate the ice transport and jamming in rivers (Lu et al. 1999, Liu and Shen 2005); and to examine the feasibility of controlling ice using ice booms by estimating the ice load on the booms (Liu and Shen 2000, Shen et al. 2000). DynaRICE has also been included into a new proprietary modeling package known as the Comprehensive River Ice Simulation System (CRISSP) (Liu et al. 2006), which is capable of simulating both thermal and mechanical processes during both the freeze-up and breakup periods (e.g. dynamic transport of surface ice and ice jam evolution; thermal growth and decay of ice cover and mechanical breakup conditions).

A different type of model is the DEM (discrete element model). Individual ice blocks within an ice jam are each considered explicitly, instead of considering the entire ice jam as granular continuum (as the above models do). The motion of each block is determined by calculating the forces applied on the block exerted by the water and the surrounding blocks. Daly and Hopkins have coupled a DEM with a one-dimensional unsteady hydraulic model to simulate the dynamic process of ice runs arrested by ice-control structures (e.g. Hopkins et al. 1996; Daly and Hopkins 1998, 2001). The forces exerted by jams on structures were also predicted, which provided valuable information for the design of ice-control structures. Limited by computational efforts, DEM technology best applies to events that occur within a short reach and last for a short duration.

1.2.5 *Discussion*

While considerable progress has been made in studying ice jam formation events, some aspects have not yet been fully addressed. There is a lack of continuous measurements of the variations in many key parameters during the dynamic formation process. The most comprehensive set of quantitative data of this kind is from the experimental study of Healy and Hicks (1999, 2001, 2006, and 2007), and should be explored fully. Several excellent sophisticated numerical models have been developed, but have not yet been fully validated. These models provide good predictions of the measured stable ice jam and water level profiles, but how they perform with regard to simulating the dynamic consolidation process is still not known. Questions also remain regarding the applicability of the steady-state stationary ice jam computational models, and so this needs further investigation.

1.3 Current Knowledge of Ice Jam Release

The release of an ice jam produces a combined water and ice wave, leading to rapidly rising water levels downstream. It is a very complex process, not only due to the highly dynamic flow, but also because of the interactions between the ice and water. Possible stoppage of the released ice run further complicates the problem. Previous research on ice jam release processes has focused on how the presence of ice in a channel changes the arrival time and magnitude of the ice jam release wave.

1.3.1 *Analytical Investigations*

Henderson and Gerard (1981) conducted the first theoretical study of the properties of wave produced by the sudden release of an ice jam in a rectangular channel. Bed slope and resistance, as well as the effects of ice after jam release, were neglected in their analytical model. This idealization, which is essentially the classic dam-break solution, predicted a positive wave with an abrupt front propagating downstream at a constant speed c, coupled with a negative wave propagating upstream, as shown in Figure 1-2. The two waves are separated by a lengthening reach of uniform flow of y_1 deep. For the positive wave, also referred to as a *surge*, the governing equations of continuity and momentum as determined by Henderson and Gerard (1981) are:

[1-2] $$c(y_1 - y_0) = V_1 y_1 - V_0 y_0$$

[1-3] $$\frac{(c - V_0)^2}{g y_0} = \frac{1}{2}\frac{y_1}{y_0}\left(\frac{y_1}{y_0} + 1\right)$$

and for the negative wave,

[1-4] $$V_2 + 2\sqrt{g y_2} = V_1 + 2\sqrt{g y_1}$$

in which, symbols are defined as in Figure 1-2. They showed that the surge height (y_1 - y_0), surge speed (c), and the water velocity behind the surge front (V_1) can be determined from the above equations, given the initial conditions upstream and downstream of the jam toe. The severity of an ice jam release events can then be assessed, with awareness of the strong simplifications made in this method.

Henderson and Gerard (1981) tested their solution using practical ice jam release data collected by Doyle and Andres (1979) on the Athabasca River at Fort McMurray. It was observed that a wave 3.6 m high traveled 11 km from the original release point in 45 minutes. Close agreement with the observed peak water level was achieved; however, a large discrepancy in terms of the surge speed was found, with their theoretical value of 11 m/s being significantly larger than the observed value of 4 m/s. From this, they presumed that the ice should slow down the surge considerably and may increase the peak stage or at least reduce the attenuation due to the reflection of negative wave.

1.3.2 *Experimental Investigations*

Wong et al. (1985) and Khan et al. (2000) both attempted to study the effects of the ice on the release wave using laboratory experiments. They both used polyethylene blocks to simulate the ice. Wong and his colleagues simulated ice jams by obstructing the polyethylene blocks with a sluice gate. There was no ice downstream of the gate. Jam release was simulated by suddenly lifting the gate. The resulting waves were monitored at various locations along the channel by recording the water levels. The times at which the front of the ice run arrived at several stations were also recorded, and thus the front speed could be calculated. They concluded that the ice had little effect on wave propagation, upon comparison with Henderson and Gerard's (1981) theoretical solution and with a one-dimensional, unsteady flow hydrodynamics model (Beltaos and Krishnappan 1982).

Khan et al. (2000) studied the effect of floating debris on dam-break surges. They considered the ice in the jam and in the receiving channel both. Different depth ratios between the water depths downstream and upstream of the jam were tested. By

comparing with the theoretical solution of Henderson and Gerard (1981), they found that the debris (the polyethylene blocks) slowed down the surge speed, and increased the surge height. They also found that the effects of the debris on the surge height reduce as the depth ratio increases, because the higher initial downstream water depth provides more vertical room for the debris.

The two experimental investigations had different findings regarding to the ice effects on the propagation of the ice jam release wave. The reason for this discrepancy could be that ice in the receiving channel was considered in one case but not the other. Less mass of ice had more room to move, thus had smaller resistance to the flow in the experimental flume. The applicability of these experimental findings to the field situation was limited by the physical constraints of the laboratory experiments. The length of the flume was only tens times the water depths; while propagation distances of thousands, or tens of thousands times the depth, are involved in actual ice jam release events. Thus, the results of laboratory studies should be only applicable to the very early stages of the wave motion. In addition, the way an ice jam is held in place in the field can not be reproduced well in the laboratory.

1.3.3 *Field Investigations*

Jasek (2003) conducted field investigations documenting ice jam release events and found that the celerity (speed) of release waves were affected by different ice conditions in the receiving channel. He found that for an *unimpeded ice run* (ice jam release with open water downstream), the majority of the ice concentration initially traveled along and slightly ahead of the peak water level. Defining release wave propagation distance in

'jam lengths' (i.e. non-dimensionalized by dividing travel distance by the original ice jam length), he observed that the ice effects seemed to be important only for the first 1 to 2 jam lengths of propagation, approximately. Within this range, he observed that the ice slowed down the flood wave, until the water crest finally overtook the ice. In contrast, an *impeded ice run* (ice jam release with solid ice cover downstream) was significantly different from, and more complex than, the case of an unimpeded ice run. The transition point between the moving fragmented ice and the stationary downstream solid ice is termed the *breaking front*. Jasek (2003) further divided the breaking front into two types: *rubble front* and *sheet front*. He found that rubble fronts tend to form where the ice sheet is confined and thus not able to be set in motion; instead the ice sheet is pulverized into smaller pieces and then incorporated into the moving ice pack. He also found that sheet fronts are common on larger and steeper rivers, which provide enough space for large ice sheets to move. Sheet fronts were documented as traveling for longer distances than rubble fronts. Wave celerity was also found to be affected by the type of breaking front and other factors. Jasek (2003) suggested that more work needs to be done in this area.

In addition to the ice jam flood events reviewed by Blench (1964), many people/agencies (e.g. Alberta Environment, Alberta Research Council, Trillium Engineering and Hydrographs Inc.) have been documenting ice jam release events on the Athabasca River, Alberta, since the late 1970's. Kowalczyk Hutchison and Hicks (2007) analyzed approximately 25 years of historical field data recorded on the Athabasca River and noted that very little quantitative data has been obtained for theoretical analysis and numerical model verification. An analysis of those events that were documented, showed that even slight deceleration of an ice run may be significant in increasing both the magnitude and

celerity of a flood wave. Since these decelerations may not be noticeable to the observers in the field, it is important to include ice effects in forecasting tools. An ongoing monitoring program led by Faye Hicks from the University of Alberta, in collaboration with Alberta Environment, successfully implemented a remote water level monitoring network along the Athabasca River in 2001. Hydrographs describing ice jam release waves were captured for events occurring during 2001, 2002, and 2003 breakup (Robichaud and Hicks 2001, Kowalczyk and Hicks 2003, 2004). This included documentation of an ice jam release wave which rose 4.07 m in the first 5 minutes (0.81 m/min), and a total overall of 4.31 m (believed to be the largest rise speed and wave magnitude measured for any ice jam release event to date). Hydrographs were measured at 7 sites downstream of the jam over a distance of 50 km, including hydrographs at, and downstream of the toe of a new jam which formed 37 km downstream. Analysis of the event using unsteady flow modeling suggested that approximately two thirds of the release wave was captured by the new ice jam which formed downstream (Kowalczyk Hutchison and Hicks 2007).

Beltaos and Burrell (2005a) used a surge meter to measure ice jam release waves. This device consists of a pressure transducer and radio transmitter combined (Beltaos et al. 1998). It provides water level hydrographs similar to those obtained from hydrometric stations; but can be easily and quickly installed along a mildly sloping bank downstream of an ice jam. Therefore, a surge meter has a higher chance than the hydrometric stations of collecting data within a short distance downstream of a jam, where most of the highly dynamic processes happen (Beltaos and Burrell 2005a). Two data sets obtained for the 2000 Restigouche River (New Brunswick) and 2002 Saint John River (New Brunswick)

release events were presented in detail. They found that the measured jam release waves, and those reported previously by others, differ from the idealized waves predicted by analytical solutions based on the classic dam break problem (e.g. Henderson and Gerard 1981). The wave celerity is the highest at very near the point of release, but still much smaller than that predicted by the analytical dam-break solution obtained by neglecting resistance effects; the rising limb of the wave is very steep at this phase, but still far from the abrupt increase predicted by the same analytical solution. They also found that the celerity of the wave's leading edge is greater than that of the wave peak, and the latter is greater than the celerity of the trailing edge. For this reason, they proposed that the term ice jam release "wave" would be more appropriate than ice jam release "surge". Beltaos (2008) has proposed a new term "jave" to describe a jam release wave, although this term has not yet been used in the literature by others. All the data sets Beltaos and Burrell (2005a) reported on also indicated that attenuation occurred as the wave was propagating downstream, with the celerity and magnitude of the releasing wave both decreasing. For example, the celerity of Saint John River release wave was calculated to be 5.5 m/s and 2.5 m/s at the front and the peak, when it traveled 6.9 km between the surge meter and a downstream gauge station at Ft Kent; and 3.5 m/s, 2.1 m/s and 1.7 m/s for the front, the peak, and the trailing edge, respectively, when the wave traveled another 32.1 km between two gauge stations at Ft Kent and Edmundston.

Though many waveforms have been recorded for ice jam release events, the corresponding initial ice jam length, thickness and water level (or ice surface) profiles are not available for most of these documented release events. Detailed pre-release data are required by numerical models for predicting flood wave released by ice jams; thus, it is

highly desirable to collect these data together with propagating wave data for the same release events. Alternatively, Beltaos and Burrell (2005b) developed an approximate analytical method to determine the hydrodynamic characteristics of ice jam release waves from the measured waveforms, without needing initial ice jam thickness and water level profiles. Unlike the analytical approach of Henderson and Gerard (1981), this method takes both resistance and the bed-slope effects into account, but does not predict the wave itself. Instead, it deduces important hydraulic parameters (e.g. wave celerity, flow velocity, discharge, and shear stress) from measured waveforms. Application of this method to the events measured in the Restigouche and Saint John Rivers in New Brunswick provided plausible quantification of the severity of ice jam release waves (Beltaos and Burrell 2005b). Flow discharge, velocity, and shear stress were shown to be greatly amplified during the passage of an ice jam release wave. The degree of amplification is the highest near the release point and decreases as the wave travels downstream. This method provides good results within the rising limb of a wave, and within the early phases of wave propagation (Beltaos and Burrell 2005b).

1.3.4 *Numerical Investigations*

Numerical modeling of ice jam release waves started in the 1980s, and has continued to the present. Although the sophistication of solution techniques and channel geometry representations increased, most of the researchers have attempted to use one-dimensional hydrodynamic models and have neglected ice effects on the propagating wave. For example, Beltaos and Krishnappan (1982) modeled the 1979 Athabasca River event (documented by Doyle and Andres 1979), using an implicit finite difference scheme to solve the St. Venant equations for one-dimensional, unsteady, water-only flow, assuming

rectangular channel geometry. The ice was treated as a portion of the water. Plausible approximations, in terms of the peak water level and the wave speed, were achieved; however, they had difficulties matching the shape of the measured stage hydrograph. Specifically, the observed stages at the recession limb of the wave were greatly underestimated by their model. This discrepancy was very likely because they did not consider the effects of ice resistance.

Hicks et al. (1992) applied the one-dimensional *Characteristic-Dissipative-Galerkin* (CDG) finite element method (Hicks and Steffler 1992) to model the propagation of ice jam release waves over a 500 km reach of the Hay River in Alberta and Northwest Territories. The gradually varied flow profile under open-water conditions was first computed using the CDG model, and the water surface profile corresponding to an ice jam of specified length (as well as the backwater profile upstream) was then superimposed on it, as the initial pre-release condition. The water depth at each section within the jam was calculated as that for an equilibrium section of a fully developed jam (Beltaos 1983). Ice mass was treated as water. Simulating the release of this approximated ice jam showed that the CDG method can provide stable solutions for the highly dynamic wave conditions (which occur during the very early phase of the wave propagation); the kinetic conditions (after the wave had traveled a long distance); and the transition between these two extremes. The modeled results were not validated with actual measurements.

Hicks et al. (1997) investigated the feasibility of applying the one-dimensional CDG hydraulic flood routing model (Hicks and Steffler 1992) to ice jam release wave modeling for the 1993 ice jam event on the Saint John River, New Brunswick

(documented by Beltaos et al. 1994). The event was modeled, with a rectangular channel approximation (of varying widths) and ice effects were neglected. The ice jam profile measured prior to release was superimposed on the computed open-channel water level profile, as was the backwater profile upstream of the jam. The model results were compared with a measured water level hydrograph at a downstream station, located within one jam length of the original jam toe. The model reproduced the propagation speed of the wave well, but was relatively inaccurate in terms of the predicted water level. They hypothesized that this discrepancy might be attributed to using the rectangular geometry assumption and/or to neglecting the ice effects.

Blackburn and Hicks (2003) conducted further analysis of the 1993 Saint John River event (Beltaos et al. 1994), again using the one-dimensional CDG method. They found that using actual channel geometry provided a better prediction of the peak water level, compared to using a rectangular channel approximation. They also increased the bed resistance in the receiving channel to approximate the ice resistance effects, and showed that the peak discharge was decreased, but the wave celerity was not significantly affected. The computed water level was increased, and although it overestimated the observed peak, it provided a better visual fit to the hydrograph shape. Increased resistance was also introduced along the length of the ice jam for the first 15 minutes, providing a delayed release of the jam as compared to instantaneous release. The only noticeable effects of this on the stage and discharge hydrographs were within the ice jam reach. Blackburn and Hicks also encountered difficulties in matching the recession portion of the stage hydrograph. Another limitation was that they only had the observed hydrograph for model evaluation at one station.

Liu and Shen (2004) further explored the ice resistance effects on the wave propagation, by applying the two-dimensional DynaRICE model mentioned in section 1.2.4. Both internal resistance and boundary friction resistance of the ice were considered. An idealized test case, which was loosely based on the 1993 Saint John River release event, was used since the actual channel geometry data is proprietary to New Brunswick Power and thus was not available to them. Comparisons between their simulation results, obtained with and without inclusion of ice dynamics, showed that the ice resistance decreased the peak discharge and slowed down the release processes. Liu and Shen (2004) also designed an idealized ice jam release event in a short channel, as a demonstration of the jam release phenomenon in a reach between run-of-river power stations. The modeled wave, with ice effects considered, attenuated much faster than that simulated without ice effects. They concluded that ice effects on the wave propagation cannot be neglected. Worth noticing is that this conclusion is only partly consistent with Jasek (2003)'s finding in the field, that the ice effects on the propagating jam release wave are important, but only for the first 1 to 2 jam lengths. Unfortunately, there is, as yet, a lack of actual data for validating this type of numerical models.

1.3.5 *Discussion*

Numerous studies on river ice jam release processes have been conducted. Observations and measurements have been widely carried out in the laboratory and in the field. Significant efforts have been devoted to the development of numerical models due to their advantages in real-time forecasting. The sophistication of models has been greatly improved. However, despite this progress, a review of previous research indicates that there are still considerably different opinions on the significance of ice effects on the

propagation of the jam release wave, specifically regarding whether or not the ice changes the characteristics of propagating waves, and when and where the ice effects are most important. Clearly the presence of ice has significantly complicated the problem and the ice-water interactions have not been well understood. As a result, our current ability to predict of ice jam related floods is limited to relatively simple conditions. Existing numerical models are in need of more, and better, validation data.

1.4 Research Objectives and Thesis Outline

The objectives of the work embodied by this thesis were as follows:

- Expand our knowledge of dynamic ice processes by collecting scientific data describing ice jam formation and release events through annual field observations during river breakup, and by extracting useful information from the existing experimental data of Healy and Hicks (2001, 2007)

- Develop and apply numerical models of ice jam dynamics that can facilitate prediction of floods related to river ice jam occurrences, and improve our understanding of ice jam dynamics by using these models to aid in the interpretation of field and experimental data.

The numerical models developed for this research project were built on the University of Alberta's public domain software *River1-D*, a one-dimensional hydrodynamic model for open-channel flow, previously known as the CDG model (Hicks and Steffler, 1992). Numerical model development involved three distinct phases. In Phase 1, simplified (empirical) ice momentum effects were incorporated into the *River1-D* model to explore

the extent of ice complexity necessary to successfully simulate flood waves produced by the sudden release of an ice jam. The Phase 1 model considered only the effects of the ice within the original jam. In Phase 2, the effects of an ice cover in the receiving channel were included for the ice jam release problem, again in a simplified manner. In Phase 3, ice effects were considered deterministically and the internal resistance of the ice accumulation was explored. Validation and application of this refined model focused on ice jam formation events under various flow conditions achieved in laboratory. The Phase 3 model also has the ability to handle ice jam release events. It was implemented to simulate hypothetical, experimental, and actual release events; and to investigate ice effects on propagating flood waves produced from ice jam release. An integral part of this study was the spring breakup field program undertaken on the Athabasca River, near Fort McMurray in northern Alberta. Field data, obtained as a result of the 2006 and 2007 breakup monitoring programs, was presented in detail and have been used in the evaluation of the numerical models.

This thesis is presented in a paper format following the guidelines for thesis preparation set forth by the Faculty of Graduate Studies and Research, University of Alberta. Three core papers and one conference paper constitute the bulk of this thesis. Chapter 2, describing the Phase 1 model, is presented as it was published in the Journal of Cold Regions Science and Technology (She and Hicks 2006a). Chapter 3, describing the Phase 2 model, is a paper presented by the author at the 18th IAHR International Symposium on Ice (She and Hicks 2006b). Chapter 4, describing the ice jam formation and release processes measured on the Athabasca River, is presented as it was accepted by the Journal of Cold Regions Science and Technology (She and Hicks *in press*).

Chapter 5, describing the Phase 3 model, is a paper that is currently under review for publication in the Journal of Cold Regions Science and Technology (She et al. *under review*). Chapter 6 provids a detailed description and discussion on applying the Phase 3 model to ice jam release events. Appendix A presents details of a sensitivity analysis conducted on the Phase 3 model. Appendix B contains a paper that will be presented by the author at the 19th IAHR International Ice Symposium (She et al. 2008). It provides details on utilizing the Phase 3 model to investigate the applicability of steady ice jam profile models.

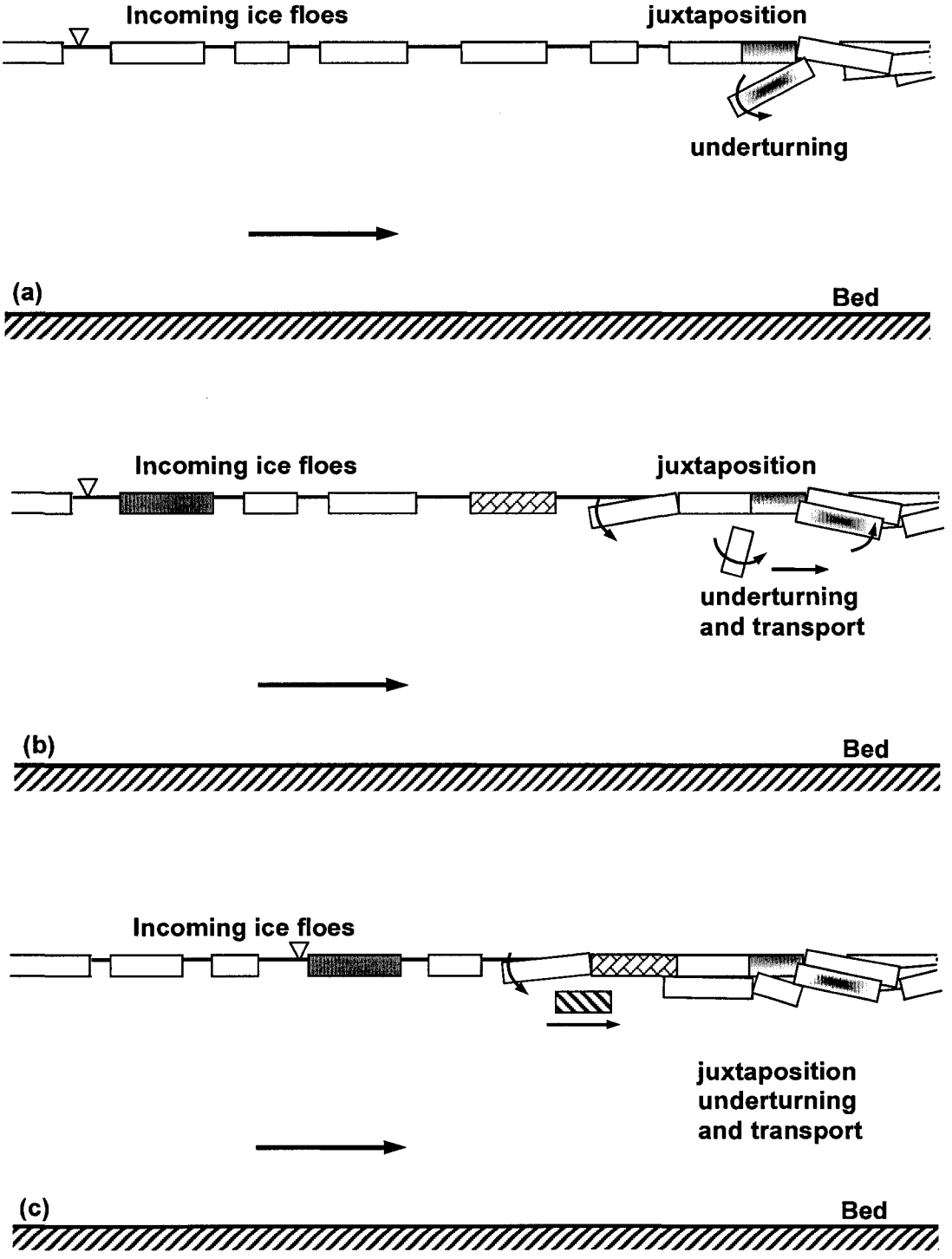

Figure 1-1 Sketch of the initiation and evolution process of an ice jam (adapted from Healy 2006, with changes)

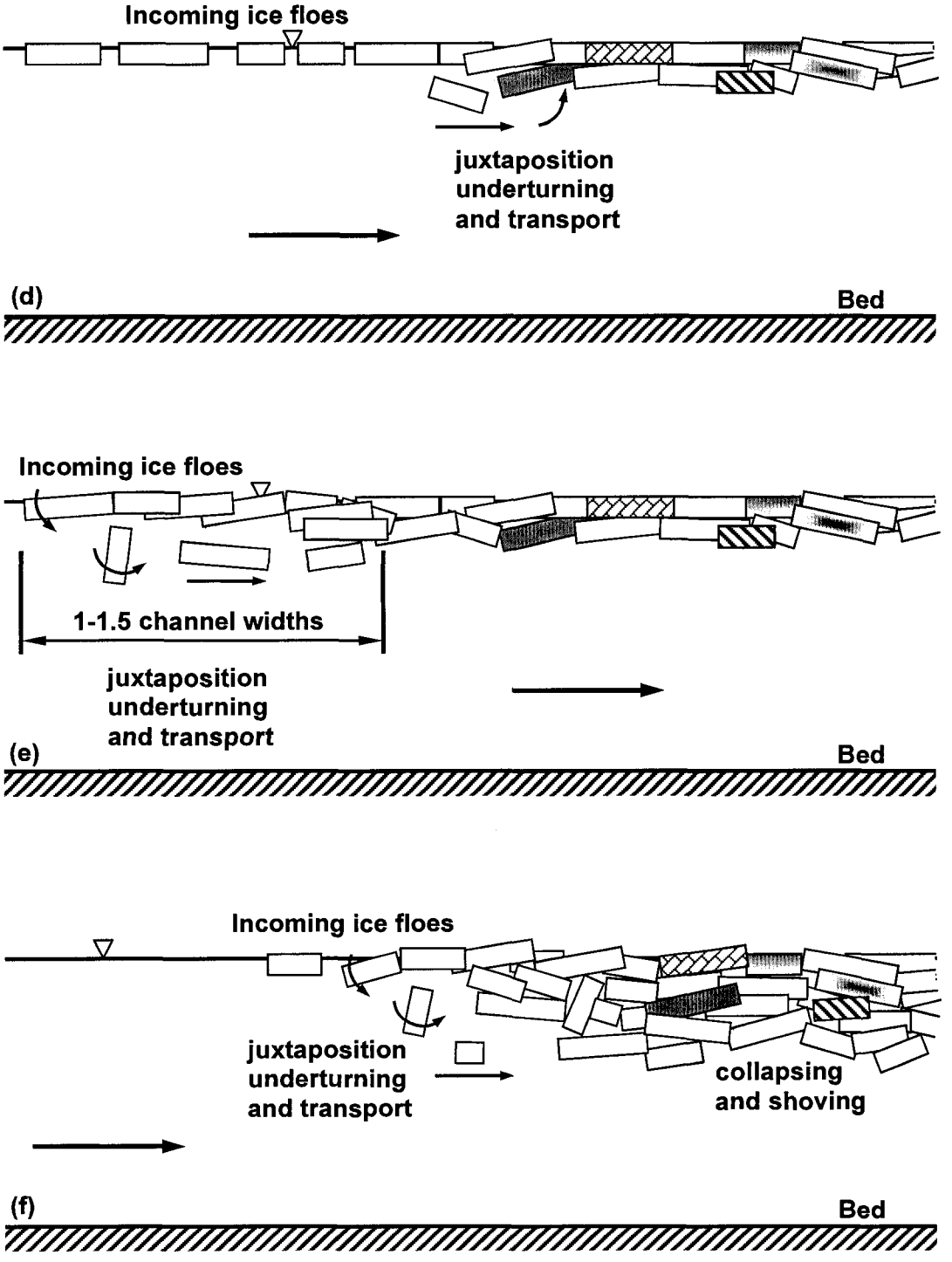

Figure 1-1 Sketch of the initiation and evolution process of an ice jam (adapted from Healy 2006, with changes) (*continued*).

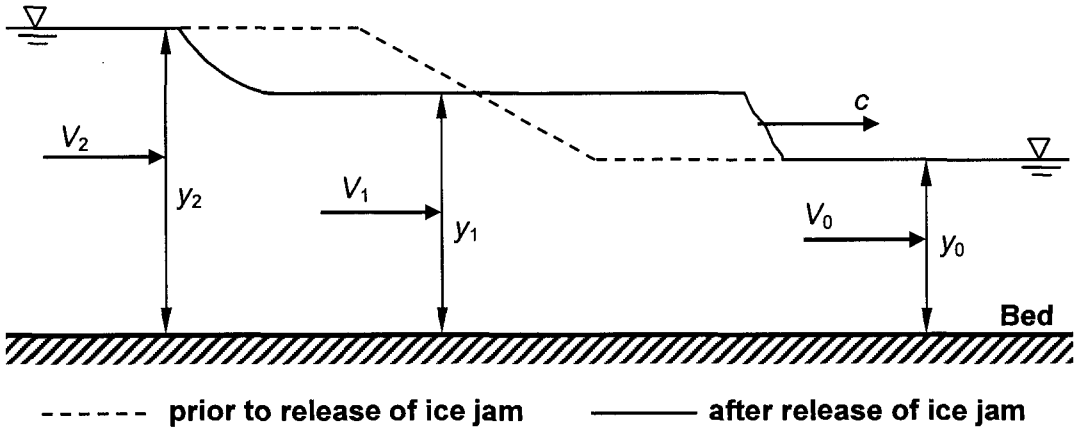

Figure 1-2 Surge propagation after release of an ice jam (adapted from Henderson and Gerard 1981, with changes).

1.5 References

Andres, D.D. (1996). Review of WSC Border Gauge Discharge Estimates. Consulting Engineering Report, Trillium Engineering and Hydrographics Inc., 23pp.

Andres, D.D. and Rickert, H.A. (1985). Observation of Breakup in the Athabasca River upstream of Fort McMurray, Alberta, 1984. Alberta Research Council, Report No. SWE 85-09.

Ashton, G.D. (1986). River and Lake Ice Engineering. Water Resources Publications, Littleton, Colorado, 485 pp.

Beltaos, S. (1983). River Ice Jams: Theory, Case Studies, and Applications. Journal of Hydraulic Engineering, 109(10): 1333-1359.

Beltaos, S. (Ed) (1995). River Ice Jams. Water Resources Publications, Highlands Ranch, Co., USA.

Beltaos, S. (1999). Flow Through the Voids of Breakup Ice Jams. Canadian Journal of Civil Engineering, 26: 177-185.

Beltaos, S. (2001). Hydraulic Roughness of Breakup Jams. ASCE Journal of Hydraulic Engineering, 127(8): 650-656.

Beltaos, S. (2008). Progress in the Study and Management of River Ice Jams. Cold Regions Science and Technology. Vol. 51: 2-19.

Beltaos, S. and Burrell, B.C. (1990). Ice Breakup and Jamming in the Restigouche River, New Brunswick: 1987-1988 Observations. National Water Research Institute, NWRI Contribution 90-169, 25pp.

Beltaos, S. and Burrell, B.C. (2005a). Field Measurements of Ice-Jam-Release Surges. Canadian Journal of Civil Engineering, 32: 699-711.

Beltaos, S. and Burrell, B.C. (2005b). Determining Ice-Jam Surge Characteristics from Measured Wave Forms. Canadian Journal of Civil Engineering, 32: 687-698.

Beltaos, S. and Krishnappan, B.G. (1982). Surges from Ice Jam Releases: A Case Study. Canadian Journal of Civil Engineering, 9(2): 276-284.

Beltaos, S. and Moody, W.J. (1986). Measurements on the Configuration of A Breakup Jam. National Water Research Institute, NWRI Contribution 86-123, 37 pp.

Beltaos, S. and Prowse, T.D. (2001). Climate Impacts on Extreme Ice Jam Events in Canadian Rivers. Hydrological Sciences Journal. 46(1): 157-182.

Beltaos, S. and Wong, J. (1986). Downstream Transition of River Ice Jams. Journal of Hydraulic Engineering, 112(2): 91-110.

Beltaos, S., Burrell, B.C., and Ismail, S. (1994). Ice and Sedimentation Processes in the Saint John River, Canada. Proc., 12th IAHR Ice Symposium, 1994, Trondheim, Norway, 11-21.

Beltaos, S., Burrell, B.C., and Ismail, S. (1996a). 1991 Ice Jamming along the Saint John River: A Case Study. Canadian Journal of Civil Engineering, 23(2): 381-394.

Beltaos, S., Ford, J.S., and Burrell, B.C. (1996b). Remote Measurements of Ice Jam Thickness Profiles. Proc., 13th IAHR International Symposium on Ice, Beijing, China, Vol.2: Beijing, Chinese Hydraulic Engineering Society, 577-584.

Blackburn, J.L. and Hicks, F.E. (2003). Suitability of Dynamic Modeling of Flood Forecasting during Ice Jam Release Surge Events. ASCE Journal of Cold Regions Engineering, 17(1): 18-36.

Blench, T., and Associates Ltd. (1964). Flood Protection Proposals for McMurray. Government of Alberta, unpublished report, 62 pp.

Carson, R.W. and Groeneveld, J.L. (1997) Evolution of the ICESIM Model. Proc. 9th Workshop on River Ice, Fredericton, New Brunswick, Committee on River Ice Processes and the Environment, Hydrology Section, Canadian Geophysical Union, 289-302.

Daly, S.F. and Hopkins, M.A. (1998). Simulation of River Ice Jam Formation. Proc., 14th IAHR Symposium on Ice, Potsdam, New York, 101-108.

Daly, S.F. and Hopkins, M.A. (2001). Estimation Forces on an Ice Control Structure Using DEM. Proc., 11th Workshop on River Ice, Ottawa, Committee on River Ice Processes and the Environment, Hydrology Section, Canadian Geophysical Union, Sidney, British Colombia, pp. 145-158.

Daly, S.F. and Vuyovich, C.M. (2003). Modeling River Ice with HEC-RAS. Proc., 12th Workshop on River Ice, Canadian Geophysical Union – Hydrology Section, Comm. on River Ice Processes and the Environment, Edmonton, Alberta, pp. 280-290.

Doyle, P.F. and Andres, D.D. (1978). 1978 Breakup in the Vicinity of Ft. McMurray and Investigation of Two Athabasca River Ice Jams. Alberta Research Council, Edmonton, AB, Report SWE 78-5.

Doyle, P.F. and Andres, D.D. (1979). 1979 Spring Breakup and Ice Jamming on the Athabasca River Near Fort McMurray. Alberta Research Council, Edmonton, AB, Report SWE 79-05.

Flato, G. and Gerard, R. (1986). Calculation of Ice Jam Thickness Profiles. Proc., 4th Workshop on Hydraulics of River Ice, Montreal, pp. C3.1-C3.25.

Gerard, R. and Stanley, S. (1988). Ice Jams and Flood Forecasting, Hay River, N.W.T. Department of Civil Engineering, University of Alberta, Report 88-6, 175 pp.

Healy, D. (2006). Experimental Observations on River Ice Accumulations. Ph.D. Thesis (supervisor F. Hicks), Department of Civil and Environmental Engineering, University of Alberta, Edmonton, AB, 380 pp.

Healy, D. and Hicks, F. (1999). An Assessment of the Applicability of Steady Flow Ice Jam Profile Models. Proc., 10th Workshop on the Hydraulics of ice Covered Rivers, Winnipeg, pp. 346-360.

Healy, D. and Hicks, F. (2001). Experimental Observations on Ice Jam Shoving. Proc., 11th Workshop on River Ice. May 2001, CGU - Hydrology Section, Comm. on River Ice Processes and the Env., Ottawa, ON, pp. 122 -144.

Healy, D. and Hicks, F. (2006). Experimental Study of Ice Jam Formation Dynamics. ASCE Journal of Cold Regions Engineering, 20(4): 117-139.

Healy, D. and Hicks, F. (2007). Experimental Study of Ice Jam Thickening under Dynamic Flow Conditions. ASCE Journal of Cold Regions Engineering, 21(3): 72-91.

Henderson, F.M. and Gerard, R. (1981). Flood Waves Caused by Ice Jam Formation and Failure. Proc., International Association for Hydraulic Research, International Symposium on Ice. Quebec city, Quebec, 1: 277-287.

Hicks, F.E. and Steffler, P.M. (1992). A Characteristic-Dissipative-Galerkin Scheme for Open Channel Flow, ASCE Journal of Hydraulic Engineering, 118(2): 337-352.

Hicks, F.E., McKay, K., and Shabayek, S. (1997). Modelling An Ice Jam Release Surge on the St. John River, New Brunswick. Proc., 9th Workshop on the Hydraulics of Ice Covered Rivers, Fredericton, N.B.: 303-314.

Hicks, F.E., Steffler, P.M., and Gerard, R. (1992). Finite Element Modeling of Surge Propagation and An Application to the Hay River, N.W.T. Canadian Journal of Civil Engineering, 19(3): 454-462.

Hopkins, M.A., Daly, S.F., and Lever, J.H. (1996). Three-Dimensional Simulation of River Ice Jams. Proc., International Conference on Cold Regions Engineering, New York, NY, 582-593.

Jasek, M. (2003). Ice Jam Release Surges, Ice Runs, and Breaking Fronts: Field Measurements, Physical Descriptions, and Research Needs. Canadian Journal of Civil Engineering, 30: 113-127.

Jasek, M., Marko, J., Fissel, D., Clarke, M., Buermans, J., and Paslawski, K. (2005). Instrument for Detecting Freeze-up, Mid-winter and Break-up Ice Processes in Rivers. Proc., 13th Workshop on the Hydraulics of Ice Covered Rivers, Hanover, NH, CGU-HS Committee on River Ice Processes and the Environment, Edmonton, Canada, pp. 150-183.

Kawai, T., Hara, F., Masaki, S., Nishihata, A., and Saeki, H. (1997). Experimental Study on the Process of Ice Jam Development. Proc., 9th Workshop on River Ice, Fredericton, NB, Canada, pp. 245-256.

Khan, A.A., Steffler, P.M. and Gerard, R. (2000). Dam-Break Surges with Floating Debris. Journal of Hydraulic Engineering, 126(5): 375-379.

Kowalczyk, T. and Hicks, F. (2003). Observations of Dynamic Ice Jam Release on the Athabasca River at Fort McMurray, AB. Proc., 12th Workshop on River Ice. 18-20 June 2003, Canadian Geophysical Union – Hydrology Section, Comm. On River Ice Processes and the Environment, Edmonton, AB, pp. 369-392.

Kowalczyk, T. and Hicks, F. (2004). Analysis of Ice Jam Release Surges on the Athabasca River near Fort McMurray, AB. Cold Regions Engineering and Construction Conference, May, 2004, Edmonton, AB, 14 pp.

Kowalczyk Hutchison, T. and Hicks F. (2007). Observations of Ice Jam Release Events on the Athabasca River, AB. Canadian Journal of Civil Engineering, 34(4): 473-484.

Lal, A.M.W. and Shen, H.T. (1992). Numerical Simulation of River Ice Dynamics. Proc., 3rd International Conference on Ice Technology, Cambridge, MA.

Liu, L. and Shen, H.T. (2000). Numerical Simulation of River Ice Control with Booms. US Army Corps of Engineers Cold Regions Research and Engineering Laboratory, Technical Report TR 00-10, Hanover, NH. USA, 28pp.

Liu, L. W. and Shen H. T. (2004). Dynamic of Ice Jam Release Surges. Proc., 17th International Symposium on Ice. St. Petersburg, Russia, 8 pp.

Liu, L. W. and Shen H. T. (2005). Numerical Modeling of 2003 Grasse River Ice Jam and Scenario Analysis. Proc., 13th Workshop on the Hydraulics of Ice Covered Rivers, Canadian Geophysical Union – Hydrology Section, Comm. on River Ice Processes and the Environment, Hanover, NH, 15 pp.

Lu, S., Shen H. T. and Crissman, R. D. (1999). Numerical Study of Ice Jam Dynamics in Upper Niagara River. Journal of Cold Regions Engineering, 13(2): 78-102.

Liu, L., Li, H., Shen, H.T. (2006). A Two-Dimensional Comprehensive River Ice Model. In: Saeki, H. (Ed.), Proc., 18th IAHR International Symposium on Ice, Sapporo, Japan, Vol. 1. Nakanishi Publishing Co. Ltd. ISBN: 4-89115-152-8, pp. 69-76.

Malcovish, C.D., Andres, D.D., and Morstert, P. (1988). Observations of Breakup on the Athabasca River near Fort McMurray, 1986 and 1987. Alberta Research Concil, Report No. SWE 88-12.

Morse, B., Hessami, M., and Bourel, C. (2003). Characteristics of Ice in the St. Lawrence River. Canadian Journal of Civil Engineering, 30(4): 766-774.

Morse, B. and Hicks, F. (2005). Advances in River Ice Hydrology. Hydrological Processes. 19(1): 247-264.

Pariset, E. Hausser, R., and Gagnon, A. (1966). Formation of Ice Covers and Ice Jams in Rivers. ASCE Journal of the Hydraulics Division, 92(HY6): 1-24.

Prowse, T.D. (2000). River-Ice Ecology. Environment Canada. National Water Research Institute, Saskatoon, SK. 64 pp.

Prowse, T.D. and Beltaos, S. (2002). Climatic Control of River-Ice Hydrology: A Review. Hydrological Processes, 16(4): 805-822.

Robichaud, C. and Hicks, F. (2001). A Remote Water Level Network for Breakup Monitoring and Flood Forecasting. Proc., 11th Workshop on River Ice, Ottawa, May, pp. 292-307.

Saade, R. G. and Saraaf, S. (1996). Phreatic Water Surface Profiles along Ice Jams – An Experimental Study. Nordic Hydrology, 27(3): 185-201.

She, Y. and Hicks, F. (2006a). Modeling Ice Jam Release Waves with Consideration For Ice Effects. Cold Regions Science and Technology, 45(3): 137-147.

She, Y. and Hicks, F. (2006b). Ice Jam Release Wave Modeling: Considering The Effects Of Ice in A Receiving Channel. Proc., 18th International Symposium on Ice. 28 Aug.-1 Sept. 2006, Sapporo, Japan, 8 pp.

She, Y. and Hicks, F. (2008a). Athabasca River Ice Jam Formation and Release Events, 2006 and 2007. Cold Regions Science and Technology, *in press*.

She, Y., Hicks, F., Steffler, P., and Healy, D. (2008b). Constitutive Model for Internal Resistance of Moving Ice Accumulations and Eulerian Implementation for River Ice Jam Formation. Submitted to Journal of Cold Regions Science and Technology, June 2008.

She, Y., Hicks, F., Steffler, P., and Healy, D. (2008c). Effects of Unsteadiness and Ice Motion on River Ice Jam Profiles. IAHR Proc., 19th International Symposium on Ice. 6 Jul. – 11 Jul. 2008, Vancouver, Canada.

Shen, H.T., Shen, H., and Tsai, S.M. (1990). Dynamic Transport of River Ice. Journal of Hydraulic Research, 28(6): 659-671.

Shen, H.T., Su, J.S. and Liu, L.W. (2000). SPH Simulation of River Ice Dynamics. Journal of Computational Physics, 165: 752-770.

Tuthill, A., Frankenstein, G., Kenney, M., and Mihm, J. (2005). Ice Tree Scar Evidence of Historic Ice Events on the Grasse River. Proc., 13th Workshop on River Ice, Hanover, NH.

Uzuner, M.S. and Kennedy, J.F. (1976). Theoretical Model of River Ice Jams. Proc., American Society of Civil Engineers, 102(HY9): 1365-1383.

Wang, J., Yi, M., Fu, H., and Sun, X. (2006). Ice Jam Processes in a Curved Channel. IAHR Proc., 18th International Symposium on Ice, Sapporo, Japan, pp. 151-158.

White, K.D., Tuthill, A.M., Vuyovich, C.M., and Weyick, P.B. (2007). Observed Climate Variability Impacts and River Ice in the United States. Proc., 14th Workshop on the Hydraulics of Ice Covered Rivers, Quebec City, Canada, June 20-22, paper No. a24.

Wong, J., Beltaos, S. and Krishnappan, B.G. (1985). Laboratory Tests on Surges Created by Ice Jam Releases. Canadian Journal of Civil Engineering, 12(4): 930-933.

Zufelt, J.E. (1990). Experimental Observations of Shoving and Thickening: Comparison to Equilibrium Thickness Theory. IAHR Proc., 10th International Symposium on Ice, Espoo, Finland, Vol.1: 500-510.

Zufelt, J.E. (1992). Modes of Ice Cover Failure during Shoving and Thickening. IAHR Proc., 11th International Symposium on Ice, Banff, Alberta, Canada, Vol.3: 1507-1514.

Zufelt, J.E., and Ettema, R. (1997). Unsteady Ice Jam Processes. CRREL Report No.97, U.S. Army Cold Regions Research and Engineering Laboratory, Hanover, N.H.

Zufelt, J.E., and Ettema, R. (2000). Fully Coupled Model of Ice Jam Dynamics. ASCE Journal of Cold Regions Engineering, 14(1): 24-41.

2 Modeling Ice Jam Release Waves with Consideration for Ice Effects[1]

2.1 Introduction

River ice jams can store a substantial volume of water which, if released, can result in the rapid propagation of ice and water, with associated high water levels and velocities. Such flood events can occur with little or no warning, and often pose a significant flood risk. Thus, it is highly desirable to be able to predict the speed and magnitude of the resulting waves of ice and water occurring upon ice jam release. This is one of the most complex problems in river ice engineering, involving not only dynamic flow hydraulics, but also the interaction between the ice and water.

A number of researchers have attempted to model the propagation of ice jam release waves, most using one-dimensional hydrodynamic models and neglecting ice effects on the propagating wave (e.g. Beltaos and Krishnappan 1982, Blackburn and Hicks 2003). Although reasonable approximations could be achieved, difficulties were encountered in matching the shapes of measured stage hydrographs, suggesting that ice effects could not reasonably be neglected. Jasek (2003) conducted field investigations documenting ice jam release events and found that the release wave celerity seemed to be affected by different ice conditions. Defining release wave propagation distance in *'jam lengths'* (i.e. non-dimensionalized by dividing travel distance by the original ice jam length), he observed that the ice effects seemed important only for the first jam length of propagation approximately. Liu and Shen (2004) further explored this issue, by applying a two-dimensional coupled flow and ice dynamic model to investigate the ice resistance effects

[1] This chapter was published in the Journal of Cold Regions Science and Technology, 2006, 45(3): 137-147.

(both internal resistance and boundary friction resistance) on ice jam release wave propagation in an idealized channel. Comparisons between their simulation results obtained with and without inclusion of ice dynamics showed that the ice effects decreased the peak discharge and slowed down the release processes.

These previous investigations clearly suggest that ice effects need to be incorporated into hydraulic flood forecasting models of ice jam release wave propagation to obtain realistic predictions; however, a number of questions still remain. For example, over what extent of the propagation length are ice effects actually significant? Also, to what level of sophistication must ice effects be considered in order to provide reliable forecasts, given that the exact effects of the ice on the propagating wave are not yet well understood? In this investigation, a simplified one-dimensional flow and ice dynamics model is presented and tested to explore these issues. In the proposed model, the ice released from the jam is assumed to move at the surface water velocity, so that the combined ice and water flow can be described by total (ice plus water) mass and momentum equations. Ice mass conservation is then considered explicitly, in an uncoupled sequence. Ice momentum effects are approximated empirically with bank-to-ice resistance introduced as a force term in the total flow momentum equation, while an empirical dispersion term is introduced in the ice mass continuity equation to approximate the longitudinal dispersion of the ice mass. In this paper, details of the basis for these terms are first provided and the modeled equations are presented. Next numerical results are compared with Liu and Shen's (2004) two-dimensional model results for a hypothetical ice jam release event. The model is then evaluated with actual data for the 2002 release event on

the Saint John River documented by Beltaos and Burrell (2005a, b), and for the 2002 ice jam release event on the Athabasca River documented by Kowalczyk and Hicks (2003).

2.2 Model Description

The hydraulic model developed in this investigation was built on the public domain software *River1-D* which employs the *characteristic-dissipative-Galerkin* (CDG) finite element scheme (Hicks and Steffler 1992) to solve the St. Venant equations for open channel flow. Ice momentum effects on the propagating release wave are evaluated based on an integral control volume approach which considers a force balance on the overall ice plus water mass, rather than employing the usual differential approach which considers the internal strength of the ice accumulation. The mobilized ice in the released jam ice is assumed to move at the mean flow velocity, which Beltaos (1986) indicated was a reasonable assumption once the ice velocity is fully developed. In this first approximation of ice effects, this assumption is made from the moment of release, thus neglecting the acceleration phase (an acknowledged limitation of the proposed model which will be addressed in future refinements). By assuming the ice and water move together at the same velocity, the equations of total (ice plus water) mass and momentum have the same form as the St. Venant equations for open channel flow, except for one additional term describing the ice resistance. The equations for rectangular channels can be written as:

[2-1] $$\frac{\partial A}{\partial t}+\frac{\partial Q}{\partial x}=0$$

[2-2] $$\frac{\partial Q}{\partial t}+\frac{\partial (VQ)}{\partial x}+gA\frac{\partial H}{\partial x}=-gAS_f+gAS_0-2\lambda_1 gBt_i S_f$$

where,

H is the depth of flow under the water surface;

A is the total area of the cross-section under the water surface, measured perpendicular to the flow;

Q is the total discharge, including both water and ice flow;

V is the ice and water velocity;

S_0 is the bed slope of the channel;

λ_I is an empirically determined resistance parameter;

B is the width of the channel;

t_i is the ice thickness;

S_f is the friction slope which can be evaluated as

$$[2\text{-}3] \quad S_f = \frac{V|V|}{gRC_*^2}$$

When using Chezy's equation (where C_* represents the non-dimensional Chezy coefficient and R is the hydraulic radius), or as

$$[2\text{-}4] \quad S_f = \frac{n^2 V|V|}{R^{4/3}}$$

when using Manning's equation (with n representing Manning's resistance coefficient).

As the ice run moves downstream there will be resistance at the interfaces between the moving ice and the bank (or the shear walls), as illustrated in Figure 2-1, and the last term in equation [2-2] empirically accounts for this effect. This force is quantified using a concept from solid mechanics; specifically, it is taken equal to the downslope component of ice weight, multiplied by a resistance parameter, λ_1. This resistance parameter, λ_1, is actually the product of two coefficients: a frictional coefficient (for ice sliding along this interface), and a lateral thrust coefficient (which represents the fraction of the longitudinal force component that is directed normal to the banks). The bank resistance is assumed to act equally at each bank.

The ice mass continuity equation is:

$$[2\text{-}5] \quad \frac{\partial t_i}{\partial t} + \frac{\partial (V t_i)}{\partial x} + \frac{V t_i}{B}\frac{dB}{dx} = \lambda_2 \frac{\partial^2 t_i}{\partial x^2}$$

where, λ_2 is an artificial dispersion parameter which empirically accounts for the longitudinal dispersion of the released ice mass.

The ice mass continuity equation [2-5] is solved in an uncoupled sequence with the coupled total (ice plus water) mass and momentum equations [2-1] and [2-2], all using the CDG finite element scheme. First the flow hydrodynamics at a given time step are determined (based on the ice solution at the previous time step), and then these flow properties are used in the subsequent solution of the ice mass continuity equation before moving on to the next time step.

For convenience in modeling ice jam release events, the *River1-D* model was also adapted to calculate initial (water surface and ice jam profile) conditions. Specifically, the

ice jam stability equation (Pariset et al. 1966, Uzuner and Kennedy 1976) was incorporated into the model and solved in an uncoupled sequence with the coupled hydrodynamic equations using a constant inflow discharge boundary condition. In this context, the unsteady hydrodynamic solution provided the mechanism for an iterative solution of an initial ice jam profile prior to release.

2.3 Model Application

2.3.1 *Hypothetical Ice Jam Release Event*

Liu and Shen (2004) developed a hypothetical test case, adapted from the 1993 release event on the Saint John River documented by Beltaos et al. (1994). In their test case, Liu and Shen (2004) approximated the Saint John River as a rectangular channel 100 km long and 600 m wide, with a bed slope of 0.0004 for the first 30 km, and a bed slope of 0.0001 for the remaining 70 km. A constant value for Manning's n of 0.030 was used for the river bed, a constant inflow discharge of 2000 m^3/s was set at the upstream boundary, and an uncontrolled condition was used at the downstream boundary. The initial steady state water surface and ice jam profiles for their test case are depicted in Figure 2-2.

An identical test case was set up for the *River1-D* model, with the exception that the downstream boundary was eliminated from consideration by extending the length of the modeled reach further downstream. Based on a series of test runs the optimal values of λ_1 and λ_2 were found to be 3.5 and 100, respectively for this case. Comparison of the simulated water level and combined ice and water discharge hydrographs at different locations downstream of the jam toe are depicted in Figure 2-3 and 2-4, respectively. Similarly, the ice jam profiles at 4, 10, 20 and 60 minutes after the jam release are shown

in Figure 2-5. Results published by Liu and Shen (2004) from their two-dimensional coupled flow and ice dynamics model (DynaRICE) are also shown for comparison purposes.

In Figure 2-3 it is interesting to note that, for both models, a second water level peak occurs at stations 60 km and 75 km. Because the ice is moving at the surface water velocity, which is slower than the dynamic release wave, the ice accumulation is eventually left behind as the wave propagates downstream. Thus, the first peak represents the water wave passing these stations, and the second peak occurs as the ice accumulation subsequently passes. Figure 2-3 also indicates an increasing discrepancy between the water level results obtained using the two models as the wave propagates farther and farther downstream. This may be explained by the reduced surface ice concentration which develops as the ice run spreads longitudinally (disperses), which would be expected to decrease the bank resistance to the moving ice accumulation. This suggests that perhaps the resistance parameter, λ_1, in the proposed approximate model should be reduced as the wave propagates.

Table 2-1 summarizes a quantitative comparison between the two models, in terms of peak water level and arrival time, as well as peak discharge (ice + water). It can be seen that the largest differences are around 10%, with many in the order of 5% or less. These results illustrate that the approximate model proposed here performs reasonably well when compared to the much more sophisticated DynaRICE model, suggesting that reasonable forecasts might be achievable with this simplified model.

2.3.2 *2002 Release Event on the Saint John River*

The *River1-D* model was next used to simulate the wave propagation event of 13 April 2002, which resulted from the release of two small ice jams on the Saint John River upstream of Ledges (Figure 2-6). According to Beltaos and Burrell's (2005b) description of ice conditions prior to release, there was a 3 km long jam with a 1.5 km reach of open-water downstream of it, followed by a 1 km long jam. Downstream, the river was open except for a short reach of fragmented ice cover just downstream of the lower jam (Figure 2-7, inset), with a sizeable open lead observed near Ledges. During the release event, water levels were measured approximately 500 m downstream of the toe of the lower (1 km long) jam, near Ledges, at Fort Kent (Water Survey of Canada (WSC) station number: 01AD002) 8.7 km downstream of the toe of the lower jam, and at Edmundston (WSC station number: 01AD004) 40.8 km downstream of the toe of the lower jam.

Figure 2-7 illustrates the initial profiles obtained with the model, estimated by performing an ice jam profile calculation using *River1-D* based on the unperturbed-flow discharge, which could be reliably determined from the two gauging stations operated by the United States Geological Survey (USGS): one is on the Saint John River at Fort Kent; the other is on the Fish River, just below the river mouth (Beltaos and Burrell 2005b). The fragmented ice cover was modeled by treating it as a portion of the ice jams, which also provides resistance to the propagating wave. The channel geometry was approximated as a varying width rectangular channel, with bed profile and widths determined based on the actual channel geometry. Open water was assumed in the receiving channel.

It is unknown whether the two ice jams released simultaneously, or if the release of the upper jam preceded that of the lower jam (or vice versa). However, the measured water level hydrograph at Ledges exhibits two peaks, suggesting that the two ice jams did not release at exactly the same time. Nevertheless, since different jam release times could not be handled with the proposed model, unsteady flow simulations were conducted assuming that both jams released simultaneously.

River1-D model results are shown in Figure 2-8, together with the measured water level rise at the Ledges, Fort Kent and Edmundston stations, for comparison. To investigate the potential significance of released ice on the resulting wave propagation, three different model simulations were conducted. In Run 1, (Figure 2-8a) these ice effects were neglected completely, by setting both λ_1 and λ_2 to zero. In Run 2, (Figure 2-8b) λ_1 and λ_2 were set to 1.5 and 300, respectively, throughout the entire simulation. Finally, in Run 3 (Figure 2-8c), in an effort to consider the potential diminishing effects of ice on the event propagation (as has been suggested by Jasek 2003), λ_1 and λ_2 were set to 1.5 and 300, respectively, for the first 2.8 hours of the event only, and set to zero thereafter. This duration, which was determined by trial and error to give the best results, reflects a travel distance of about 2 jam lengths. The optimal values of λ_1 and λ_2 were also determined based on a sensitivity analysis involving a series of test runs.

As Figure 2-8a illustrates, completely neglecting ice effects leads the model to underestimate the water level for the receding limb of the stage hydrographs at all three stations. The peak is overestimated at the Fort Kent station (8.7 km downstream), and the wave appears to be traveling too fast (i.e. the computed peaks precede the observed peaks). Incorporating constant ice effects for the entire duration of the simulation (Figure

2-8b) improves the results near the toe of the lower jam (Ledges) considerably, and provides improved results at Fort Kent (8.7 km downstream) as well. However, this causes the peak of the stage hydrograph computed for Edmundston (40.2 km further downstream) to be more diffused than the observed.

Figure 2-8c illustrates the interesting result obtained when only considering ice effects for the initial part of the simulation. In this case, the results for Ledges and Fort Kent are the same as in Figure 2-8b, while the simulation results for Edmundston are much more similar to the observed water levels. These results suggest that ice effects on the propagating water wave diminish as it travels downstream, which might be expected as the water wave eventually moves out ahead of the ice run.

The sensitivity of the proposed model to variation of the parameters λ_1 and λ_2 was also examined. Two additional runs were conducted setting λ_1 and λ_2 to 1.5 and 0 and 0.0 and 300 respectively. A comparison to the results of Run 1, which neglected ice effects completely, shows that the ice resistance term ($\lambda_1 > 0$, $\lambda_2 = 0$) tends to delay the arrival time of the peak and to slow the wave recession, but does not have significant influence on the peak water level. The ice dispersion term ($\lambda_1 = 0$, $\lambda_2 > 0$) changes the shape of the ice accumulation profile, but has no effect on the water stage hydrograph.

2.3.3 *2002 Release Event on the Athabasca River, AB*

The *River1-D* model was next tested using actual data obtained during a large ice jam release event measured on the Athabasca River, AB in 2002 (Kowalczyk and Hicks 2003). Figure 2-9 illustrates the study reach of the Athabasca River, which extends from Crooked Rapids (approximately 35 km upstream of Fort McMurray) to the Water Survey

of Canada gauge (about 1 km downstream of Fort McMurray). During the 2002 event, an ice run from an upstream ice jam release arrested briefly at Crooked Rapids, just upstream of station G140. Upon re-releasing, this new jam caused the water level at station G140 to rise more that 4 m in less than 15 minutes. The propagating release wave was measured with water level sensors as it passed stations G140, G135 and G130, before arresting again to form a new jam with its toe near station G104. Based on an analysis of pre-event hydraulics, it was estimated the channel discharge was fairly steady at about 850 m^3/s prior to the ice jam release event.

The resistance characteristics along the study reach are listed in Table 2-2. Due to the remote location and the time of day (near midnight), the profile of the ice jam at Crooked Rapids could not be measured. Therefore, this initial condition was estimated using the *River1-D* model, first by assuming an ice jam length and calculating the ice profile using the jam stability equation, then releasing the ice jam and comparing measured and calculated stage hydrographs at station G140. Since the Athabasca River can be characterized as a wide and shallow channel, the channel could reasonably be approximated as a variable width rectangular section. The ice jam roughness height was estimated to be 2 m, based on calibration of numerous historical ice jams at Fort McMurray (Friesenhan 2004). By trial and error, it was determined that the release of a 10 km long ice jam provided the best match with the measured stage hydrograph at station G140 (Figure 2-10).

The computational results obtained by including the effects of releasing ice on the propagating wave ($\lambda_1 = 0.25$ and $\lambda_2 = 100$), and without consideration of this ice ($\lambda_1 = 0.0$ and $\lambda_2 = 0.0$) are shown in Figure 2-11 together with the measured stage hydrographs at

several stations downstream of the release point. It should first be pointed out that open water in the receiving channel was assumed for these simulations, since the current version of the proposed model could not handle interactions between released ice from jams and ice in the receiving channel. This was not considered a significant limitation in this case, since the ice in the receiving channel was quite thermally decayed with many large open leads. As a consequence, water levels after the event match well when comparing observations and model results (e.g. at stations G140 and G130). However, the model results are lower than the observations for the antecedent situation (because of the added resistance effects of the ice in the receiving channel, which are not considered by the model).

As Figure 2-11 illustrates, inclusion of the effects of released ice on the propagating wave did not seem to improve the model's ability to reproduce the measured water level hydrographs. In fact, much better results were obtained at station G130, 16 km downstream of the released jam, by neglecting these ice effects completely. Results at the intermediate station (G135) are inconclusive, as the sudden drop in the observed stage hydrograph suggests that the water level sensor (pressure transducer) shifted position when the ice run arrived. Similarly, at station G104, results were inconclusive since the ice run arrested at this point forming a new ice jam.

Focusing then on the results for station G130, the finding that ice effects do not seem important at this location may be consistent with the observations of Jasek (2003) on other rivers. He found that ice effects on the propagating wave were significant only for about one jam length of propagation, whereas for this case, station G130 is located beyond this limit, at 1.6 jam lengths downstream of the release point. In comparison to

the Saint John River event, ice effects may also be less relevant here as the bed slope of the Athabasca River is much steeper, (about 0.001 compared to <0.0005 for Saint John River). As a result, the relative magnitude of the driving force (gravity) compared to the resisting force (bank resistance to the ice), would be much larger for the study reach of the Athabasca River.

In a manner similar to the Saint John River event simulations, additional runs were conducted for this event in an attempt to simulate the diminishing effects of ice on the propagating wave. Specifically, λ_1 and λ_2 were set to 0.25 and 100, respectively, for only the first hour of the event, and then set to zero thereafter. This duration reflects a travel distance of about one jam length. This resulted in an improved agreement between the model and the observations at station G130, as compared to considering constant ice effects for the entire event (not shown in Figure 2-11 to retain clarity). However, the best results were still achieved by neglecting ice effects completely. Unfortunately, the existing data are insufficient to provide a conclusive interpretation. However, it is clear that the objective of future field studies of ice jam release events should be to focus on obtaining data close to the toe of the released jam.

2.4 Summary and Conclusion

The *River1-D* model was adapted to consider ice jam resistance effects on propagating ice jam release waves. In the proposed model, the total (ice plus water) mass and momentum conservation equations are solved together with a conservation of ice mass equation, in an uncoupled sequence. Ice resistance effects are approximated through an empirical term in the total flow momentum equation and an empirical ice dispersion

approximation in the ice continuity equation. The resulting model appears to perform reasonably well when compared to the two-dimensional ice dynamic model DynaRICE for a hypothetical ice jam release event (Liu and Shen 2004).

The model was further tested for two observed ice jam release events: one which occurred on the Saint John River in 2002 (Beltaos and Burrell 2005a, b) and one which occurred on the Athabasca River in 2002 (Kowalczyk and Hicks 2003). The results for the former case suggest that ice effects are only significant in the first stage of release wave propagation. For the Athabasca River event, inclusion of ice effects did not seem to improve results when compared to measured stage hydrographs more than 1 to 2 jam lengths downstream of the released toe. Clearly more comprehensive field data is still needed to provide further validation of models of this type, and it is recommended that future efforts be focused on obtaining detailed water level data at a number of sites all located within one to two jam lengths downstream of the toe of a releasing ice jam.

Table 2-1 Percent difference in the results of the proposed model from Liu and Shen's (2004) published results, for a hypothetical ice jam release event.

Location:	45km	50km	60km	75km
Peak Water Level				
1st peak	3.48	4.24	0.62	2.63
2nd peak	-	-	4.25	10.11
Peak Arrival Time				
1st peak	10.53	6.94	1.00	5.10
2nd peak	-	-	7.78	1.04
Peak Discharge				
1st peak	9.00	0.75	9.65	4.60
2nd peak	-	-	7.80	1.45

Table 2-2 Bed roughness characteristics for the Athabasca River study reach.

From (km)	To (km)	Manning's n (dimensionless)	Roughness height k (m)
0 *	296.55	0.030	0.24
296.6	300.4	0.020	0.02
300.45	319.4	0.030	0.24
319.45	400	0.035	0.61

* Station 0 km is set at the mouth of the Athabasca River at Lake Athabasca

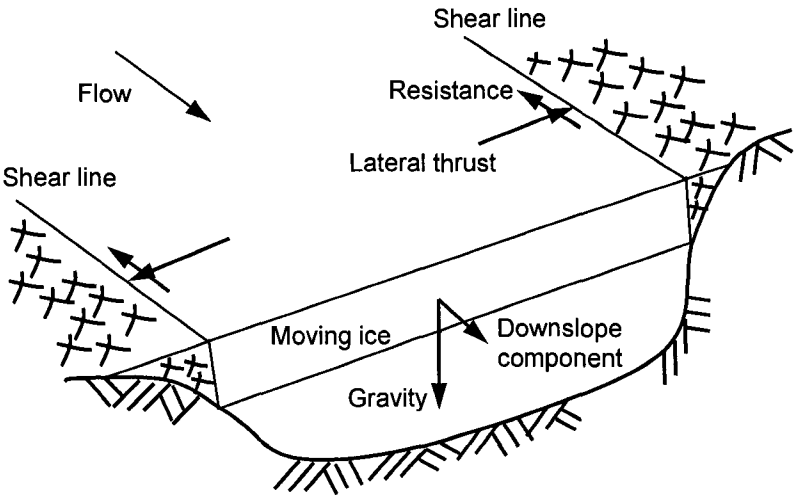

Figure 2-1 Forces acting on the moving ice pack in a river channel.

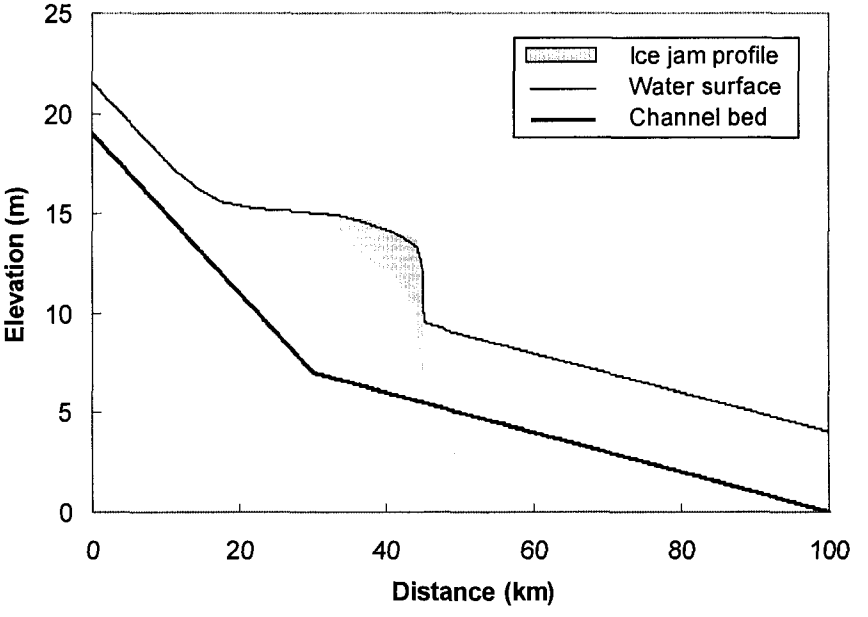

Figure 2-2 Initial condition of Liu and Shen's (2004) test case for ice jam release simulation.

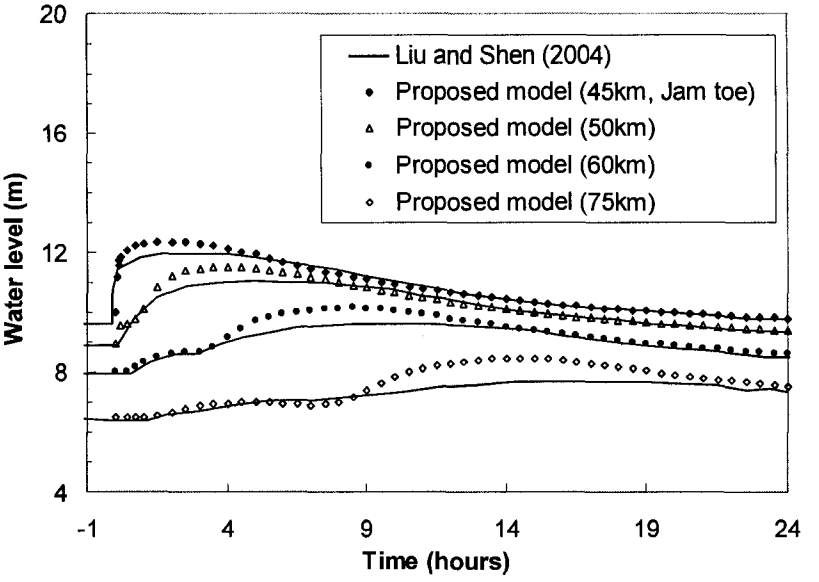

Figure 2-3 Comparison of the proposed model with Liu and Shen's (2004) simulation results for water level, $\lambda_1 = 3.5$, $\lambda_2 = 100$.

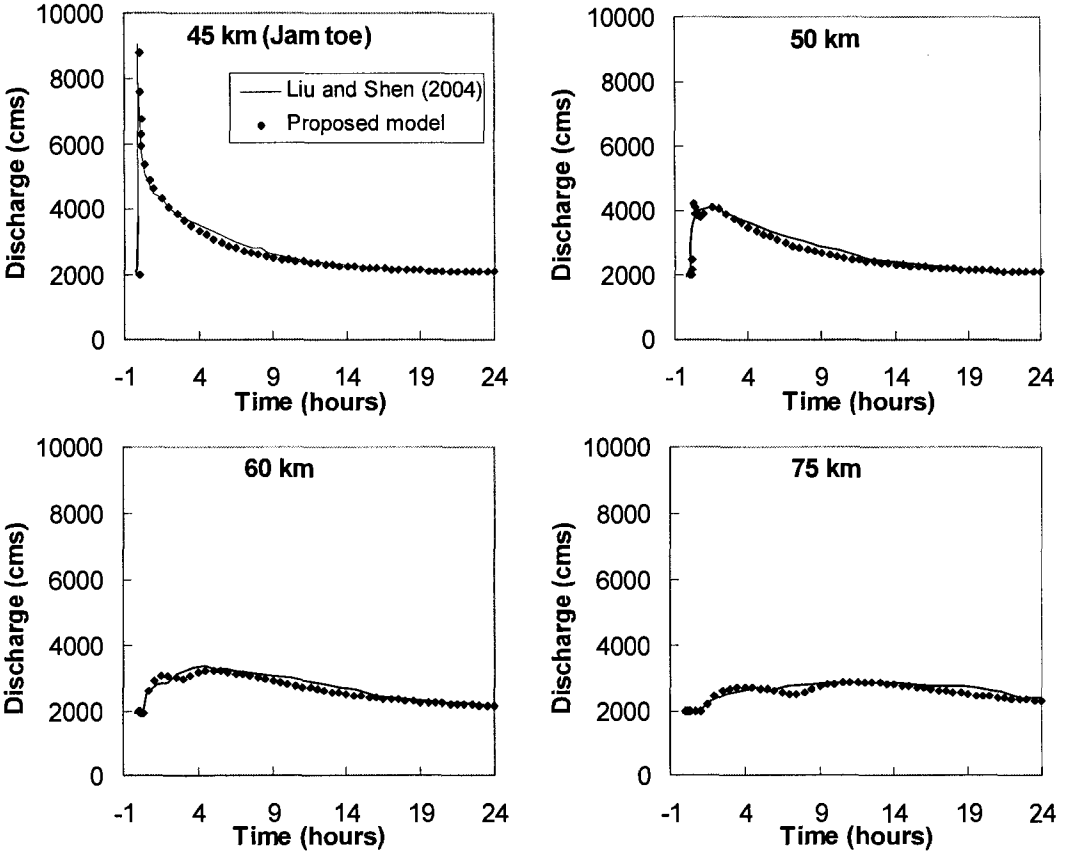

Figure 2-4 Comparison of the proposed model with Liu and Shen's (2004) simulation results for combined water and ice discharge, $\lambda_1 = 3.5$, $\lambda_2 = 100$.

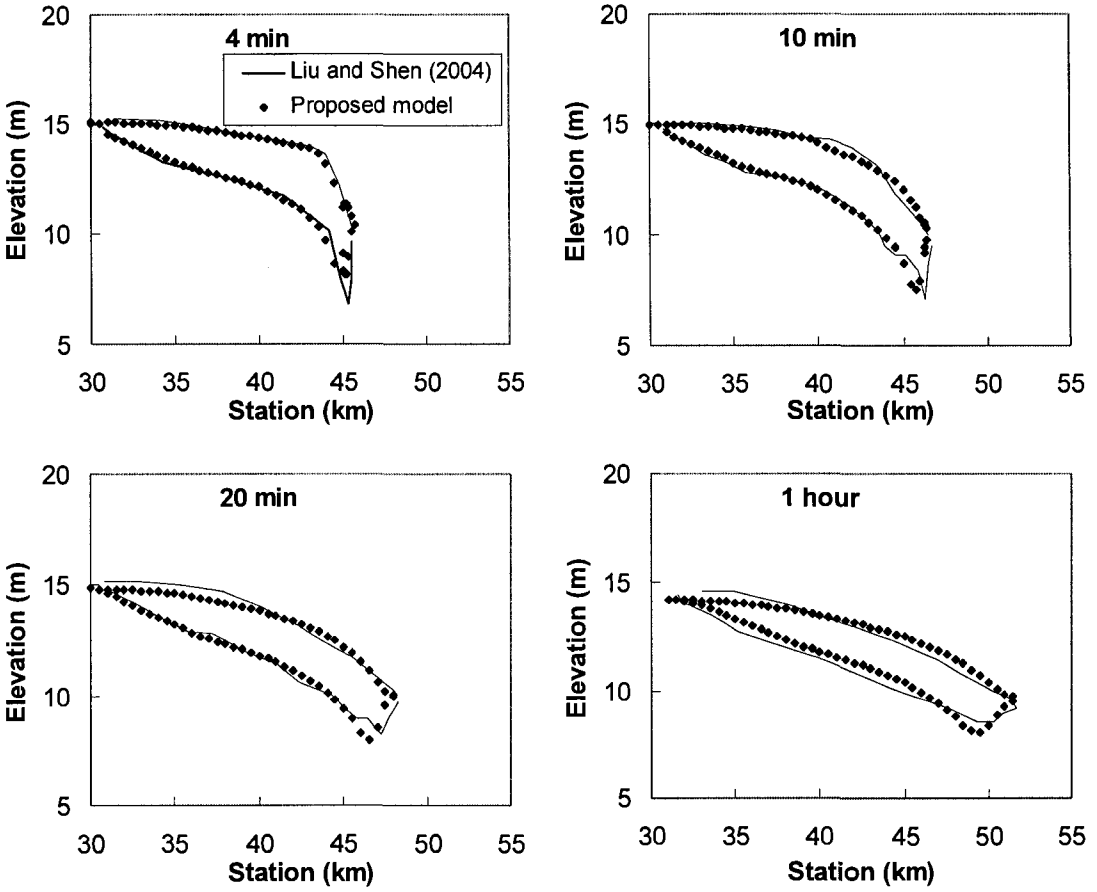

Figure 2-5 Comparison of the proposed model with Liu and Shen's (2004) simulation results for ice jam profiles at different time after the release, $\lambda_1 = 3.5$, $\lambda_2 = 100$.

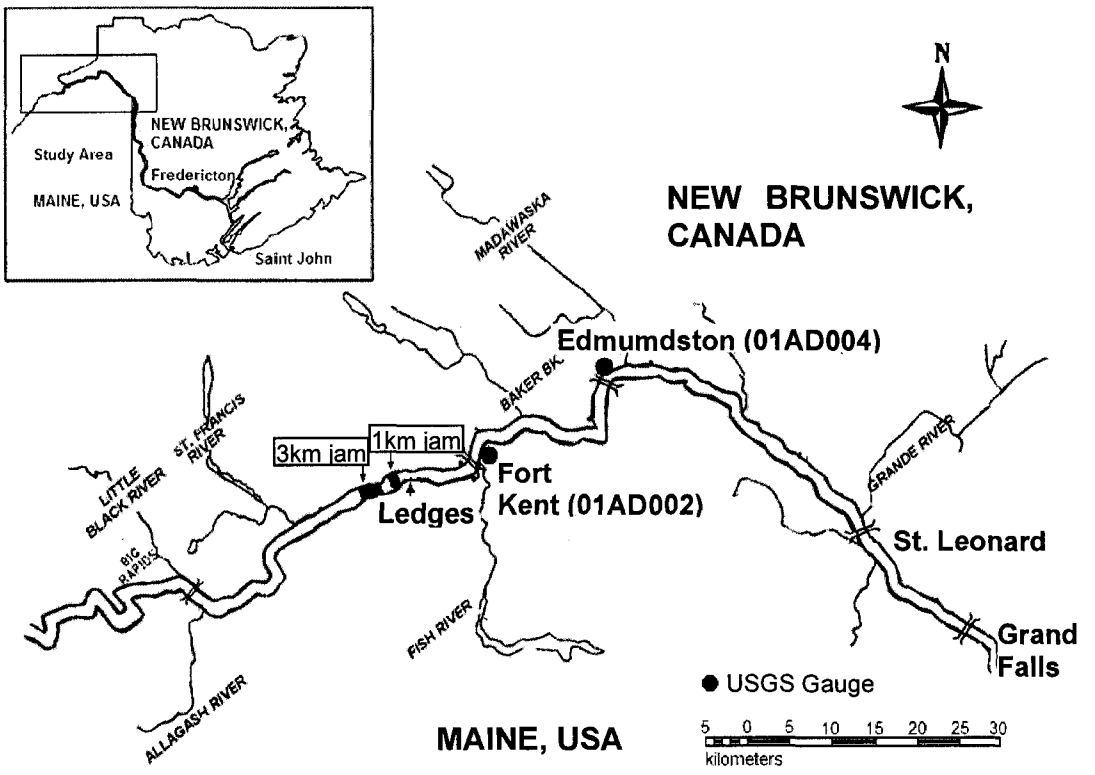

Figure 2-6 Study reach on the Saint John River, New Brunswick, Canada and Maine, US.

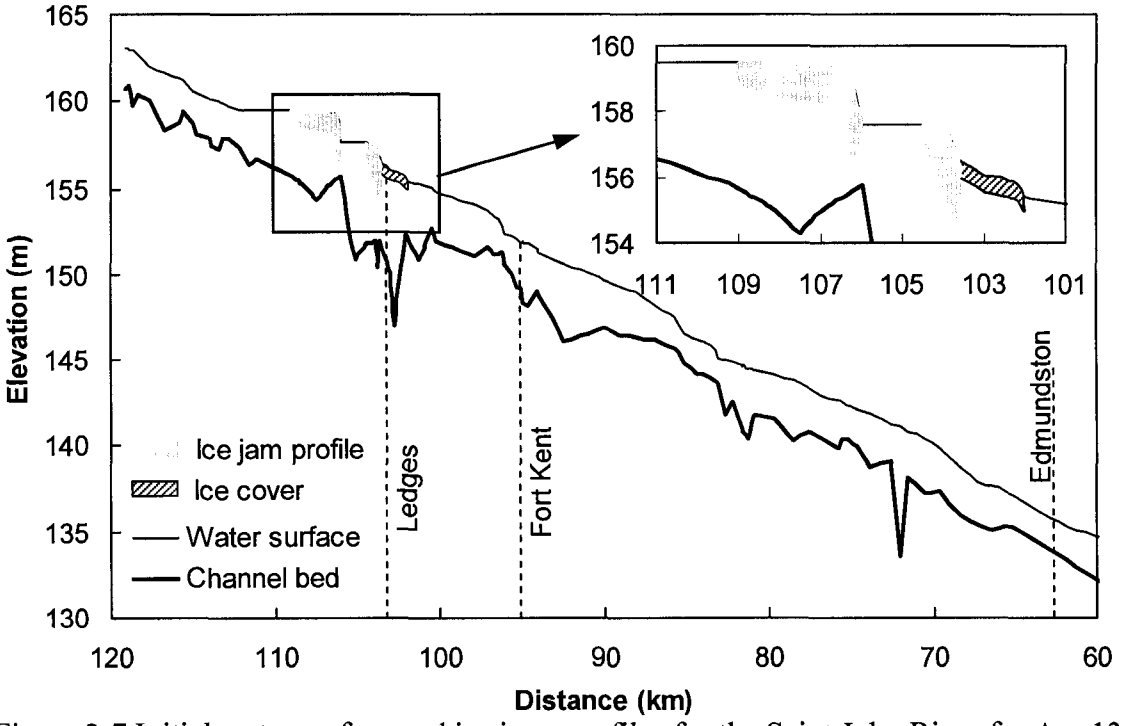

Figure 2-7 Initial water surface and ice jams profiles for the Saint John River for Apr 13, 2002 prior to release, both computed using *River1-D*.

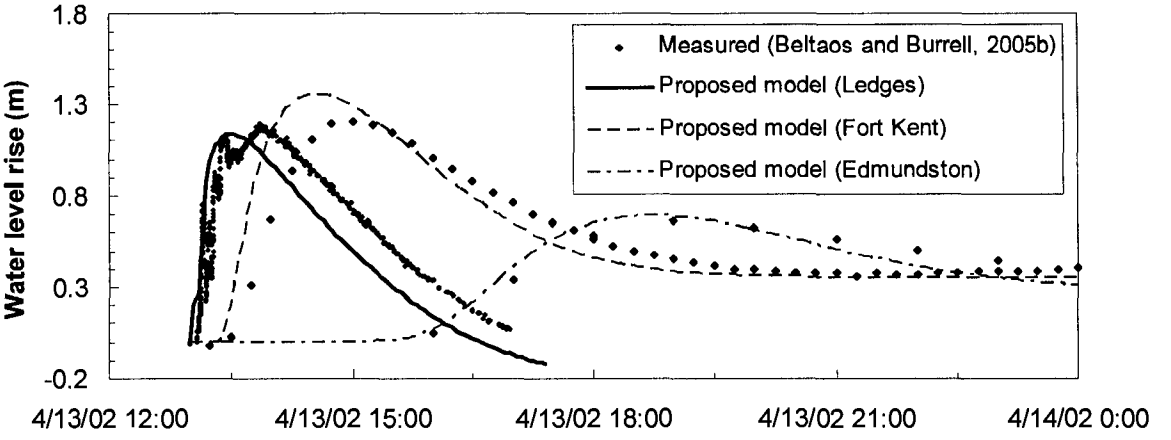

(a) $\lambda_1 = 0.0$, $\lambda_2 = 0$ throughout entire simulation

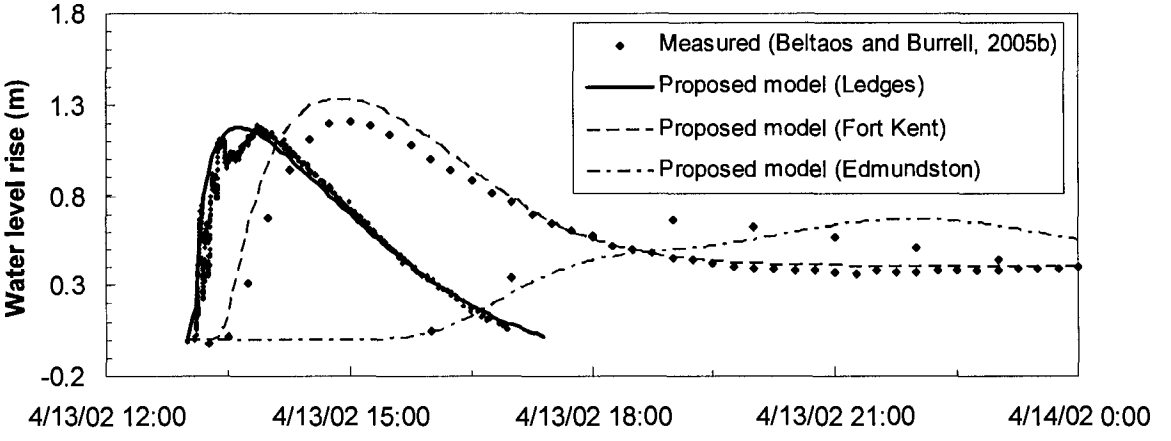

(b) $\lambda_1 = 1.5$, $\lambda_2 = 300$ throughout entire simulation

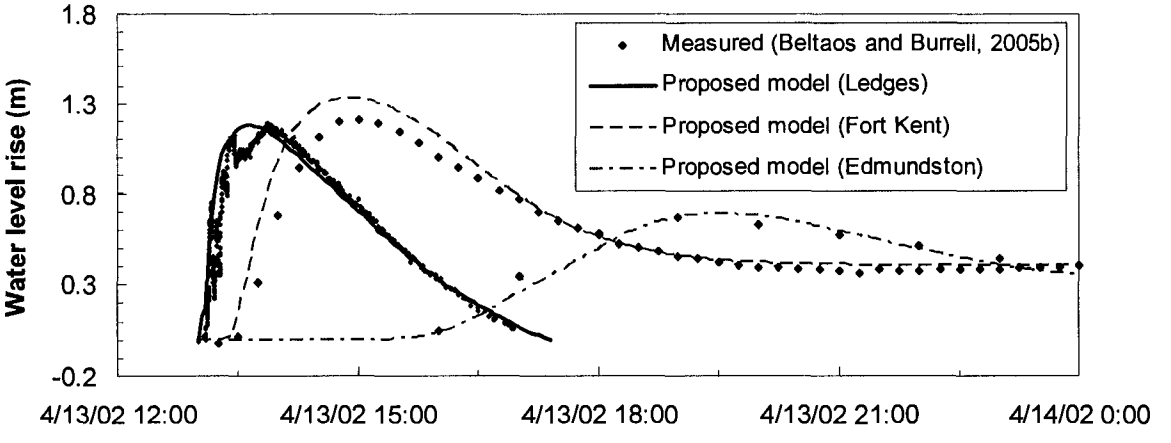

(c) $\lambda_1 = 1.5$, $\lambda_2 = 300$ for first 2.8 hrs, $\lambda_1 = 0.0$, $\lambda_2 = 0$ for the remaining time

Figure 2-8 Comparison of measured and computed water level rise at different downstream stations for Saint John River 2002 ice jam release event.

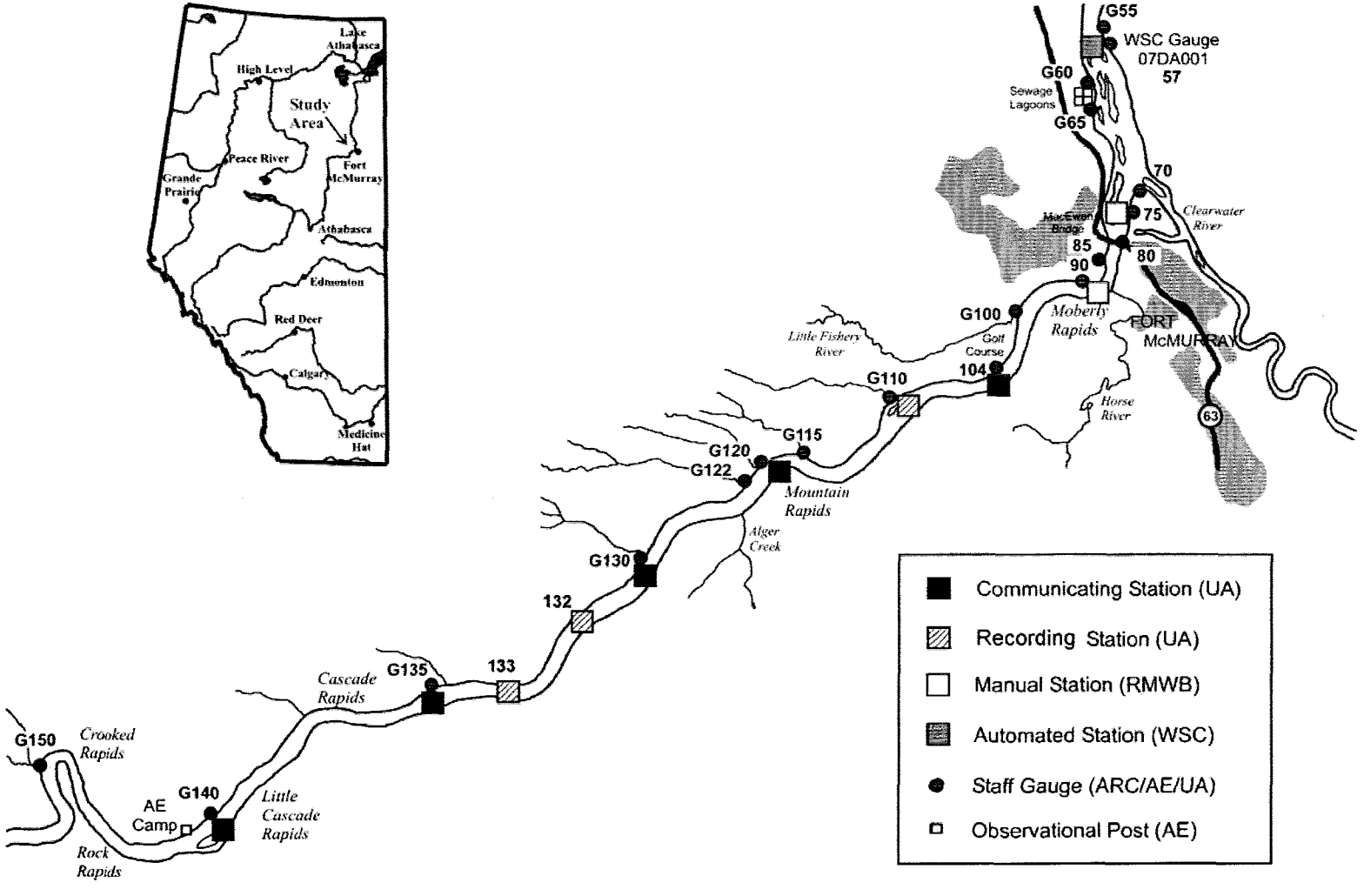

Figure 2-9 Study reach of the Athabasca River (adapted from Kowalczyk and Hicks 2003.

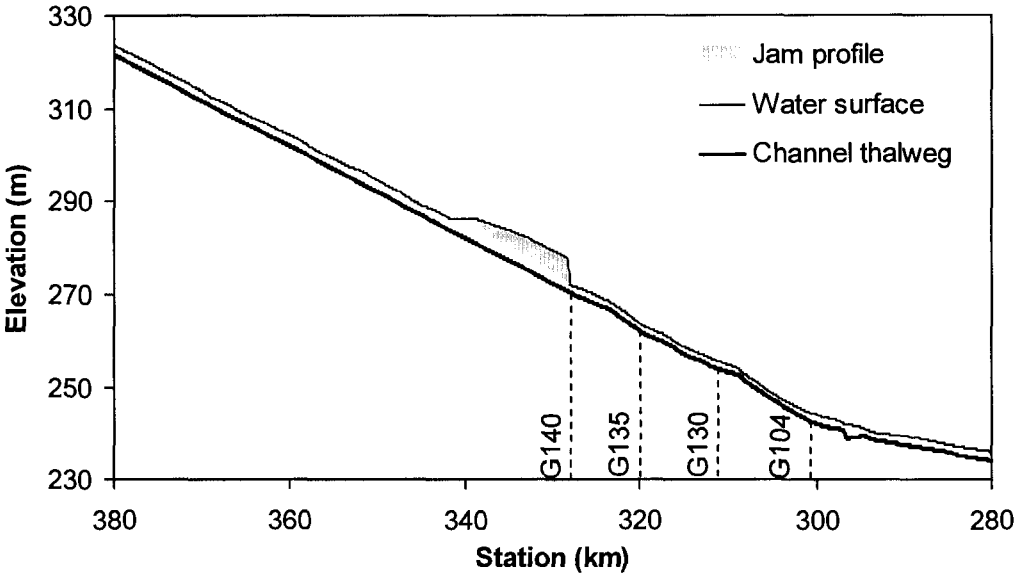

Figure 2-10 The initial water surface and ice jam profile on the Athabasca River, both computed using *River1-D*.

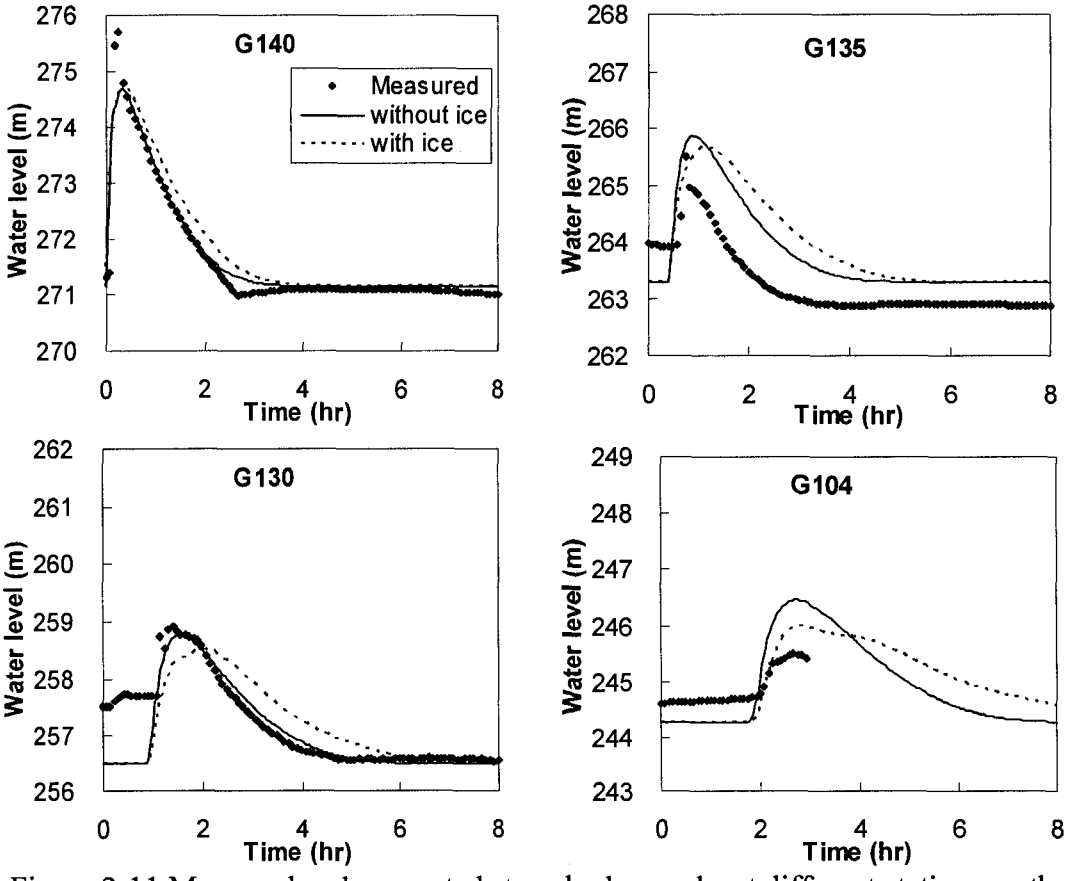

Figure 2-11 Measured and computed stage hydrographs at different stations on the Athabasca River for the 2002 event, $\lambda_1 = 0.25$, $\lambda_2 = 100$ for the case with ice.

2.5 References

Beltaos, S. and Krishnappan, B.G. (1982). Surges from Ice Jam Release: A Case Study. Canadian Journal of Civil Engineering, Vol. 9: pp. 276-284.

Beltaos, S., Burrell, B. C., and Ismail, S. (1994). Ice and sedimentation processes in the Saint John River, Canada. Proc., 12th International Association for Hydraulic Research Symposium on Ice, Norwegian Institute of Technology, Trondheim, Norway, pp. 11–21.

Beltaos, S., Burrell, B. C. (2005a). Field Measurements of Ice-Jam-Release Surges. Canadian Journal of Civil Engineering, Vol. 32: pp. 699-711.

Beltaos, S., Burrell, B. C. (2005b). Determining Ice-Jam Surge Characteristics from Measured Wave Forms. Canadian Journal of Civil Engineering, Vol. 32: pp. 687-698.

Blackburn, J. and Hicks, F. (2003). Suitability of Dynamic Modeling for Flood Forecasting during Ice Jam Release Surge Events. Journal of Cold Regions Engineering, Vol. 17, No. 1, pp. 18-36.

Friesenhan, Evan. (2004). Modeling of Historic Ice Jams on the Athabasca River at Fort McMurray. Report prepared in partial fulfillment of the requirements for the degree Master of Engineering (supervisor F. Hicks), Dept. of. Civil and Environmental Engineering, University of Alberta, 64 pp.

Hicks, F.E. and Steffler, P.M. (1992). A Characteristic-Dissipative-Galerkin Scheme for Open Channel Flow. ASCE Journal of Hydraulic Engineering, Vol. 118, No.2, pp. 337-352.

Hicks, F.E., McKay, K. and Shabayek, S. (1997). Modelling an Ice Jam Release Surge on the St. John River, New Brunswick. Proc., 9th Workshop on the Hydraulics of Ice Covered Rivers, Fredericton, N.B, pp. 303-314.

Jasek, M. (2003). Ice Jam Release Surges, Ice Runs, and Breaking Fronts: Field Measurements, Physical Descriptions, and Research Needs. Canadian Journal of Civil Engineering, Vol. 30: pp. 113-127.

Kowalczyk, T. and F. Hicks (2003). Observations of Dynamic Ice Jam Release on the Athabasca River at Fort McMurray, AB. Proc., 12th Workshop on River Ice. 18-20 June 2003, CGU - Hydrology Section, Comm. on River Ice Processes and the Env., Edmonton, AB, pp. 369-392.

Liu, L.W. and Shen, H.T. (2004). Dynamics of Ice Jam Release Surges. Proc., 17th International Symposium on Ice. St. Petersburg, Russia, 8 pp.

Pariset, E., Hausser, R. and Gagon, A. (1966). Formation of Ice Covers and Ice Jams in Rivers. Journal of Hydraulics Division, Proc. of the American Society of Civil Engineers, Vol. 92, No. HY6, pp. 1-23.

Uzuner, M. S. and Kennedy, J. F. (1976). Theoretical Model of River Ice Jams. Proc., American Society of Civil Engineers, Vol. 102, No. HY9, pp. 1365-1383.

3 Ice Jam Release Wave Modeling: Considering the Effects of Ice in a Receiving Channel[2]

3.1 Introduction

It is believed that, when propagating water and ice from a released ice jam encounter and break up the intact ice in a receiving channel, the interaction can vary between two extremes. One is termed a "sheet front" propagation, in which ice in the receiving channel is pushed ahead of the propagating release wave. The other is a "rubble breaking front", in which the moving ice accumulation ploughs through the intact ice in the receiving channel, incorporating it into the ice run. In either case, the highly dynamic flow situation, combined with the ice-water interactions, makes this one of the most complex problems in river ice engineering. A further complication, and one of intense interest in flood forecasting, is the potential for such an ice run to arrest and reform a new jam.

From a flood forecasting perspective, it is desirable to be able to model the propagation of the ice and water waves that result from an ice jam release. A number of researchers have attempted to do this using one-dimensional water-only hydrodynamic models, neglecting ice effects on the propagating wave (e.g. Beltaos and Krishnappan, 1982; Blackburn and Hicks, 2003). Difficulties were encountered in matching the shapes of measured stage hydrographs, suggesting that ice effects could not reasonably be neglected. More recent modeling efforts have included consideration of ice effects (Liu

[2] This chapter was published in the Proceeding of the 18th IAHR International Symposium on Ice, Sapporo, Japan, 125-132. The paper was also presented by the first author at this conference in August 2006.

and Shen, 2004; She and Hicks, 2005), and indicated that the ice decreases the peak discharge and slows down the release processes. However, those studies only considered the effects of the moving ice accumulation itself; to date no one has attempted to include the effects of ice in the receiving channel, though these are likely equally important.

In this study, we investigate numerical approaches for including consideration of the effects of ice in a receiving channel when modeling the propagation of an ice jam release wave and its associated ice run. Specifically, a simplified one-dimensional flow and ice dynamics model was developed to simulate the dynamic progress of an ice jam release event in a rectangular, ice-covered, receiving channel. In the proposed model, equations of water mass and momentum are solved, alternating with ice mass conservation in an uncoupled sequence. Longitudinal dispersion of the ice mass is approximated with an empirical dispersion term in the ice mass continuity equation. The resulting equations are solved using the Characteristic-Dissipative-Galerkin (CDG) finite element method (Hicks and Steffler, 1992). The model is tested here using an idealized rectangular channel loosely based on the geometry of the Saint John River in New Brunswick, Canada, where ice jam release events often occur.

3.2 Model Description

The hydraulic model developed in this investigation was built on the public domain software *River1-D*, developed at the University of Alberta (Hicks and Steffler, 1992). For a rectangular channel, the mass equation for the under-ice water was modified slightly to the following form to include the mass exchange across the ice-water interface:

[3-1] $$\frac{\partial A_w}{\partial t}+\frac{\partial Q_w}{\partial x}=-\frac{Bs_i t_i}{1-p}\frac{dp}{dt}$$

where, A_w is area of the cross-section under the ice, measured perpendicular to the flow; Q_w is the under-ice water discharge; B is the channel width; s_i is specific gravity of the ice; t_i is the ice thickness; and p is the effective aerial porosity of the ice cover in the receiving channel, which is allowed to change with time (e.g. to facilitate consideration of the closing of open leads). The term on the right hand side of equation [3-1] accounts for the discharge to/from the voids in the ice layer due to porosity changes.

The momentum equation for the under-ice water layer can be written as:

[3-2] $$\frac{\partial Q_w}{\partial t}+\frac{\partial(V_w Q_w)}{\partial x}+gA_w\frac{\partial H_w}{\partial x}=-gA_w(S_f-S_0)-gA_w s_i\frac{\partial t_i}{\partial x}$$

where, H_w is the under-ice water depth; V_w is the under-ice water velocity; and S_f is the friction slope, which can be evaluated as:

[3-3] $$S_f=\frac{V_w|V_w|}{gRC_*^2}$$

using Chezy's equation. R is the hydraulic radius; and C_* is the non-dimensional Chezy coefficient, defined as:

[3-4] $$C_*=2.5\ln\left(\frac{R}{k_o}\right)+6.2$$

where k_o is the composite roughness height, in meters. It represents the combined roughness of the ice underside, k_i, and of the channel bed, k_b. The composite roughness is calculated using Sabaneev's formula:

$$[3\text{-}5] \quad k_o = \left[\frac{k_i^{1/4} + k_b^{1/4}}{2} \right]^4$$

The ice mass continuity equation is taken as:

$$[3\text{-}6] \quad \frac{\partial t_i}{\partial t} + \frac{\partial (V_i t_i)}{\partial x} = \frac{t_i}{1-p} \frac{dp}{dt} + \lambda_2 \frac{\partial^2 t_i}{\partial x^2}$$

in which V_i is the ice velocity and λ_2 is an artificial dispersion parameter which empirically accounts for the longitudinal dispersion of the released ice mass.

The distribution of ice velocity in the longitudinal direction is believed to vary depending upon whether the situation involves a rubble breaking front or sheet front propagation. Figure 3-1 depicts a definition sketch of the approach taken to deal with this in the proposed model. The ice accumulation is assumed to move at the water velocity ($V_i = V_w$); the shaded zone indicates the ice accumulation profile at time t, and the solid line depicts the new profile and location of the ice accumulation at time $t + \Delta t$. There is a small portion of the downstream ice sheet, termed the 'displacement zone' (cross hatched portion), which will either be displaced or consumed by the moving ice accumulation during the interval Δt. In the case of sheet front propagation, the moving ice accumulation is assumed to create a "transition zone" of moving ice sheets ahead of it. Our field observations indicate that the length of this transition zone is generally several river

widths, within which the ice sheets shift position, closing open leads and forming pressure ridges. In the model, it is assumed that the ice in the displacement zone is pushed into this transition zone: decreasing its effective aerial porosity (as leads close); increasing its effective thickness due to ridging (approximated as a uniform increase in thickness in the transition zone); and initiating some movement ($V_i < V_w$). In contrast, for the case of a rubble breaking front, it is assumed that the ice in the displacement zone is incorporated directly into the advancing ice accumulation, increasing its total volume of ice (and water). In this case, there is no consideration of a transition zone; instead, all sheet ice downstream is assumed to remain stationary until it is consumed by the advancing ice accumulation. As a third possibility, it was considered that an intermediate behavior might occur, with some of the sheet ice in the displacement zone being consumed and some being pushed ahead.

A parameter β is used in the model to control the propagation behavior, representing the percentage of the ice sheet in the displacement zone being pushed into the transition zone. A value of $\beta = 0$ indicates a pure rubble breaking front, $\beta = 1$ indicates a pure sheet front propagation, and $0 < \beta < 1$ indicates the intermediate case. Therefore, at each time step, a proportion of the total ice volume in the displacement zone ($\Delta \forall$) is removed and either added to the ice accumulation ($(1-\beta)\Delta \forall$) and/or the transition zone ($\beta \Delta \forall$).

3.3 Model Application

An idealized case based on the geometry of the Saint John River is used to investigate the behavior of the proposed model for varying types of breaking fronts. The test case consists of a rectangular channel, 70 km long and 600 m wide, having a bed slope of

0.0005 and a 0.8 m thick ice cover in the receiving channel. Based on earlier calibrations for the prototype case, roughness heights of 0.243 m and 0.004 m were used for the river bed and the underside of the intact ice, respectively. A constant water discharge of 850 m^3/s was used as the upstream inflow boundary condition and the downstream boundary effect was eliminated from consideration by extending the modeled reach far downstream of the area of interest. The initial water surface and ice jam profiles were established using the *River1-D* model, by solving the steady ice jam profile equation, together with the hydrodynamic equations, in a decoupled iterative sequence. Ice jam roughness, again based on previous calibrations, for the prototype case, was taken as 2 m. Figure 3-2 illustrates the resulting initial condition used for the ice jam release tests, showing only the portion of the reach near the initial ice jam.

Three test scenarios were considered in this investigation to examine the behavior over the full range, from one extreme of a rubble breaking front, to the other extreme of a sheet front propagation and the intermediate behavior between these two extremes. For each of the three runs, a time step increment 10 s was used, corresponding to a Courant number ranging from about 0.1 to 0.4, considering that a Courant number of 0.5 is indicated appropriate for the CDG scheme in order to assure good phase accuracy (Hicks and Steffler, 1992). A dispersion parameter $\lambda_2 = 100$ was found to provide optimal results for dispersion of the ice run and also reduced numerical oscillations at the interface between the moving ice accumulation and the ice in the receiving channel.

3.3.1 *Case 1: Rubble breaking front*

In Case 1, a rubble breaking front was simulated, by assuming that the ice sheet ahead of the breaking front was broken and incorporated into the moving accumulation as the ice run ploughed through the receiving channel ($\beta = 0$). Figure 3-3 presents the computed water surface and ice profiles at a time 30 minutes after release of the ice jam (lower graph), as well as the flow discharge under the ice as a function of location at this same time (upper graph). Note that again, for clarity of detail, only a portion of the total channel length is shown. The location of original jam toe is also indicated. As the figure illustrates, the ice concentrates at the front of the moving ice accumulation and quickly grounds on the river bed. The corresponding flow discharge under the ice approaches zero, indicating that the flow can only pass through the voids of the ice accumulation. At this point the simulation breaks down, since the proposed model does not account for seepage through ice voids.

3.3.2 *Case 2: Sheet breaking front*

In Case 2, a sheet front propagation was simulated by assuming that the ice in the receiving channel was pushed ahead of the moving accumulation ($\beta = 1$). Run 2a assumed that the length of the transition zone was three river widths ($3B$). In this case, the fractured ice being pushed ahead of the moving ice accumulation was assumed to thicken the ice cover in the transition zone, and the effective aerial porosity of the transition zone was not affected. The computed water and ice profile together with the under-ice discharge 30 minutes after release are shown in Figure 3-4a. The location of original jam toe is also indicated. Comparison to Case 1 in Figure 3-3 shows that, in this case, the ice

accumulation progresses downstream at a higher speed than for the case of the rubble breaking front (Figure 3-3), indicating that the resistance offered by the ice in the receiving channel is smaller here. Of particular interest in Run 2a is that the transition zone ice thickness increases rapidly, becoming even thicker than that of the moving ice accumulation. Run 2b was similar to 2a, with only the length of the transition zone changed ($5B$ instead of $3B$). As Figure 3-4b illustrates, again the ice thickness in the transition zone increases to exceed that of the moving ice accumulation, although at a slower rate than in Run 2a.

Run 2c was the same as Run 2a, except that in this case, the aerial porosity of the ice cover, initially taken as 40%, was allowed to decrease in the transition zone (i.e. first closing open leads before any thickness change due to ridging). Simulation results 30 minutes after release of the original ice jam are shown in Figure 3-5a where it is seen that the ice sheet in the transition zone is still compressing at this time. Extending the simulated duration, it was found that the aerial porosity decreased to zero by 50 minutes, after which thickening occurred in the transition zone (Figure 3-5b).

In all of these test runs considered in Case 2, the transition zone was assumed to be constant in length (either $3B$ or $5B$). This assumption implies that the sheet front is progressing at the same velocity as the front of the moving ice accumulation. However, these simulations raise a doubt as to the validity of that assumption. Jasek (2003) presented some quantitative data of the celerity of sheet front propagation; he observed the celerity of a sheet front for a reach of the Hay River, Northwest Territories, Canada, breakup on 2 May 1989 to be above 4 m/s, while the wave crest traveled at about 2 m/s. Another sheet front propagation documented on 6 May 1997 on the Yukon River showed

a sheet front celerity of 7.7 m/s, due to extra space provided by a large open lead. These sheet front celerities are all much larger than the velocity at which the ice accumulation can travel. Clearly, the available space within the downstream ice cover is a key factor for the celerity of the sheet front. Application of a moving control volume to the sheet front yields a relation between the front celerity c_b and the ice velocity V_i of:

[3-7] $$c_b = V_i / p$$

For example, a moving ice accumulation with velocity of 1.5 m/s and a downstream ice cover porosity of 40%, produces a sheet front celerity of 3.75 m/s, or 2.5 times larger. This is a quite plausible result in comparison to Jasek's field observations. Therefore, the length of the transition zone must actually increase as the moving ice accumulation progresses downstream, providing more space for the ice volume being pushed into this reach, and preventing the unreasonably excessive accumulation and thickening of ice volume.

Also worthy of notice in the simulation results (e.g. Figure 3-4) is that the under-ice water discharge is quite large in the transition zone, indicating higher flow velocities. Thus, any ice accumulated under the ice cover in this zone could possibly be carried further downstream by this relatively faster flow. This would also tend to mitigate the thickening process in this zone.

3.3.3 *Case 3: intermediate mode*

In Case 3, a mode between the two extremes was simulated. In this case, the fractured ice sheet ahead of the moving ice accumulation was partly consumed by the moving ice and

partly pushed ahead. β was set at 0.7, which means that 70% of the ice volume in the displacement zone was assumed to be pushed ahead, and 30% was assumed to be consumed. Here again, the length of the transition zone was set to $3B$. Run 3a assumed only thickening within the transition zone, while in Run 3b the aerial porosity was first decreased to zero before thickening. Results are shown in Figure 3-6, again after 30 minutes of simulation time. Here again, a lengthening transition region is needed to avoid excessive thickening in the transition zone.

3.4 Conclusions

The effects of ice in a receiving channel are included into a one-dimensional simplified flow and ice dynamic model when modeling the propagation of an ice jam release wave and its associated ice run. Specifically, the behavior of a rubble breaking front, sheet front propagation, and an intermediate mode are simulated. The results show that the ice accumulates rapidly at the rubble breaking front, quickly leading to grounding of the simulated ice run. For the case of sheet front propagation, a lengthening transition zone representing the fact that the breakup front travels faster than the flow velocity, is needed to avoid excessive thickening. For this case, the celerity of the sheet front depends on the effective aerial porosity of the ice cover downstream. These numerical experiments appear to validate the generally accepted interpretations of field observations. More work is needed in this area, both in terms of numerical model enhancement and additional field observations.

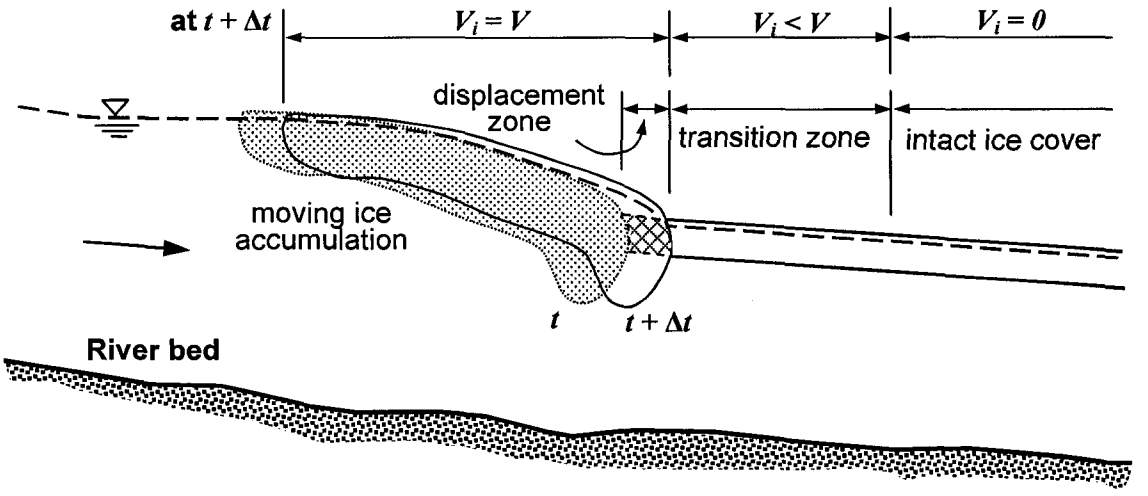

Figure 3-1 Definition sketch of the proposed breaking front model.

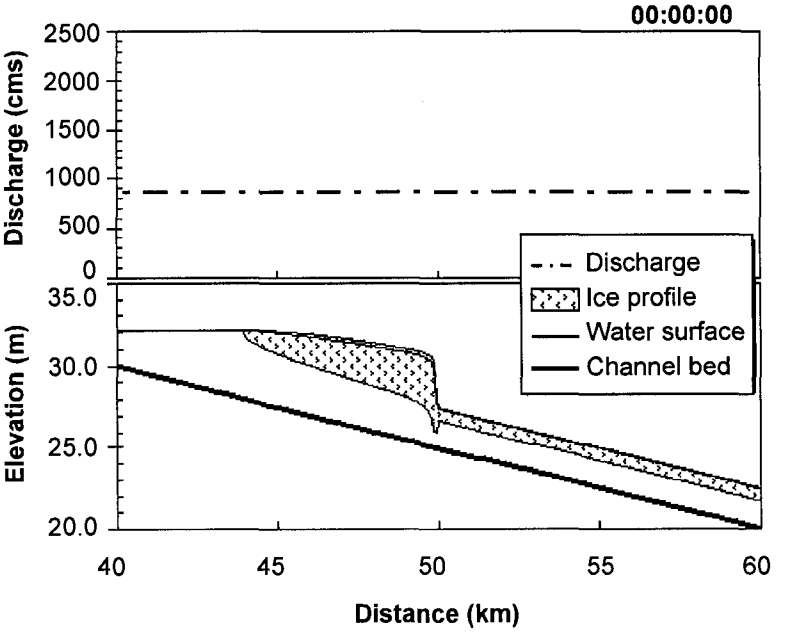

Figure 3-2 Initial water surface and ice jam profiles and discharge under the ice.

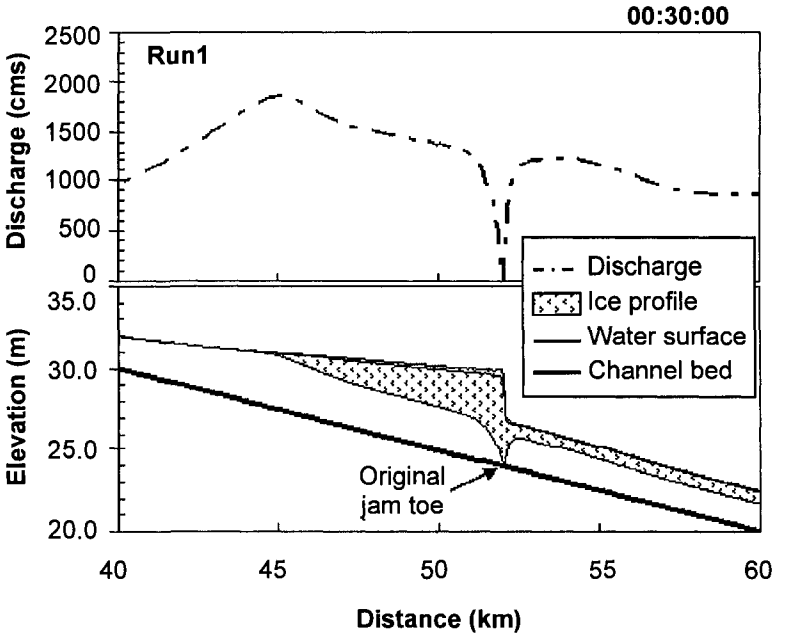

Figure 3-3 Water and ice profiles and discharge under the ice of a rubble front release.

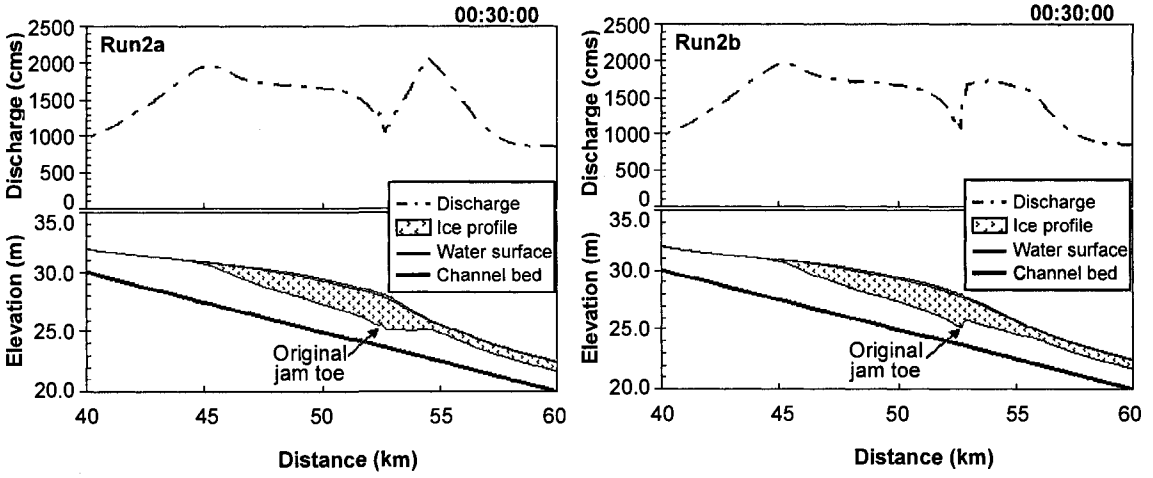

Figure 3-4 The water and ice profiles and flow discharge under the ice of a sheet breaking front: a) 3B transition zone; b) 5B transition zone

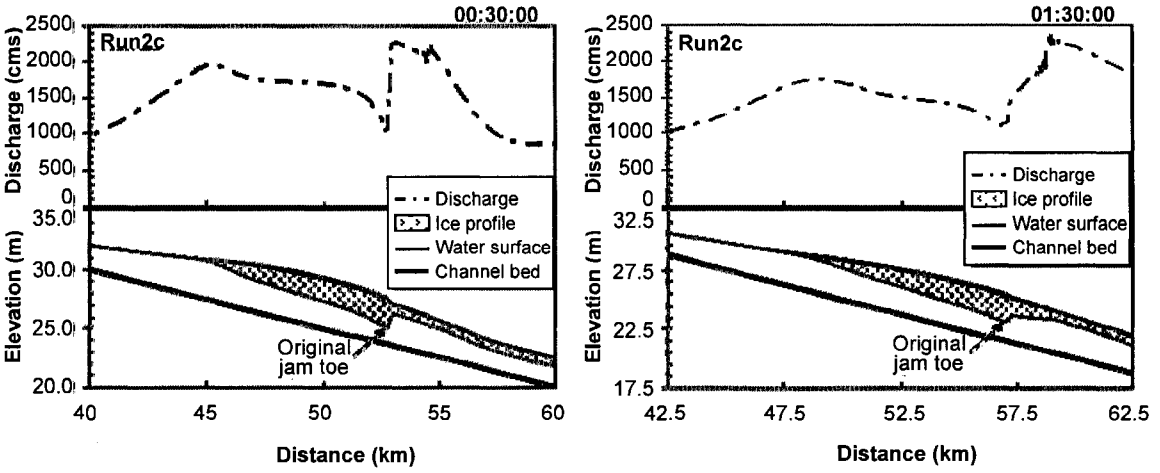

Figure 3-5 The water and ice profiles and flow discharge under the ice of a sheet breaking front: open leads close before any thickening.

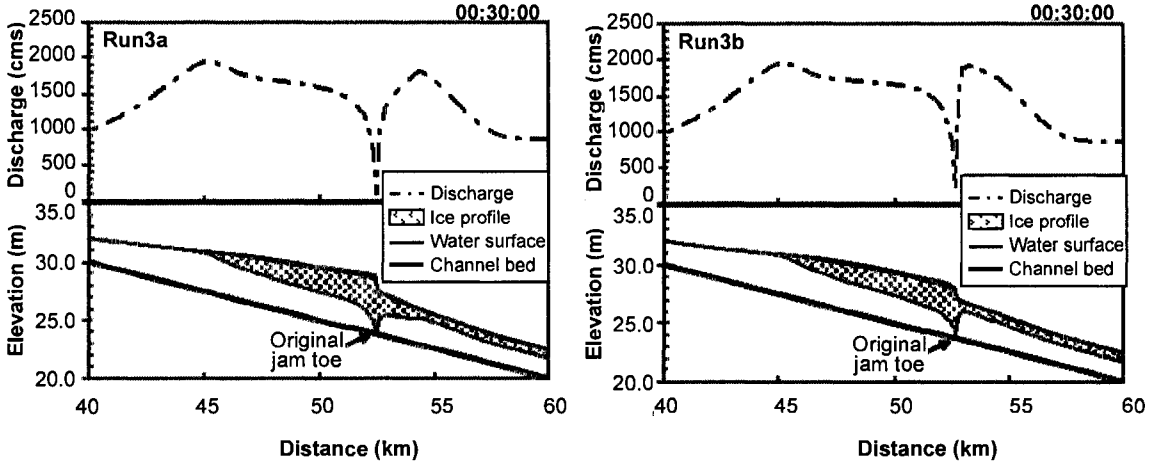

Figure 3-6 The water and ice profiles and flow discharge under the ice of a mode between the rubble and sheet breakup: a) thicken only; b) compress and thicken.

3.5 References

Beltaos, S. and Krishnappan, B. G. (1982). Surges from ice jam release: a case study. Canadian Journal of Civil Engineering, Vol. 9, pp. 276-284.

Hicks, F. E. and Steffler, P. M. (1992). A Characteristic-Dissipative-Galerkin scheme for open channel flow. ASCE Journal of Hydraulic Engineering, Vol. 118, No.2, pp. 337-352.

Jasek, M. (2003). Ice jam release surges, ice runs, and breaking fronts: field measurements, physical descriptions, and research needs. Canadian Journal of Civil Engineering, Vol. 30, pp. 113-127.

Liu, L. W. and Shen, H. T. (2004). Dynamics of ice jam release surges. Proc., 17th International Symposium on Ice (IAHR2004), Saint Petersburg, Russia, 8pp.

She, Y. T. and Hicks, F. (2005). Incorporating ice effects in ice jam release surge models. Proc., 13th Workshop on River Ice, CGU-HS CRIPE, Hanover, NH, pp. 470-484.

4 Athabasca River Ice Jam Formation and Release Events, 2006 and 2007[3]

4.1 Introduction

River ice breakup in northern regions can be very dynamic, involving both ice jam formation and release events. Because they cause violent ice runs and rapidly increasing water levels, ice jam release events are analogous to, but are far more complex than, a small-scale dam break event. Flooding can be particularly severe and difficult to predict if the resulting ice runs are stalled or arrested by a solid ice cover, or by geometry constrictions downstream. Unfortunately, reliable field data describing the water levels, flow rates, ice thicknesses, as well as shoving and breaking front speeds during dynamic ice events are often difficult to acquire due to the rapid nature of, and variable locations, for such events.

Published data regarding the dynamic aspects of ice jam consolidation and release are scarce. This lack of data limits our understanding of how the ice and water components in an ice-jam-related flood may be interacting, and also hinders full validation of the existing models. In terms of ice jam formation, many of the experimental ice jam studies conducted to date have been case specific investigations, rather than generic process models. Also, they have been almost exclusively steady flow experiments (e.g. Saade and Sarraf 1996). Unsteady ice jam consolidation experiments were conducted by Zufelt and Ettema (1990, 1992); however, variations in water level and ice thickness during ice jam

[3] This chapter was accepted for publication in Journal of Cold Region Science and Technology, 2008.

consolidation events were documented only qualitatively. Healy and Hicks (2006, 2007) provide the only comprehensive quantitative experimental data describing ice jam formation dynamics to date. In the field, in-situ ice jams have been documented by a number of researchers, with the formative work in this field conducted by Beltaos (e.g. Beltaos, 1978, 1983 and Beltaos and Moody, 1986). However, ice jams are notoriously difficult to predict and measure and as a result very little has been documented on the consolidation process in the field. Andres et al. (2005) provide unique data for a freeze-up consolidation event on the Peace River in Alberta, Canada, but to the authors' knowledge, no other dynamic ice jam consolidation events have been measured in the field.

Data is equally scarce for ice jam release events. Laboratory studies (e.g. by Wong et al. 1985 and Khan et al. 2000) have elucidated some of the physics of ice jam release events. However, they have been limited by physical size constraints in the laboratory setting (i.e. channel length) and thus field studies are essential to facilitate a comprehensive investigation of release wave attenuation. Doyle and Andres (1979) reported a 3.6 m increase in water level on the Athabasca River at the MacEwan Bridge in Fort McMurray which occurred within 45 minutes of the release of an ice jam located 11 km upstream. Beltaos et al. (e.g. 1994, 1998, 2005) report on ice jam release events measured on the Saint John River, NB, in 1993, 1996 and 2002, respectively. For the 1993 and 1996 events, water levels were measured 5 km downstream of the toe of the released jam, documenting 1.1 m and 2.3 m high waves, respectively. Water levels were measured at the toe of the releasing jam in 2002 (rising 1.2 m) and its propagation was documented with additional stage hydrograph measurements 8 and 32 km further downstream. Beltaos

and Burrell (2005) also report on a notable ice jam release event which occurred on the Resitgouche River, New Brunswick, Canada in 2000, involving a water level rise near the jam toe of 2.85 m in only 6 minutes (~0.5 m/min). Kowalczyk Hutchison and Hicks (2007) documented a particularly extreme event on the Athabasca River in Alberta, Canada in 2002, involving a 4.31 m release wave which rose at a rate 0.81 m/min at the jam toe. Stage hydrographs were also measured at seven sites downstream as this wave propagated over a 40 km reach, before eventually arresting to form a new ice jam. These studies cited above represent some of the most impressive measurements of ice jam formation and release events to date; however, considerably more data is critically needed before we can build a comprehensive picture of the physics of ice jam release wave propagation.

The Athabasca River near Fort McMurray, Alberta (AB), Canada annually experiences multiple ice jam formation and release events, making it an ideal site for scientific studies of this phenomenon. Since 1998, the University of Alberta (UA), in collaboration with Alberta Environment (AENV), has conducted annual field observations of breakup along the Athabasca River near Fort McMurray. Kowalczyk Hutchison and Hicks (2007) present a compilation of data describing ice jam events obtained from 1977 to 2005, as well as analyses of these data from a flood forecasting perspective. Valuable and unique scientific data on a number of large ice jam formation and release events have since been collected in an expanded field program at this site. This paper presents the data and analyses obtained as a result of the 2006 and 2007 breakup monitoring programs, conducted as part of a number of intersecting studies investigating ice jam dynamics, ecological impacts of river ice and remote sensing of river ice. To aid in the interpretation

of the data, the current version of the UA *River1-D* ice jam release model is employed to analyze some of these documented ice jam release events. She and Hicks (2006a, b) provided detailed description of the *River1-D* ice jam release model.

4.2 Study Reach

Figure 4-1 illustrates the relevant portion of the Athabasca River, extending from the Town of Athabasca (~400 km upstream of Fort McMurray) to Bitumount (~80 km downstream of Fort McMurray). Station numbers shown on the figure indicate distance in river km measured upstream from the mouth of the Athabasca River. Upstream of Fort McMurray, the river is relatively steep (bed slope ~0.001) and is characterized by numerous rapids and knick points, which play a key role in instigating a dynamic breakup each year (Kowalczyk Hutchison and Hicks 2007). The Clearwater River joins the Athabasca River at Fort McMurray, and downstream of this point the Athabasca River bed slope flattens considerably (to ~0.0003), and contains numerous islands and bars.

Breakup in the reach of the Athabasca River upstream of Fort McMurray is generally quite dynamic and, although event magnitudes and timings are highly variable, breakup typically involves a very consistent pattern of events. First, border flow and local surface runoff initiates thermal deterioration of the ice cover. Next, ice sheet cracking is initiated by increasing flow velocities and water levels (due to snowmelt runoff from the upper basin). Small ice accumulations ("mini" jams) develop and toe-out over the many knick points (rapids) along the reach. The waves caused by this shifting ice tend to break off additional segments of the intact (but thermally deteriorated) ice cover upstream, increasing the length of these small jams. Eventually, these accumulations build sufficient

head to slip over the knick points, and the result is a sequence of small ice jams and ice runs, progressing to larger ice jams and ice runs. Thus ice jams forming in the reach upstream of Fort McMurray are often dislodged by incoming ice runs, occurring as a result of ice jam releases occurring further upstream.

Breakup in the reach downstream of Fort McMurray tends to be dominated by thermal processes, with open water development believed to be accelerated by industrial thermal outfalls from the oil sands mining operations in this area. Because of the abrupt decrease in river slope at Fort McMurray, and the numerous bars and islands in the channel just downstream of the Clearwater River confluence, ice runs from releasing upstream jams may arrest in the vicinity of the confluence, obstructing its outflow. Water can then back up along the Clearwater River, flooding downtown Fort McMurray. Some of the most significant floods on record have occurred as a result of events of this type, most recently in 1997 and 1977. However, because the channel downstream of Fort McMurray often melts out before any significant ice runs occur, many ice runs have been observed to pass right by Fort McMurray.

4.3 Instrumentation

Figure 4-2 presents the portion of the study reach in which the majority of the instrumentation and monitoring efforts were focused. Most of the reach is remote, with no road access. Furthermore, in the reach upstream of Fort McMurray, the rapids make access by boat or snowmobile difficult and dangerous; consequently, installation of monitoring equipment in this reach requires the use of a helicopter. The monitoring network has been continuously expanded and improved since its first installation,

particularly in terms of the number of stations and the range of instruments used to conduct the measurements, as described below. Figure 4-2 shows the instruments employed to monitor the breakup in 2007.

4.3.1 *Meteorological Stations*

Environment Canada operates a meteorological station at the Fort McMurray Airport; however, it does not collect data on incoming solar radiation. The University of Alberta operates a meteorological station between the Athabasca and Clearwater Rivers (Figure 4-2) that measures rainfall, air temperature, barometric pressure, incoming solar radiation, and wind speed all on 30 minute intervals. Air temperature is also monitored at station M216.7, located approximately 80 km downstream of Fort McMurray (Figure 4-1).

4.3.2 *Ice and Water Level Monitoring*

The Water Survey of Canada (WSC), in cooperation with Alberta Environment, operates a water level and discharge gauging network along the Athabasca River, with real-time reporting stations at the Town of Athabasca (RATHATH) and just downstream of Fort McMurray (RATHMCM), as shown on Figure 4-1and 4-2, respectively. As part of their river ice flood monitoring program, Alberta Environment operates additional water level stations in the reach upstream of Fort McMurray. These are shown in Figure 4-1 (WATHGRAN: Grand Rapids), and Figure 4-2 (RATHCKRP: Crooked Rapids, RATHCARP: Cascade Rapids and RATHMTRP: Mountain Rapids). These stations employ compressed air systems, recording water levels every 5 minutes for archival purposes, and reporting hourly water levels for forecasting purposes (via satellite). An additional, acoustic, water level sensor was employed at the Grand Rapids station as a

backup in 2007. These stations are also capable of signaling an alarm if rapid water level rises are detected, thus providing warning of dynamic ice events occurring in the remote reach upstream of Fort McMurray. Pull wires are also employed at each of these sites as a backup for the alarm system. Robichaud (2006) and Mahabir and Garner (2007) provide detailed information on the provincial ice monitoring network.

For breakup in 2007, additional water level sensors were installed along the study reach by the researchers from UA and Université Laval (ULAVAL). The locations and instrument types are illustrated in Figure 4-2. Standard (unvented) pressure transducers were installed at stations M303.3 and M300.3 (upstream of Fort McMurray). Laser rangefinders were also installed at these same locations as a backup, since the pressure sensors were expected to be lost in the event of a major ice jam event. The laser rangefinders were angled downward from a high bank, in order to measure the distance to a point on the ice cover. As the water and/or ice level varied, this distance would change. Measurement of the tilt angle on the laser rangefinder enabled the conversion of these distance changes into water level changes by simple geometry. Simultaneous measurement of water level with the pressure sensor and the laser rangefinder facilitated confirmation of this angle, and manual water level measurements were also conducted to provide geodetic reference elevations. The laser rangefinders were set to take readings every 3 seconds, recording to a USB memory stick, while the pressure transducers were programmed to take readings every 6 minutes, recording to a data logger. Standard pressure transducers were also installed at four sites downstream of Fort McMurray, extending over 80 km (stations M288.1, M268.1, M245.5 and M216.7 in Figure 1), each sampling on 30 minute intervals.

Ice/water levels were also monitored manually by UA and ULAVAL researchers. For 2006 breakup, lath lines tied in to temporary benchmarks were set up at the water intake site (M296.3) and the Clearwater River confluence (M293.0). Water levels were read from the lath as significant waves passed by. A laser rangefinder was employed at the water intake site in 2007, to enhance the resolution and accuracy of the measurements. The laser rangefinder was sampling manually approximately every 10 seconds. Staff gauges were also installed along the remote reach upstream of Fort McMurray, to facilitate photographic measurement of ice jam profiles from a helicopter (Figure 4-2).

The accuracy of these instruments is pretty high. The vertical precision of the laser rangefinders is ~ ± 1 cm. The maximum error of the pressure transducers is about ~1 cm over the range of measured depths. However, this level of accuracy is not possible to achieve when measuring the water levels associated with large ice runs in shallow water. A conservative estimate of the error would be approximately ± 10 to 15 cm (Kowalczyk 2005). The error of manual measurements using a rod and level can be even larger.

4.3.3 *Photographic Monitoring*

One still camera was installed by UA researchers at station M300.3 in advance of the 2006 breakup, to facilitate monitoring the corresponding ice conditions with water levels. The camera was programmed to take photos every minute during daylight hours (i.e. 05:00 to 22:00). For breakup in 2007, additional still cameras were installed at monitoring stations both upstream of Fort McMurray (stations M303.8, M303.3, M300.3), and downstream of Fort McMurray (station M288.1). These were programmed to take pictures every 15 minutes. The upstream cameras at stations M303.3 and M300.3 were

controlled by a data logger connected to a trip wire, and programmed to take one picture every 5 seconds for 10 minutes when triggered, then one every 15 seconds for 60 minutes, before returning to the 15 minute interval. The upstream camera at M303.8 was operated as a webcam, with photos obtained by dial-up digital cellular modem. For both years, the Regional Municipality of Wood Buffalo (RMWB) operated a webcam at the bridge in Fort McMurray (located at station M294.8), and these images were captured and archived to supplement the observations. Video cameras were employed during the ice jam release event at the water intake site (M296.3) for both years and at the bridge as well (M294.8) in 2007.

4.4 Observation of Ice Jam Events

Breakups in 2006 and 2007 were both highly dynamic, involving numerous ice jam formation and release events along the Athabasca River. The monitoring network successfully recorded water and/or ice level hydrographs at numerous stations during the ice jam formation and release events in both years. Aerial and ground observations of ice conditions provided valuable complementary data in both years. Additionally, a helicopter was used to monitor and track the speeds of ice runs, regressive waves, shoving fronts, and a breaking front during the 2007 breakup.

4.4.1 *Breakup 2006*

Breakup in 2006 progressed as a cascade of ice jam formation and release events over an extended reach from Grand Rapids to Fort McMurray from April 13 to April 20. Water and/or ice level hydrographs were obtained at 8 monitoring stations. Figure 3 presents the water levels obtained from the four AENV stations located upstream of Fort McMurray

while Figure 4-4 presents the water level (or top of ice) measured at the four stations in and downstream of Fort McMurray.

On April 13, the reach from Grand Rapids to Crooked Rapids (see Figure 1) was mainly open with sections of intact ice cover, minor ice runs and small ice jams (~ 1 to 1.5 km long). The toe of the most downstream ice jam was located at the Crooked Rapids station (RATHCKRP). Downstream of this to the Clearwater River confluence, the ice cover was mainly intact, but thermally deteriorated.

Water level fluctuations at the Crooked Rapids gauge (RATHCKRP) triggered an automated alarm at 01:30 on April 14, suggesting ice movement and a possible ice jam release (Robichaud, 2006). Observations that afternoon revealed that the ice runs observed on April 13 had created a 5 km ice jam with its toe at Long Rapids. The Crooked Rapids ice jam had released and broke 2 km of intact ice cover before coming to rest as a 4 km ice jam with its toe at Cascade Rapids. Downstream of this to the Clearwater River confluence, ice conditions had changed very little. This event (denoted "A" in Figure 4-3) caused the water level reading at Crooked Rapids (RATHCKRP) gauge to drop 1.63 m and later become non-operational. Also, although the ice run stopped near Cascade Rapids, part of the water continued propagating underneath the ice cover without fracturing it, as seen in the Cascade Rapids (RATHCARP) and Mountain Rapids (RATHMTRP) gauge records (Figure 4-3c and d, respectively). Based on the timing of the water level peaks, the jam release wave progressed under the ice cover at approximately 1.13 m/s, having traveled 8.1 km between those stations in 120 minutes.

Due to cooler, overcast weather, ice conditions did not change significantly from April 14 to April 17 except that 1 km of ice had melted at the head of the Long Rapids ice jam. On the morning of April 17, a wave was recorded at Grand Rapids (WATHGRAN), which passed through the Long Rapids ice jam and caused the water level at Cascade Rapids (RATHCARP) start to rise at 14:00 the same day (denoted "B" in Figure 4-3). The Long Rapids ice jam released at approximately 17:00, causing the water level at the Cascade Rapids gauge to increase further. As these two waves passed by, the Cascade Rapids ice jam stayed in position, but the ice cover downstream became dislodged. The broken ice cover was forced downstream and reformed to create a small ice jam with its toe positioned just upstream of Mountain Rapids, and water level fluctuations were observed at the nearby gauge (RATHMTRP).

This new ice jam released on April 18, pushing the ice cover downstream (denoted as event "C" in Figure 4-3d and Figure 4-4). The exact time of release is not known, but the water level at Mountain Rapids (RATHMTRP) had dropped almost one meter by 14:00 and station M300.3 (downstream) captured a 1.05 m high wave, peaking at 14:50. At 14:37, UA researchers observed initial ice movement at the water intake site (M296.3), and a 2.20 m water level increase over only 15 minutes was documented at this manual station. At approximately 15:15, this ice run arrested at the water intake site and the water level stopped rising. Consolidation continued until the jam head stopped in front of the camera at M300.3 by 16:00 that afternoon. The resultant jam was 4 km long. The WSC gauge (RATHMCM) further downstream captured a 0.44 m high wave by 17:45 as a result of the wave that had escaped downstream of this newly formed ice jam.

By April 19, the total length of the Cascade Rapids ice jam had reduced from 4 km (on April 14) to approximately 1 km, due to melting. Aerial reconnaissance at 17:00 revealed that this ice jam was releasing (event "D" denoted in Figure 4-3 and Figure 4-4). The river was open downstream of this to the head of the water intake ice jam, with only a limited remnant ice sheet at station RATHCARP, where a 0.78 m water level increase was recorded at 17:54. Unfortunately, the Mountain Rapids gauge (RATHMTRP) had malfunctioned by this time, but photos taken by the camera at station M300.3 show that the ice run originating at Cascade Rapids arrived at the head of the water intake ice jam at 19:50 and instigated its release at 20:50. Water level readings could not be obtained at the water intake site because the lath line was destroyed when the ice jam formed there. The peak of the release wave was manually documented passing the Clearwater River confluence (station M293) at 21:50. Further downstream at the WSC gauge (RATHMCM) a 0.58 m water level increase was recorded, peaking at 22:30.

4.4.2 *Breakup 2007*

Breakup in 2007 was particularly dynamic, with an extensive reach of river (several hundred km) breaking up during the late evening and early morning of April 18 and 19. Water and/or ice level hydrographs were successfully obtained at 10 of the 12 monitoring stations (Figures 1 and 2). The pressure transducers at stations M245.5 and M216.7 were pulled out by the violent ice runs so that no data were obtained at these two stations. Figure 4-5 presents the water levels obtained from the four AENV stations located upstream of Fort McMurray while Figure 4-6 and 4-7 present the water level (or top of ice) measured at five stations in and downstream of Fort McMurray.

Observations by fixed wing aircraft first indicated signs of ice cover deterioration by mid-April. By the late afternoon of April 17 ice was reported to be running bank to bank at the Town of Athabasca. Breakup began in the late afternoon of April 17 with the reach just upstream of Fort McMurray to Crooked Rapids experiencing small ice jams on all the rapids, with the largest open stretch being between Little Cascade Rapids and Cascade Rapids. Later that evening it rained steadily in Fort McMurray for approximately one hour (an atypical occurrence). By 08:00 on April 18, the small ice jams in the reach upstream of Fort McMurray had all lengthened. The most downstream of these (~1 to 1.5 km long) was at Mountain Rapids, with the toe located just upstream of station M303.8. By 14:30, the water level had increased by 1.13 m at Grand Rapids (WATHGRAN) as two ice runs approximately 10 and 7 km in length passed. This event, marked as "A" in Figure 4-5, 4-6 and 4-7, could be tracked in the water level record all the way down past Fort McMurray. Note that the water level reading at station RATHCKRP dropped 1.43 m and flat-lined during this event, indicating the sensor there was pushed to a higher location by the ice run. As a result, water levels below 4.5 m at this location could not be recorded. Based on the time of travel of peak water level, the wave speed was calculated to be approximately 1.92 m/s, having traveled 8.1 km from RATHCARP to RATHMTRP in 70 minutes. By 02:00 on April 19, these ice runs had all reached Mountain Rapids and pushed the toe of the jam down to the water intake site (M296.3). The head of the resultant jam was located at Mountain Rapids near station 308 km (making it 11 km long).

On the morning of April 19, another incoming ice run caused the water level at Grand Rapids (WATHGRAN) to increase by 1.61 m (denoted as "B" in Figure 4-5). This gauge peaked at 06:30, and by 16:10 aerial reconnaissance confirmed that the front of an ice run

more than 30 km long was approaching Crooked Rapids. A helicopter was used to track the speed of this ice run upstream of Crooked Rapids as summarized in Table 4-1. The speed of the wave associated with this event was calculated to be approximately 4.71 m/s between the Crooked Rapids and Cascade Rapids gauges and 2.42 m/s between the Cascade Rapids and Mountain Rapids gauges, based on travel times of 35 and 50 minutes, respectively. Of particular interest is the fact that the shape of the stage hydrograph for event "B" was nearly identical at those stations (Figure 4-5c and d).

By 17:56, the front of the ice run (30-50% ice coverage) was getting close to the head of the ice jam near Mountain Rapids; however, its observed speed had slowed to 2.73 m/s by this time. Preceding it was a wave front that impacted the ice jam at approximately 17:30, creating a series of regressive waves propagating upstream at 0.83 m/s. These waves attenuated completely upon arriving at the front of the incoming ice run. Within the upper portion of the jam, this precursor wave initiated a series of shoving events (initially spanning the channel width), and when the ice run itself impacted the jam, a complex 2-D pattern of shoving fronts was observed. These shoving episodes stopped, started and split a number of times, continuing until at least 20:00. A summary of the observed shoving front speeds is presented in Table 4-2.

At 18:30, an open lead began developing at the toe of the jam at the water intake site, with ice running within it by 19:00. The ice jam released at 20:00, initially propagating as a sheet breaking front at a high speed. The foremost sheet pushed through the intact ice cover, with the back end of the sheet quickly developing transverse cracks. Observations at the breaking front indicated that the breaking mechanism varied, with the moving ice sheet alternating between riding up on to the intact ice, and diving below as it progressed.

As the breaking front and corresponding water wave passed the Clearwater River confluence (M293), a noticeable water surface gradient was observed, and ice on the Athabasca River quickly developed longitudinal cracks (oriented perpendicular to the Clearwater channel). As a result, a rush of water and ice quickly began moving up the Clearwater River as the breaking front continued moving downstream at a slower rate of only 1.88 m/s by the islands downstream of the confluence. A summary of the breaking front speeds documented by helicopter are presented in Table 4-3.

Pressure sensors at station M303.3 and M300.3 were ripped out as the ice jam formed, but did provide event timing information. Also, unfortunately, the laser rangefinder at station M300.3 malfunctioned for unknown reasons; and no data could be retrieved. Water and ice levels were successfully recorded with the laser rangefinder at M303.3, however, as shown in Figure 4-6. Staff gauge readings conducted from a helicopter on April 19 confirmed the top of ice level recorded at M303.3. Figure 4-6 shows that the top of ice level increased by 2.3 m between 00:50 and 01:30 on April 19 as the ice jam formed (denoted "A"). Later in the day (between 19:20 and 21:00 on April 19), when the second extensive ice run hit this jam (event "B"), the consolidations pushed the top of ice level up by an additional 2.5 m. The ice jam toe released at 20:00 and the water level recorded with the laser rangefinder started dropping at 21:00; therefore, it took 1 hour for the regressive wave to reach station M303.3 and the speed of this regressive wave was 1.94 m/s. Close examination of the data obtained did not reveal any indication of any small amplitude, short period waves preceding or during the event (e.g. see Beltaos and Roswell, 2001); however, this might reflect a limitation of the measurement system (vertical precision ~ ± 1 cm).

Top of ice levels measured with the laser rangefinder at the water intake site (M296.3), approximately 500 m upstream of the toe of the Fort McMurray ice jam, are presented in Figure 4-7a. The ice level initially rose 1.1 m at 18:30 and remained steady for 90 minutes, which likely corresponds to the event "B" wave (which had earlier instigated the series of consolidations in the upper jam) arriving at this location. At 19:50 the ice level again begin rising, and was up by another 0.5 m at the time the jam released. It continued to rise until 20:21, peaking at 248.82 m (geodetic elevation), with a total increase of 2.6 m occurring over those 31 minutes.

This ice jam release wave was also captured at three stations downstream of Fort McMurray (event "B" in Figure 4-7b, c, and d). The first two were within one jam lengths' distance from the jam toe: RATHMCM at station 289km (7.3 km downstream from release point) and M288.1 (8.2 km downstream). The water level rose 0.96 m peaking at 22:00 at RATHMCM and rose 2.19 m peaking at 02:00 (April 20) at M288.1. The significant increase in wave height suggests that the jam stalled at least briefly between these two stations. As Figure 4-2 illustrates, there are numerous islands as well as a noticeable constriction between these two stations, which lends credibility to this interpretation. Also, similar tendencies have been noted historically (Kowalczyk Hutchison and Hicks, 2007).

Further downstream at station M268.1 (28.2 km downstream of the release point), the water level rose 1.56 m, peaking at 09:30 on April 20 (giving a wave peak speed of 0.75 m/s between these stations). It is also interesting to notice that both stations M288.1 and M268.1 showed two peaks, with the first one related to the dynamic forerunner, and the second one corresponding to the ice run itself (again lending credibility to the

interpretation that the ice run stalled between the WSC gauge and M288.1). Of interest also in Figure 4-7b, c, and d is the appearance of a small disturbance, about 24 hours in advance of the release event. The peaks arrived at 03:30 (RATHMCM), 03:30 (M288.1), and 05:00 (M268.1). It is possible that this small disturbance represents part of the water from event "A" which escaped downstream as the jam formed at the water intake site (M296.3).

4.5 *River1-D* Modeling of Ice Jam Release Events

To facilitate further interpretation of the data, the current version of the *River1-D* model's ice jam release modeling component (She and Hicks, 2006a) was employed to analyze three of the ice jam release events described above. In particular, the importance of the ice effects, both within the original ice jam, and in the receiving channel, on the propagating ice jam release wave could be evaluated. The geometric model used was based on a limited geometry (rectangular) channel approximation, due to a lack of river bathymetry data in the rapids infested reach of the Athabasca River upstream of Fort McMurray.

4.5.1 *Cascade Rapids – Water Intake Ice Jam Release in 2006*

On April 19 in 2006, an approximately 1 km long ice jam was positioned with its toe at Cascade Rapids (323.5 km) and another 4 km long ice jam was positioned with its toe at the water intake site (M296.3). The channel was mostly open downstream from the toe of the Cascade Rapids ice jam to the head of the water intake ice jam, with only a limited length of ice sheet at station RATHCARP (M320.1). Downstream of the water intake ice jam, there was a limited length ice cover from the jam toe to the Grant MacEwan Bridge

(294.9 km). This ice cover was dark and significantly deteriorated, and contained a large open lead. The river was fully open downstream of the bridge. Figure 4-8 illustrates the initial ice jam profiles calculated with the *River1-D* model, based on the unperturbed-flow discharge estimated from the two WSC gauging stations: Athabasca River below Fort McMurray (RATHMCM) and Clearwater River at Draper (RCLEDRAP). The water intake ice jam profile was surveyed about 9 hours before its release (20:50), and the surveyed top of ice elevations are also shown on Figure 4-8 for comparison.

At about 17:00, April 19, the Cascade Rapids ice jam released, later triggering the release of the water intake ice jam at around 21:00 (denoted as event "D" in Figure 4-3 and 4-4). The *River1-D* ice jam release model was first used to simulate the release of the Cascade Rapids ice jam. The empirical resistance and dispersion parameters λ_1 and λ_2 (as defined in Chapter 2) used here are 1.0 and 100 for the first 0.4 hours, and 0.0 and 0 for the remaining simulation time. Results are shown in Figure 4-9a and b, together with the recorded wave at station RATHCARP (about 3 jam lengths downstream from the original jam toe) and RATHMTRP (about 11 jam lengths downstream from the original jam toe). Note that in the figures, 258.68 m and 251.06 m were added to the measured water level at these two stations, respectively, to match the simulated unperturbed water level to the observed, since the actual geodetic elevation is unknown.

Figure 4-9a interestingly shows a spike in the water level hydrograph at station RATHCARP. The water level first increased 0.45 m, then dropped for a period of time before it rose another 0.33 m. *River1-D* modeling the of Cascade Rapids ice jam release event indicated that the spike was due to the dislodgement of the limited length of ice sheet at this station, which occurred as the ice jam release wave increased the water level

by 0.45 m. The average thickness of the ice cover was measured to be about 0.5 m in the late winter. Thus, the 0.45 m water level increase is a reasonable value for lifting off of the hinge line between the ice cover and the shorefast ice. Ice resistance effects (both internal resistance and friction between the ice and the river bank, as discussed in She and Hicks (2006a) were incorporated into the model for the first half-hour after release, and became unimportant after that. The model could not achieve agreement with the gauge record at RATHMTRP (Figure 4-9b); however, as mentioned in the previous section (4.4.1), it was confirmed with Alberta Environment that this station was not working properly during this time (Robichaud, 2006).

Although the water intake ice jam release was triggered by the ice run coming from the Cascade Rapids ice jam release, it was simulated separately assuming a constant inflow; since the current version of the *River1-D* model cannot handle a cascade of ice jam release and reformation events. The model results are shown in Figure 4-9c and d, together with the measured water level hydrographs as the ice jam release wave passed by the stations at the Clearwater River confluence and at RATHMCM (both within 1 jam length of the original jam toe). Again, the ice effects were only considered for the first 0.5 hours (empirical resistance and dispersion parameters: $\lambda_1 = 1.0$; $\lambda_2 = 100$) of the simulation time. For both sites, the water levels predicted by the model are vertically offset from the measured geodetic elevations. This elevation difference can likely be attributed, at least in part, to the approximate geometry used in the model (as demonstrated by Blackburn and Hicks, 2002). Nevertheless, as Figure 4-9c shows, the model results for the station at the Clearwater River confluence were consistent with the measured data in terms of the timing of the peak arrival. For the WSC gauge site

(RATHMCM) the model results appear to peak slightly late, and the relative increase in water level seems to be 1.7 times the observed.

The characteristics of the ice jam release waves, as determined from the *River1-D* model output, are summarized in Table 4-4. Wave attenuation is seen in the downstream direction, both in terms of magnitude and celerity. There is one exception, in that the wave peak celerity increased between the Cascade Rapids gauge (RATHCARP) and the Mountain Rapids gauge (RATHMTRP). This might possibly be attributed to resistance effects of the remnant ice near the Cascade Rapids station, impeding the wave. Alternatively, the larger wave speed further downstream might reflect the diminishing ice resistance effect on the wave after a longer travel distance (as the water wave moved out ahead of the ice rubble). The narrower channel section between the Cascade Rapids and the Mountain Rapids could also be a possible factor.

From Table 4-4, it is also seen that the wave celerity is the highest for the leading edge, lower for the peak, and the lowest for the trailing edge of the water level hydrograph. Also of interest is the destructive potential of an ice jam release wave, which could be estimated from the maximum values of several hydraulic parameters of the passing wave. As Table 4-4 illustrates, the wave released from the 1 km long ice jam at Cascade Rapids led to a peak discharge of nearly 3 times that of the unperturbed flow; and the flow shear stress was 2 times the unperturbed value. The release of the 4 km long water intake ice jam led to a discharge of almost 3.5 times that of the unperturbed flow; and the flow shear stress increased to a value close to 5 times the unperturbed value. Although these ice jam release waves attenuate as they propagate downstream, their power was yet not negligible for a location farther downstream from the release point, such as station

Mountain Rapids in the first case (11.5 km downstream) and Fort McMurray in the second case (7.3 km downstream), as the results in Table 4-4 illustrate.

4.5.2 *Water Intake Ice Jam Release in 2007*

On April 19 2007, an 11 km long ice jam was in position with its toe at the water intake site, and there was a lengthy intact ice cover downstream. An extensive ice run hit this ice jam and caused it to release at 20:00. As there was insufficient data with which to estimate the discharge in the impacting wave, this ice jam release event was modeled assuming a constant inflow. The large amount of ice in the extensive ice run was also neglected, since the current version of the *River1-D* ice jam release model does not handle this complexity.

Figure 4-10 shows the initial water surface and ice jam profiles obtained with the *River1-D* ice jam profile model, based on the unperturbed-flow discharge which was again estimated from the two gauging stations: Athabasca River below Fort McMurray (RATHMCM) and Clearwater River at Draper (RCLEDRAP). Also shown in the figure are the top of ice measurements obtained using the staff gauges installed along the remote reach upstream of Fort McMurray. These were photographed from a helicopter just prior to the ice jam release, after the shoving events had diminished.

The *River1-D* model's ice jam release component was employed to simulate the water intake ice jam release event (event "B" in Figure 4-5, 4-6 and 4-7), with incorporation of the effects of the ice cover in the receiving channel (She and Hicks, 2006b). The ice jam release was simulated as a 'sheet breaking front' propagation (as observed in the field), with a transition zone ahead of the releasing ice jam. In these release events, the ice sheet

in the transition zone is fractured and pushed forward by the moving rubble releasing from the jam, and the resulting ice sheet fragments within the transition zone then shift position, closing open leads and forming pressure ridges. These physical processes are represented in the *River1-D* model as described by She and Hicks (2006b).

In these model simulations, the celerity of the sheet breaking front was set to be 2.5 times the local ice velocity at the front of the moving ice accumulation. Figure 4-11 provides a comparison of the modeled and observed locations of the breaking front as a function of time, where it is seen that this approach provides a reasonably good representation of breaking front celerity (i.e. comparing the gradient of the data to the gradient of the model results). Figure 4-12 depicts the celerity of the sheet breaking front in more detail, by comparing the actual computed celerities to the observed values. (Note in this case, GPS tracking refers to the velocities calculated by the helicopter's GPS as the aircraft matched the breaking front speed). The variability in the computed ice front celerity was likely due to the variable geometry conditions in the reach. Slight differences between the modeled and observed celerities are seen in the first 10 minutes after the ice jam release, during which most of the highly dynamic processes happened. After this, the model agreement with the observations is improved. These results and observations confirm the assertion of She and Hicks (2006b) that the transition zone of a sheet breaking front must be ever lengthening as it propagates downstream.

4.6 Summary

River breakup on the Athabasca River at Fort McMurray was quite dynamic in both 2006 and 2007, with numerous ice jam formation and release events observed. Using a variety

of water and ice level monitoring techniques, as well as other ground and aerial observation methods, unprecedented quantitative and qualitative data describing the ice jam formation and release behaviour was obtained. The current version of the *River1-D* model was used to analyze and further interpret the data set. These data contribute to a better understanding of the nature of such events, and also provide valuable validation data for numerical models of dynamic river ice processes.

Table 4-1 Speeds of ice run documented upstream of Crooked Rapids on April 19, 2007.

Time (hh:mm)	Location (km)	Speed (m/s)	Descriptions
15:23	337.8		Front of ice run located just u/s of Crooked Rapids
	~ 395.0	4.17	50 ~ 80% ice coverage
	~377.5	2.50	100% ice coverage, inside of bend
	~357.5	3.61	100% ice coverage
16:10	328.6	3.26	Front of ice run traveled 9.2 km in 47 minutes

Table 4-2 Speeds of shoving fronts documented on April 19, 2007.

Time (hh:mm)	Location (km)	Speed (m/s)	Descriptions
17:42	306.5	1.11	Bank-to-bank shoving
18:13	306.0	1.39	
18:14	305.6		
18:15	304.8	3.09	
18:20		Ice run hit the ice jam	
18:28	300.9		
18:32	300.7	1.70	
18:35	300.3	1.70	
18:37		1.11	Moving ice split to left and right banks
18:47	299.0	0.97	Shoving front stopping by big ice sheets
19:03		Ice running in open lead at the jam toe	
19:14	304.5		
19:31	303.8	0.82	
19:43	307.1		
19:46	306.2	1.34	Bank-to-bank shoving
19:52	304.5	1.13	

Table 4-3 Speed of breaking fronts on April 19, 2007.

Time (hh:mm)	Location (km)	Speed (m/s)	Tracking	Descriptions
20:03	295.2		Video/GPS	Sheet front ridging
20:04	295.0	3.85	Video	
20:05	294.8	3.77	Video	Sheet front hit bridge piers
20:07	294.7	3.50	GPS	
20:08	294.5	3.89	GPS	
20:09	294.2	2.19	Video	
20:13		3.61	GPS	
20:13	293.4	3.56	Video	
20:15	293.3		GPS	
20:19		3.24	GPS	
20:21	291.8	2.57	GPS	
20:27		1.88	GPS	Ice pushing on island

Table 4-4 Characteristics of the 2006 jam release waves, as determined by the *River1-D*.

Hydraulic Parameters	Cascade Rapids jam release		Water intake jam release	
	RATHCARP (320.1km)	RATHMTRP (312km)	Confluence (293.2km)	RATHMCM (289km)
Wave magnitude, ΔH (m)	0.78	0.57	1.27	0.99
Leading-edge celerity, C_L (m/s)	4.74	3.13	6.20	4.38
Wave peak celerity, C_P (m/s)	1.98	2.08	1.29	0.88
Trailing-edge celerity, C_T (m/s)	1.46	1.25	0.51	0.39
Ice front celerity, C_I (m/s)	2.34	1.72	3.1	1.51
Undisturbed values of hydraulic parameters before the event				
Initial flow, Q_0 (m^3/s)	550	550	550	550
Initial velocity, V_0 (m/s)	0.74	1.30	0.69	0.64
Undisturbed friction slope, S_{f0}	0.00072	0.00149	0.00038	0.00023
Initial shear stress, τ_0 (Pa)	10.5	15.9	4.5	3.5
Maximum values of hydraulic parameters during the event				
Discharge, Q (m^3/s)	1479	1071	1889	1215
Velocity, V (m/s)	1.47	1.65	1.24	0.94
Friction slope, S_f	0.00131	0.00160	0.00101	0.00041
Ratio, S_f / S_{f0}	1.82	1.07	2.66	1.78
Shear stress, τ (Pa)	25.0	22.4	21.6	8.97

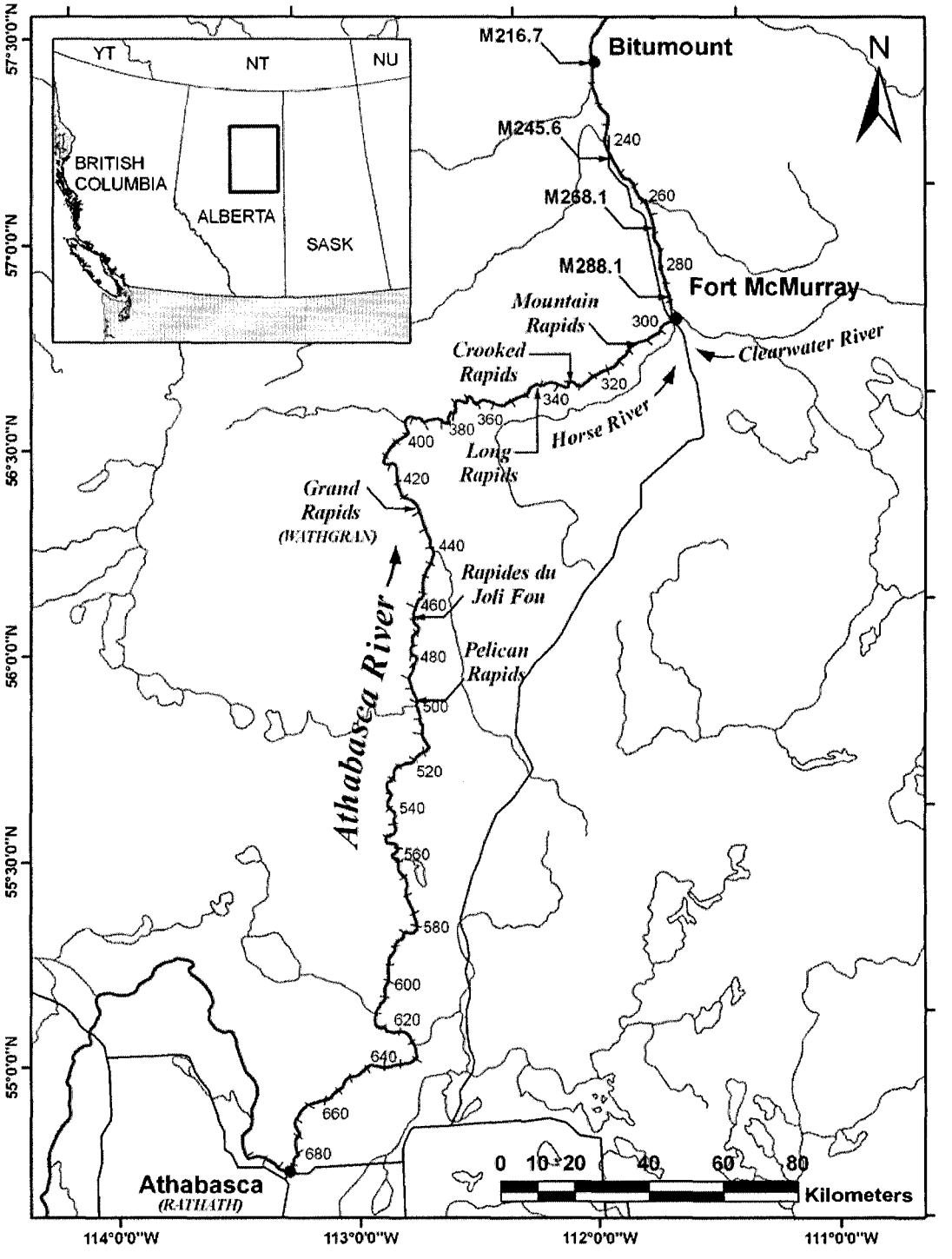

Figure 4-1 Athabasca River from Athabasca to Bitumount, AB.

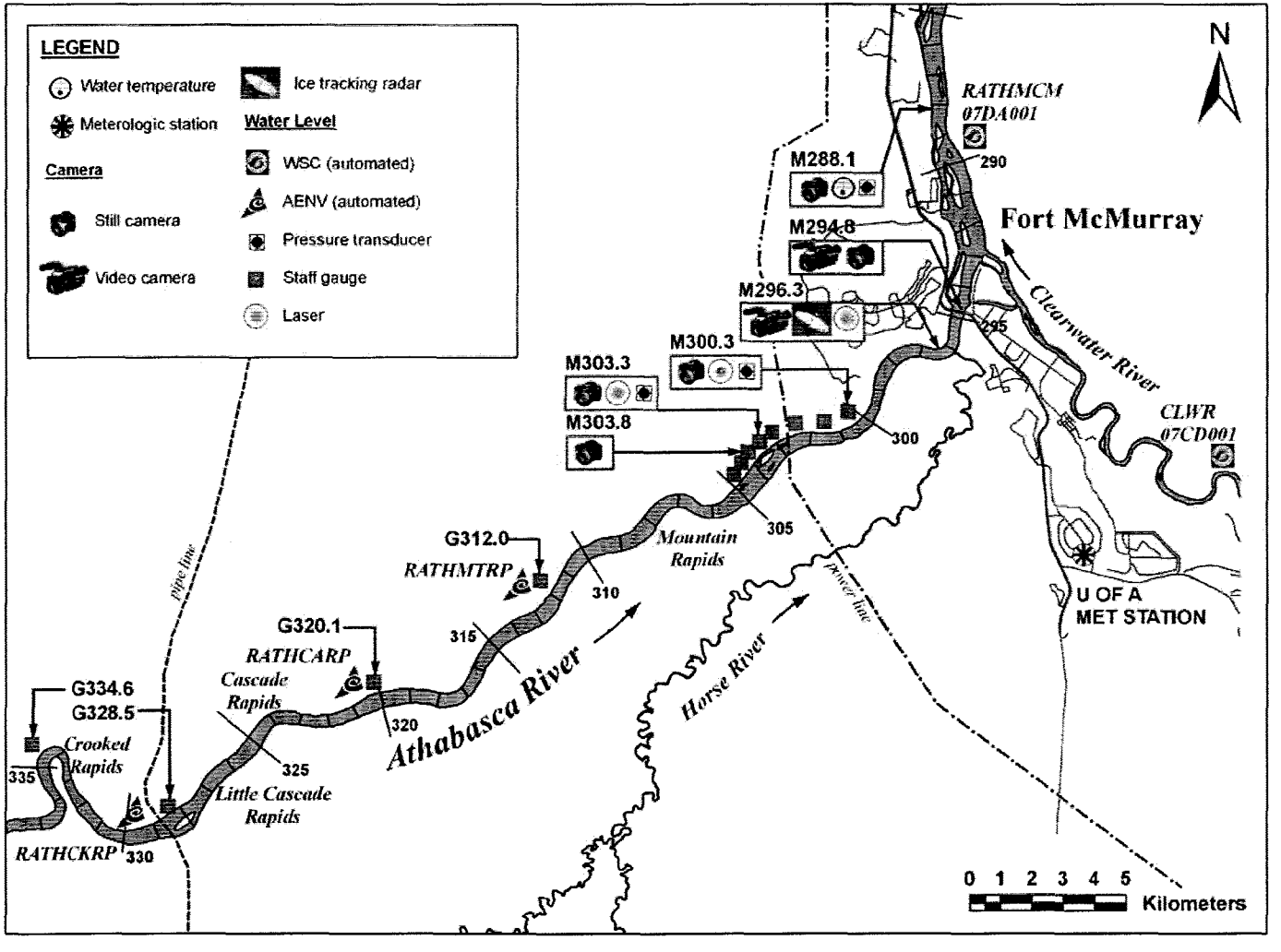

Figure 4-2 Map illustrating monitoring stations installed in the vicinity of Fort McMurray, AB in 2007.

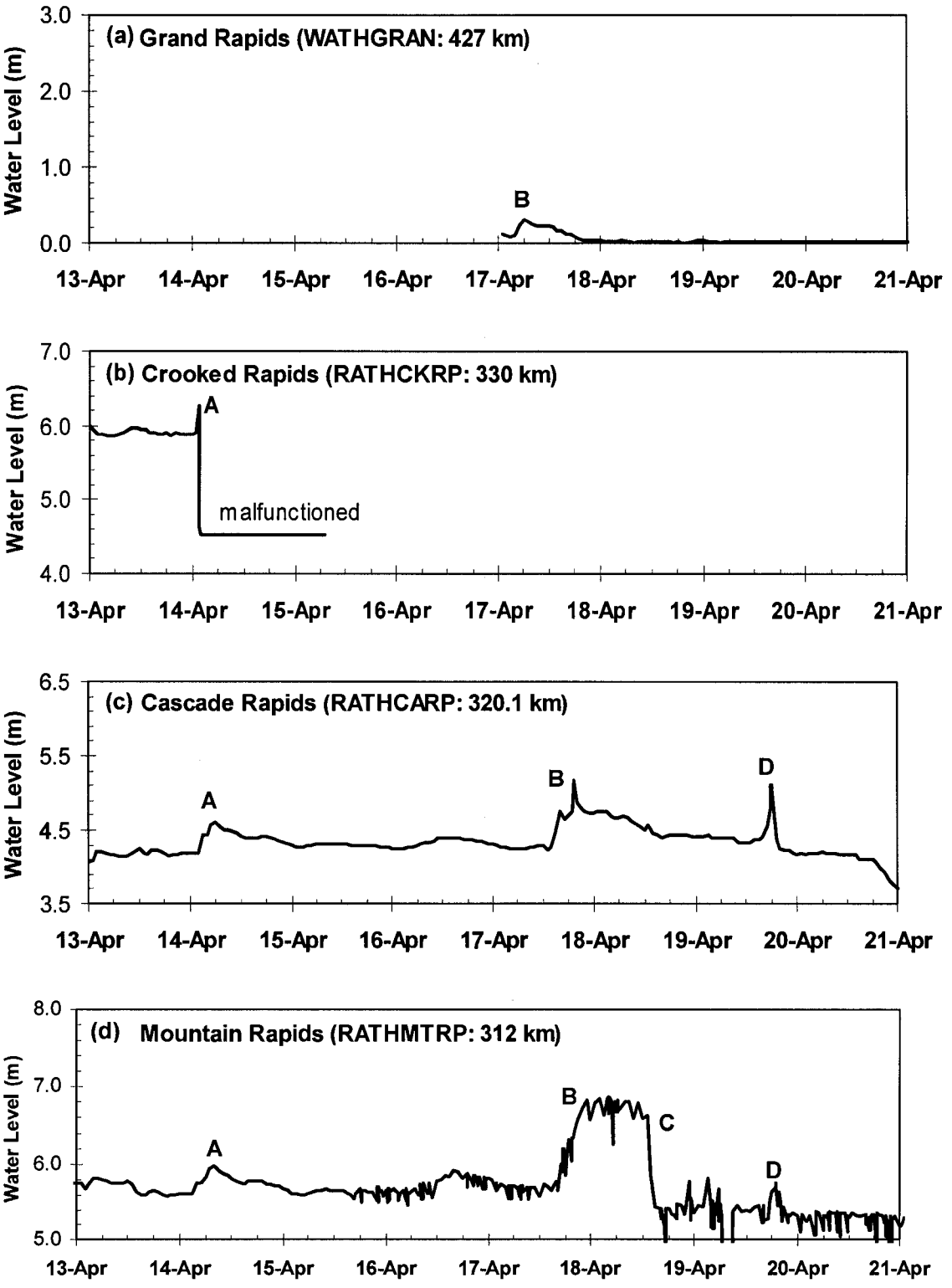

Figure 4-3 Water levels measured at remote stations WATHGRAN, RATHCKRP, RATHCARP, RATHMTRP during the 2006 breakup.

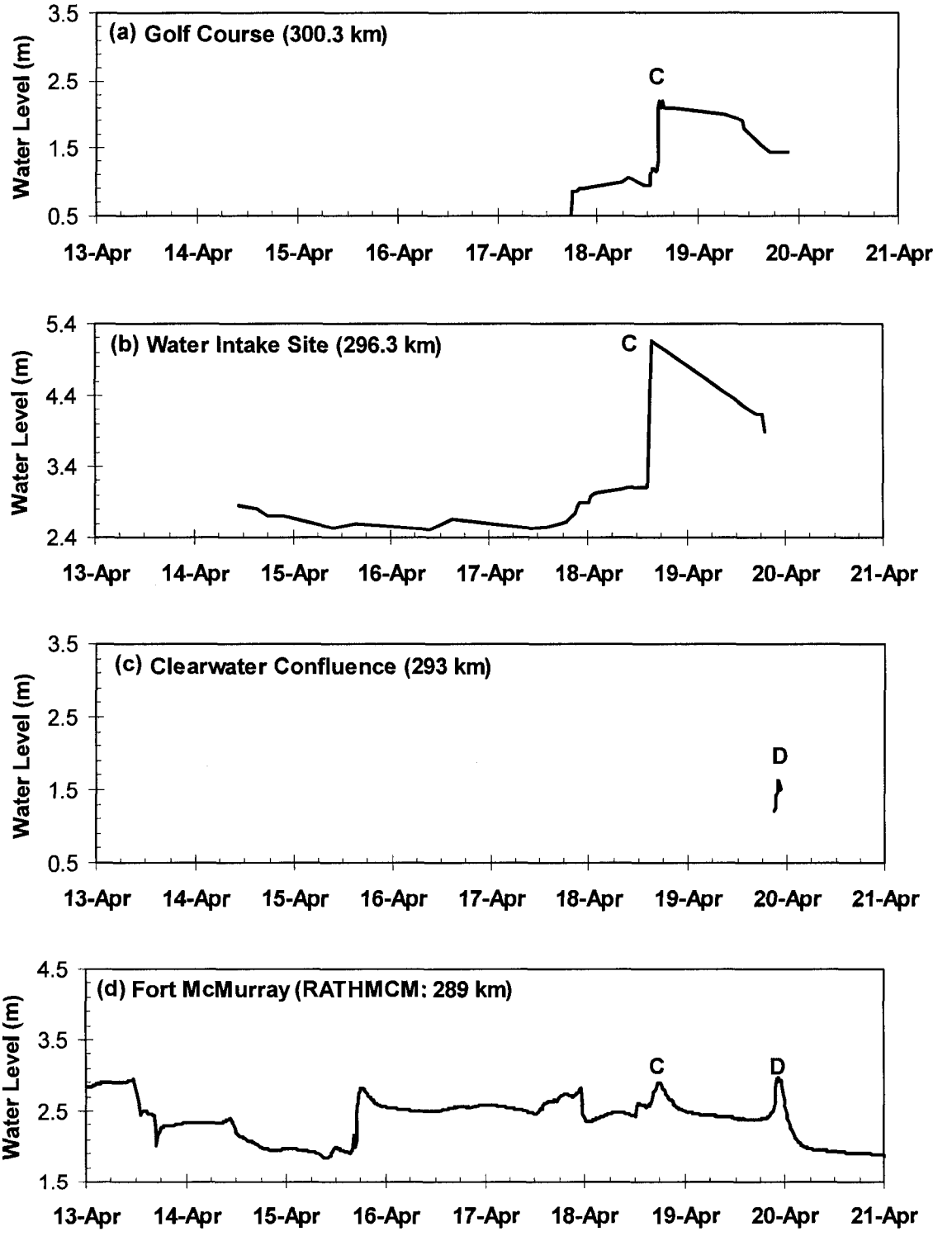

Figure 4-4 Top of ice and/or water levels measured at M300.3, water intake site, Clearwater River confluence, RATHMCM during the 2006 breakup.

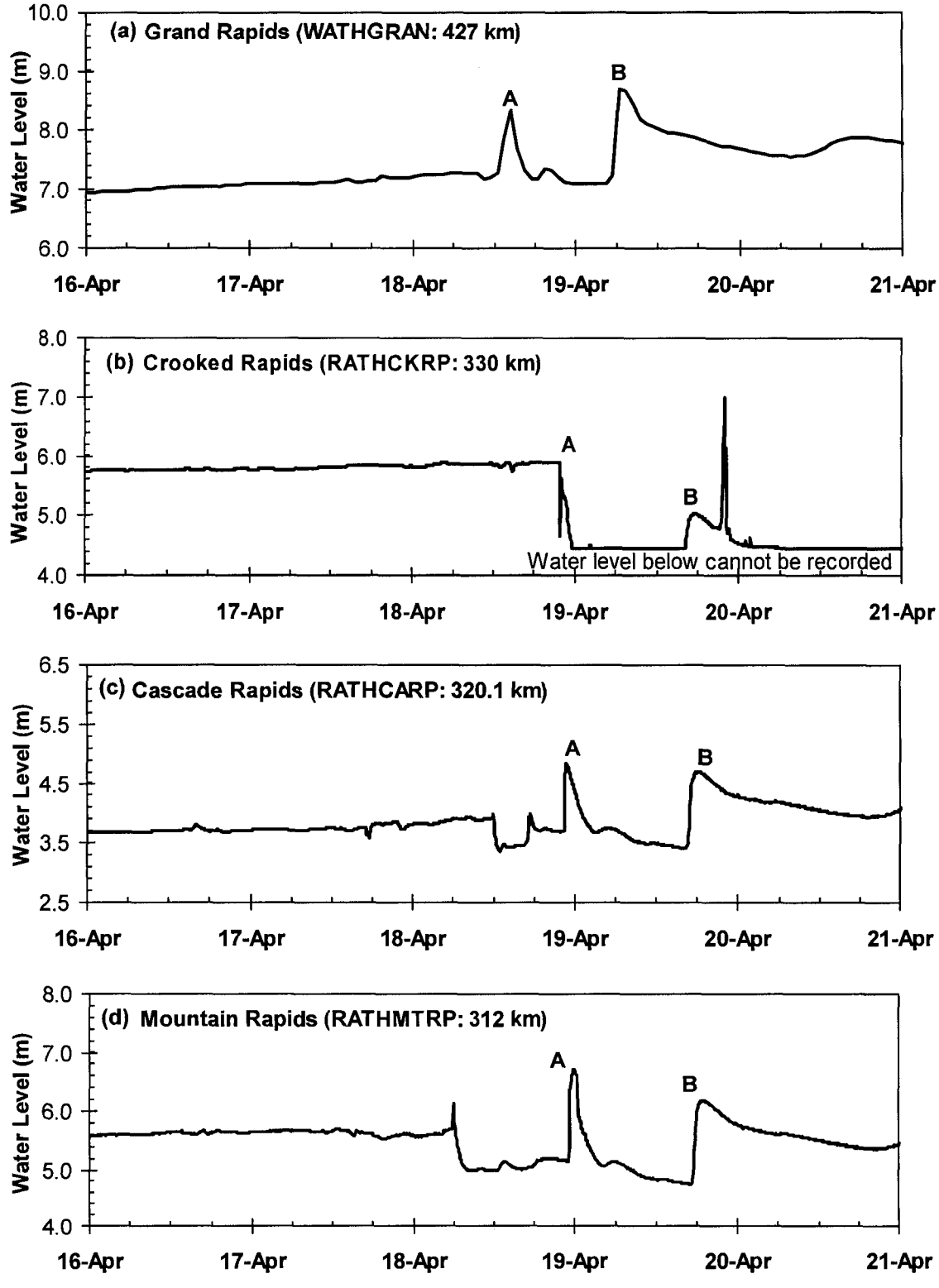

Figure 4-5 Water levels measured at remote stations WATHGRAN, RATHCKRP, RATHCARP, RATHMTRP during the 2007 breakup.

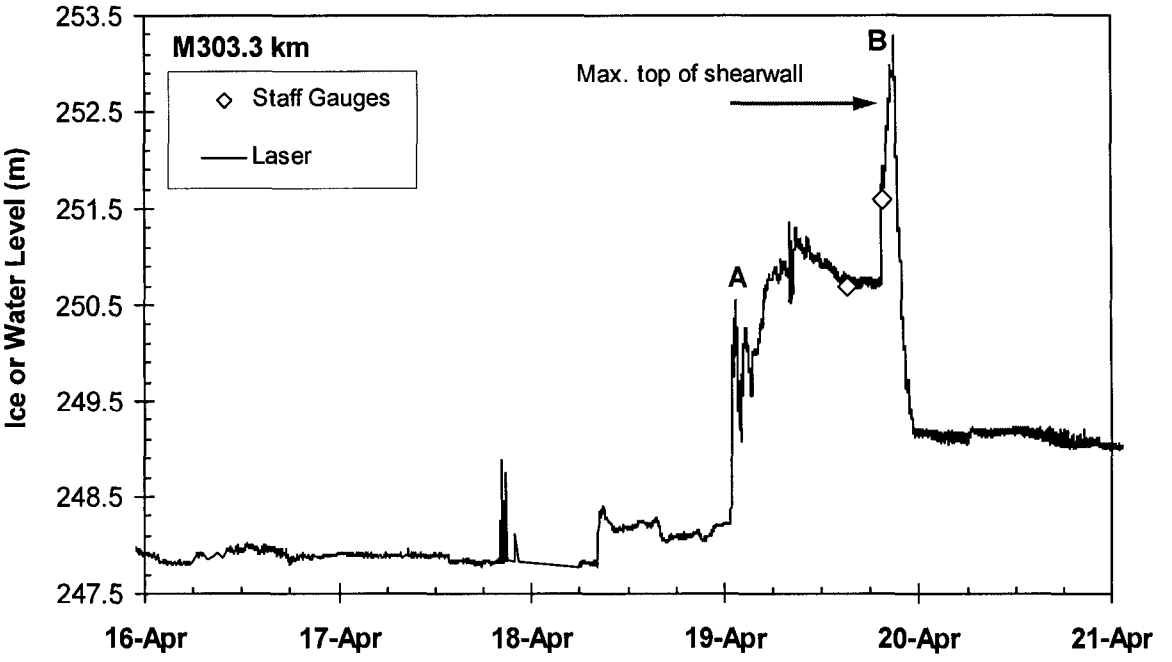

Figure 4-6 Water and ice levels measured at station M303.3 using laser rangefinder and staff gauges.

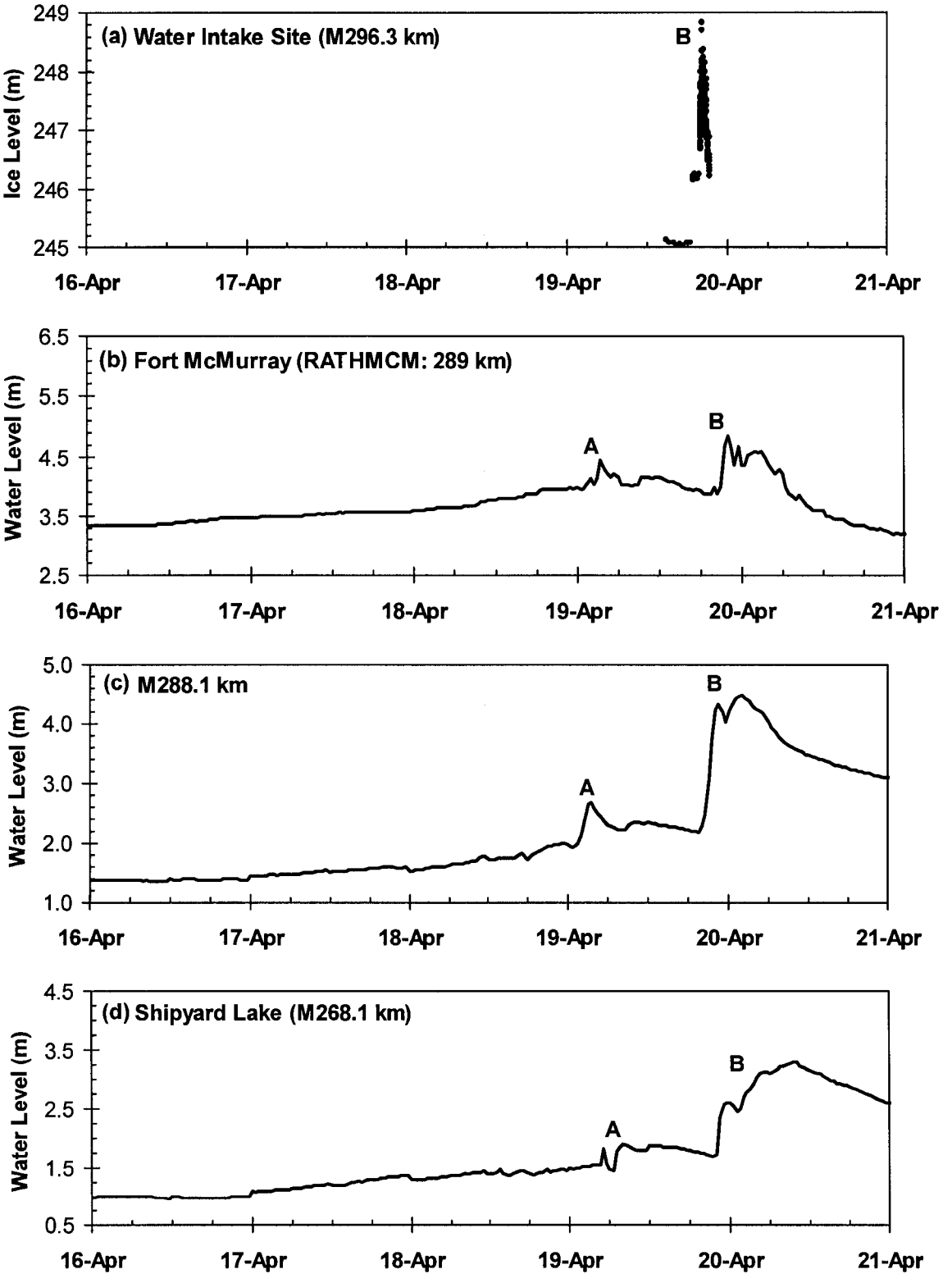

Figure 4-7 Top of ice level measured at water intake site and water level measured at RATHMCM, M288.1 and M268.1 during the 2007 breakup.

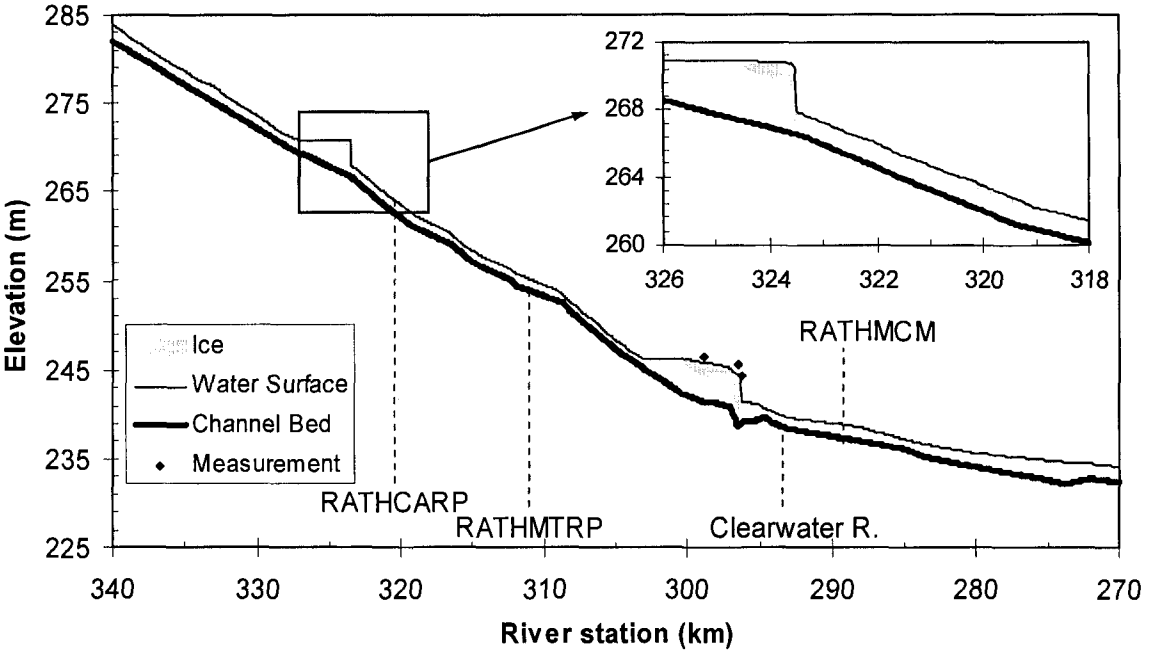

Figure 4-8 The initial water surface and ice jam profile on April 19, 2006, both computed using *River1-D*.

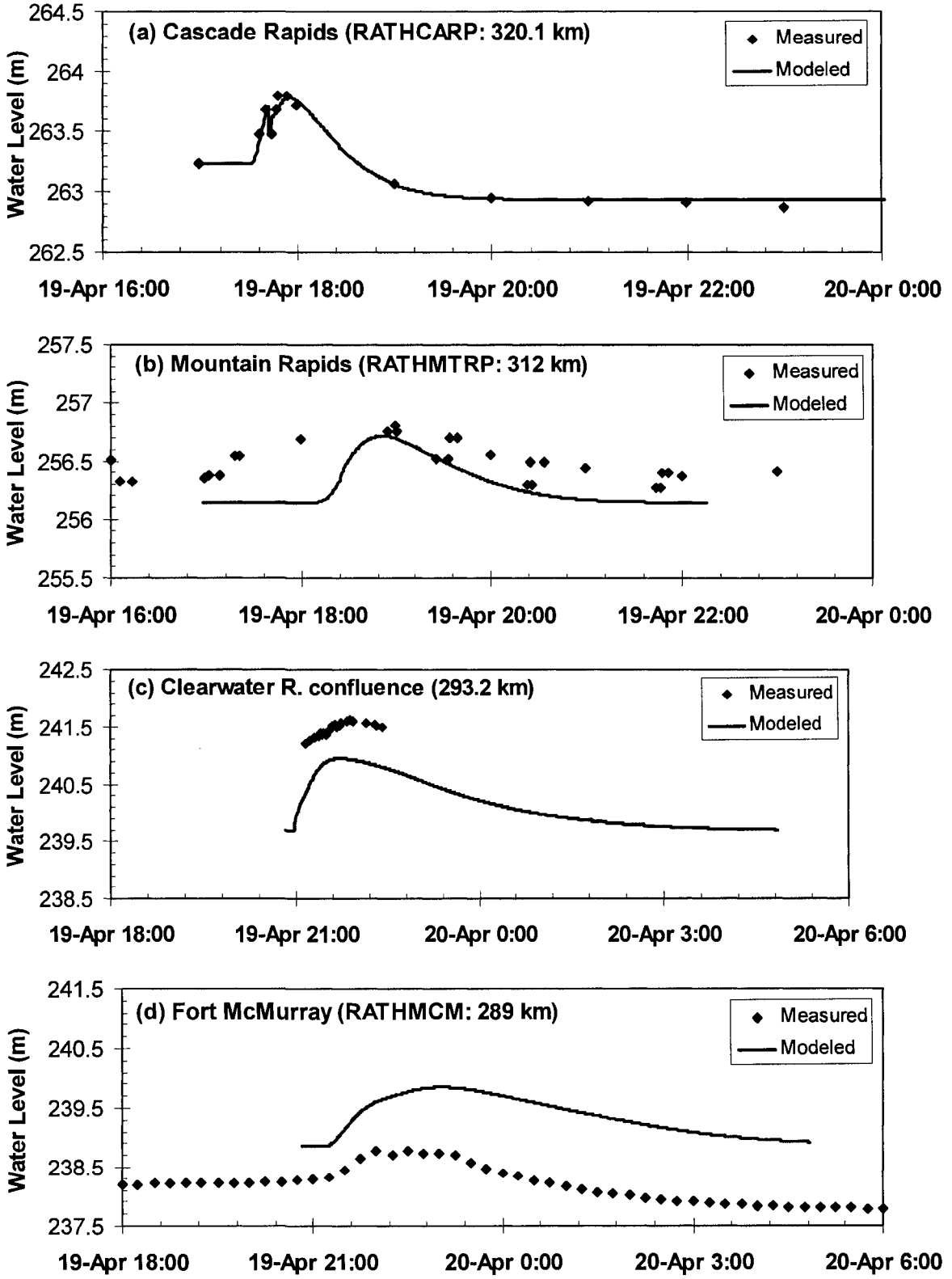

Figure 4-9 Comparison of measured and modeled stage hydrographs using *River1-D* at 4 stations during the ice jam release events of April 19, 2006.

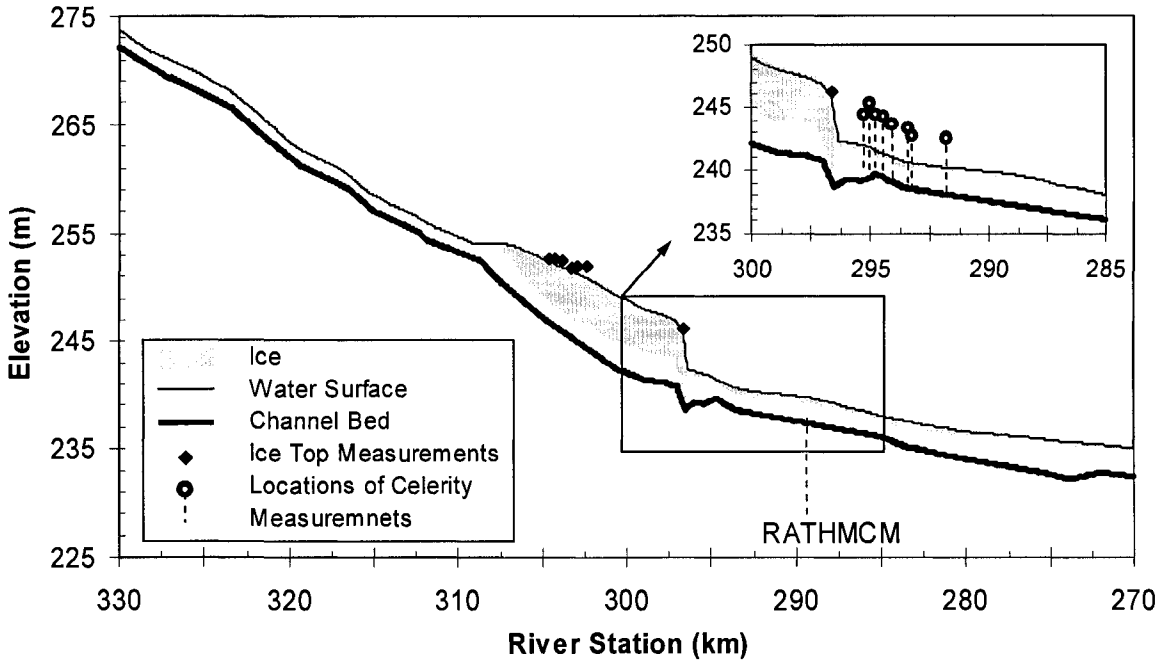

Figure 4-10 The initial water surface and ice jam profile of April 19, 2007, both computed using *River1-D*.

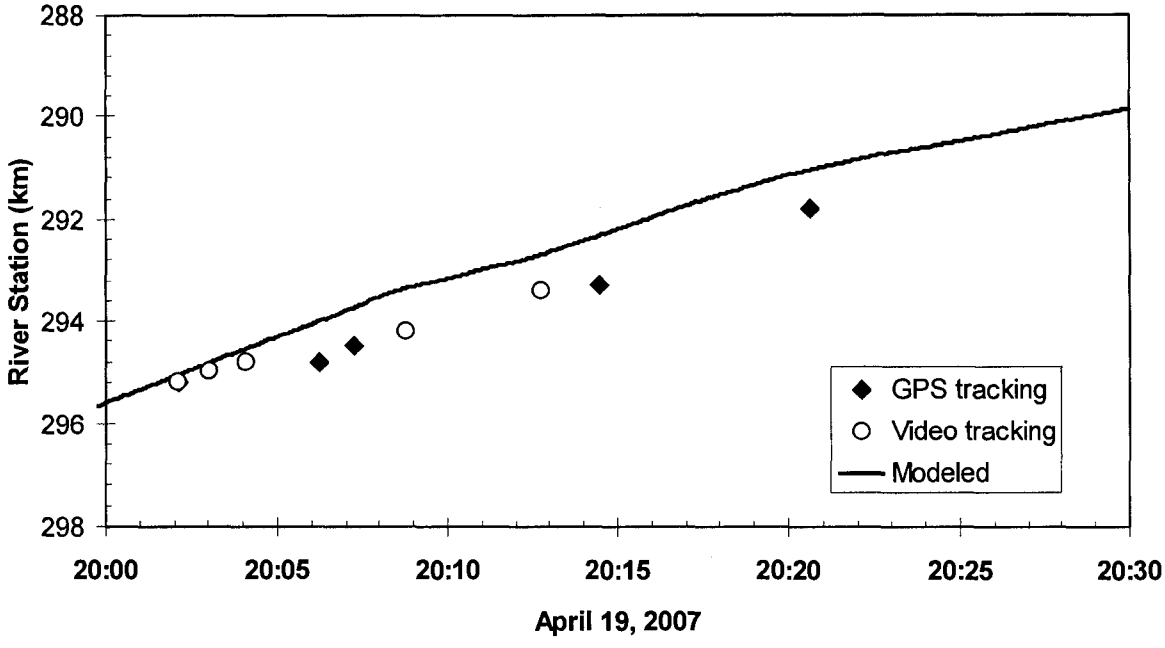

Figure 4-11 Comparison of observed and modeled breaking front location for the April 19, 2007 ice jam release event.

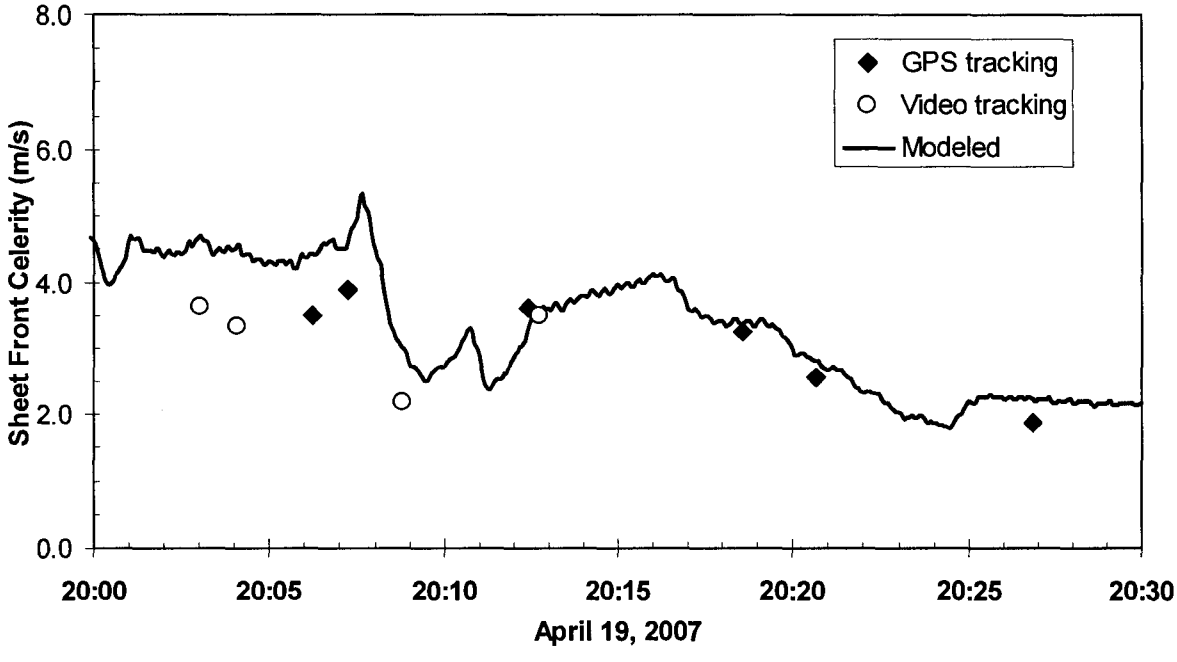

Figure 4-12 Comparison of observed and modeled breaking front celerity for the April 19, 2007.

4.7 References

Andres, D., Jasek, M. and Fonstad, G. (2005). Field and Theoretical Study of the Toe Region of a Consolidated Ice Cover. Proc., 13th Workshop on River Ice, CGU - Hydrology Section, Comm. on River Ice Processes and the Env., Hanover, NH, 22 pp.

Beltaos, S. (1978). Field investigations of river ice jams. Proc., 5th IAHR Symposium on Ice, Lulea, Sweden.

Beltaos, S. (1983). River ice jams: Theory, case studies and applications. Journal of Hydraulic Engineering, 109(10): 1338-1359.

Beltaos, S. and Moody, W.J. (1986). Measurements of the configuration of a breakup jam. NRWI Contribution 86-123, National Water Research Institute, Burlington, Ontario.

Beltaos, S., Burrell, B.C. and Ismail, S. (1994). Ice and Sedimentation Processes in the Saint John River, Canada. Proc., 12th IAHR Symposium on Ice, Trondheim, Norway, The Norwegian Institute of Technology, Trondheim, Norway, Vol. 1, pp. 11-21.

Beltaos, S., Ford, J.S., Burrell, B.C., Pedrosa, M., and Madsen, N.K. (1998). Remote measurements of temperature and surge levels in ice-laden rivers. Proc., 14th IAHR Symposium on Ice, Potsdam, N.Y., U.S.A. A.A. Balkema, Rotterdam, The Netherlands. Vol. 1. pp. 35–40.

Beltaos, S. and Roswell, R. (2001). Field Study of Pre-Breakup River Waves. Proc., 11th Workshop on River Ice, Ottawa, pp. 4-17.

Beltaos, S., and Burrell, B.C. (2005). Field Measurements of Ice-jam-release Surges. Canadian Journal of Civil Engineering, 32(4): 699-711.

Blackburn, J. and Hicks, F. (2002). Suitability of Dynamic Modeling for Flood Forecasting During Ice Jam Release Surge Events. American Society of Civil Engineering: Journal of Cold Regions Engineering, 17 (1): 18-36.

Doyle, P.F. and Andres, D.D. (1979). 1979 Spring Breakup and Ice Jamming on the Athabasca River Near Fort McMurray. Alberta Research Council, Edmonton, AB, Report SWE-79/05.

Healy, D. and Hicks, F. (2006). Experimental Study of Ice Jam Formation Dynamics. ASCE Journal of Cold Regions Engineering, 20(4): 117-139.

Healy, D. and F. Hicks (2007). Experimental Study of Ice Jam Thickening under Dynamic Flow Conditions. American Society for Civil Engineering, Journal of Cold Regions Engineering, 21(3):72- 91.

Khan, A.A., Steffler, P.M. and Gerard, R. (2000). Dam-Break Surges with Floating Debris. ASCE Journal of Hydraulic Engineering, 126(5): 375-379.

Kowalczyk, T.K. (2005). Analysis of Ice Jam Release Surges on the Athabasca River at Fort McMurray, AB. M.Sc. Thesis (supervisor F. Hicks), Department of Civil and Environmental Engineering, University of Alberta, Edmonton, AB.

Kowalczyk Hutchison, T.K. and Hicks, F. (2007). Observations of Ice Jam Release Events on the Athabasca River, AB. Canadian Journal of Civil Engr., 34(4): 473-484.

Mahabir, C. and Garner, L (2007). Athabasca River Ice Observations 2006-2007. Report of River Ice Engineering Team, Water Management Operations, Alberta Environment, Edmonton, AB.

Robichaud, C. (2006). Athabasca River Ice Observations 2005-2006. Report of River Engineering Team Regional Services, Alberta Environment, Edmonton, AB.

Saade, R.G. and Sarraf, S. (1996). Phreatic Water Surface Profiles along Ice Jams - An Experimental Study. Journal of Nordic Hydrology, 27(3): 185-202.

She, Y. and Hicks, F. (2006a). Modeling Ice Jam Release Waves with Consideration for Ice Effects. Cold Regions Science and Technology, 45(3): 137-147.

She, Y. and Hicks, F. (2006b). Ice Jam Release Wave Modeling: Considering the Effects Of Ice in A Receiving Channel. Proc., 18th IAHR Symposium on Ice. 28 Aug.-1 Sept. 2006, Sapporo, Japan, 125-132.

Wong, J., Beltaos, S. and Krishnappan, B.G. (1985). Laboratory Tests on Surges Created by Ice Jam Releases. Canadian Journal of Civil Engineering, 12(4): 930-933.

Zufelt, J.E. (1990). Experimental Observations of Shoving and Thickening: Comparison to Equilibrium Thickness Theory. Proc., 10th IAHR Symposium on Ice, Helsinki, Finland, pp. 500-510.

Zufelt, J.E. (1992). Modes of Ice Cover Failure during Shoving and Thickening. Proc., 11th IAHR Symposium on Ice, Banff, Alberta, pp. 1507- 1514.

5 Constitutive Model for Internal Resistance of Moving Ice Accumulations and Eulerian Implementation for River Ice Jam Formation[4]

5.1 Introduction

River ice jams occur when discrete ice floes amass to form a very thick and rough accumulation obstructing the passage of river flow. Ice jams can occur during freeze-up, as the ice cover is developing, or during mid-winter thaws; however, the most severe accumulations tend to develop during the breakup period, when the river discharge increases due to significant snowmelt runoff events. The obstruction of a river channel by an accumulation of ice floes can lead to rapid increases in upstream water levels, often occurring at rates far in excess of those observed for typical open water flood events. Peak water levels associated with ice jams can also be significantly higher than those observed under open water conditions at much higher discharges. Floods resulting from ice jams represent the greatest hazard presented by river ice (Ashton, 1986), which pose a significant threat to property and public safety.

Given the considerable magnitudes and rates of water level rise associated with ice jams, it is highly desirable to be able to predict the potential impacts of river ice jam occurrence. Most of the currently available numerical models for determining ice jam profiles and associated water levels (e.g., RIVJAM: Beltaos and Wong 1986, ICEJAM: Flato and Gerard 1986, and HEC-RAS: Daly and Vuyovich 2003), are based on static ice jam

[4] This chapter was submitted for publication in Journal of Cold Regions Science and Technology. It was submitted in June 2008 and is under review.

stability theory (Pariset et al. 1966, Uzuner and Kennedy 1976) and a steady gradually varied flow approximation. Steady flow models produce excellent results for stable ice jams configurations, but provide no information on the dynamics of ice jam formation and cannot determine the impacts of unsteady flow conditions on ice jam dynamics (e.g., as a result of hydro-peaking, snowmelt runoff and/or ice jam releases from upstream). Also, these static ice jam profile models cannot simulate the spatial and temporal variations in ice thickness, water level and discharge that occur during the jamming process even under steady carrier (ambient) flow conditions. Furthermore, since ice motion is not considered, these static ice jam models cannot predict when and where an ice jam will form.

More recently, numerical models have been developed to capture the dynamic aspects of ice jam formation. Shen et al. (1990) proposed the first model for dynamic ice transport in rivers. By considering the ice as a granular continuum, constitutive relationships of the internal stresses and bank shear were formulated based on limited knowledge at that time. The model provided a theoretical framework for analyzing the process of ice jam evolution, which cannot be described by the static ice jam models. Zufelt and Ettema (2000) developed a one-dimensional dynamic model to account for unsteady flow and ice momentum effects in ice jam formation. In their model, the ice jam was considered as a floating granular mass, following Rankine's passive pressure and the Mohr-Coulomb failure criterion. Such a stress theory describes the compressive strength of granular materials, and assumes that an ice jam is always at its limit equilibrium state. Their model was applied to explore the effects of unsteady inflow hydrographs on ice jam profiles in hypothetical situations. Since the approach based on Rankine's passive pressure and the

Mohr-Coulomb failure criterion is not compatible with the known relation between stress and deformation, Shen et al. (1993, 2000) in their two-dimensional ice dynamics model, DynaRICE, utilize a viscous-plastic constitutive model (Hibler 1979, with changes) in conjunction with a Mohr-Coulomb criterion to relate the internal resistance of the moving surface ice with the motion of ice, so that time-dependent forces and stresses can be handled. The hydrodynamic component of that model uses an Eulerian finite element method, while the ice dynamics component uses the Lagrangian method of smoothed particle hydrodynamics (SPH). DynaRICE has been used to simulate the ice transport and jamming processes on the upper Niagara River (Lu et al. 1999), and to evaluate the feasibility of using ice booms to reduce jamming (Liu and Shen 2000, Shen et al. 2000).

This paper presents a new one-dimensional numerical model for simulating the dynamics of ice jam formation. It is unique in that it employs a purely Eulerian frame of reference for both the ice dynamics and the hydrodynamic components of the model. Specifically, mass and momentum conservation equations, for the water and for the ice, are solved using the *Characteristic-Dissipative-Galerkin* (CDG) finite element method (Hicks and Steffler 1992) in an uncoupled sequence. Furthermore, a new constitutive model for determining the internal ice resistance is proposed, which eliminates the need for an artificial stoppage criteria for ice jam consolidation, as has been required by earlier models (e.g., Hibler 1979, Shen et al. 2000). This new constitutive model is shown to properly describe the stress and strain rate data obtained from an earlier experimental study of ice jam consolidation events (Healy and Hicks 2001, 2007; Healy 2006). The proposed model is tested with an analytical solution and compared to results obtained using Hibler's viscous-plastic constitutive model. The proposed model is also validated

with a series of experimental ice jam consolidation events (Healy 2006, Healy and Hicks 2007).

5.2 Model Description

The proposed model is built on the University of Alberta's public domain software *River1-D* which employs the CDG finite element scheme to solve the St. Venant equations for open channel flow. For the current application, a rectangular channel geometry formulation is used. Figure 5-1 shows the definition sketch of the ice-covered flow and the Cartesian coordinate system used: x is the longitudinal coordinate which follows the channel bed, and z is the depth coordinate. Mass and momentum conservation equations for the ice are incorporated into the *River1-D* model; and the open channel flow equations are accordingly revised for ice-covered flow. The two sets of equations for water and ice respectively are then solved using CDG method in an uncoupled sequence.

5.2.1 *Hydrodynamic Equations*

Assuming a floating ice accumulation (Figure 5-1), the conservation equation of water and ice mass can be written as:

$$[5\text{-}1] \quad \frac{\partial}{\partial t}\left[\rho A_w + \rho(1-N)s_i B t_i + \rho_i A_i\right] + \frac{\partial}{\partial x}\left[\rho Q_w + \rho Q_u + \rho_i Q_i\right] = 0$$

where: A_w and Q_w are the area and discharge of flow under the ice layer; ρ and ρ_i is the density of water and ice respectively; N is the volumetric ice concentration; s_i is the specific gravity of ice; A_i the ice volume per unit length, is defined as $A_i = NBt_i$; B is the channel width; and t_i is the ice thickness. Q_u is the water seepage discharge within the ice

layer, which is calculated in a similar way as in Shen et al. (2000); and Q_i is the ice discharge.

The conservation equation of the ice mass only is:

$$[5\text{-}2] \quad \frac{\partial}{\partial t}[\rho_i A_i] + \frac{\partial}{\partial x}[\rho_i Q_i] = 0$$

Combining equation [5-1] and [5-2] and dividing through by ρ, the mass conservation equation for water flow can be obtained:

$$[5\text{-}3] \quad \frac{\partial A_w}{\partial t} + \frac{\partial Q_w}{\partial x} = -\frac{\partial}{\partial t}[(1-N)s_i B t_i] - \frac{\partial Q_u}{\partial x}$$

The momentum equation of the water flow under the ice layer is:

$$[5\text{-}4] \quad \frac{\partial Q_w}{\partial t} + \frac{\partial (Q_w V_w)}{\partial x} + gA_w \frac{\partial H_w}{\partial x} = gA_w\left(S_o - \frac{\partial s_i t_i}{\partial x}\right) - \frac{\tau_b (B + 2H_w) + \tau_i NB}{\rho}$$

where: V_w and H_w are the velocity and the depth of flow below the ice layer respectively; S_o is the bed slope; and τ_b and τ_i are the shear stresses on the river bed and on the underside of the ice, respectively. The shear stresses are determined using Manning's equation:

$$[5\text{-}5] \quad \tau_b = \frac{n_b^2 |V_w| V_w}{R_b^{1/3}} \rho g$$

$$[5\text{-}6] \quad \tau_i = \frac{n_i^2 |V_w - V_i| (V_w - V_i)}{R_i^{1/3}} \rho g$$

in which n_b and n_i are the Manning's roughness coefficients for the channel bed and the ice bottom respectively; R_b and R_i are the hydraulic radius of the bed-affected, and ice-affected areas, respectively. Specifically:

$$[5\text{-}7] \quad R_b = \frac{1}{1+\alpha_H}\frac{A_w}{(B+2H_w)}$$

$$[5\text{-}8] \quad R_i = \frac{\alpha_H}{1+\alpha_H}\frac{A_w}{B}$$

where α_H is the ratio of the water flow area affected by the ice friction to the flow area affected by the bed friction; determined as (adapted from Shen et al. 1990, with changes):

$$[5\text{-}9] \quad \alpha_H = \left[\frac{n_i^2}{n_b^2}\frac{N(V_w - V_i)^2}{V_w^2}\right]^{3/4}\frac{B}{(B+2H_w)}$$

5.2.2 *Ice Dynamic Equations*

Considering the floating ice accumulation in the river as a continuum, the mass conservation equation for the ice layer can be written as:

$$[5\text{-}10] \quad \frac{\partial A_i}{\partial t} + \frac{\partial(V_i A_i)}{\partial x} = \lambda_2 \frac{\partial^2 A_i}{\partial x^2}$$

which is equation [5-2] divided through by ρ_i and added a dispersion term. V_i is the ice velocity; and λ_2 is a parameter accounting for longitudinal dispersion due to the non-uniform velocity distribution across the river (Fischer et al. 1979). In this model, λ_2 is assumed to be proportional to the ice velocity.

The momentum conservation equation can be written as:

$$[5\text{-}11]\quad \rho_i A_i\left(\frac{\partial V_i}{\partial t}+V_i\frac{\partial V_i}{\partial x}\right)=\mathbf{G}+\mathbf{P}+\mathbf{R}-\mathbf{F_B}+\mathbf{F_w}$$

in which the L.H.S. is the ice mass multiplying its acceleration; **G** is the downslope component of gravitational force; **P** is the pressure force; **R** is the internal ice resistance; $\mathbf{F_B}$ is the bank-to-ice friction force; and $\mathbf{F_w}$ is the water drag at the ice-water interface. Substituting the expression of each force and dividing through by ρ_i, equation [5-11] can be rewritten as:

$$[5\text{-}12]\quad \begin{aligned} &A_i\left(\frac{\partial V_i}{\partial t}+V_i\frac{\partial V_i}{\partial x}\right)+gA_i\frac{\partial(s_i t_i)}{\partial x}\\ &=gA_i\left(S_o-\frac{\partial H_w}{\partial x}\right)+\frac{1}{\rho_i}\frac{\partial(A_i\sigma)}{\partial x}-\frac{2A_iK_{xy}\tan\phi}{\rho_i B}\sigma+\frac{\tau_i NB}{\rho_i}\end{aligned}$$

in which σ is the internal resistance stress of the ice; K_{xy} is the lateral thrust coefficient; and $\tan\phi$ is the bank-to-ice friction coefficient.

Equations [5-10] and [5-12] are solved for A_i and V_i. The ice concentration N is calculated by:

$$[5\text{-}13]\quad N=\frac{A_i}{Bt_{io}}$$

in which t_{io} is the thickness of a single layer of ice. t_{io} is an input to the model, and can be taken as the average thickness of the ice blocks within the jam, or the thickness of the ice cover prior to breakup. If the calculated ice concentration is bigger than its maximum

allowable value, N_{max} , then it is set to be equal to N_{max}; and the ice thickness is modified to $t_i=A_i/(BN_{max})$, representing thickening due to consolidation.

5.2.3 *Constitutive Model for the Internal Resistance of the Ice Accumulation*

A constitutive model is needed to relate the internal resistance of the ice accumulation to its deformation. Here the focus is on compressive behaviour only, since the ice accumulation will strongly resist compressive deformation, while allowing dilation to occur with little or no stress (Hibler 1979). Hibler's viscous-plastic constitutive model has been widely used in sea ice mechanics and adapted with changes for river ice dynamic models (e.g. Shen et al. 2000). In the one-dimensional case, Hibler's viscous-plastic rheology is (Hibler 1979):

[5-14] $$\sigma = \eta\dot{\varepsilon} - \frac{P}{2}$$

in equation [5-14]: $\dot{\varepsilon}$ is the strain rate; and $\eta = P/(2|\dot{\varepsilon}|)$ is the viscosity, which becomes infinite for a zero strain rate. The value of σ would also jump from $-P$ (for negative strain rates) to zero (for positive strain rates). To avoid this singularity, Hibler (1979) bounded the viscosity with a very large value ($\eta_{max} = P/(2\dot{\varepsilon}_c)$; $\dot{\varepsilon}_c = 10^{-8}\sim10^{-6}\ s^{-1}$) when the strain rate is small ($|\dot{\varepsilon}| \le \dot{\varepsilon}_c$). Therefore, the relatively motionless status of the ice accumulation is actually approximated as a very slow flow, which is the reason that an artificial stoppage criterion must be employed in conjunction with Hibler's viscous-plastic constitutive model.

This paper proposes a new formulation of the constitutive model; as shown in Figure 5-2, it has a similar shape to that of Hibler's viscous-plastic constitutive model for the portion describing tensile strain rate, where the stress quickly goes to zero and remains there; whereas the stress corresponding to the compressive deformation is formulated based on a one-m^{th} power law as follows:

$$[5\text{-}15] \quad \sigma = P(\dot{\varepsilon})^{1/m} T^{1/m} - P$$

in which T is a time scale parameter which is used to give the right dimensions; and m is an integer representing which power law is adopted. The model was not found to be exceptionally sensitive to the values of T and m chosen. Values of T and m equal to 1 and 7, respectively, were employed for illustrative purpose. The pressure term P is formulated as:

$$[5\text{-}16] \quad P = \tan^2\left(\frac{\pi}{4} + \frac{\phi}{2}\right)(1 - s_i)\frac{N}{N_{\max}}\frac{\rho_i g t_i}{2}$$

in which ϕ is the internal friction angle of ice; the other symbols are the same as defined in the former sections.

The main differences of the proposed constitutive model from Hibler's viscous-plastic constitutive model can be seen from Figure 5-2. First, the slope of the proposed model (i.e., the stiffness of the ice accumulation) increases as the strain rate decreases, which provides a much steeper slope than Hibler's model for very small strain rates. Thus, the proposed constitutive model achieves a better representation of the relatively motionless status of the ice accumulation. Second, the stress determined by this new constitutive

model does not have a constant value for compressive strain rates, but instead increases with increasing strain rate. In addition, the proposed constitutive model is a continuous function for compressive stresses and strain rates, which has obvious numerical advantages.

Data from an earlier experimental study of ice jam consolidation events (Healy and Hicks 2001, 2007) was analyzed to evaluate whether the proposed constitutive model appropriately describes the internal resistance of moving and stationary ice accumulations. In each of the experiments in that study, an accumulation of polyethylene model ice pieces was first allowed to form a stable floating cover in a flume at a low carrier discharge. This initial ice accumulation was then collapsed by means of a rapid increase in discharge, shoving to a much shorter and thicker ice jam. Tracking particles placed on the surface of the accumulation were monitored throughout the consolidation process. In addition, flow depths and discharges were measured at discrete points within the consolidating ice jam. Healy and Hicks (2001, 2007) provide a complete description of the experimental apparatus and methods. For this investigation, strain rates at numerous locations within the ice accumulations during consolidation were determined from the trajectories of the tracking particles. Specifically, the velocity of the tracking particles was first determined as the slope of their trajectories on an x-t plane. Then the strain rates were calculated as the velocity difference between two adjacent tracking particles divided by their initial distance. The corresponding internal resistance stresses were then determined by conducting a force balance calculation at discrete points along the ice accumulation. Specifically, the external applied force at a specific location was calculated as the sum of the down-slope component of ice weight and the cumulative water drag on

the bottom of the ice accumulation upstream of that point. The internal resistance stress at a specific location within the ice accumulation was then calculated as the total external force divided by the cross-sectional area of the ice at that location. Considering the error involved in the experimental measurements, a conservative estimation of the error for the strain rate and stress data obtained here is ±15% and ±20%, respectively.

Healy and Hicks (2001, 2007) conducted a total of 40 experimental simulations, from which thousands of data points (strain rate, stress) can be obtained. Figure 5-3 shows an example of the data, to provide a visual image of the constitutive relationship observed. Negative values in the figure denote compressive stress and deformation. The data are grouped in accordance with the ice thickness and the increase in discharge (ΔQ) used to initiate the shoving event, two obvious factors affecting the stress-strain rate relationship. Each subfigure in Figure 5-3 shows the data points obtained for the same ice thickness; while the differing symbols in each subfigure represent proportionally high (85%), medium (55%) and low (38%) discharge increases instigating the consolidation. In this manner, nine sets of data in total are presented. Also shown in Figure 5-3 are the stress and strain rate relationships determined using the proposed constitutive model and Hibler's viscous-plastic model.

Although the data did not collapse well enough to deduce a numerical formulation of the stress-strain rate relationship, Figure 5-3 still shows that the proposed constitutive model provides an improved visual agreement with the trend in the experimental data as compared to Hibler's model. First, all of the data sets show that the compressive stress increases as the strain rate increases, which supports the proposed constitutive model. Second, the stress-strain rate curve determined using the new model (solid curve in

Figure 5-3) is closer to the middle of the experimental data band, thus more representative of the data than that determined using Hibler's model (dashed curve in Figure 5-3). Also worth noticing is that, although the proposed constitutive model does not match any particular one of the three data sets in the same subfigure, it captures the flat portion of the data set with high discharge increase, and the steep slope of the data set with low discharge increase (as can be seen most clearly from Figure 5-3c).

5.3 Comparison of Constitutive Models

Both the proposed constitutive model and Hibler's viscous-plastic constitutive model were incorporated into the one-dimensional numerical model, and compared for a hypothetical ice jam formation event (adapted from Shen et al. 2000) for which an analytical steady-state solution is obtainable. Specifically, for a straight, uniform, rectangular channel with constant flow field, considering only the internal ice resistance and the water drag on the ice bottom, the analytical solution for the static ice jam profile can be written as:

$$[5\text{-}17] \quad t_i = \left(t_{io}^2 + \frac{2n_i^2 V_w^2 / R_i^{1/3}}{\tan^2(\pi/4 + \phi/2)(1 - s_i)s_i} x_j \right)^{1/2}$$

where x_j is the distance from the jam head.

For the same case, if bank friction is incorporated, the analytical solution for the static ice jam profile can be obtained by revising the solution of Pariset et al. (1966):

$$[5\text{-}18] \quad t_i = t_{eq}\left(1 - e^{-(2K_{xy}\tan\phi/B)x_j}\right)^{1/2}$$

where t_{eq} is the equilibrium ice thickness (Pariset et al. 1966):

$$[5\text{-}19] \quad t_{eq} = \left(\frac{Bn_i^2 V_w^2 / R_i^{1/3}}{K_{xy} \tan^2(\pi/4 + \phi/2) \tan\phi s_i (1 - s_i)} \right)^{1/2}$$

For the test case used here, the hypothetical channel is 4500 m long and 500 m wide. The constant flow field has a water velocity of 0.6 m/s and a zero water surface slope. Initially, the entire channel is covered by a single layer of ice 0.2 m thick, with an ice concentration of 60%. Manning's coefficient for the ice bottom is 0.053 and the internal friction angle of the ice accumulation is 46°. The ice moves downstream in response to the flow drag, and no ice is allowed to pass the downstream boundary. The results of the numerical simulation using the two alternative approaches for the constitutive model are shown in Figure 5-4 (no bank friction) and 5-5 (with bank friction), along with the analytical solutions. For clarity, only the portion of the domain containing the final ice jam profile is shown.

According to the analytical solution for the case where bank friction is neglected, the 4500 m-long initial ice cover should consolidate to an 825 m-long ice jam. The simulated ice thickness profile calculated using Hibler's viscous-plastic constitutive model (Figure 5-4a) experiences oscillations at 2 hours and the ice accumulation continues to consolidate in the following hours, resulting in a shorter and thicker ice jam than found by the analytical solution. The simulated ice jam continues consolidating indefinitely, even though quite a large bounding viscosity (~ 10^{10} Pas^{-1}) was used in this simulation. This demonstrates why an artificial stoppage criterion is required in conjunction with Hibler's viscous-plastic constitutive model. For instance, Shen et al. (2000) defined a

stoppage criterion based on the following conditions: (1) the ice velocity is less than 0.001 m/s; (2) the ice parcel is decelerating; and (3) the ice strain rate is less than 10^{-4} s^{-1}. When these conditions are satisfied, the stress is calculated by a linear extrapolation of its critical value (the value of the stress when the above three conditions are satisfied for the first time). Also, to avoid the indefinite creeping problem, Ji et al. (2004) extended the viscous-plastic law to a viscoelastic-plastic law, which is currently used in the updated DynaRICE model.

Figure 5-4b presents the numerical simulation results using the constitutive model proposed herein. It can be seen that the ice jam thickness profile approaches the analytical solution at 5 hours, and changes only very slightly during the ensuing 5 hours. Hence, the very steep slope of the proposed constitutive model for small deformation rates is effective at describing the stiffness of an ice accumulation approaching static state. The numerical and analytical solutions show a better agreement than that between Hibler's model and the analytical solutions.

Similar results were obtained for the case with bank friction considered as well (Figure 5-5). For this case, the analytical solution indicates that the final ice jam is longer (925 m in length) and thinner than the ice jam formed without considering the bank friction. Again, Hibler's viscous-plastic constitutive model cannot simulate the stoppage of the ice jam, and produces an ice jam that is shorter and thicker than produced by the analytical solution (Figure 5-5a). Again also, the proposed constitutive model provides a better match with the analytical solution (Figure 5-5b) than the Hibler's viscous-plastic constitutive model.

5.4 Model Application

The proposed model was next evaluated by comparing simulation results to measured experimental ice jam consolidation events (Healy and Hicks 2001, 2007). The experiments were conducted in a 32 m-long, 1.22 m-wide rectangular flume set to a slope of 0.00164. Discharges ranging from 33 to 63 L/s were supplied to the head tank and water levels at the downstream end were controlled by a weir and guide vanes. A 1.9 cm-thick, 1.22 m-long plywood sheet was positioned 24.5 m downstream of the head tank to simulate a free-floating intact ice cover, and a wire screen was fixed to its upstream edge to facilitate initiation of an ice accumulation. Manning's n for the flume ranged from 0.020 to 0.025 under open water conditions (Healy and Hicks 2007). The specific gravity of the model ice was 0.92 and the angle of repose was found to be 46^{o} (Healy and Hicks 2001).

For the hydrodynamic component of the proposed numerical model, the inflow hydrograph measured during each experiment was specified as the upstream boundary condition. Since the numerical model is not set up to incorporate the complex weir and vane arrangement in place at the downstream end of the experimental flume, the domain length in the simulated channel was extended a sufficient distance downstream of the ice jam toe, to allow a normal depth downstream boundary condition to be used without affecting the model reach of interest. For the ice dynamic component of the model, to be consistent with the experiments, the ice discharge was set to zero at the upstream boundary (no incoming ice during the shoving events) and at the location of the wire screen (no ice passing the toe). The roughness for the flume bed was calibrated to be 0.020 for the events simulated.

The model was first calibrated for one experimental consolidation event, which was instigated by a medium discharge increase. The calibrated parameters from this run were then used for all the test runs presented here. Manning's n for the ice was calibrated against the initial water levels along the ice accumulation prior to consolidation. It varies with the thickness of the ice accumulation based on:

[5-20] $$n_i = n_{io}\left(\frac{t_i}{t_{io}}\right)^{1/3}$$

in which n_{io} is Manning's coefficient for a single-layer ice; a value of n_{io} = 0.020 was used in the model. According to equation [5-20], Manning's n for the ice ranges from 0.020 to ~0.050 for all the experiment tests.

Healy and Hicks (2007) conducted experiments both with and without a wire mesh placed along the flume sidewalls, and found no significant difference in the water level and ice jam thickness measurements obtained for the two configurations. This suggests that the wire mesh used was insufficient to introduce a significant increase in the sidewall-to-ice friction effect, compared to the Plexiglas side wall alone. This finding suggests that it is appropriate to use a small lateral thrust coefficient, K_{xy}, in the numerical model. Therefore a value of 0.05 was used in the proposed model.

Of the 40 experimental tests conducted, three were selected for detailed presentation in this paper, representing a small (24%), medium (55%), and large (85%) step increase in inflow discharge. A summary of the salient parameters of these tests is provided in Table 5-1. The initial conditions for each numerical simulation were obtained by conducting a steady flow simulation using the proposed model, with the ice thickness profile set to be

equal to the measured thickness of the initial stable ice accumulation under the initial steady carrier discharge. These modeled initial conditions are shown in subfigure (a) of Figure 5-6 to 5-8. The measured water surface and ice accumulation profiles are also shown for comparison.

Subfigure (b) of Figure 5-6 to 5-8 presents the simulated and measured final stable ice jam profiles resulting from the rapid increase in discharge. It can be seen that the numerically simulated results match the measurements very well, both in terms of the water surface and the ice jam profile. A quantitative comparison between the modeled final profiles and the measurements is summarized in Table 5-2, where it is seen that the largest differences are around 5%. Small discrepancies are found to occur at the head of the jam, where the observed ice jam presents a "hook-like" shape and thus shows shorter length than the numerically simulated jam. Healy and Hicks (2007) indicated that the "hook-like" features were caused by the localized hydraulic thickening at the head (due to entrainment and deposition of ice floes at the leading edge) after the bulk of the ice consolidation was complete. This entrainment process is not considered in the current version of the proposed numerical model. Comparison between Figure 5-6a and b shows that the 24% increase in discharge only causes the ice jam to shorten and thicken slightly compared to the initial ice accumulation. For the other two tests with a 55% increase (Figure 5-7) and an 85% increase (Figure 5-8) in discharge, respectively, the final ice jam is much shorter and thicker than the initial ice accumulation. The initial jam profiles for these two tests are comparable (Figure 5-7 and 5-8) as they were formed under the same initial discharge condition. Comparing the final ice jam profiles for the two cases

(measured and modeled) it can be seen that the ice accumulation had been consolidated more for the higher step increase in discharge.

It is also of great interest to examine how well the proposed model simulates the highly dynamic aspects of these shoving events. Although the water level, ice thickness and discharge variations during actual ice jam formation events are difficult and dangerous to measure in the field, such information was provided by the experimental study. Figure 5-9 to 5-11 present the continuous time series data obtained at a station located 20 m downstream of the head tank for each of these same three experimental tests, respectively. Each figure contains three components. Subfigure (a) shows the continuous discharge measured at station 20 m, with the measured inflow discharge included for comparison. Subfigure (b) presents the continuous time series water level; and subfigure (c) presents the continuous time series continuous ice thickness (both for station 20 m). It can be seen from Figure 5-9 to 5-11 that the proposed model results are consistent with the continuous measurements at this location. The results are also compared quantitatively in Table 5-2, which indicates that the differences in many cases are in the order 5% or less (and therefore within the accuracy of the experimental tests). The largest discrepancy (35.98%) occurs between the modeled and measured ice thickness for the 24% increase in discharge (Figure 5-9c). This may be explained by the fact that, for this case, station 20 m is relatively close to the jam head and therefore the ice thickness measured at this station was influenced by localized hydraulic thickening, which (as discussed above) is not considered in the proposed numerical model.

For each test case, the step increase in inflow introduced a steep-faced dynamic wave front to the flume. By comparing subfigures (b) and (c) to (a) in Figure 5-9 to 5-11, it can

be seen that the water surface and ice thickness at station 20 m increased immediately in response to this step increase in inflow discharge. Also, by comparing the inflow hydrograph to that at station 20 m, it can be seen that the wave attenuated as it progressed downstream and water went into storage within both the ice jam and the backwater zones (Figure 5-9 to 5-11a). The volume of water that went into storage during the ice jam consolidation event can be determined by integrating the inflow and outflow hydrographs and calculating the difference between these two volumes. Table 5-3 presents the storage volume calculated in this manner for the three test runs considered here. The model results and the measurements appear to be consistent (the percentage differences are less than 15%), considering the cumulative error in the measurements of system outflow. It also can be seen from Table 5-3 that more water went into storage in response to the higher increases in discharge. This has important implications for flood forecasting. During river breakup, if the inflow discharge and the contributing ice volume could be estimated, then the flooding potential of an ice jam could then be evaluated using the proposed model.

5.5 Summary and Conclusion

This paper presents a one-dimensional numerical model for ice jam formation dynamics in rectangular channel. Both the hydrodynamic and ice dynamic components of the model use the pure Eulerian finite element method. Of particular interest is the development of a new formulation of the constitutive model for determining the internal resistance of the moving ice accumulation. The proposed constitutive model was shown to be supported by the stress-strain rate relationship observed during experimental studies of ice jam consolidation events. In comparison to the widely used Hibler's viscous-plastic

constitutive model, the proposed model shows numerical advantages and improved accuracy when applied to a hypothetical test with a known analytical solution. This new formulation of the constitutive model for determining the internal resistance of the moving ice accumulation could be easily adapted into other dynamic ice models.

The proposed numerical model was further validated using measurements obtained from a series of experimental ice jam shoving events caused by rapid increases in discharge. Three tests with proportionally low (24%), medium (55%), and high (85%) step increases in discharge were simulated with the model and it was found that both the profiles and thicknesses of the resulting stable ice jams were well simulated. Continuous measurements of the variations in discharge, water level, and ice thickness at a key station within the consolidating ice jams were also well reproduced by the proposed model.

Future development of the proposed model should include consideration of natural channel geometries, such as varied channel widths, channel sinuosity, bars and islands, giving the model the capability of predicting when and where an ice jam may form due to geometry constrictions. It is also desirable to include into the numerical model the influence of incoming ice runs on ice cover consolidation.

Table 5-1 Salient parameters of three experimental test runs.

Test date	Discharge (L/s)		Increase in discharge	Porosity	
	Initial	Final		Initial	Final
19-Jul-2001	42.9	53.0	24%	0.50	0.50
31-Jul-2001	33.7	52.4	55%	0.52	0.51
1-Aug-2001	33.5	61.9	85%	0.56	0.53

Table 5-2 Percent difference between the proposed model simulations and measurements for the three experimental test runs.

Increase in discharge	Final jam profile		Time series at Station 20 m		
	Water level	Ice Volume	Discharge	Water level	Ice thickness
24%	0.51%	5.74%	3.24%	0.95%	35.98%
55%	0.51%	4.68%	4.44%	0.86%	6.92%
85%	2.48%	4.23%	5.31%	1.07%	22.37%

Table 5-3 Comparison of proposed model simulations and measurements of the storage volume estimated from inflow minus outflow.

Test date	Increase in discharge	Measured (m^3)	Simulated (m^3)	Percent difference
19-Jul-2001	24%	0.52	0.49	5.43%
31-Jul-2001	55%	0.96	1.05	9.98%
1-Aug-2001	85%	1.88	1.61	14.21%

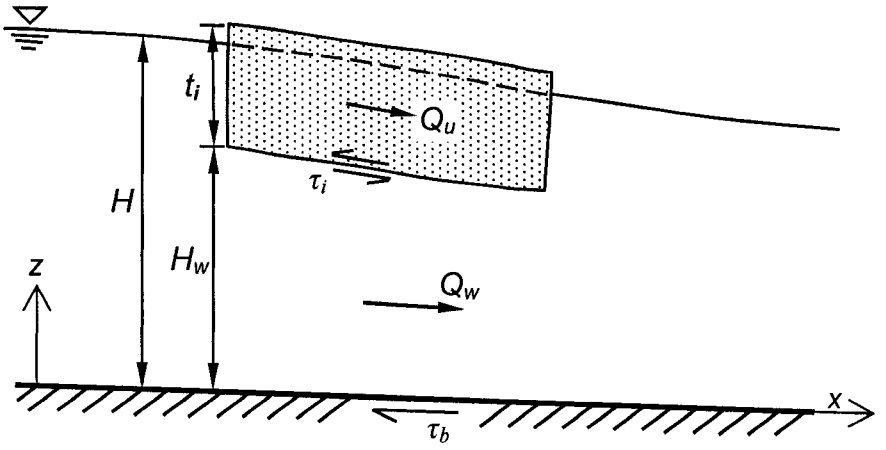

Figure 5-1 Definition sketch of ice-covered flow.

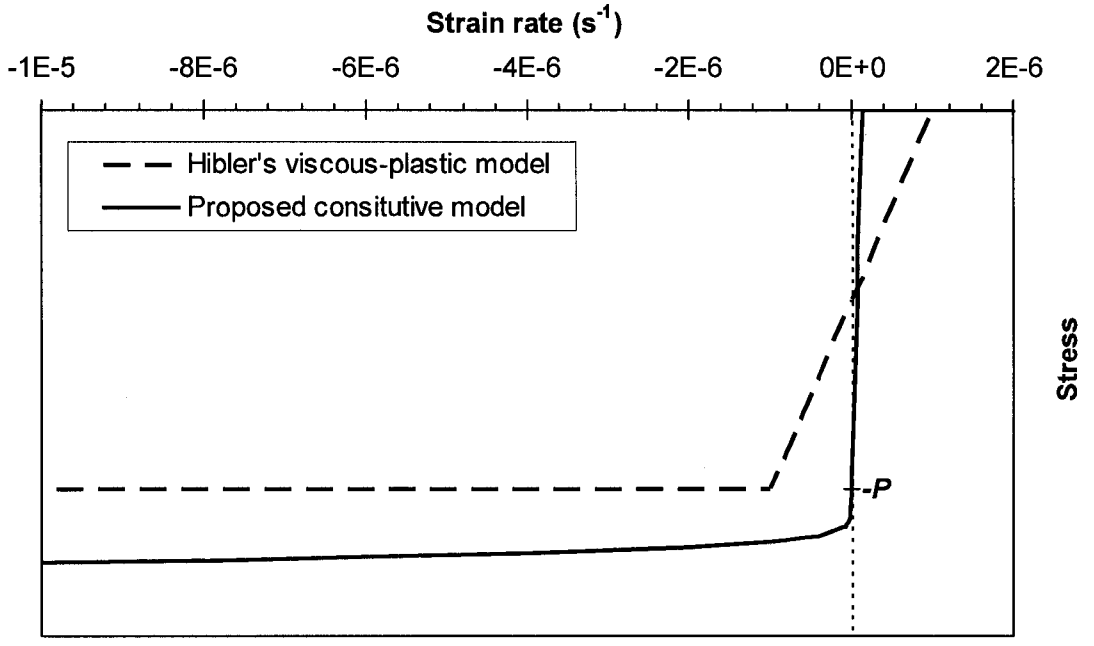

Figure 5-2 Comparison between the Hibler's viscous-plastic constitutive model (adapted from Hibler 1979 with changes) and the proposed constitutive model.

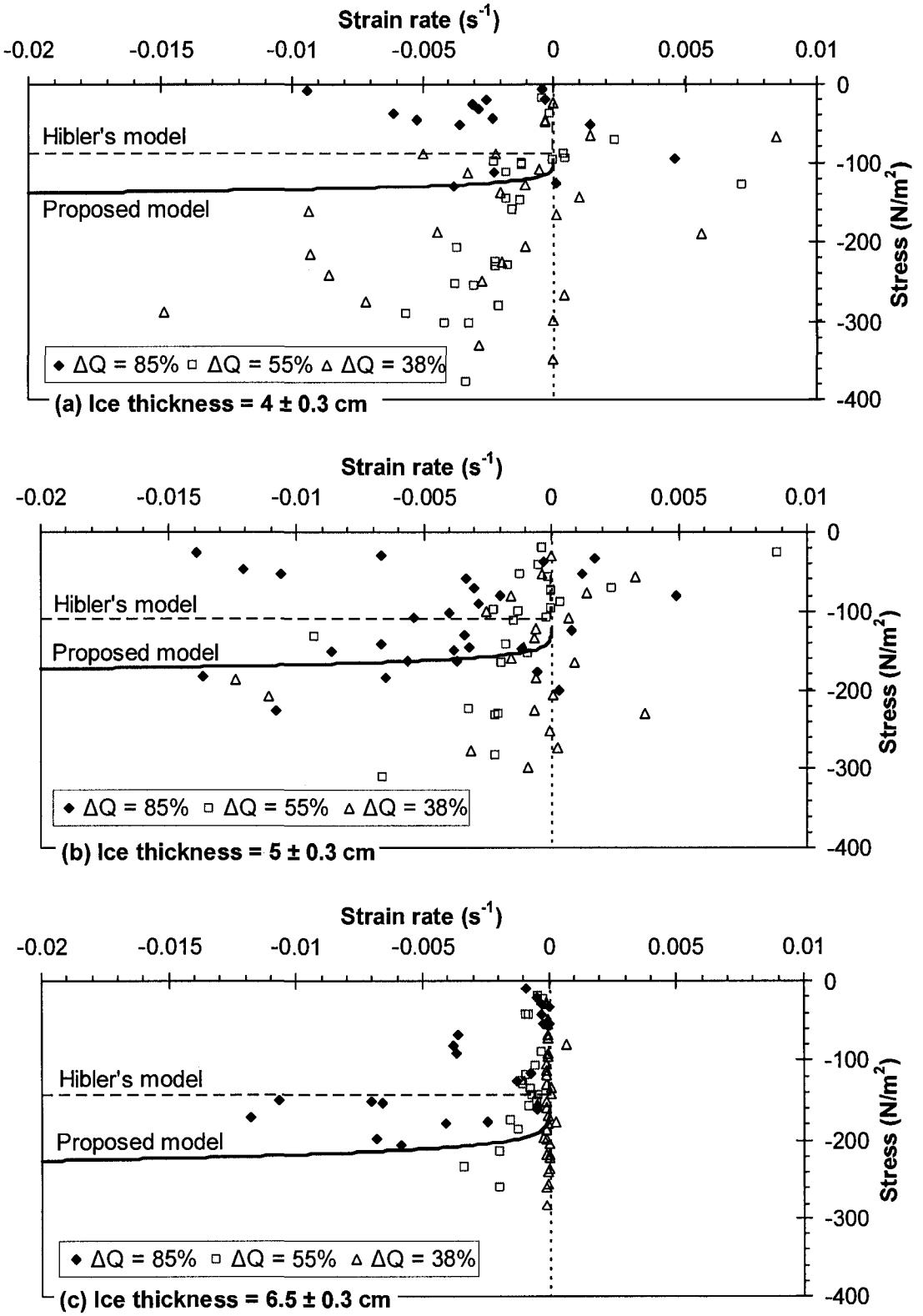

Figure 5-3 Stress-strain rate relationship obtained from laboratory experiments, and those determined using Hibler's viscous-plastic and the proposed constitutive models.

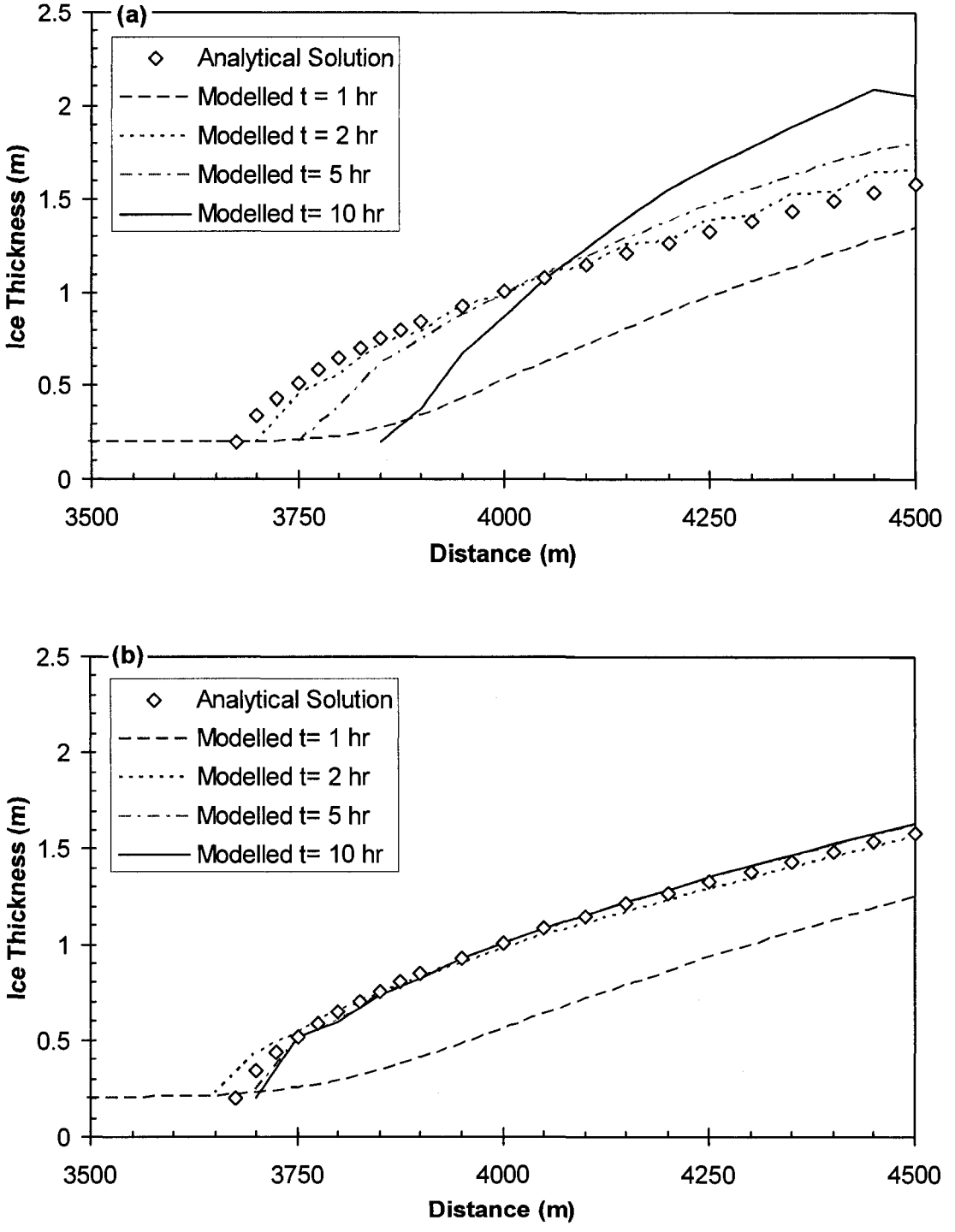

Figure 5-4 Comparison of simulation results using the two constitutive models with the analytical solution, for the case where bank resistance is neglected: (a) Hibler's viscous-plastic model; (b) proposed model.

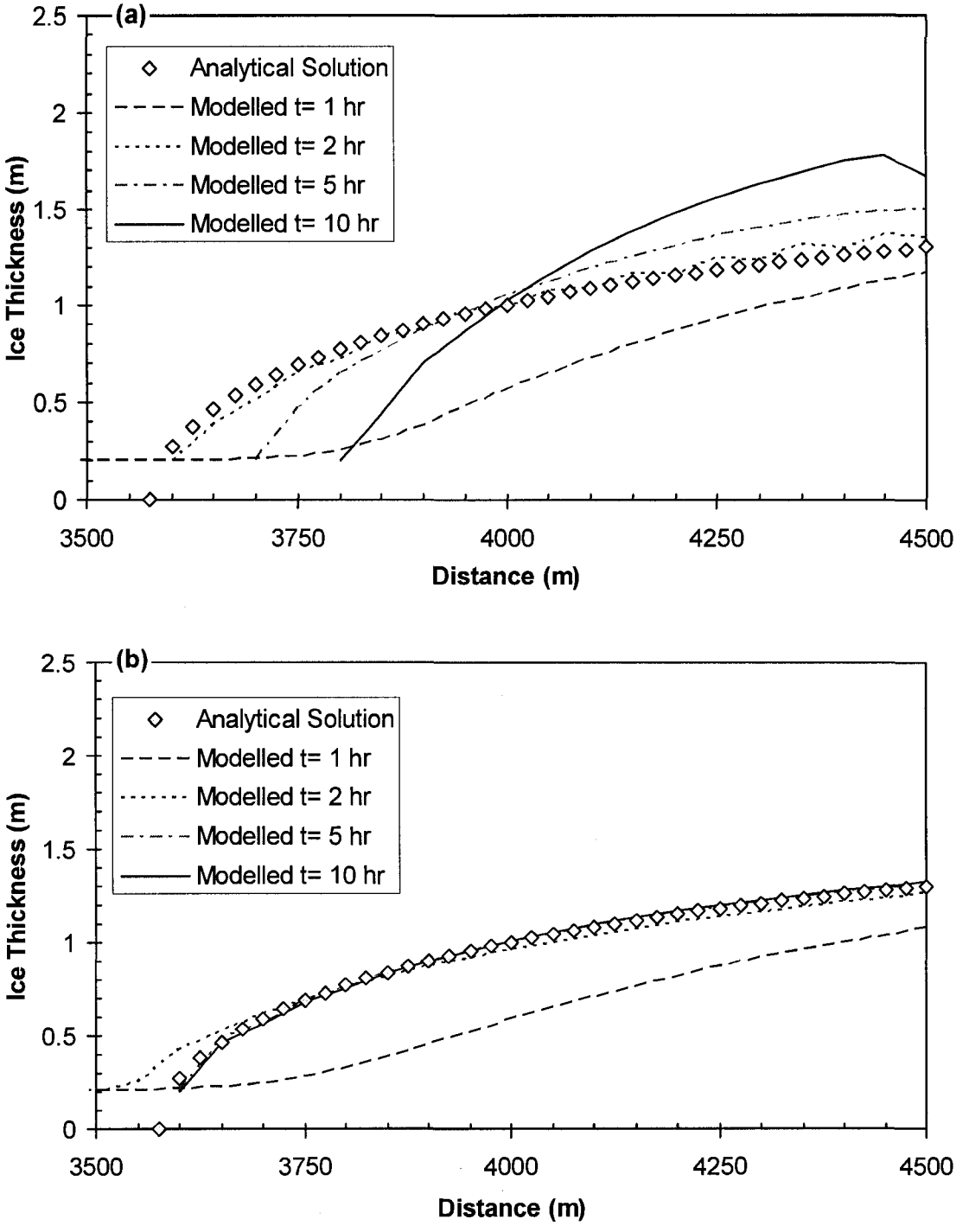

Figure 5-5 Comparison of simulation results using the two constitutive models with the analytical solution, for the case where bank resistance is included: (a) Hibler's viscous-plastic model; (b) proposed model.

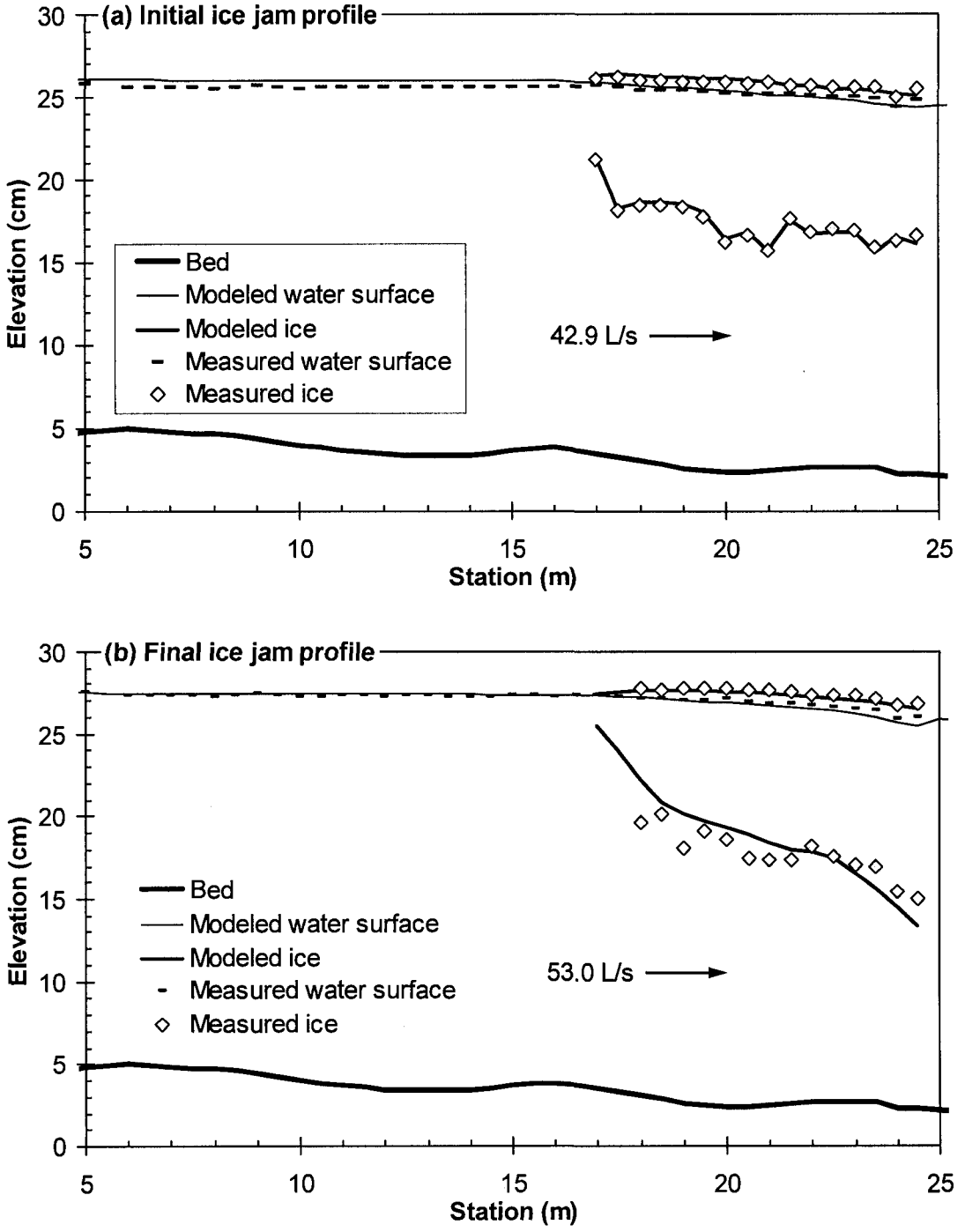

Figure 5-6 Comparison of proposed model results to experimental measurements for a 24% increase in discharge (a) initial ice jam profile (ice thickness input to model, water surface profile computed), and (b) final ice jam profile (both ice thickness and water surface profile computed).

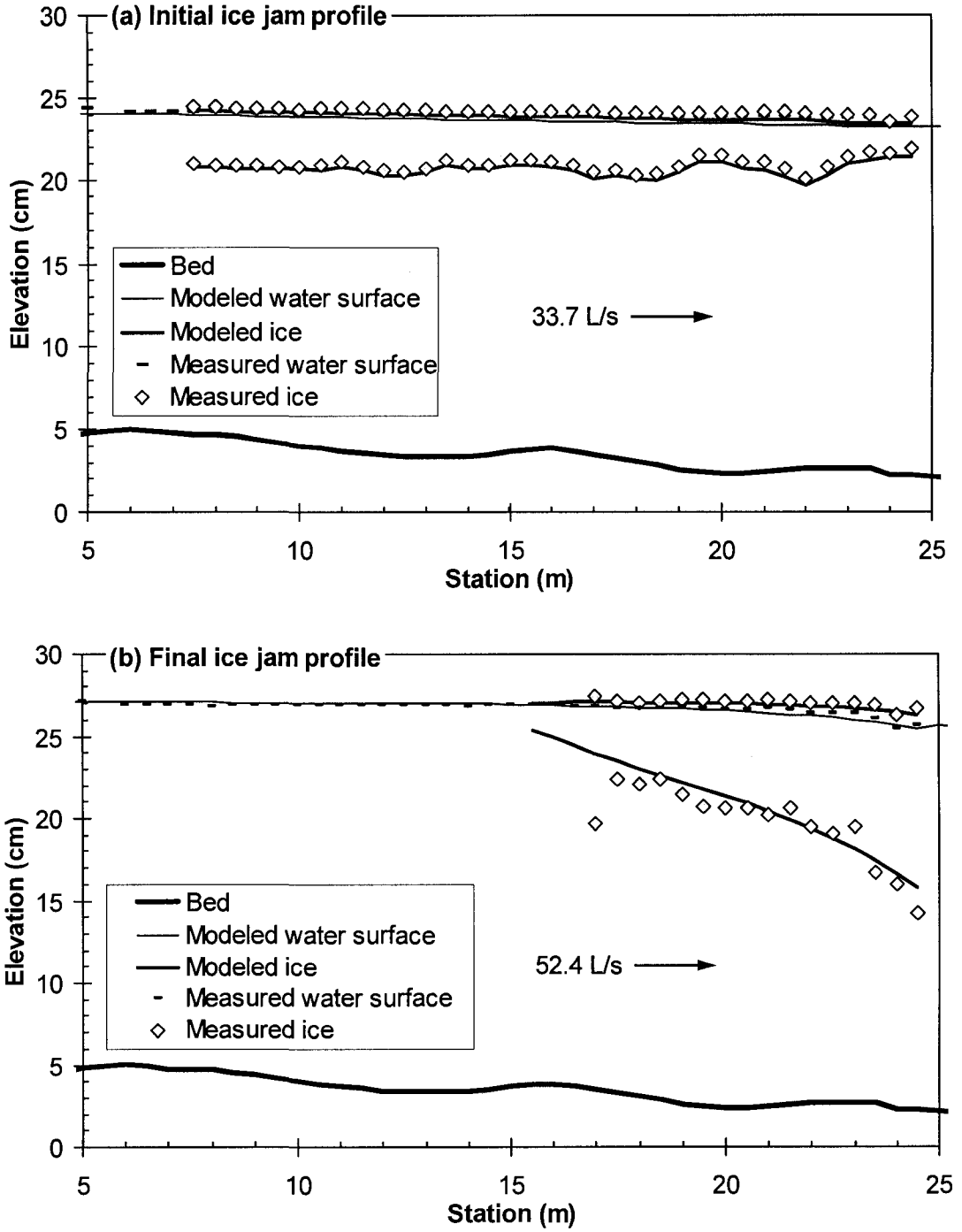

Figure 5-7 Comparison of proposed model results to experimental measurements for a 55% increase in discharge (a) initial ice jam profile (ice thickness input to model, water surface profile computed), and (b) final ice jam profile (both ice thickness and water surface profile computed).

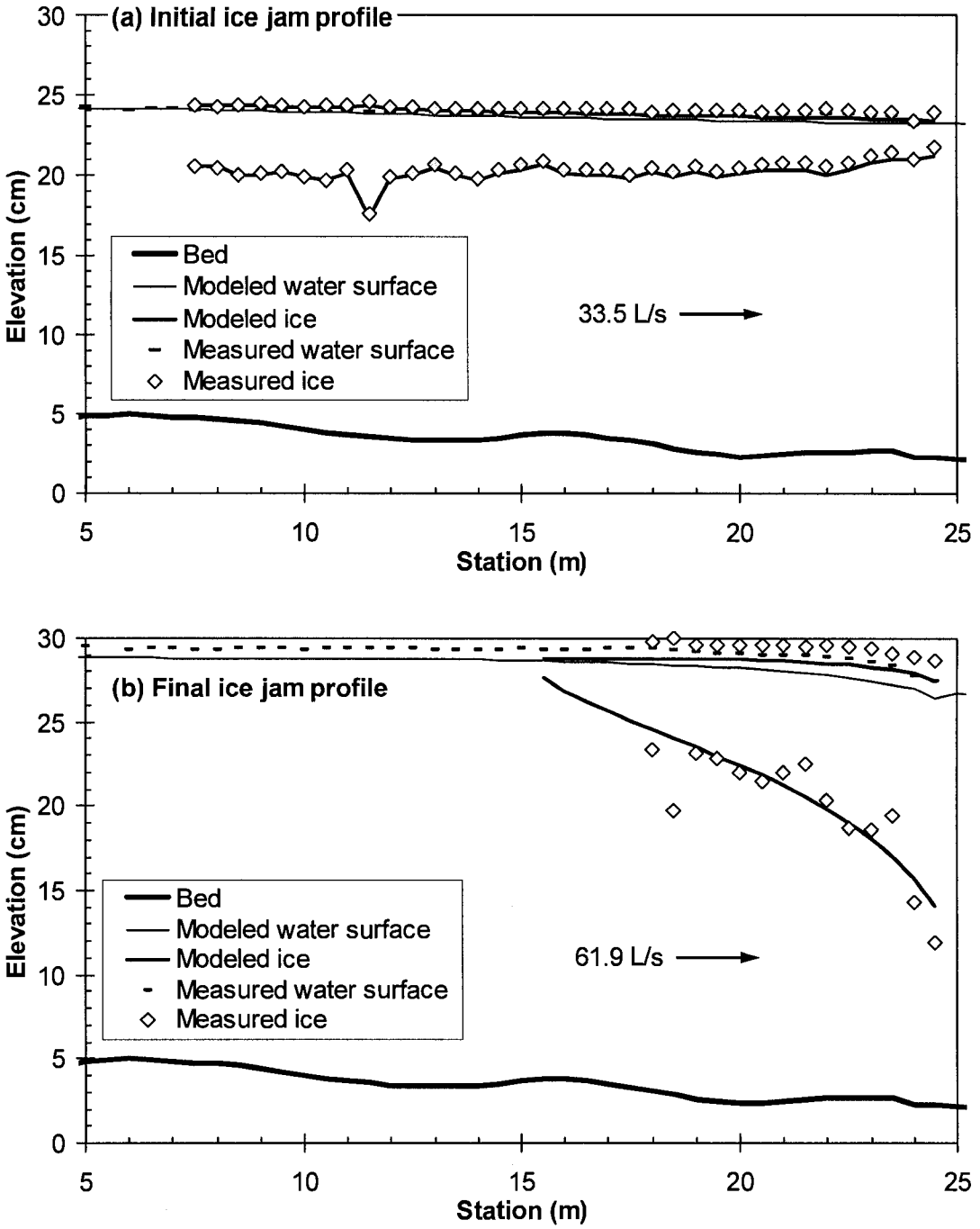

Figure 5-8 Comparison of proposed model results to experimental measurements for a 85% increase in discharge (a) initial ice jam profile (ice thickness input to model, water surface profile computed), and (b) final ice jam profile (both ice thickness and water surface profile computed).

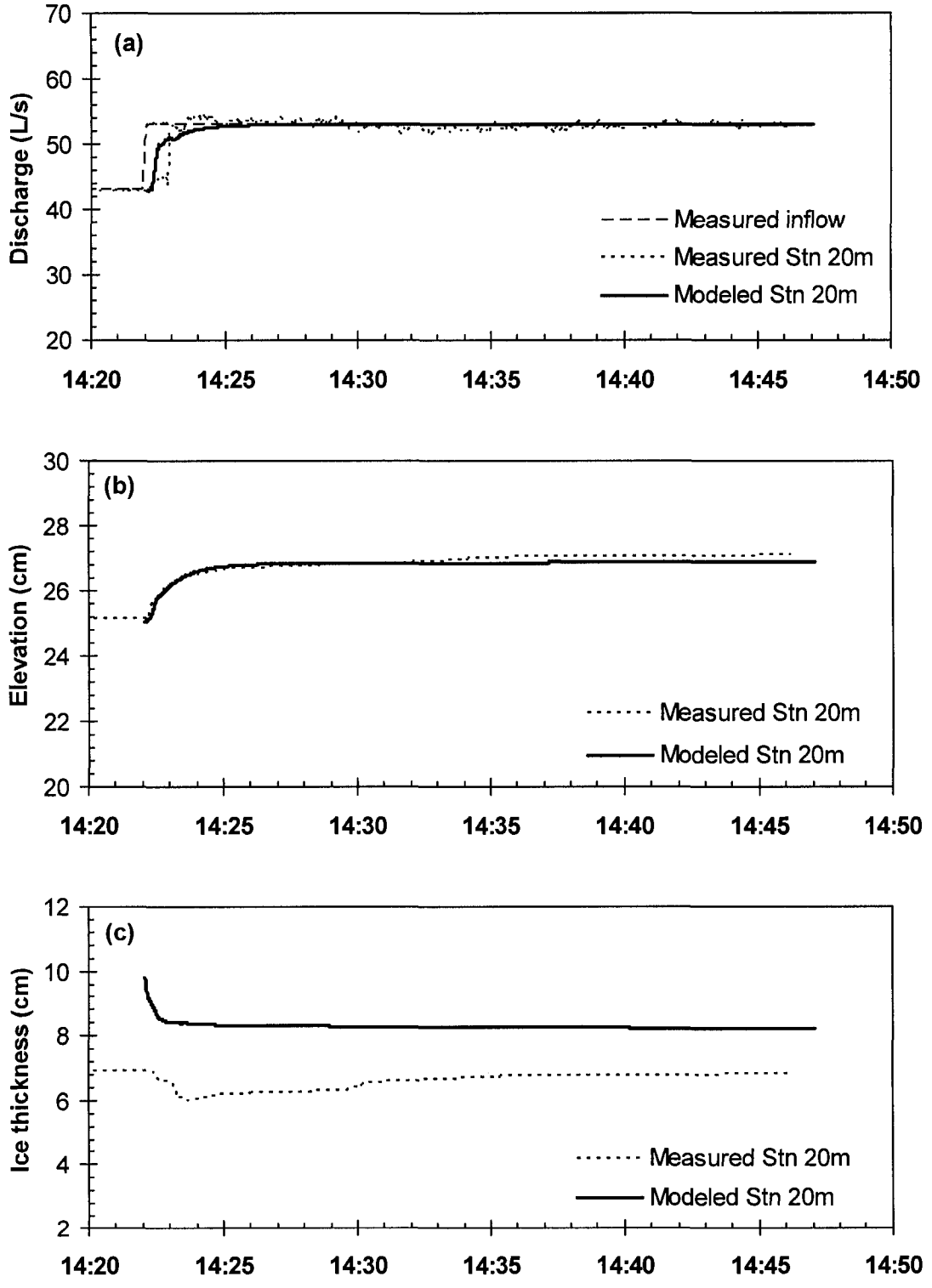

Figure 5-9 Comparison of proposed model results with continuous observations of (a) discharge; (b) water level; (c) ice thickness at station 20 m for 24% increase in discharge.

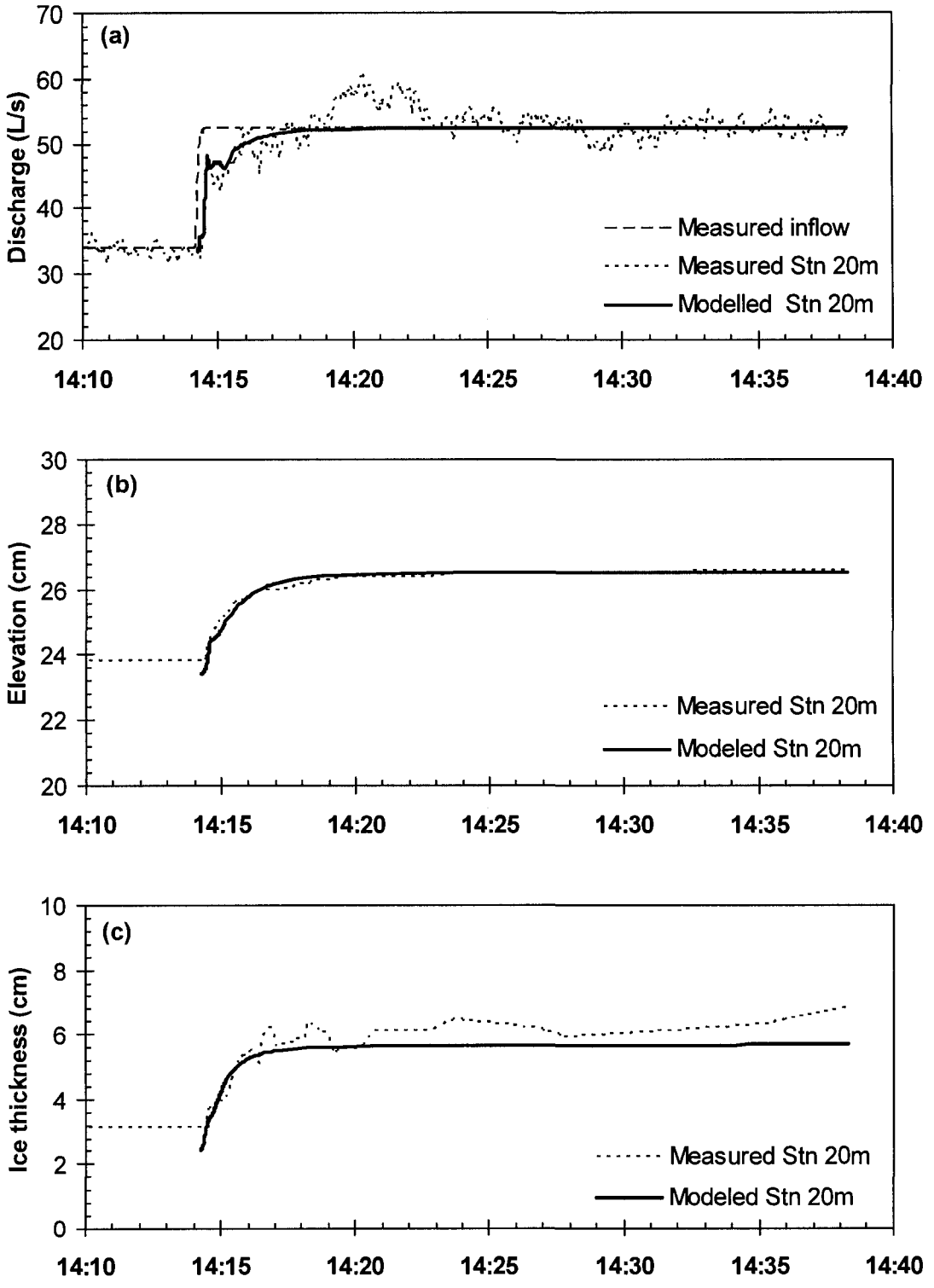

Figure 5-10 Comparison of proposed model results with continuous observations of (a) discharge; (b) water level; (c) ice thickness at station 20 m for 55% increase in discharge.

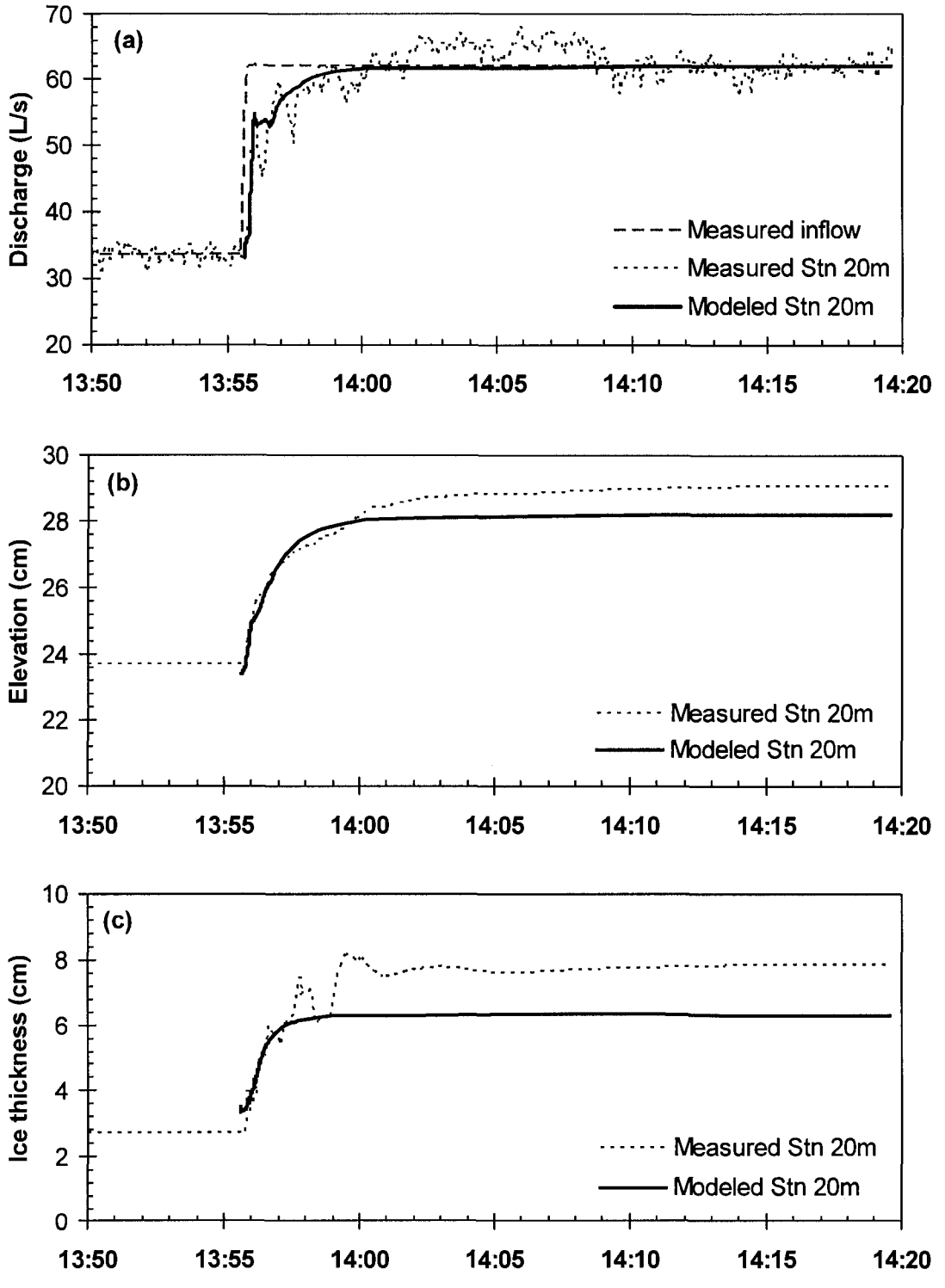

Figure 5-11 Comparison of proposed model results with continuous observations of (a) discharge; (b) water level; (c) ice thickness at station 20 m for 85% increase in discharge.

5.6 References

Ashton, G.D. (Ed.) 1986. River and Lake Ice Engineering. Water Resources Publications, Littleton, Co. USA.

Beltaos, S. and Wong, J. (1986). Downstream Transition of River Ice Jams. Journal of Hydraulic Engineering, 112(2): 91-110.

Daly, S. F., and Vuyovich, C. M. (2003). Modeling River Ice with HEC-RAS. Proc., 12th Workshop on River Ice, Canadian Geophysical Union–Hydrology Section, Calgary, Canada, 280–290.

Fischer, H.B., List, E.J., Koh, C.R., Imberger, J., and Brooks, N.H. (1979). Mixing in Inland and Coastal Waters. 5.1 Turbulent Mixing in Rivers. Academic Press, USA, 105-109.

Flato, G., and Gerard, R. (1986). Calculation of Ice Jam Thickness Profiles. Proc., 4th Workshop on Hydraulics of River Ice, Subcommittee of Hydraulics of Ice Covered Rivers, National Research Council of Canada, Montreal.

Healy, D. and Hicks, F. (2001). Experimental Observations on Ice Jam Shoving. Proc., 11th Workshop on River Ice. May 2001, CGU - Hydrology Section, Comm. on River Ice Processes and the Env., Ottawa, ON, pp. 122 -144.

Healy, D. (2006). Experimental Observations on River Ice Accumulations. Ph.D. Thesis (supervisor F. Hicks), Department of Civil and Environmental Engineering, University of Alberta, Edmonton, AB, 380 pp.

Healy, D. and Hicks F. (2007). Experimental Study of Ice Jam Thickening under Dynamic Flow Conditions. ASCE Journal of Cold Regions Engineering, 21(3): 72-91.

Hibler, W.D. (1979). A Dynamic Thermodynamic Sea Ice Model. Jounal of Phys, Oceanogr. 9: 815.

Hicks, F.E. and Steffler, P.M. (1992). A Characteristic-Dissipative-Galerkin Scheme for Open Channel Flow. ASCE Journal of Hydraulic Engineering, 118(2): 337-352.

Ji, S., Shen, H.T., Wang, Z., Shen, H., and Yue, Q. (2004). Ice Dynamics Model with A Viscoelastic-Plastic Constitutive Law. Proc., 17th International Ice Symposium, St. Peterburg, 274-281.

Liu, L. and Shen, H.T. (2000). Numerical Simulation of River Ice Control with Booms. US Army Corps of Engineers Cold Regions Research and Engineering Laboratory, Technical Report TR 00-10, Hanover, NH. USA, 28pp.

Lu, S., Shen, H.T. and Crissman, R.D. (1999). Numerical Study of Ice Jam Dynamics in Upper Niagara River. ASCE Journal of Cold Regions Engineering. 13(2): 78-102.

Shen, H.T., Chen, Y.C., Wake, A., and Crissman, R.D. (1993). Lagrangian Discrete Parcel Simulation of River Ice Dynamics. International Jounral of Offshore and Polar Engineering, 3(4): 328-332.

Shen, H.T., Shen, H., and Tsai, S.M. (1990). Dynamic Transport of River Ice. Journal of Hydraulic Research. 28(6):659-671.

Shen, H.T., Su J. and Liu, L. (2000). SPH Simulation of River Ice Dynamics. Journal of Computational Physics. 165: 752-770.

Pariset, E., Hausser, R. and Gagon, A. (1966). Formation of Ice Covers and Ice Jams in Rivers. Journal of Hydraulics Division, Proc. of the American Society of Civil Engineers, 92(HY6): 1-23.

Uzuner, M. S. and Kennedy, J. F. (1976). Theoretical Model of River Ice Jams. Proc. of the American Society of Civil Engineers, 102(HY9): 1365-1383.

Zufelt, J. E. and Ettema, R. (2000). Fully Coupled Model of Ice-Jam Dynamics. ASCE Journal of Cold Regions Engineering , 14(1), 24-41.

6 Application of *River1-D*: *Ice Jam* Model for Ice Jam Release Events

6.1 Introduction

The proposed model *River1-D*: *ice jam* is capable of simulating the formation process of ice jams, and its performance was presented in Chapter 5; the same model also has the capability to handle ice jam release events. What follows in this chapter is first a brief review of the available data for ice jam release events collected both in the laboratory and in the field. Some test cases were then chosen to evaluate the performance of the proposed model on predicting the ice jam release wave propagation, and the model results are then presented and discussed.

Wong et al. (1985) simulated a series of unimpeded ice jam release events (open water downstream of the released jam) via laboratory experiments. It was shown that the ice had little effect on wave propagation, upon comparison with Henderson and Gerard's (1981) theoretical solution and with a one-dimensional, unsteady flow, water-only numerical model (Beltaos and Krishnappan 1982). Khan et al. (2000) also conducted an experimental study, modeling ice jam release events with ice in the receiving channel. They found that the ice slowed down the wave speed, and increased the wave height. Both experiments were constrained by limited flume lengths, which represent only the very early phase of the release wave propagation compared to the extensive reaches over which ice jam release waves can propagate in actual rivers.

Field studies are therefore essential to facilitate a comprehensive investigation of the ice effects on the release wave propagation. Doyle and Andres (1979) reported a 3.6 m

increase in water level on the Athabasca River at the MacEwan Bridge in Fort McMurray, which occurred within 45 minutes of the release of an ice jam located 11 km upstream. Beltaos et al. (e.g. 1994, 1998, and 2005) reported on ice jam release events measured on the Saint John River, New Brunswick, in 1993, 1996 and 2002, respectively. Beltaos and Burrell (2005) also reported on a notable ice jam release event which occurred on the Resitgouche River, New Brunswick, in 2000. Kowalczyk Hutchison and Hicks (2007) documented a particularly extreme event on the Athabasca River in Alberta, in 2002, involving a 4.31 m release wave which rose at a rate 0.81 m/min at the jam toe. Stage hydrographs were also measured at seven downstream sites as this wave propagated over a 40 km reach.

Scientific data for river ice jam events is still quite challenging to obtain, and therefore scarce, especially from the perspective of model validation. Ideally one would have measurements of the initial ice jam thickness and water level profiles, and water level and/or discharge hydrographs at multiple stations downstream of the release point. It is also important to know the prevailing flow discharge, the nature of incoming waves and ice runs that impact on the ice jam, and the ice conditions in the receiving channel downstream of the jam.

Unimpeded ice jam release events for model validation and application were designed or chosen from the above citations to test the proposed model *River1-D: ice jam*. For this case, the ice cover in the receiving channel is not considered because it has a totally different failure mode compare to that of the ice accumulation itself, and this aspect of ice jam release is not included in the current version of the proposed model. Instead, the effects of ice from the released jam on the propagating release waves were explored.

Whether to choose the ice dynamics model (Phase 3 model), the model with simplified ice effects (Phase 1 model, as presented in Chapter 2), or the water-only model, under specified circumstances is also discussed.

6.2 Model Description

As described in Chapter 5, the *River1-D*: *ice jam* model employs the Characteristic-Dissipative-Galerkin (CDG) finite element scheme (Hicks and Steffler 1992) to solve two sets of equations for water and ice in an uncoupled sequence. The mass and momentum conservation equations for water flow under ice are:

$$[6\text{-}1] \quad \frac{\partial A_w}{\partial t} + \frac{\partial Q_w}{\partial x} = -\frac{\partial}{\partial t}\left[(1-N)\frac{s_i A_i}{N}\right] - \frac{\partial Q_u}{\partial x}$$

$$[6\text{-}2] \quad \frac{\partial Q_w}{\partial t} + \frac{\partial (Q_w V_w)}{\partial x} + gA_w \frac{\partial H_w}{\partial x} = gA_w\left(S_o - \frac{\partial s_i t_i}{\partial x}\right) - \frac{\tau_b (B + 2H_w) + \tau_i NB}{\rho}$$

The mass and momentum conservation equation for the upper ice layer are:

$$[6\text{-}3] \quad \frac{\partial A_i}{\partial t} + \frac{\partial (V_i A_i)}{\partial x} = \lambda_2 \frac{\partial^2 A_i}{\partial x^2}$$

$$[6\text{-}4] \quad \begin{aligned} & A_i\left(\frac{\partial V_i}{\partial t} + V_i \frac{\partial V_i}{\partial x}\right) + gA_i \frac{\partial (s_i t_i)}{\partial x} \\ & = gA_i\left(S_o - \frac{\partial H_w}{\partial x}\right) + \frac{1}{\rho_i}\frac{\partial (A_i \sigma)}{\partial x} - \frac{2A_i K_{xy} \tan\phi}{\rho_i B}\sigma - \frac{\beta_b V_i^2 A_i}{B} + \frac{\tau_i NB}{\rho_i} \end{aligned}$$

The constitutive model describing the compressive stress of the ice accumulation is:

$$[6\text{-}5] \quad \sigma = P(\dot{\varepsilon})^{1/m} T^{1/m} - P$$

in which the pressure term is also the same as that defined in Chapter 5:

$$[6\text{-}6] \quad P = \tan^2\left(\frac{\pi}{4}+\frac{\phi}{2}\right)(1-s_i)\frac{N}{N_{\max}}\frac{\rho_i g t_i}{2}$$

Notice that the ice accumulation would be mostly in its dilation status shortly after its release. Figure 6-1 shows a definition sketch of the proposed constitutive model with the emphasis on the dilation portion. When the tensile strain rate exceeds a very small value (e.g. 10^{-9} s^{-1}), the one-m^{th} power law (shown as the dashed line) is replaced by a straight line, following which the stress goes to zero linearly and then remains zero.

After an ice jam release, the bank-to-ice friction arising from the lateral confinement of the accumulation between the river banks ($2K_{xy}\tan\phi\sigma Nt_i$) quickly diminishes; while the friction arising from the collisions of ice rubble with the banks (or the remnant ice) becomes dominant. Therefore, this effect was included into the model, by introducing a new term $\beta_b V_i^2/B$ into the ice momentum equation [6-4]. β_b is an empirical constant which needs to be calibrated. All of the other variables in the above equations are the same as defined in Chapter 5.

6.3 Model Application

6.3.1 *Hypothetical Ice Jam Release Event in a Long Channel*

Liu and Shen (2004) developed a hypothetical ice jam release event in a long channel. The rectangular channel was 100 km long and 600 m wide. The channel slope of the first 30 km was 0.0004, and the remaining 70 km downstream was 0.0001. A constant inflow discharge of 2000 m^3/s was set at the upstream boundary. The water depth at the

downstream boundary changed automatically with water discharge. Manning's resistance coefficient was 0.030 for the channel bed and less than or equal to 0.060 for the underside of the ice accumulation. The Manning's n for the ice, n_i, was determined as a linear function of the ice thickness t_i:

$$[6\text{-}7] \quad n_i = n_{io}\left(\frac{t_i}{t_{io}}\right) \quad \text{and} \quad n_i \leq 0.060$$

in which: the single-layer ice thickness t_{io} was taken as 0.5 m; the Manning's roughness coefficient for a single-layer of ice n_{io} was taken as 0.025.

An identical test case was set up for the *River1-D: ice jam* model, except that the channel was extended for 50 km further downstream and a specified normal water depth was specified at the downstream boundary (to eliminate boundary effects from affecting the wave propagation solution). The initial steady state ice jam and water surface profiles calculated using the *River1-D: ice jam* are shown in Figure 6-2. The initial condition used for Liu and Shen's study (2004) is also shown in the same figure for comparison. It can be seen that the initial ice jam configuration computed using *River1-D: ice jam* is close to, although not exactly the same as, the one obtained by Liu and Shen (2004). The percentage difference of the ice jam profile is only slightly bigger than 5% (width-averaged longitudinal profile of ice jam was used for the one obtained by Liu and Shen when calculating the percentage difference). As can be seen in Figure 6-3, the longitudinal thickness profile computed from one-dimensional *River1-D: ice jam* model appears to be an upper envelope of that obtained from the two-dimensional DynaRICE model, which included the cross-channel variations. The data for the DynaRICE model presented in Figure 6-3 was provided by Dr. Hung Tao Shen (2008).

Once the initial conditions were established, the ice jam was then released for a simulation period of 24 hours. Both the internal resistance and the bank friction were included in the model *River1-D*: *ice jam* model; with the bank-to-ice friction coefficient, β_b, being set to 5. The dispersion parameter λ_2 used in this case was 10. These values were determined by trail and error to produce optimal results for this test case. The simulated water level hydrographs at five different stations at, and downstream of, the original jam toe are presented in Figure 6-4; the simulated total water and ice discharge hydrographs at these five stations are presented in Figure 6-5. The corresponding results published by Liu and Shen (2004) from their two-dimensional flow and ice dynamics model (DynaRICE) are also shown in the corresponding figure. Although similar results were obtained at the five stations in comparison with Liu and Shen's results using the proposed model, discrepancies in both the water level and total discharge hydrographs were noted. By comparing the two models' results, it can be seen that the moving ice accumulation provides smaller resistance to the dynamic forerunner of the released wave in the proposed model than in the DynaRICE model. Specifically, the first peak is higher and arrives earlier than that simulated by DynaRICE (Liu and Shen 2004) for each site. This is primarily because of the different methods of determining the internal ice resistance and bank-to-ice friction used in *River1-D: ice jam* and in DynaRICE. In addition, the discrepancy can also be attributed, in part, to the one-dimensional approximation of the original two-dimensional case.

A simulation was also carried out for the same test case neglecting the ice resistance effects in the proposed model. In this case, the ice mass was treated as water. The results from the above simulations with and without ice resistance effects are shown in Figure

6-6. It can be seen that the ice has significant effects on both water level and discharge hydrographs during the ice jam release event. The peak wave with ice resistance arrives much later, and the wave recedes much slower than the case without ice resistance. The ice resistance also greatly lowers the peak discharge, while it does not have any obvious effect on the peak water level at all of the five sites.

6.3.2 *Hypothetical Ice Jam Release Event in a Short Channel*

Liu and Shen (2004) developed a hypothetical ice jam release event in a short channel, as a demonstration of the jam release phenomenon in a reach between run-of-river power stations. In their test case, a constant water discharge of 3600 m^3/s was specified at both the upstream and downstream boundary of a 28 km long and 600 m wide rectangular channel. The bed slope of the channel was 0.00012. The Manning's roughness coefficient was 0.018 for the channel bed and less than or equal to 0.050 for the underside of the ice accumulation. The Manning's n for the ice, n_i, was determined as a linear function of the ice thickness t_i:

$$[6\text{-}8] \quad n_i = n_{io}\left(\frac{t_i}{t_{io}}\right) \quad \text{and} \quad n_i \le 0.050$$

in which: the single-layer ice thickness t_{io} was taken as 0.5 m and the Manning's roughness coefficient for a single-layer of ice n_{io} was taken as 0.030.

An identical test case was set up for the *River1-D: ice jam* model. The *River1-D: ice jam* is first used to calculate the initial steady state ice jam and water surface profiles prior to release, as shown in Figure 6-7. The initial condition used for Liu and Shen's study (2004) is also shown in the same figure for comparison. It can be seen that the initial ice jam

configuration computed using *River1-D: ice jam* is close to, although not exactly the same as, the one obtained by Liu and Shen (2004). The percentage difference of the ice jam profile is only slightly bigger than 5% (width-averaged longitudinal profile of ice jam was used for the one obtained by Liu and Shen when calculating the percentage difference). Also, as can be seen in Figure 6-8, the longitudinal thickness profile computed from one-dimensional *River1-D: ice jam* model appears to be an upper envelope of that obtained from the two-dimensional DynaRICE model. The ice thickness data for the DynaRICE model presented in Figure 6-8 was provided by Dr. Hung Tao Shen (2008).

Once the initial condition for the unsteady simulation was achieved, the ice jam was then released. Both the internal resistance and the bank friction (bank-to-ice friction coefficient β_b was set to 5) were included in the model *River1-D*: *ice jam*. The dispersion parameter λ_2 used in this case was 10, being the same as in the previous test case. The simulated water level hydrographs at four different locations along the channel are plotted in Figure 6-9; the simulated total water and ice discharge hydrographs at the jam toe, and 8 km downstream of the toe are presented in Figure 6-10. The corresponding results published by Liu and Shen (2004) from their two-dimensional flow and ice dynamics model (DynaRICE) are also shown in Figure 6-9 and Figure 6-10 respectively. It can be seen that the proposed model provided similar water level and discharge hydrographs as compare to the DynaRICE model results at all the four stations examined. For the water level hydrographs, the maximum percentage difference between the two models results is less than 5%; but for the total water and ice discharge hydrographs, the maximum percentage difference can reach 20%. Differences can be attributed to the one-

dimensional approximation of the original two-dimensional case; and to different methods used to describe the internal ice resistance and bank-to-ice friction of the moving ice accumulation.

A simulation was carried out using the proposed model, but with ice resistance effects neglected. Ice mass was treated as water. The simulated water level and discharge hydrographs at the same four stations are shown in Figure 6-11 and Figure 6-12 respectively, along with the corresponding model results with ice resistance effects considered. It can be seen that the ice resistance has significant damping effects on the ice jam release wave. When neglecting ice resistance effects, the water level and discharge hydrographs showed that the released wave had been reflected several times before dissipation; while with ice dynamics fully considered, the released wave had been damped very quickly.

6.3.3 *Experimental Ice Jam Release Events*

Wong et al. (1985) carried out a series of laboratory tests to study the waves from ice jam release. The experiments were conducted in a 25.9 m long, 1.0 m wide and 0.75 m deep rectangular flume. Water entered the channel through a head box, and the water depth in the channel was controlled by a tailgate mounted at the downstream end. Ice jams were created by obstructing the passage of polyethylene ice floes with a porous gate. Lifting the gate rapidly led to release of the jams. The resulting waves were monitored at various locations along the channel by recording water levels. The speeds of the ice runs were also measured by measuring the time required for the model ice accumulation to travel a known distance between two specified locations. Five runs in total were made. Wong et

al. (1985) compared the experimental results with the model prediction of Beltaos and Krishnappan (1982), which considered ice as a portion of water and neglected the ice effects on the propagating wave. They reported that the agreement between the measured and predicted water levels was good for all stations and the predictions of ice speeds were fair. They concluded that ice has no discernible effect on the propagating wave, and that ice jam release events can therefore be appropriately simulated by a one-dimensional, open-channel flood routine model.

The *River1-D: ice jam* model was used to simulate two of the five experimental ice jam release events. The salient parameters for the two runs (Run No. 1 and Run No. 4) are listed in Table 6-1. The Manning's roughness coefficient for the flume bed was taken as 0.011, which is equivalent to the roughness height of 0.05 cm provided by Wong et al. (1985). Unfortunately, neither the total volume of the ice, nor the length of the ice jam was available. Thus approximate ice jam profiles, which gave the best match to the measured water levels, prior to release, were setup as the initial conditions for the model. Also not available was the downstream boundary condition, which was a time-dependent water level controlled by a tailgate in the experiments (Wong et al. 1985). In the proposed model, the flume length was extended to reduce the influence of the unknown downstream boundary condition. The initial condition setup for the *River1-D: ice jam* model is shown in Figure 6-13 (Run No. 1) and Figure 6-14 (Run No. 4). The locations where water levels were measured are also marked in the figures, with "F" and "W" denote float probe and wire probe respectively (see Wong et al. 1985).

The simulated time-series water level at various stations along the flume after jam release are presented in Figure 6-15 (Run No. 1) and Figure 6-16 (Run No. 4), along with the

measured wave (Wong et al. 1985) and the predictions of the model of Beltaos and Krishnappan (1982). Both were obtained by digitizing published graphs, since the numerical data is no longer available (personal communication with Spyros Beltaos). The bank-to-ice friction coefficient β_b was calibrated to be 1 based on the measured arrival time of ice front for Run No. 1. Ice speed measurements were unavailable for Run No. 4, thus the same value of β_b was used as for Run No. 1. The dispersion parameter λ_2 was set to 0.5 for both test runs. It can be seen that the predictions of *River1-D: ice jam* model do not match well with either the measurements or the predictions of Beltaos and Krishnappan's model. Clearly, since important information is missing, the model setup here has not fully reproduced the experimental setup. However, the predictions of *River1-D: ice jam* model do captured every wave passing by each station. In all the subfigures of Figure 6-15 (Run No. 1) and Figure 6-16 (Run No. 4), the first larger wave was due to the jam release, and all the following smaller waves were due to boundary reflections.

The ice effects on the propagating release wave in the two experimental runs were further studied. A simulation was carried out for both Run No. 1 and Run No. 4 using the same initial and boundary conditions as above, but neglecting the ice resistance effects by treating the ice mass as water. The simulated water level hydrographs at various stations downstream of the release point are shown in Figure 6-17 (Run No. 1) and in Figure 6-18 (Run No.4) respectively. The simulated results of water level hydrographs and ice thickness, with ice resistance considered, are also presented in the corresponding figure. It can be seen that for both runs, the ice resistance effects are not significant. This agrees with the conclusion of Wong et al. (1985) that the propagating wave was not affected by the presence of ice in the laboratory flume, and these experimental ice jam release events

can be appropriately simulated by a water-only model. Worth noticing is that the volume of modeled ice is relatively small comparing to the volume of water stored by and behind the ice jam in all these experimental test runs. Thus, the illustration that ice does not affect the propagating ice jam release wave may just reflect the fact that the ice volume was a very small proportion of the total ice-water mass released for these particular experiments.

6.3.4 *2002 Release Event on the Saint John River*

The *River1-D: ice jam* model was then applied to an actual event documented by Beltaos and Burrell (2005a and b): the 2002 ice jam release event on the Saint John River at the border of New Brunswick, Canada and Maine, United States. On 13 April 2002, two consecutive small ice jams formed near Ledges in the upper Saint John River. Figure 6-19 illustrates the study reach and shows the ice conditions prior to release. Although the profiles of the ice jams were not measured, Beltaos and Burrell (2005b) provided a description of ice conditions prior to release. There was a 3 km long ice jam with a 1.5 km long reach of open water downstream of it, followed by a 1 km long jam. Downstream of the second, shorter jam, there was a fragmented ice cover with a sizeable open lead observed near Ledges. The river was all open below this ice cover. The river upstream of the first, longer jam was also free of ice.

Figure 6-20 presents the initial steady-state ice jam and water surface profiles obtained with the proposed model. The channel geometry was approximated as a varying width rectangular channel, with bed profile and widths determined based on the actual channel geometry. Variation of the channel width along the study reach is shown in Figure 6-21,

from which it can be seen that the channel is much wider at the jam site than else where along the channel. Unperturbed flow discharge was reliably determined from concurrent water levels recorded at two hydrometric gauging stations operated by the United States Geological Survey (USGS) (Beltaos and Burrell 2005b): one is on the Saint John River at Fort Kent; the other is on the Fish River, just below the river mouth (Figure 6-19). The Manning's resistance coefficient of the river bed was taken as 0.035 upstream of Edmundston and 0.022 downstream of Edmundston, based on previous calibration under open water conditions of Beltaos and Burrell (2005b). The Manning's n for the ice, n_i, increased linearly with the increase of ice thickness, with a maximum value of 0.060.

At approximately 13:00 that day, the two ice jams released and sent waves and ice runs propagating downstream. It is unknown whether the two ice jams released simultaneously, or if the release of the upper jam preceded that of the lower jam (or vice versa). Water levels as the waves were passing by three downstream stations were monitored by Beltaos and Burrell (2005b). These stations are: near Ledges at approximately 500 m downstream of the toe of the lower jam; Fort Kent (Water Survey of Canada (WSC) station number: 01AD002) 8.7 km downstream of the toe of the lower jam; and Edmundston (WSC station number: 01AD004) 40.8 km downstream of the toe of the lower jam.

This simulation assumed that both jams released simultaneously. *River1-D: ice jam* model simulation results are shown in Figure 6-22, together with the measured water level rise at the Ledges, Fort Kent and Edmundston stations, for comparison. It can be seen that the proposed model successfully reproduce the wave as it passed by the station near Ledges. The rising limb of the water level hydrograph at the three stations is also

well captured. However, the modeled recession portions of the waves as they passed by Fort Kent and Edmundston do not agree well with the measurements. Reasons that may cause this discrepancy between the model and the field measurements include: the initial ice jam profiles are unknown and the calculated profiles are inaccurate; the loss of ice during the release event was not considered; the roughness of the underside of the ice accumulation was only crudely estimated; errors were introduced from the rectangular channel and one-dimensional approximations. Owing to the many complexities of ice jam release events in actual rivers, a simplified ice effects model (e.g. such as the Phase 1 model), which lumps many influencing factors into two empirical parameters (resistance parameter and dispersion parameter as discussed in Chapter 2), can sometimes provide better results than a much more sophisticated model (e.g. the Phase 3 model).

A simulation was also carried out for the same release event, but neglecting the ice resistance effects in the proposed model. The simulated water level hydrographs are shown in Figure 6-23. The results from the above simulation with ice resistance considered are also shown in the same figure to show the ice effects. It can be seen that the ice does have a significant effect on the waveforms as the wave propagates downstream. However, it is not as straightforward as in the former hypothetical cases. The ice lowered the wave peak at one station, but increased it at another station; it slowed down the recession of the wave at one station, but sped it up at another station. This is due to the highly variable bed slopes and channel widths, as can be seen from Figure 6-20 and Figure 6-21. Due to these geometry variations, the moving ice accumulation had been decelerated and accelerated several times as it traveled downstream.

6.4 Summary and Conclusions

The proposed *River1-D: ice jam* Phase 3 model was used to simulate hypothetical, experimental, and actual ice jam release events. The ice effects on the propagating wave produced by ice jam release events were investigated. It is found that the ice resistance effects are significant in the two hypothetical test cases and the actual release event; while not obvious in the experimental test cases. Comparing to the field cases, the experimental test cases had relatively deeper water and a smaller proportion of ice; thus the ice would not be able to greatly affect the water. Also, the length of the flume was much shorter (length about ten times the water depth) than those propagation lengths involved in the field test cases (thousands of water depths). Therefore, strong reflection by the boundaries may have concealed the ice effects on the ice jam release waves.

The model results of the two hypothetical ice jam release events showed that the ice resistance significantly changed the characteristics of the propagating release wave: that is, it lowered its peak discharge and caused the wave to recede much slower. Note that a constant value of the bank-to-ice friction coefficient in the proposed model was selected to give the best match with the model results obtained using the DynaRICE model. Whether or not it effectively represents the bank resistance to the moving ice accumulation for actual release events is still a question requiring further investigation.

Application of the proposed model to the 2002 Saint John River ice jam release event showed that the presence of ice in the river changed the characteristics of the propagating wave. The ice effects are not as simple and clear as in the two hypothetical events, as the wave height was lowered at one station, while increased at another; and the wave speed

was decelerated at one station, while accelerated at another. The many complexities and unknowns in the real world prevented accurate prediction of the flood wave propagation. A better prediction was actually obtained using the Phase 1 model with simplified ice effects (discussed in Chapter 2), since it lumped together many influence factors and thus their effects may be fortuitously counteracting each other, and this may be a case specific effect. However, deceleration of ice runs and reformation of new ice jams can only be simulated using a model with deterministic ice dynamics. More field measurements of river ice jam release events are necessary for further validation of the proposed model, and other existing models of this kind.

Table 6-1 Salient parameters of two experimental test runs.

Run No.	Discharge (m^3/s)	Flume slope	Level difference at the jam toe (cm)	Downstream depth (cm)
1	0.026	0.00005	15.0	18.0
4	0.020	0.00014	4.0	16.0

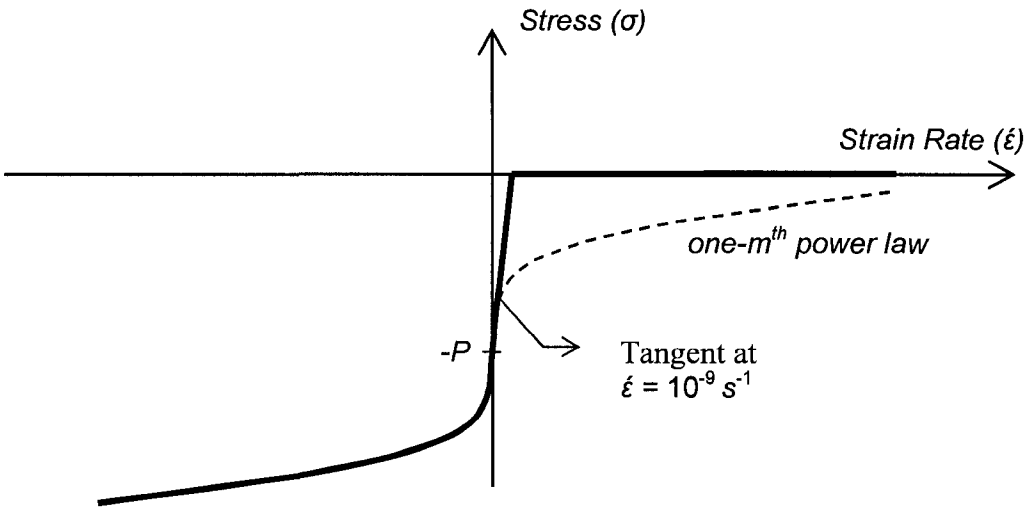

Figure 6-1 Sketch of the constitutive model with the emphasis on the dilation portion.

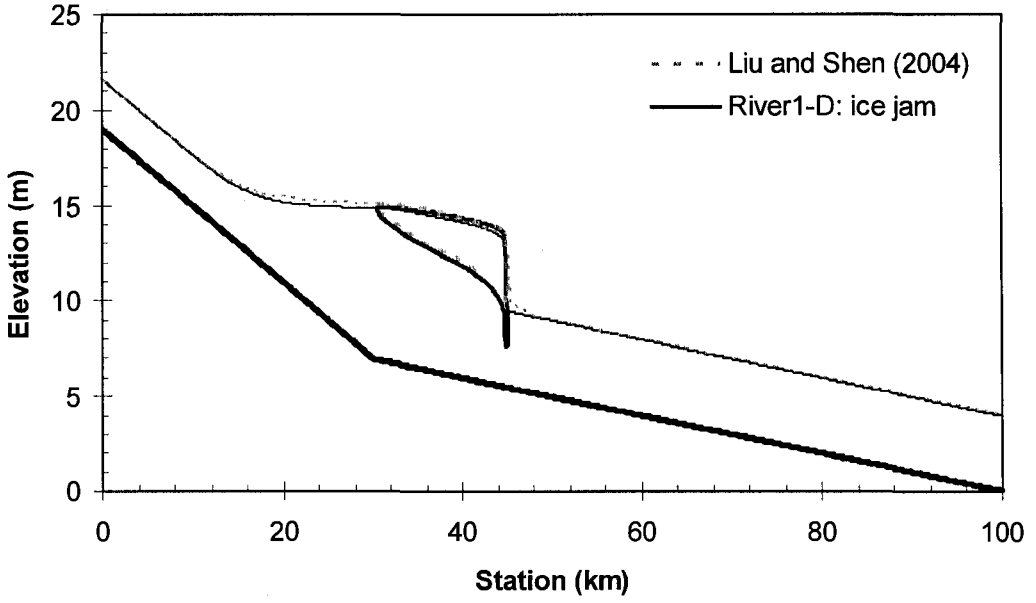

Figure 6-2 Simulated stable ice jam configuration and initial condition for the hypothetical ice jam release event in long channel.

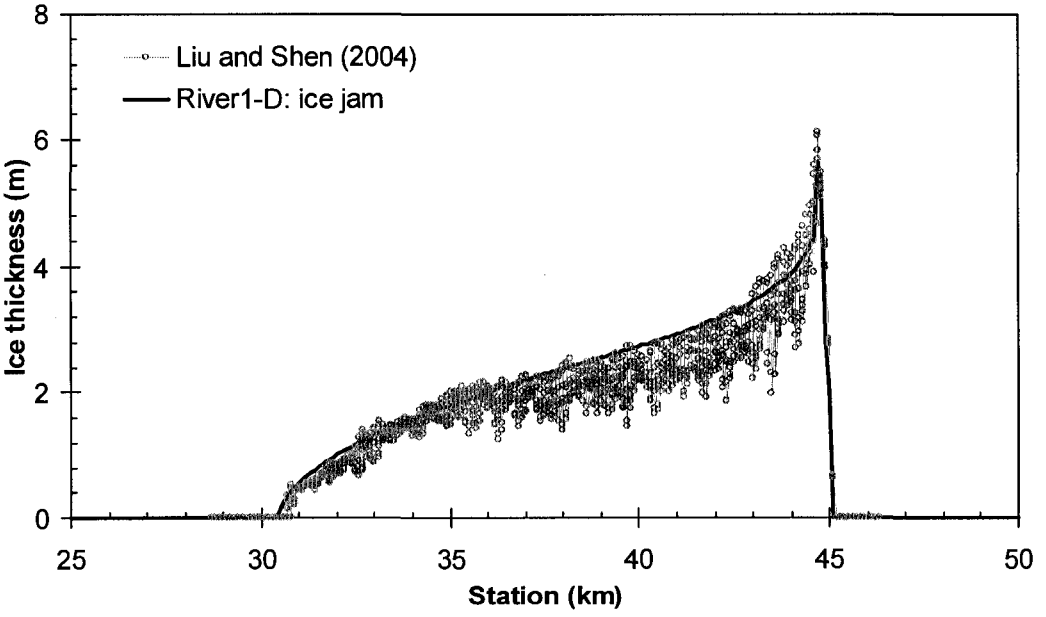

Figure 6-3 Simulated thickness profile of the initial jam obtained using *River1-D: ice jam* in comparison with that for the DynaRICE model (the hypothetical release event in long channel).

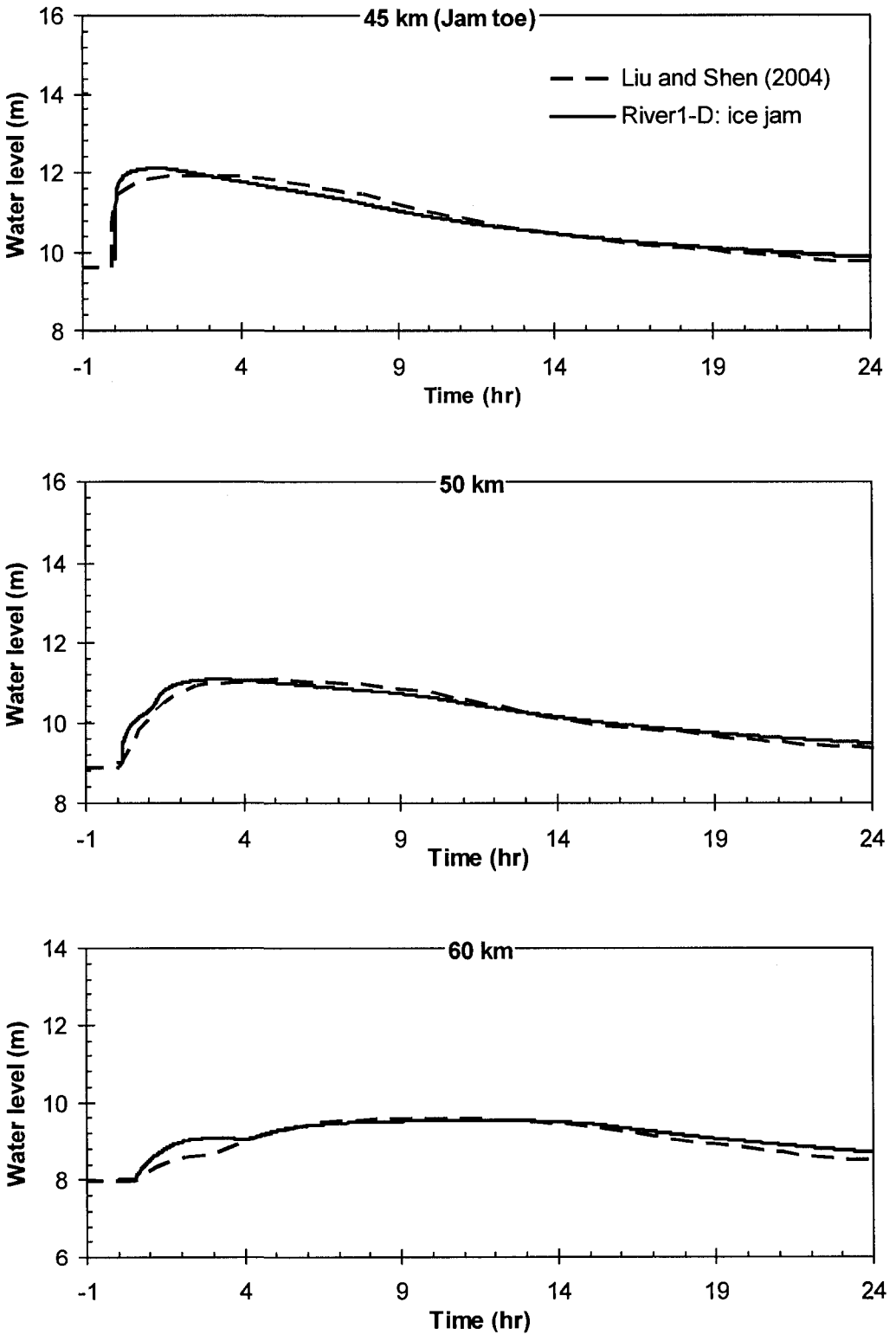

Figure 6-4 Simulated water level hydrographs at different stations along the long channel, with ice resistance effects included.

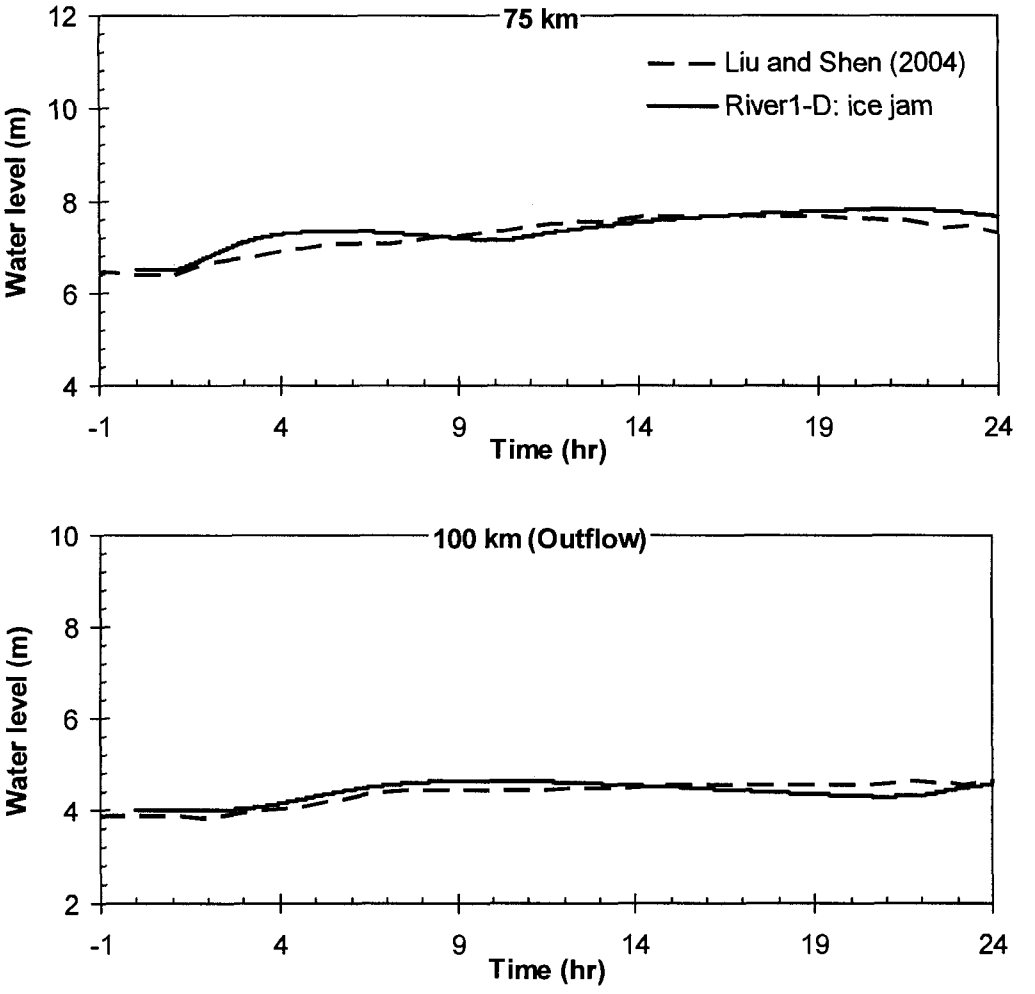

Figure 6-4 Simulated water level hydrographs at different stations along the long channel, with ice resistance effects included (continued).

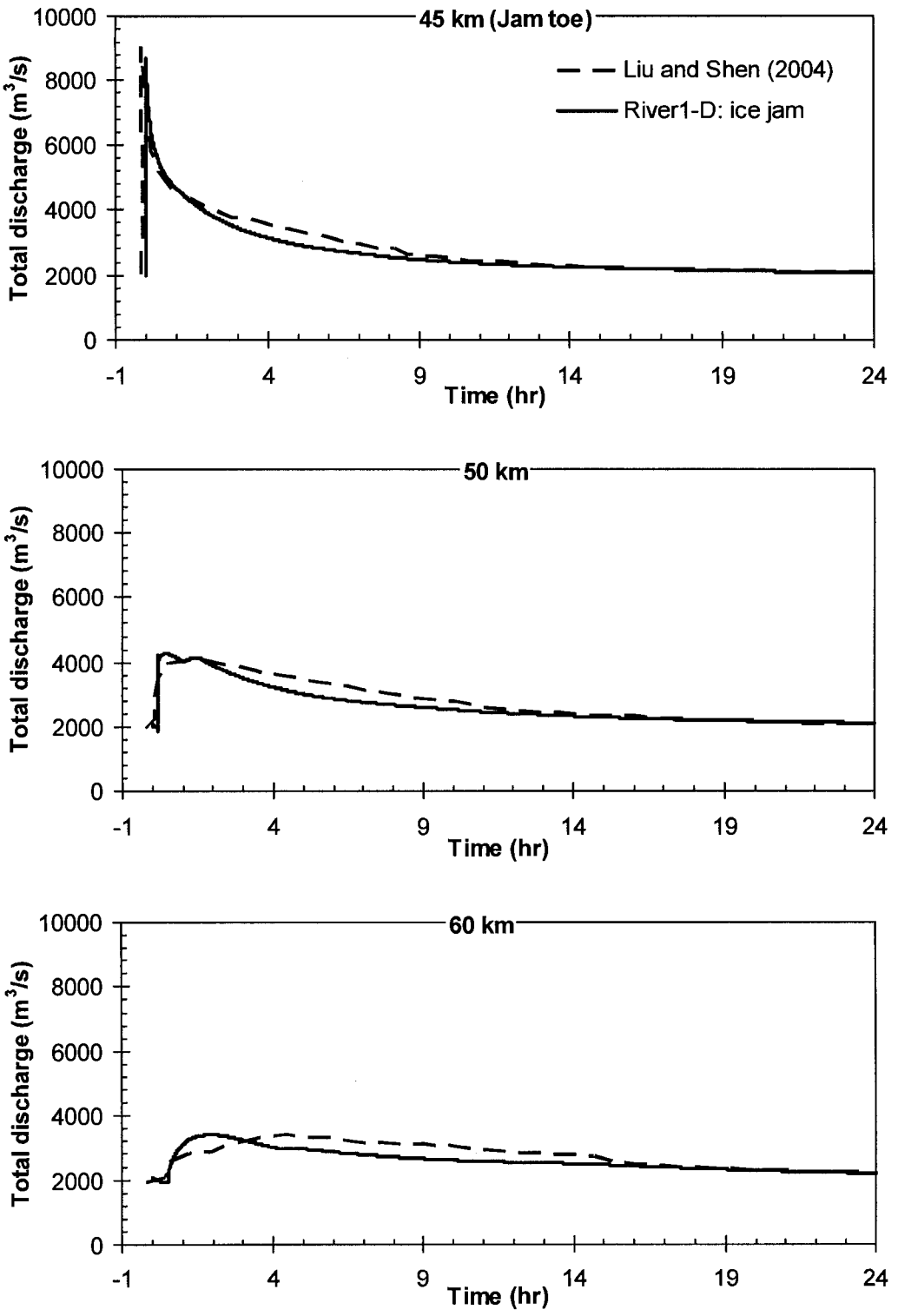

Figure 6-5 Simulated water and ice discharge hydrographs at different stations along the long channel, with ice resistance effects included.

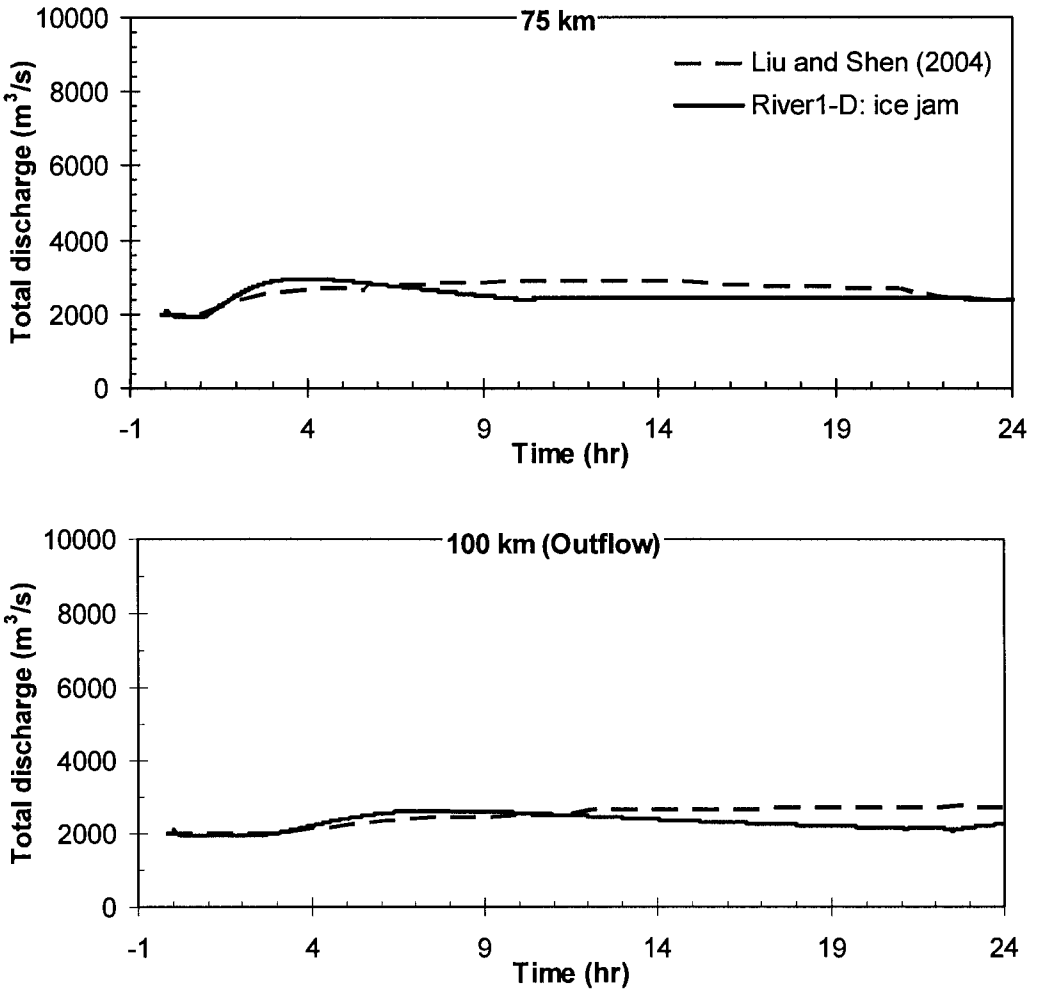

Figure 6-5 Simulated water and ice discharge hydrographs at different stations along the long channel, with ice resistance effects included (continued).

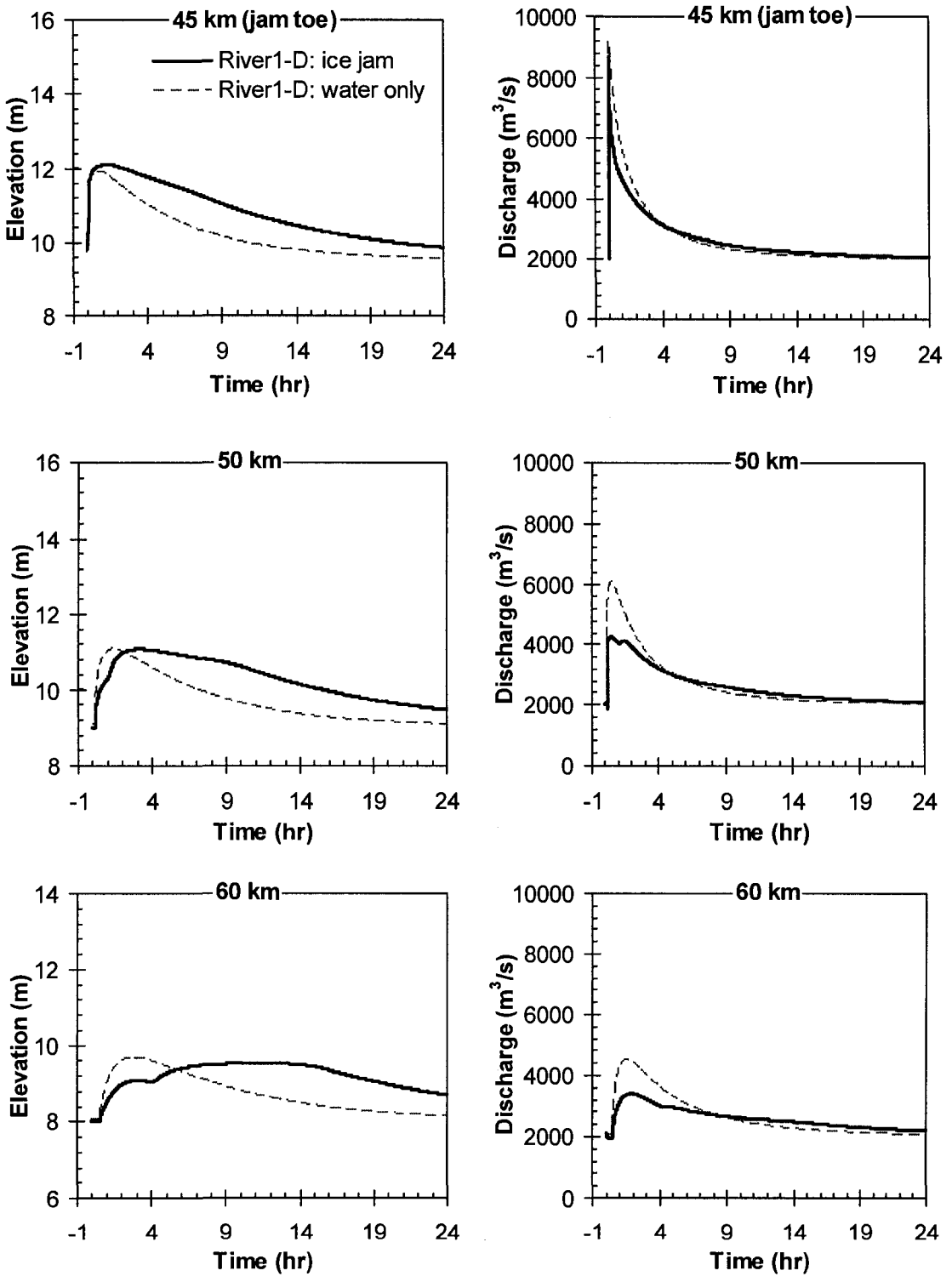

Figure 6-6 Effects of ice resistance on water level and discharge hydrographs at different stations along the long channel.

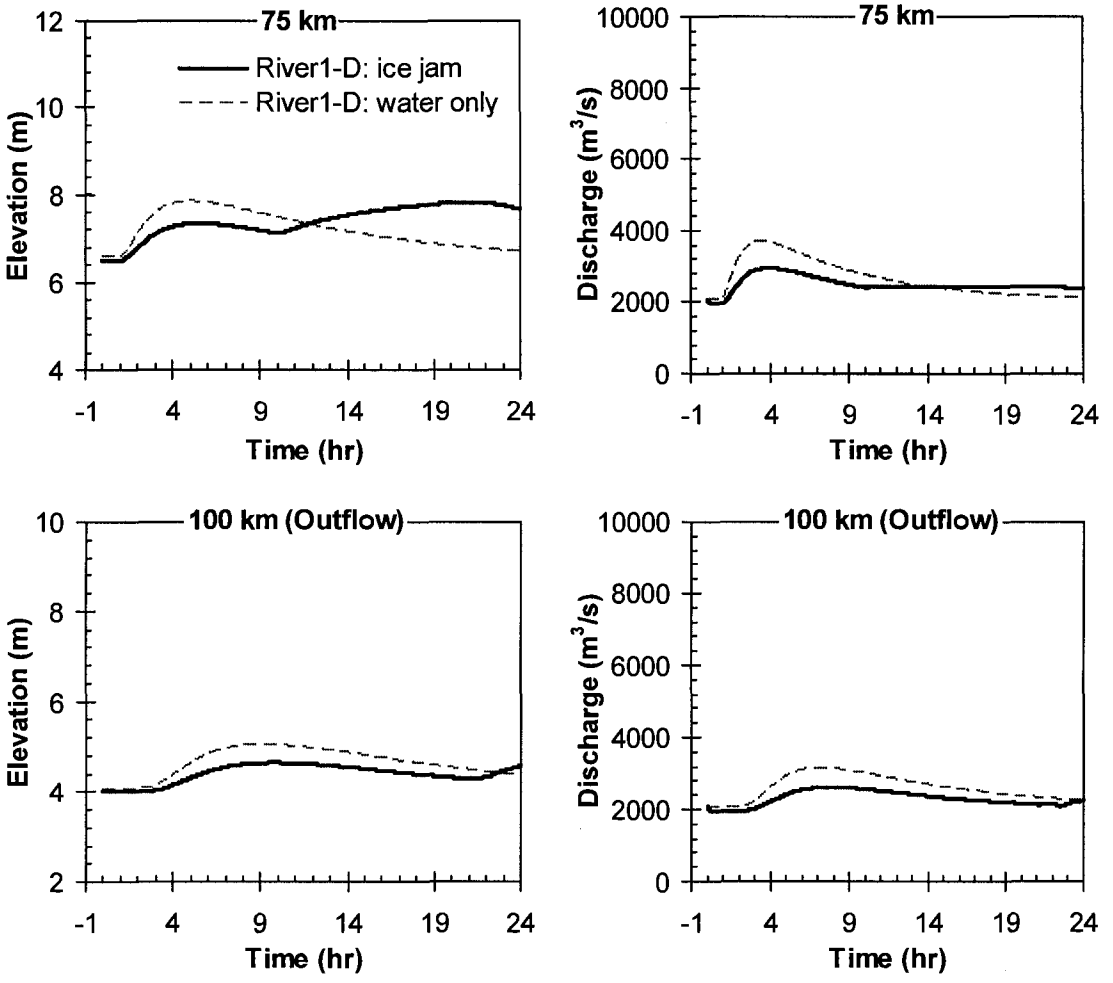

Figure 6-6 Effects of ice resistance on water level and discharge hydrographs at different stations along the long channel (continued).

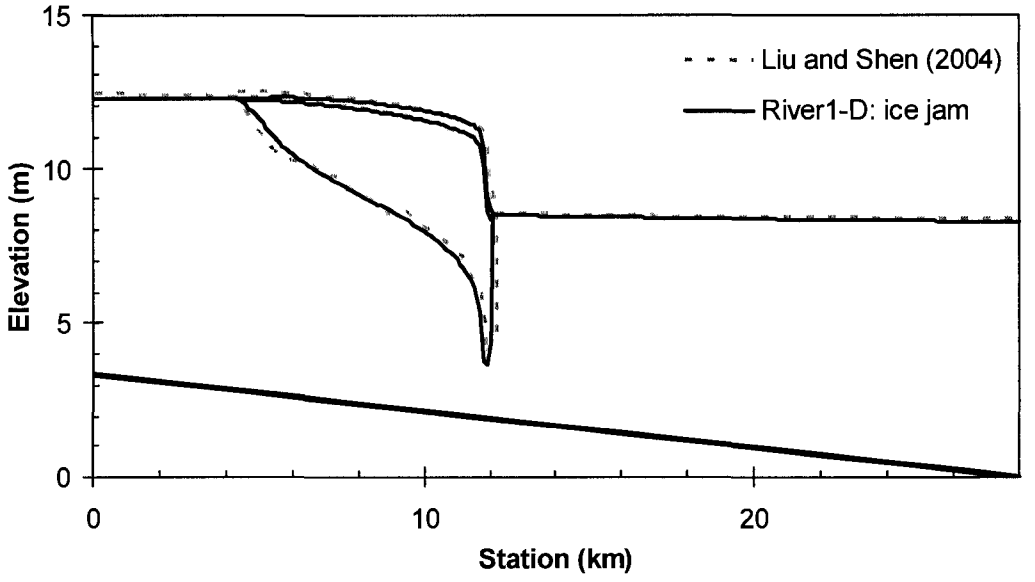

Figure 6-7 Simulated stable ice jam configuration and initial condition for the hypothetical ice jam release event in short channel.

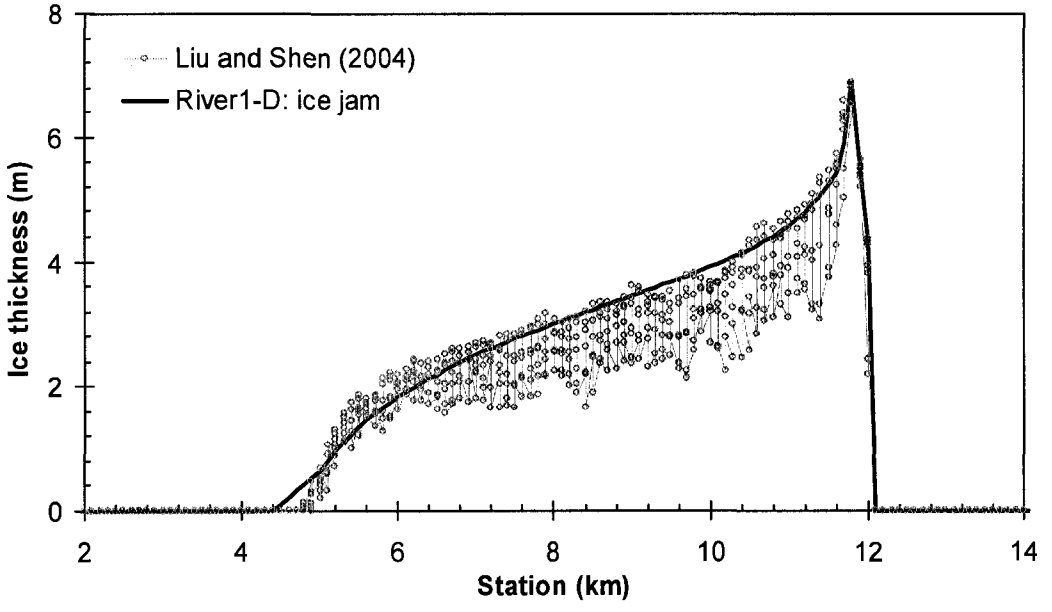

Figure 6-8 Simulated thickness profile of the initial jam obtained using *River1-D: ice jam* in comparison with that for the DynaRICE model (the hypothetical release event in short channel).

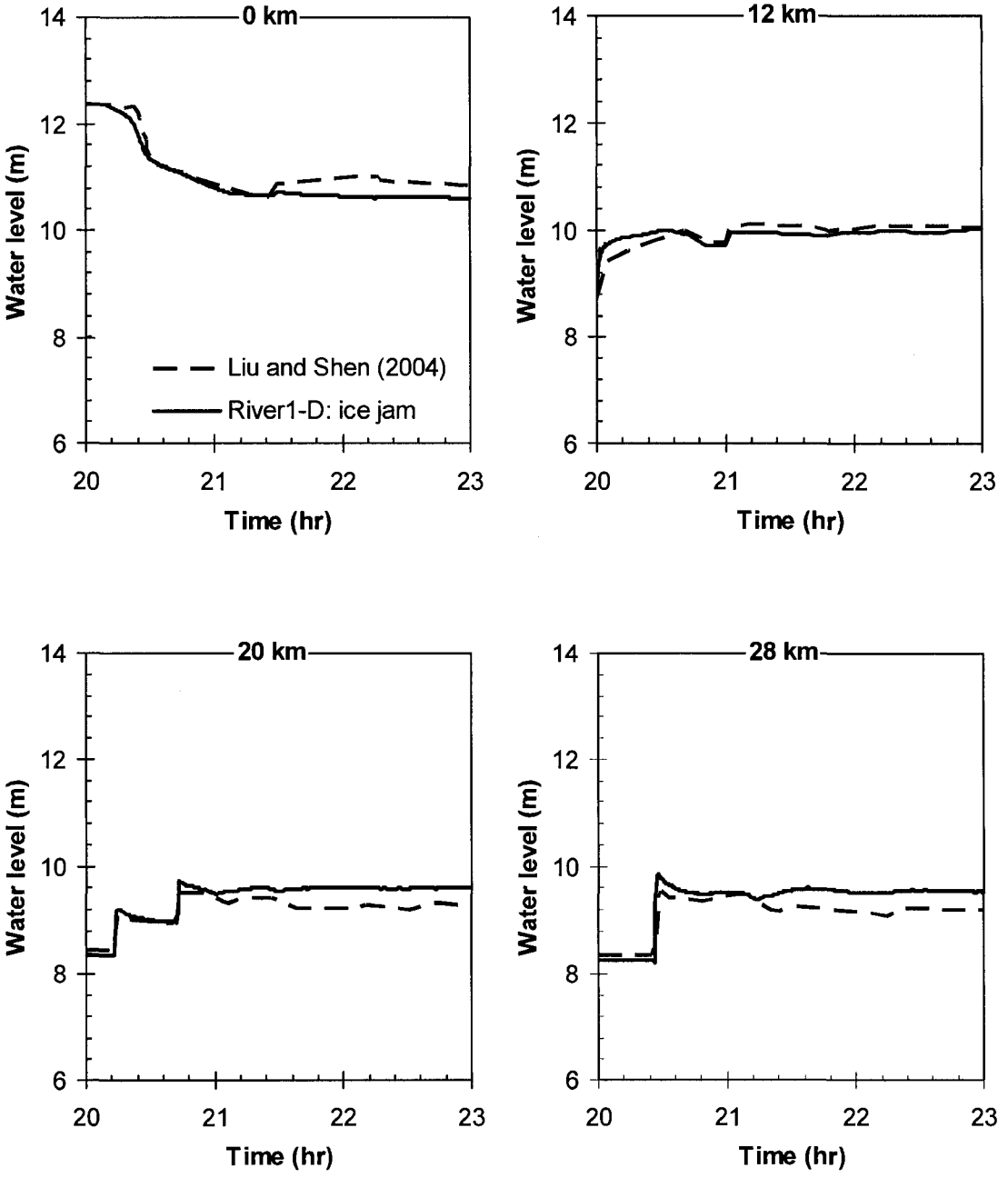

Figure 6-9 Simulated water level hydrographs at different stations along the channel, with ice resistance effects included (the hypothetical release event in short channel).

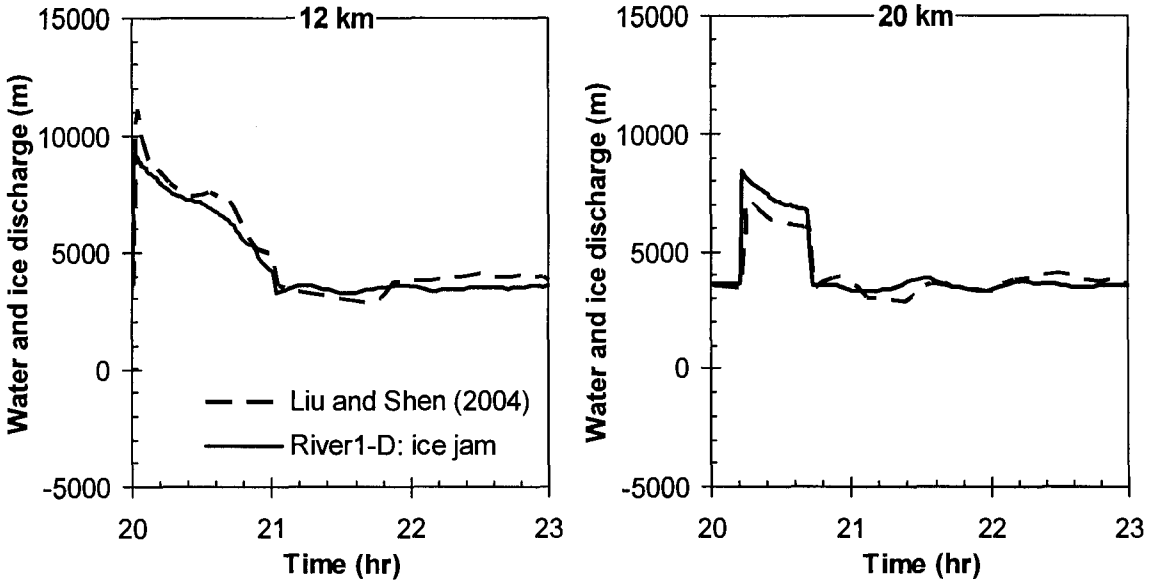

Figure 6-10 Simulated water and ice discharge hydrographs at different stations along the channel, with ice resistance effects included (the hypothetical release event in short channel).

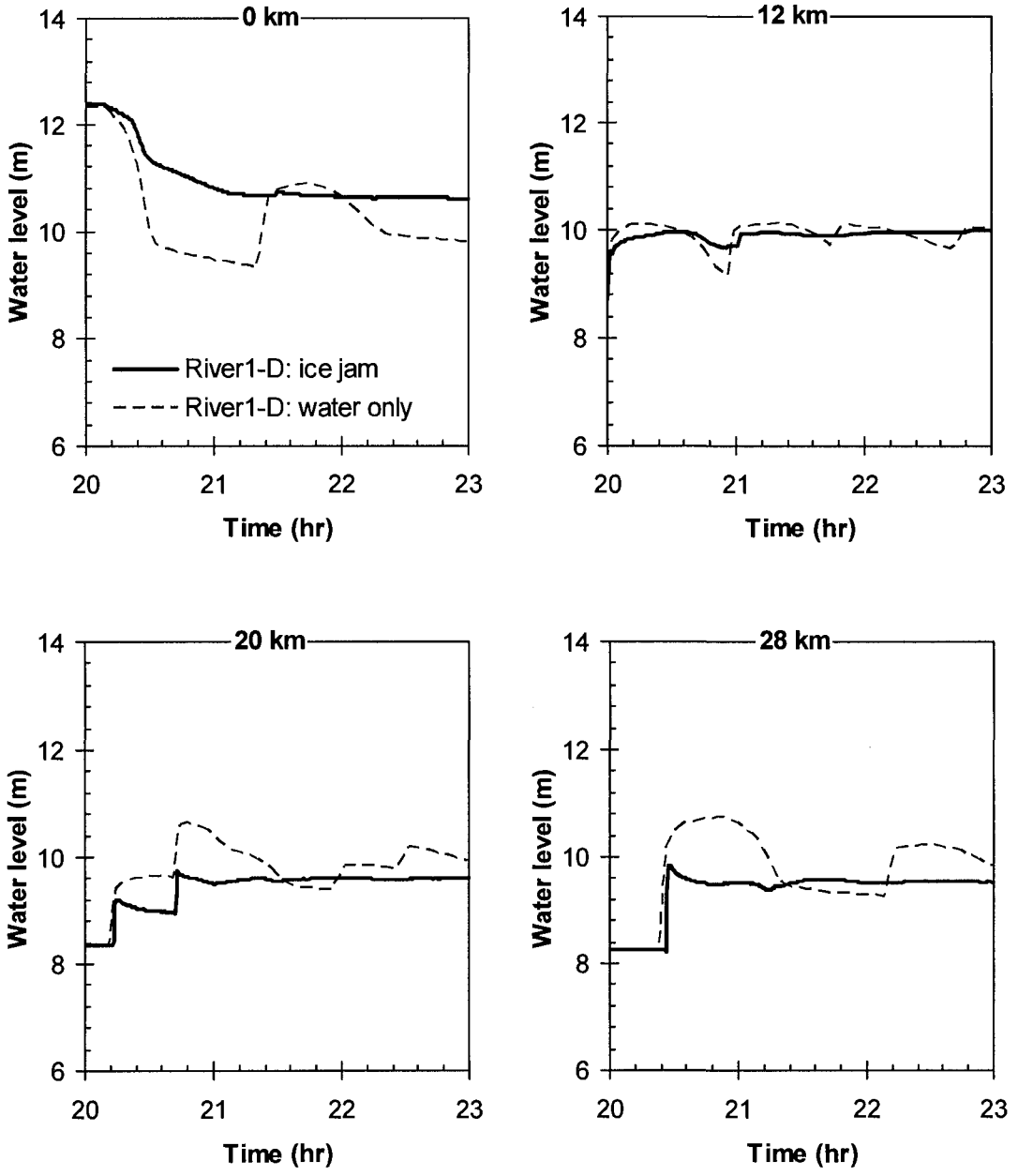

Figure 6-11 Effects of ice resistance on water level hydrographs at different stations along the short channel.

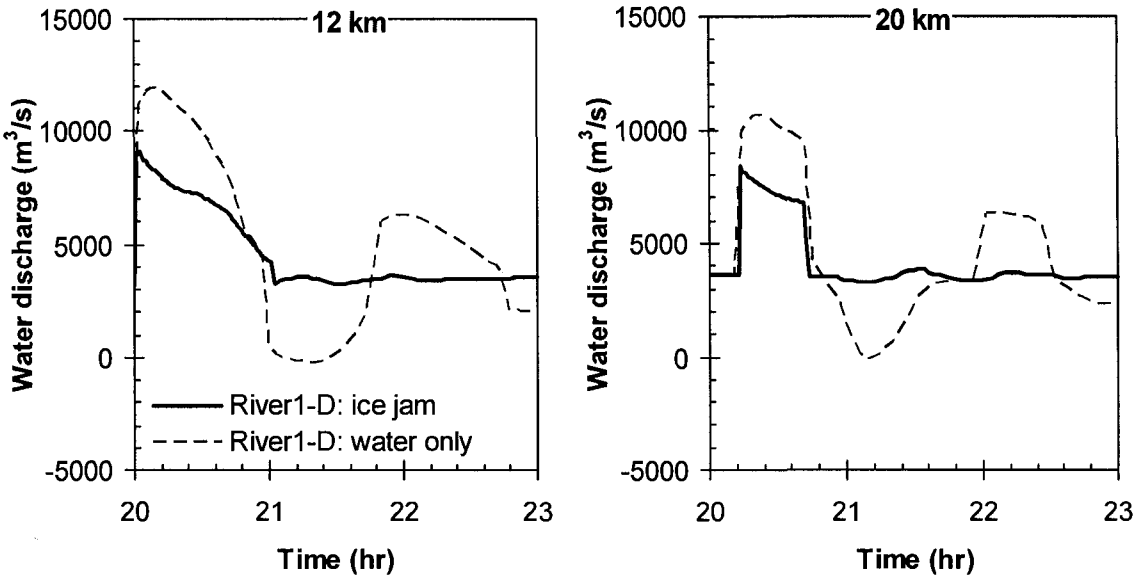

Figure 6-12 Effects of ice resistance on discharge hydrographs at different stations along the short channel.

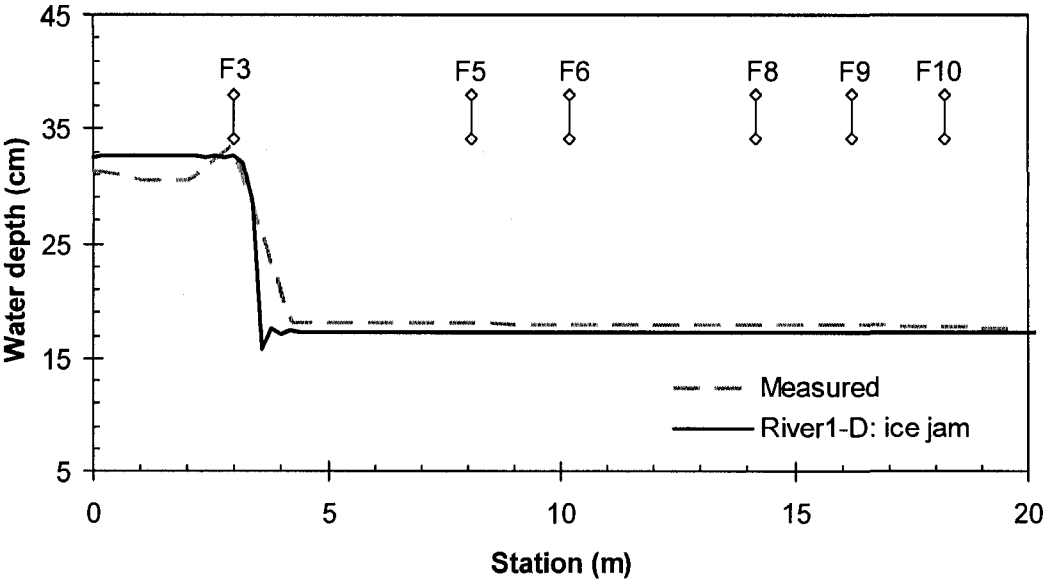

Figure 6-13 Initial water surface profile prior to jam release for Run No. 1.

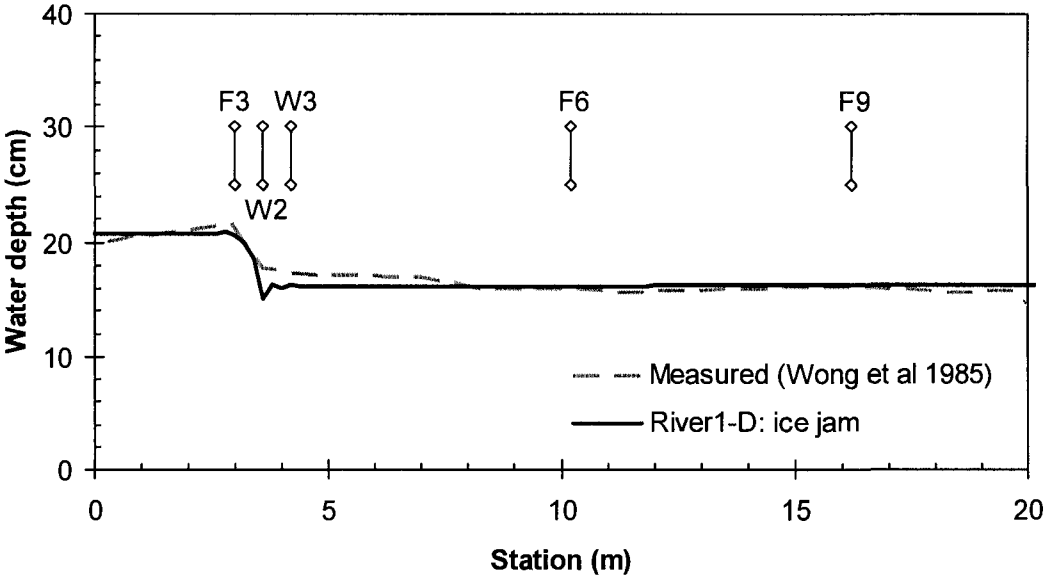

Figure 6-14 Initial water surface profile prior to jam release for Run No. 4.

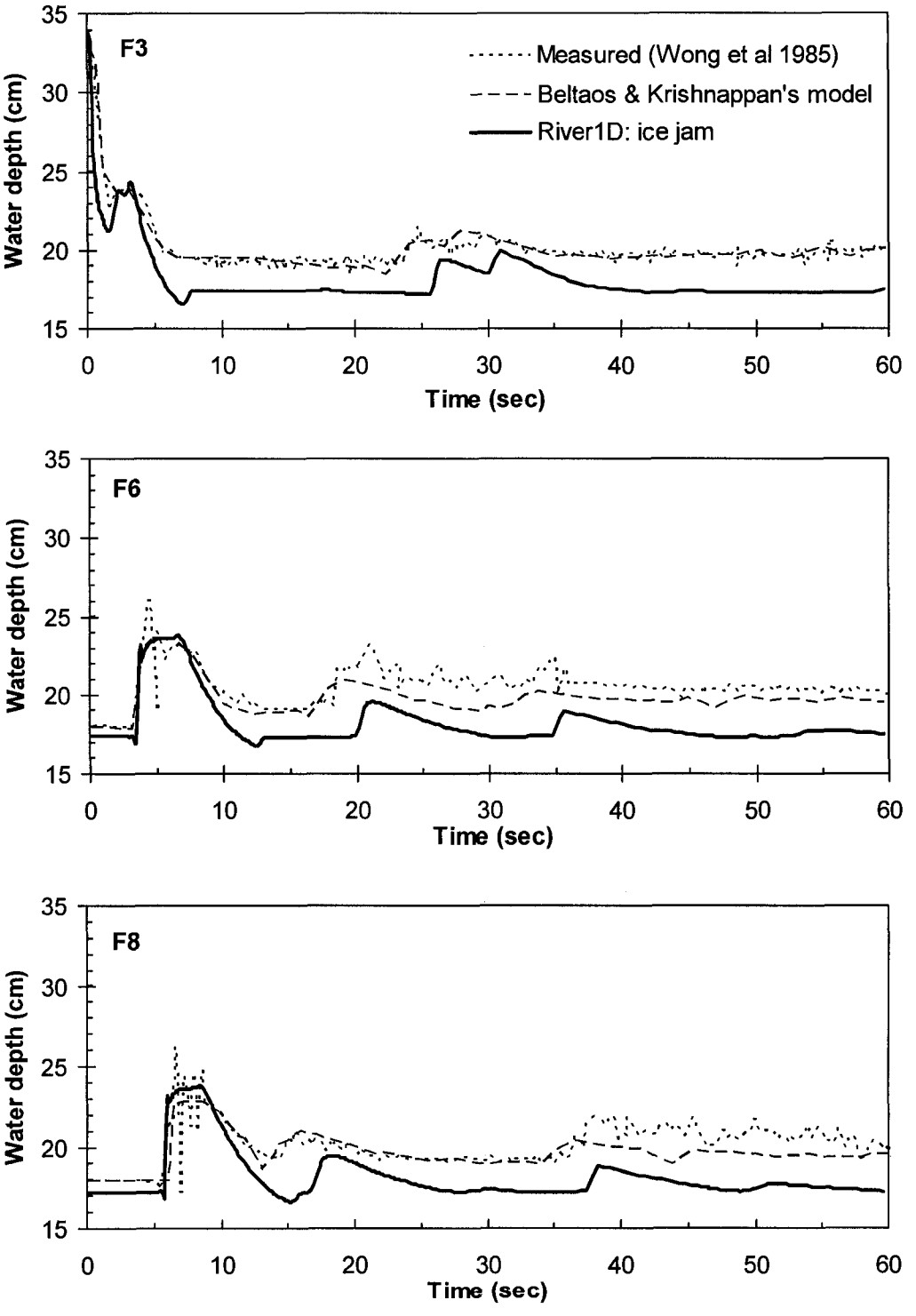

Figure 6-15 Time-series water depth at various stations for Run No. 1.

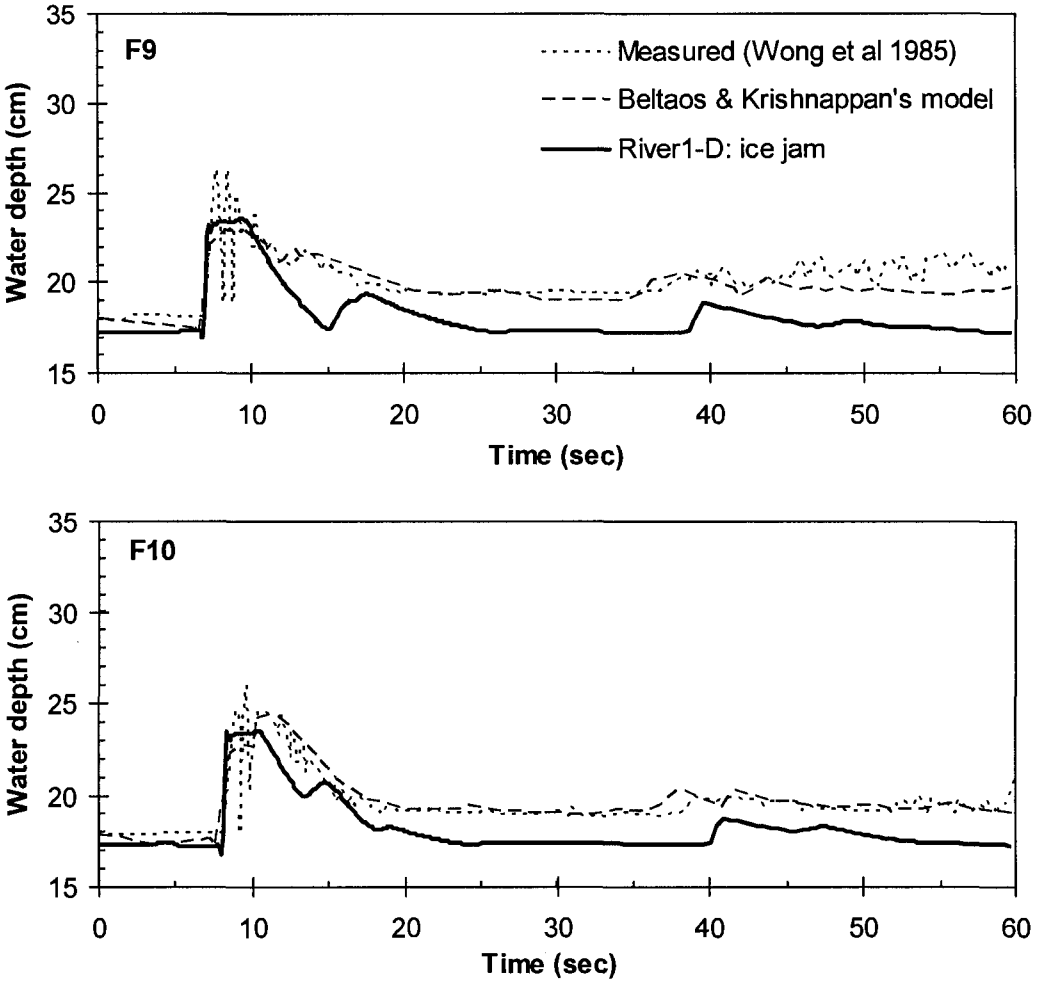

Figure 6-15 Time-series water depth at various stations for Run No. 1 (continued).

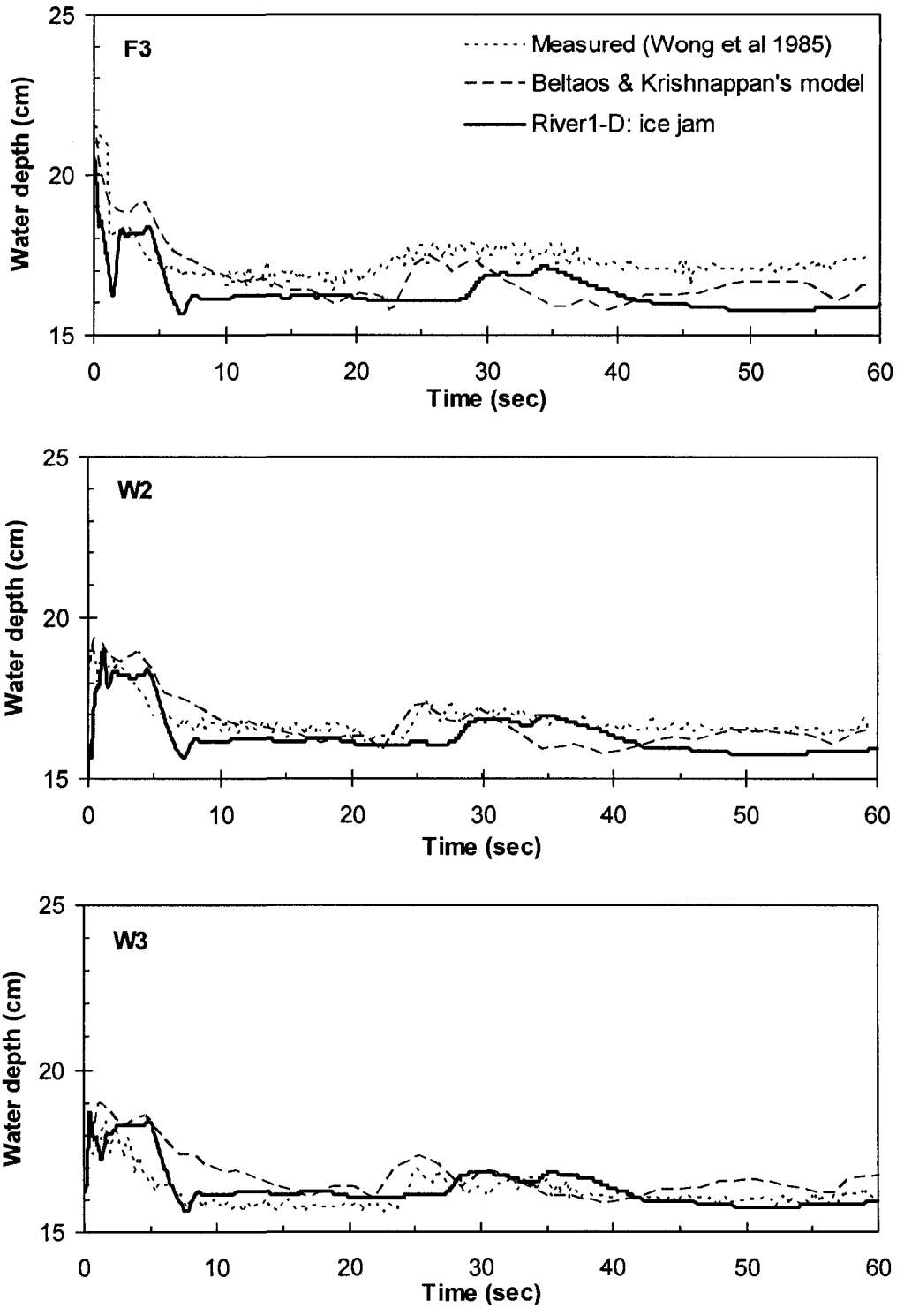

Figure 6-16 Time-series water depth at various stations for Run No. 4.

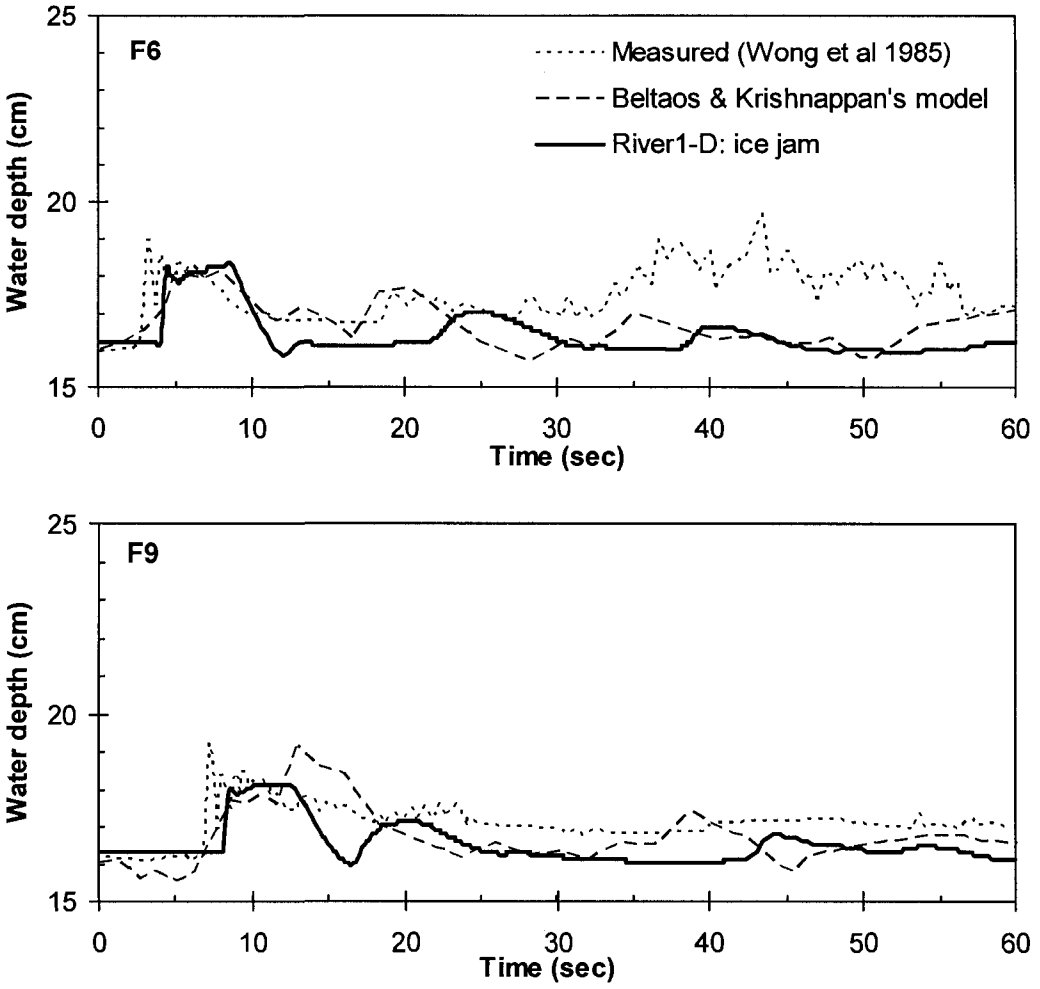

Figure 6-16 Time-series water depth at various stations for Run No. 4 (continued).

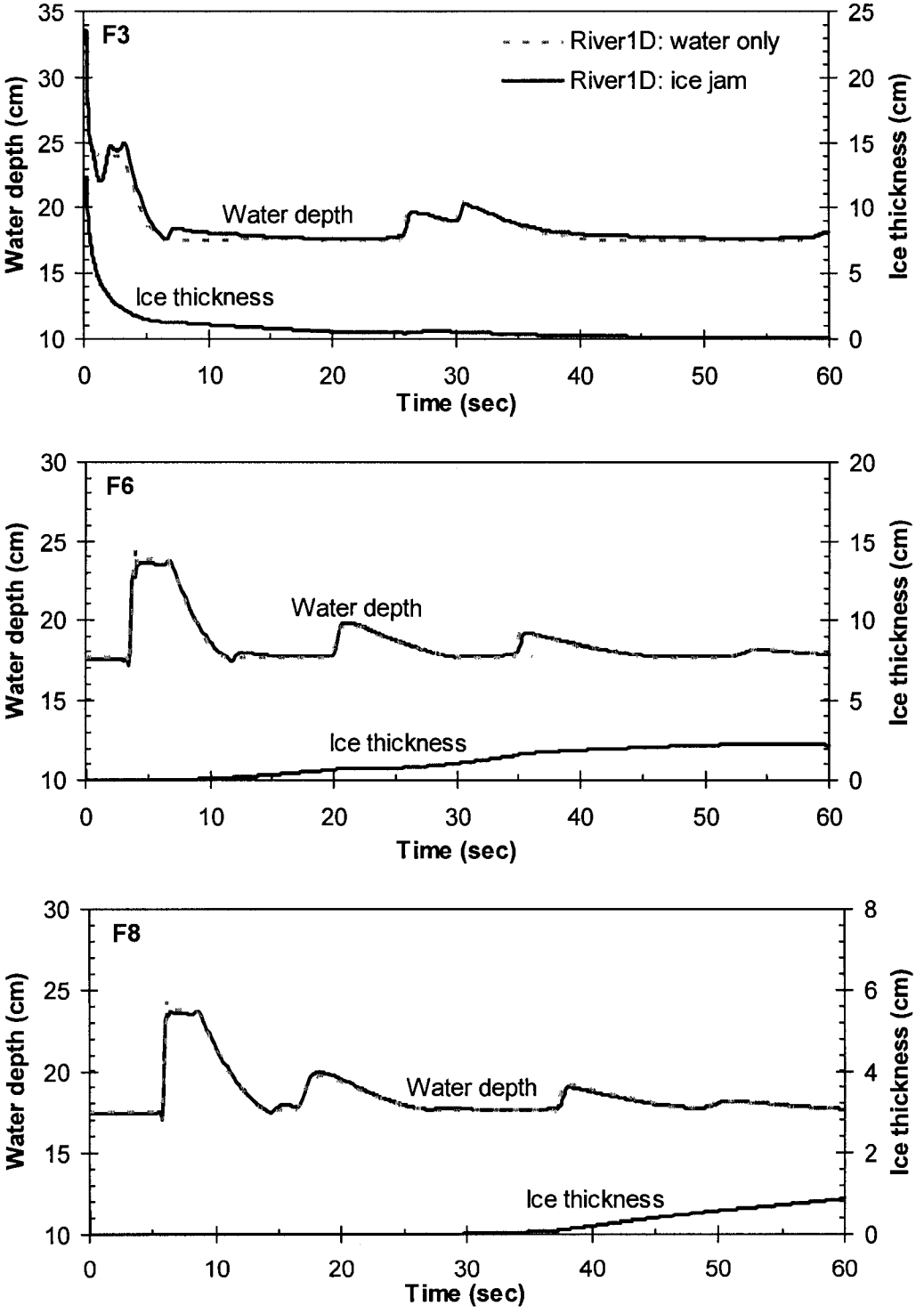

Figure 6-17 Ice effects on water depth hydrographs at various stations for Run No. 1.

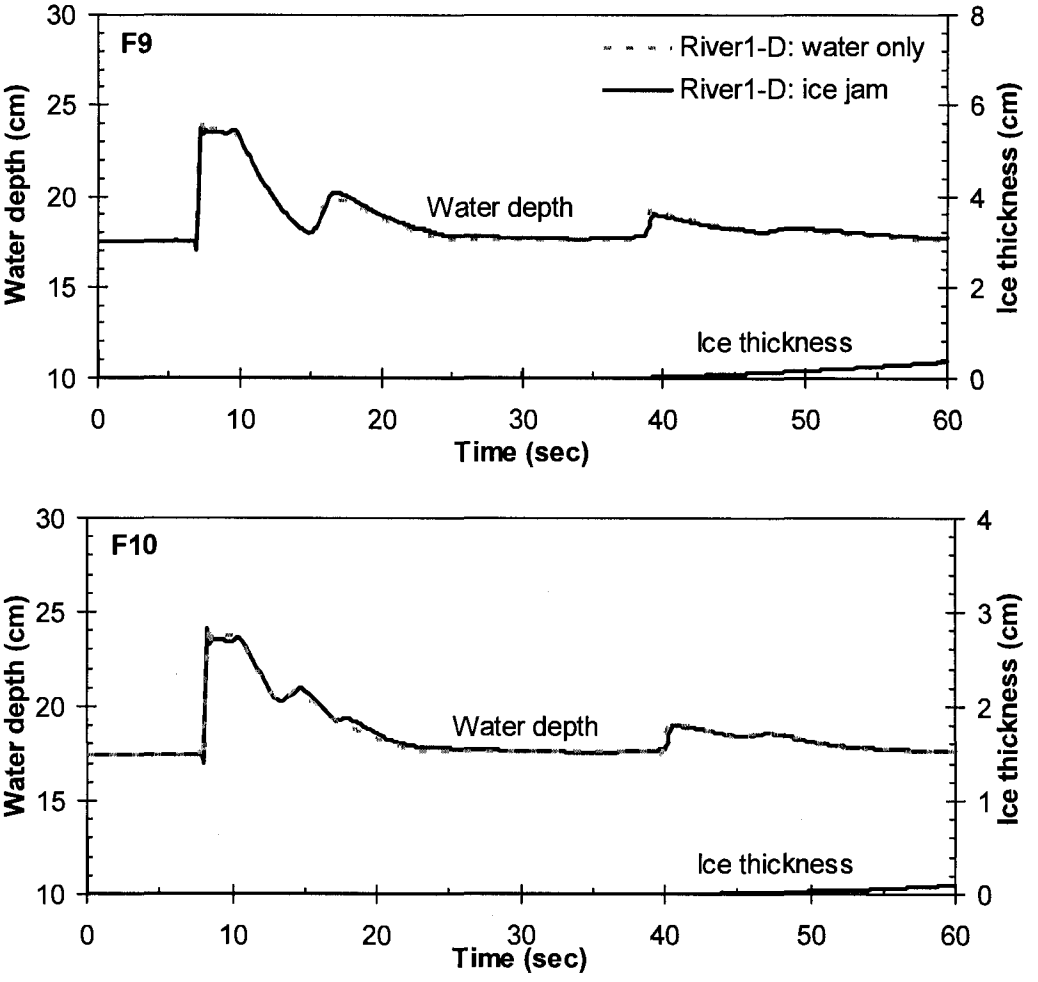

Figure 6-17 Ice effects on water depth hydrographs at various stations for Run No. 1 (continued).

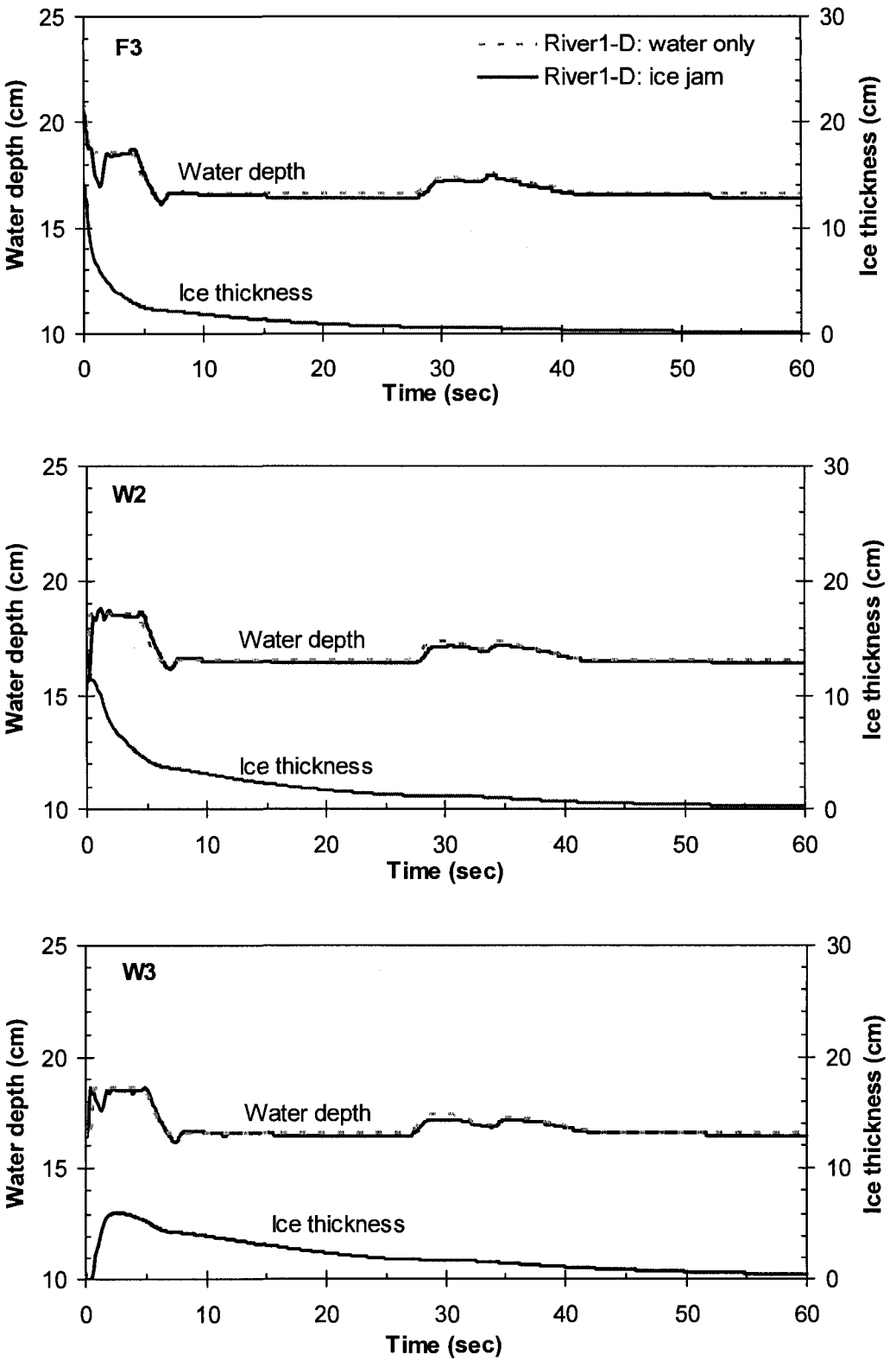

Figure 6-18 Ice effects on water depth hydrographs at various stations for Run No. 4.

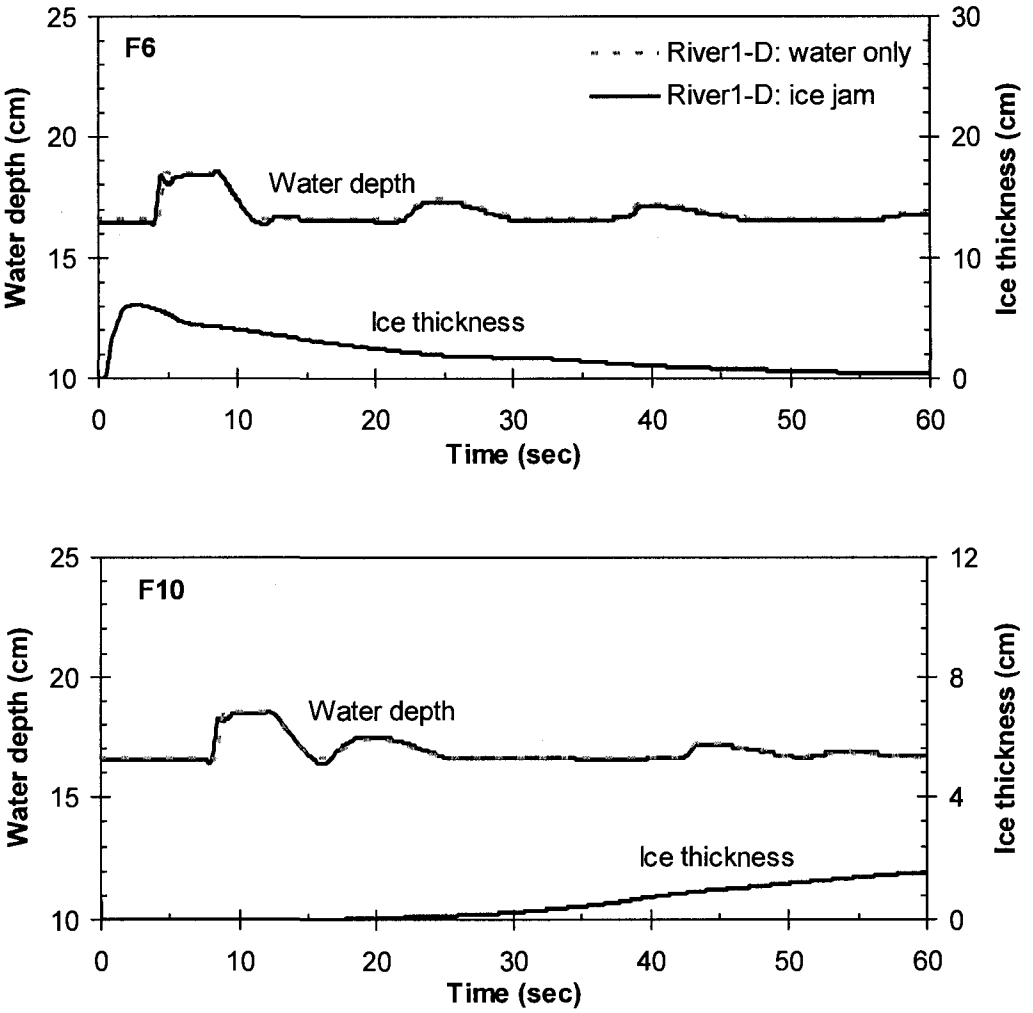

Figure 6-18 Ice effects on water depth hydrographs at various stations for Run No. 4 (continued).

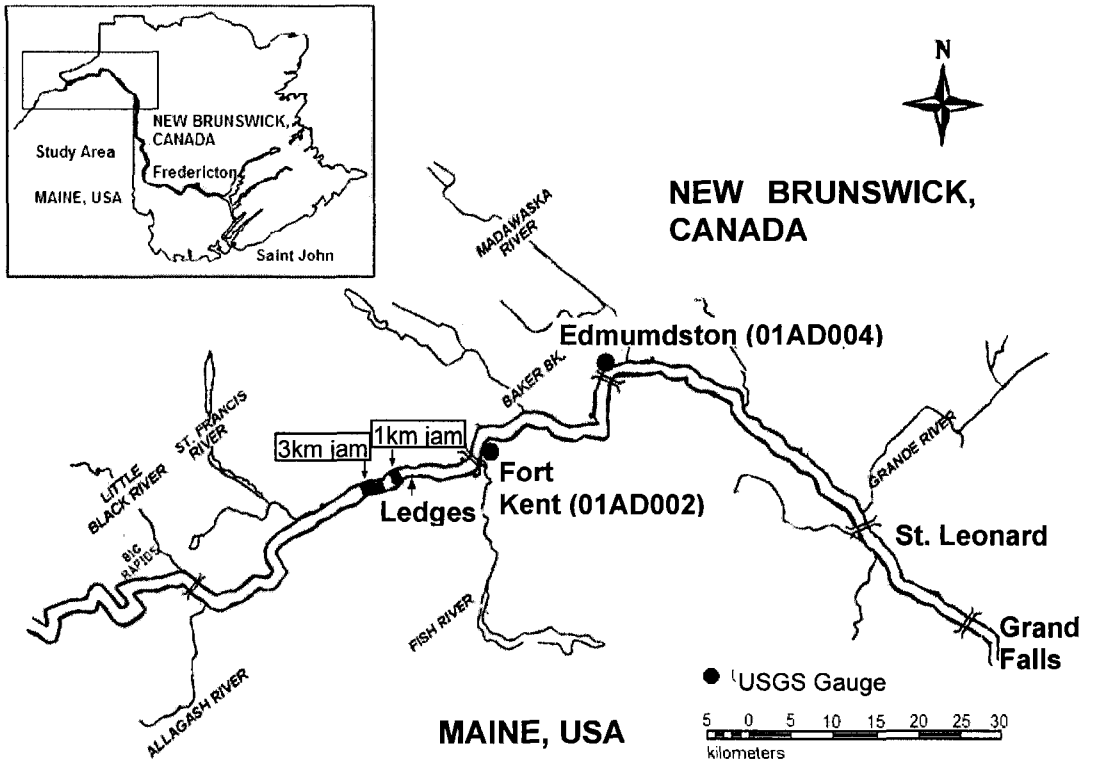

Figure 6-19 Study reach on the Saint John River, New Brunswick, Canada and Maine, United States.

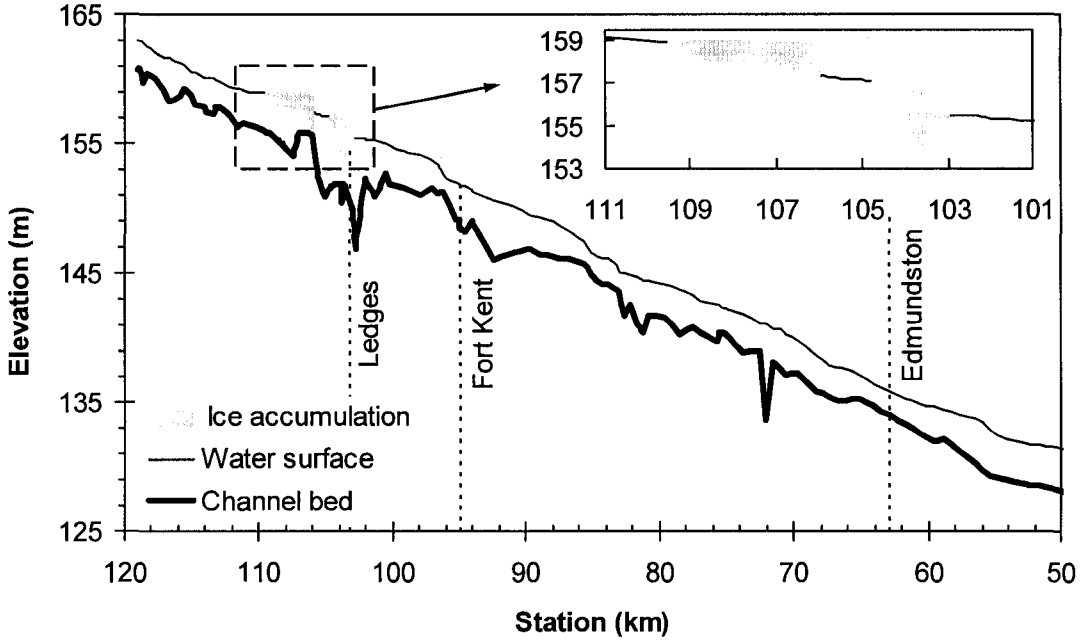

Figure 6-20 Initial water surface and ice jam profiles for the Saint John River for April 13, 2002 prior to release.

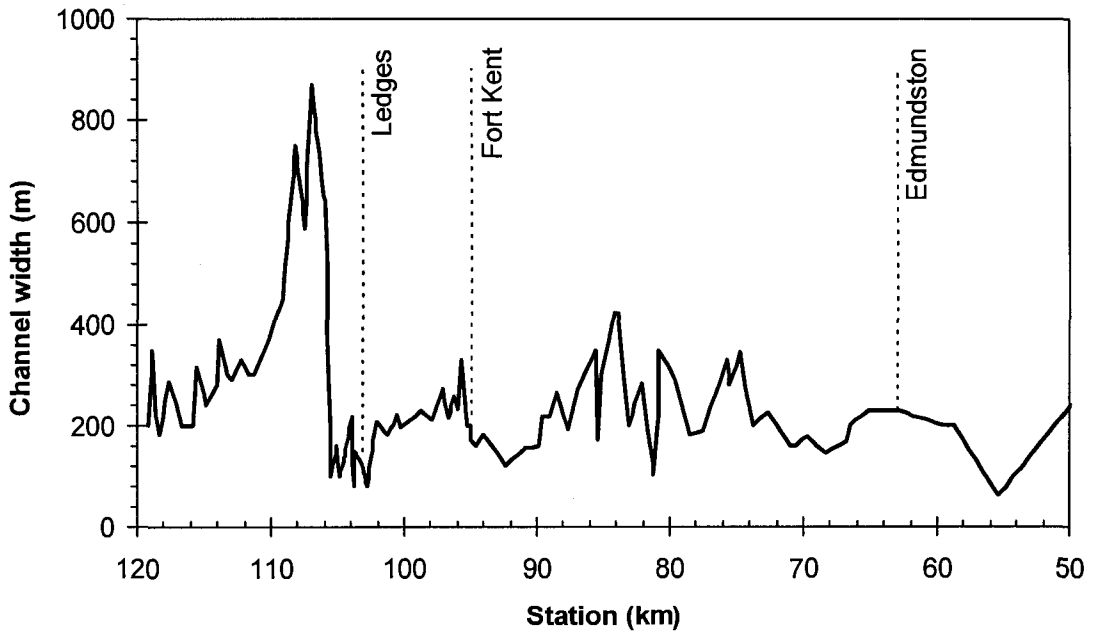

Figure 6-21 Channel width along the study reach of Saint John River based on rectangular channel geometry approximation.

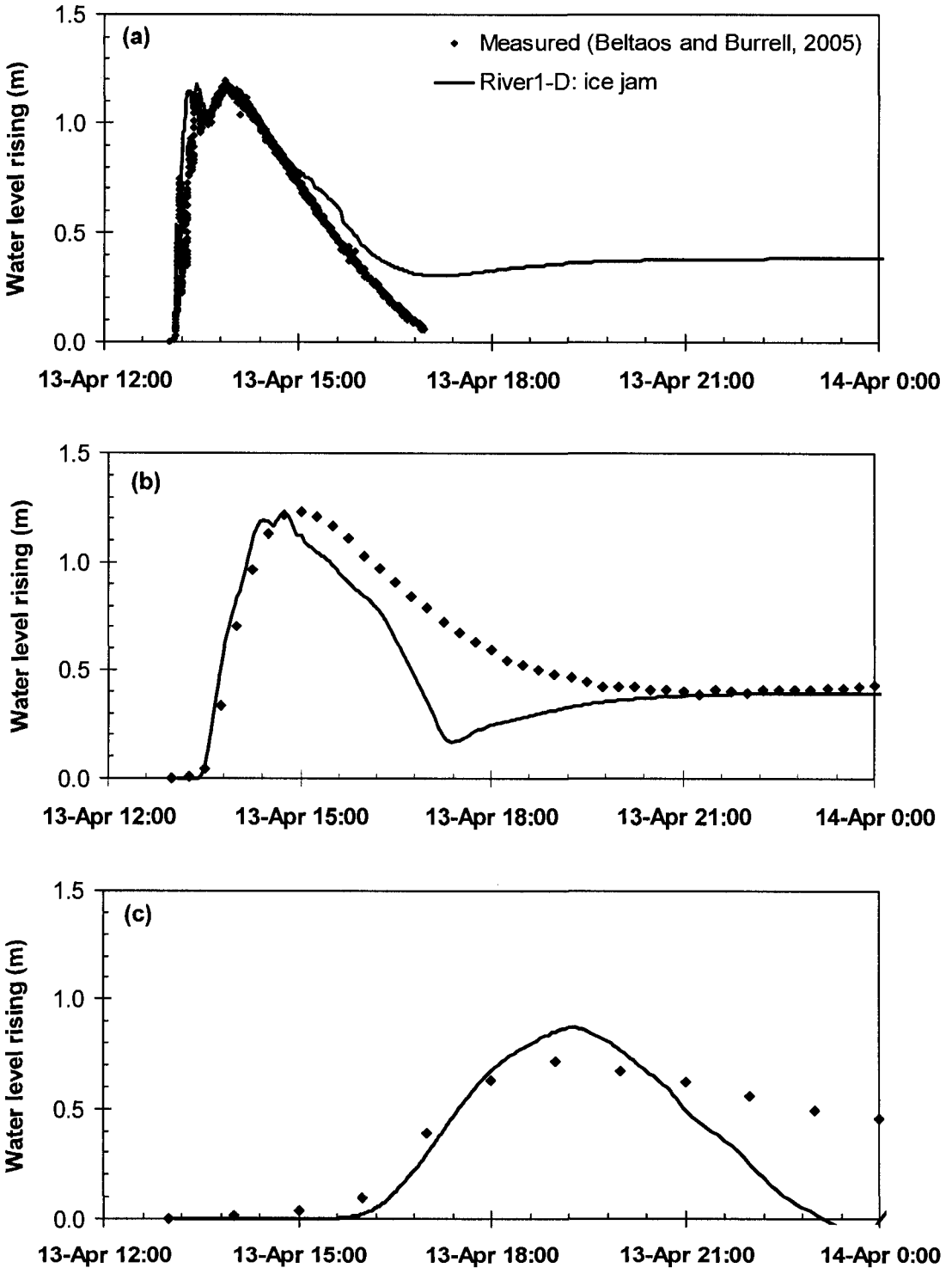

Figure 6-22 Comparison of simulated water level rising with measurements due to ice jam release at 3 downstream stations: (a) Ledges; (b) Fort Kent; (c) Edmundston.

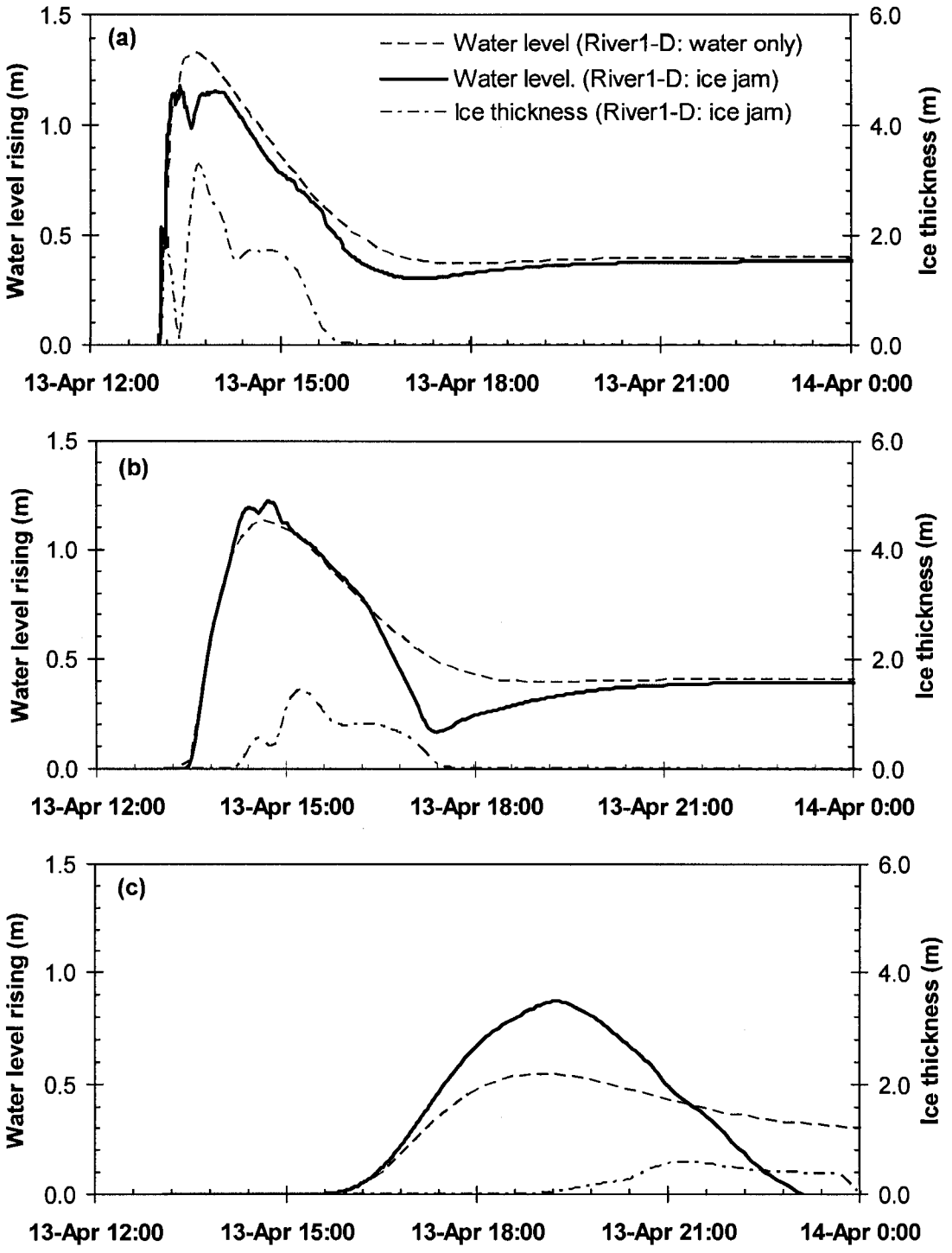

Figure 6-23 Comparison of simulated water level rising due to ice jam release with and without ice resistance effects at 3 downstream stations: (a) Ledges; (b) Fort Kent; (c) Edmundston.

6.5 References

Beltaos, S. and Krishnappan, B.G. (1982). Surges from Ice Jam Release: A Case Study. Canadian Journal of Civil Engineering, Vol. 9: 276-284.

Beltaos, S., Burrell, B. C., and Ismail, S. (1994). Ice and sedimentation processes in the Saint John River, Canada. Proc., 12th IAHR Symposium on Ice, Norwegian Institute of Technology, Trondheim, Norway, pp. 11–21.

Beltaos, S., Ford, J.S., Burrell, B.C., Pedrosa, M., and Madsen, N.K. (1998). Remote measurements of temperature and surge levels in ice-laden rivers. Proc., 14th IAHR Symposium on Ice, Potsdam, N.Y., U.S.A. A.A. Balkema, Rotterdam, The Netherlands. Vol. 1: 35–40.

Beltaos, S., Burrell, B. C. (2005a). Field Measurements of Ice-Jam-Release Surges. Canadian Journal of Civil Engineering, Vol. 32: 699-711.

Beltaos, S., Burrell, B. C. (2005b). Determining Ice-Jam Surge Characteristics from Measured Wave Forms. Canadian Journal of Civil Engineering, Vol. 32: 687-698.

Blackburn, J. and Hicks, F. (2003). Suitability of Dynamic Modeling for Flood Forecasting during Ice Jam Release Surge Events. Journal of Cold Regions Engineering, 17(1): 18-36.

Doyle, P.F. and Andres, D.D. (1979). 1979 Spring Breakup and Ice Jamming on the Athabasca River Near Fort McMurray. Alberta Research Council, Edmonton, AB, Report SWE-79/05.

Henderson, F.M. and Gerard, R. (1981). Flood Waves Caused by Ice Jam Formation and Failure. Proc., IAHR Symposium on Ice. Quebec city, Quebec, Vol. 1: 277-287.

Hicks, F.E. and Steffler, P.M. (1992). A Characteristic-Dissipative-Galerkin Scheme for Open Channel Flow. ASCE Journal of Hydraulic Engineering, 118(2): 337-352.

Khan, A.A., Steffler, P.M. and Gerard, R. (2000). Dam-Break Surges with Floating Debris. Journal of Hydraulic Engineering, 126(5): 375-379.

Kowalczyk Hutchison, T. and F. Hicks (2007). Observations of Ice Jam Release Events on the Athabasca River, AB. Canadian Journal of Civil Engineering, 34 (4) 473-484.

Liu, L.W. and Shen, H.T. (2004). Dynamics of Ice Jam Release Surges. Proc., 17th IAHR Symposium on Ice. St. Petersburg, Russia, 8 pp.

She, Y. and Hicks, F. (2006). Modeling Ice Jam Release Waves with Consideration For Ice Effects. Cold Regions Science and Technology, 45(3): 137-147.

She, Y., Hicks, F., Steffler, P., and Healy, D. (2008). Constitutive Model for Internal Resistance of Moving Ice Accumulations and Eularian Implementation for River Ice Jam Formation. Submitted to Journal of Cold Regions Science and Technology, June 2008.

Wong, J., Beltaos, S. and Krishnappan, B.G. (1985). Laboratory Tests on Surges Created by Ice Jam Releases. Canadian Journal of Civil Engineering, Vol. 12: 930-933.

7 Summary and Conclusions

River ice jams are often associated with dangerously high water levels as they obstruct the passage of flow. Furthermore, the sudden release of an ice jam can produce a violent ice run and rapidly increasing water levels downstream, leading to extremely destructive flash floods. Although the ice jam release wave attenuates as it propagates downstream, deceleration of the ice run and possible reformation of new ice jam can cause the water levels to rise again, thus increasing the severity and unpredictability of ice jam related floods.

Significant efforts have been made in the last few decades to understand and predict ice jam events. Despite the progress, many questions remain unanswered, particularly related to the dynamic processes of ice jam formation and release. Physical knowledge and prediction capabilities are limited, mainly constrained by the lack of reliable scientific data describing such events. Therefore, the objective of this thesis research was to expand our knowledge of ice jam dynamics through the collection and analysis of scientific data, and through the development and application of numerical models.

This study offers three key original contributions, as follows.

1. A numerical investigation of the effects of ice on ice jam release wave propagation has been conducted, considering both ice from the jam itself and ice in the receiving channel. Development of new numerical models of varying levels of complexity also provides a means of assessing sensitivity of results to model sophistication.

2. A new constitutive model for ice internal resistance has been formulated, and has been shown to provide an appropriate representation of the stress and strain rate relationship obtained through a new analysis of experiment data. It has the ability to simulate the ice accumulation both moving and approaching a static state, and has been implemented in a purely Eulerian one-dimensional model capable of handling ice jam formation, release, deceleration and reformation.

3. New and unique scientific data have been obtained from a field study documenting multiple ice jam release and formation events. The numerical models developed in this study provide the means to aid the interpretation of this field data, enhancing our understanding of these complex ice processes.

Each of these contributions is discussed below; results are assessed and recommendations for further research are offered.

7.1 Effects of Ice on Ice Jam Release Wave Propagation

The effects of ice on ice jam release wave propagation were first explored in a simplified manner, using the Phase 1 model with ice resistance and dispersion considered empirically. Although greatly simplified, it provided very promising results that were comparable to those obtained using a much more sophisticated model for an idealized ice jam release event. The model was also applied to two actual unimpeded ice jam release events (field events). The model results suggested that it is important to include ice effects for accurately predicting the peak and arrival time of ice jam release waves, particularly in the very early stage of wave propagation (1 to 2 jam lengths downstream

of the toe of a releasing ice jam). After that, the ice effects diminish and thus can be neglected in the model.

The more complicated situation, impeded ice jam release, was also studied. This is the first attempt to explore the behaviour of the two very different breaking fronts (sheet versus rubble breaking fronts) using a numerical model (i.e. the Phase 2 model). Instead of worrying about the highly complicated and not well understood mechanics, the Phase 2 model was developed with simplified ice momentum based on empirical knowledge obtained from field observations. It was found that for a sheet breaking front, the front between the moving ice and the stationary ice travels faster than the ice rubble released from the ice jam, forming a lengthening transition zone between the moving ice accumulation and the intact ice. The ice rubble in this case, moves downstream at a much higher speed that propagates as a rubble breaking front, in which the intact ice cover provides more resistance to the releasing jam. Also, the breaking ice accumulates rapidly at a rubble breaking front, quickly leading to grounding. Thus, the friction from the river bed further reduces the propagating speed of the released ice jam.

The development and comparison of numerical models incorporating ice effects both empirically and deterministically, facilitates direct comparison and assessment of the level of sophistication required in order to provide reliable ice jam flood forecasts. It was found that the simplified (Phase 1) model provided comparable results to those obtained using more sophisticated models for a hypothetical ice jam release event. It also provided better reproduction of the measured flood waves in some actual events, as compared to the more sophisticated Phase 3 model. For these cases tested at least, it appears advantageous to lump many of the contributing factors into several empirical parameters,

given that the exact effects of the ice on the propagating wave are not yet well understood. However, it is important to note that the simplified model is not applicable to cases where the ice run released from a jam is decelerating or stopping, which would significantly affect the height and celerity of the propagating wave. From the literature (e.g. Kowalczyk Hutchinson and Hicks 2007) this would appear to be a common scenario, at least for some sites. The Phase 3 model, which incorporated full ice momentum effects, has the capability to simulate the variations of wave characteristics as ice runs pass by geometry restrictions (e.g. channel width and slope variations) or if arrested by man-made obstacles (e.g. ice retention structures).

7.2 Development and Implementation of a New, Robust Constitutive Model for Internal Resistance of Ice Accumulations

It was realized during the work of this thesis, that the release and formation of ice jams are intimately connected to each other. Therefore, the Phase 3 model (*River1-D: ice jam*) was developed with the ability of handling both ice jam formation and release, by including the ice momentum explicitly and deterministically. Unlike most of the existing models, which use the Eulerian approach for the hydrodynamic component only, and the Lagrangian approach for ice dynamic component, the proposed Phase 3 model employs a purely Eulerian finite element method for both the hydrodynamic and ice dynamic components. This is a unique aspect of the model, which offers the advantage of eliminating the requirement to interpolate back and forth between the Lagrangian particles and the Eulerian grid.

The proposed *River1-D: ice jam* model is unique also for the new constitutive model for internal resistance of ice accumulations. It is the first effort to explore the internal resistance of ice accumulations in rivers based on experimental data, which is, specifically, stress and strain rate calculated from the existing measurements of many key parameters during experimental ice jam consolidation events. The newly formulated constitutive model was not only supported by the experimental stress-strain rate relationship, but also showed numerical advantages than the widely used Hibler's viscous-plastic constitutive model and has the ability to simulate both moving and stationary ice accumulations, without the need for any additional artificial stoppage criteria.

The proposed *River1-D: ice jam* model, incorporating this new constitutive model, was successfully applied to a series of experimental ice jam consolidation events. The model was shown to be capable not only of reproducing the final ice jam configuration (ice thickness and water level), but is also able to capture the time-variations of many key parameters (e.g. water level, ice thickness, flow discharge, ice discharge) during the formation processes. In addition to assessing flood levels caused by ice jams, it can provide valuable information for the design of ice-control structures since the model can predict the forces exerted by ice jam on such structures.

7.3 Scientific Documentation and Interpretation of Ice Jam Processes in the Field

The scarcity of comprehensive field data has limited our knowledge about the physics of ice jam formation and release dynamics. Thus, there is always a need for more field data. Using a variety of water and ice level monitoring techniques, as well as other ground and

aerial observation methods, unprecedented quantitative and qualitative data describing ice jam formation and release behaviours was obtained during the 2006 and 2007 breakup on the Athabasca River, AB. The most comprehensive data set, which is probably the most complete documentation of ice jam dynamics by any group to date, was obtained during the 2007 breakup and includes the following.

(1) The top of the ice profile along an ice jam was measured just hours before its release.

(2) Water levels were measured at multiple stations along the river, not only downstream of the original jam toe, but also upstream and within the jam, before, during, and after its release.

(3) A regressive wave was observed for the first time and its speed was documented.

(4) An ice run was observed to impact the ice jam, causing it to shove and then release. The entire shoving process was videotaped and the speed of the shoving front was documented.

(5) A sheet breaking front was observed and its speed was recorded as the ice jam released into the downstream intact ice cover.

Such information provides a comprehensive view of the entire ice jam event and facilitates validation of the existing numerical models in more aspects than just the downstream propagation of flood waves.

The Phase 1 and 2 numerical models were used to analyze one unimpeded, and one impeded, ice jam release event observed. In addition to good reproduction of key parameters (peak water level, wave celerity, waveform, and the speed of the breaking

front), the numerical modeling effort also aided in the interpretation of the data sets. As discussed in Chapter 4, water levels were observed varying in the field, and numerical modeling can explain what exact ice movement caused the variation; the speed of the sheet breaking front was measured in the field, and numerical modeling can determine the relation between front speed and the local velocity of the ice rubble released from the original jam.

7.4 Future Recommendations

To further improve the model's capability of predicting when and where an ice jam may form, future development of the numerical model recommended by the author would be:

- to include appropriate breaking criteria of ice cover in the receiving channel, which will facilitate a further investigation of the breaking fronts, and prediction of the possible stoppage of ice runs when encountering competent ice cover;

- to include natural channel geometries, such as channel sinuosity, bars and islands, which will facilitate the prediction of the changes of ice movements due to geometry restrictions other than the variation of channel width and slope.

The author also strongly recommends continuing collection of scientific data in the field. Qualitative documentations and quantitative measurements of any aspects prior, during and after ice jam events are important for further improving our understanding of these highly complicated processes. This will also serve to provide more complete validation data set for existing numerical models like those proposed in this thesis.

Appendix A – Sensitivity Analysis of *River1-D: Ice Jam* Model

A.1 Introduction

Some of the input parameters required by *River1-D: ice jam* model are difficult or even impossible to quantify based on field measurements, mainly because it is generally unsafe to make direct measurements of breakup ice jams. Therefore, a sensitivity analysis is carried out on the various input parameters for *River1-D: ice jam* model. The objective is to identify which parameters could reasonably be left constant during the model calibration and accordingly reduce the calibration efforts. Effects of three groups of parameters: i.e. mechanical parameters of ice jams, flow conditions, and empirical constants, were investigated.

A baseline configuration was first designed to provide a standard against which the other runs with different values of parameters could be compared. It simulates a very common scenario during river break-up that incoming ice runs are stopped by obstacles (man-made or natural) to form an ice jam. Each parameter was varied ±10% from the default value one at a time; and the percentage difference in the output compare to the baseline run was then calculated. If the output varied less than ±10%, it is deemed that the proposed model is not particularly sensitive to the parameter variation. Focus was not only given to the configuration of the final ice jam, but also to the continuous time-series variables (e.g. water level, water discharge, ice thickness, ice discharge) at representative locations.

A.2 Parameters

Scaling the ice mass and momentum conservation equations to find out the governing non-dimensionalized parameters facilitates an understanding of physics. The ice mass and momentum conservation equations presented in Chapter 5 are written here with slight changes for the convenience of this sensitivity analysis. Instead of using A_i and V_i as in Chapter 5, variables A_i and Q_i are used in these equations. Also, the dispersion term is neglected.

[A-1] $$\frac{\partial A_i}{\partial t}+\frac{\partial Q_i}{\partial x}=0$$

[A-2] $$\frac{\partial Q_i}{\partial t}+\frac{\partial (V_i Q_i)}{\partial x}+gA_i\frac{\partial H}{\partial x}=gA_iS_0+A_i\frac{(V_w-V_i)|V_w-V_i|}{t_iC_*^2}+\frac{1}{\rho_i}\frac{\partial(\sigma A_i)}{\partial x}-\frac{2K_{xy}\tan\phi A_i}{\rho_i B}\sigma$$

in which: C_* is the non-dimensional Chezy coefficient; all the other variables are the same as defined in Chapter 5.

The non-dimensional variables to be used in this analysis are:

[A-3] $$x'=\frac{x}{L};t'=\frac{t}{T};A_i'=\frac{A_i}{A_0};t_i'=\frac{t_i}{A_0/B};Q_i'=\frac{Q_i}{Q_0};V_w',V_i'=\frac{V_w,V_i}{V_0};$$
$$H',R_i'=\frac{H',R_i}{Y_0};\text{and},\sigma'=\frac{\sigma}{P}$$

The ice mass conservation equation can be rewritten as:

[A-4] $$\frac{\partial A_i'}{\partial t'}+\frac{Q_0T}{A_0L}\frac{\partial Q_i'}{\partial x'}=0$$

If $\frac{Q_0 T}{A_0 L} = V_0 \frac{T}{L} = 1$, i.e., $V_0 = \frac{L}{T}$, equation [A-4] becomes:

[A-5] $$\frac{\partial A_i'}{\partial t'} + \frac{\partial Q_i'}{\partial x'} = 0$$

The ice momentum equation can be rewritten as:

[A-6] $$\frac{\partial Q_i'}{\partial t'} + \frac{\partial (V_i' Q_i')}{\partial x'} + \frac{1}{F^2} A_i' \frac{\partial H'}{\partial x'} = \frac{L}{Y_0 C_*^2}\left[1 + \frac{A_w}{A_0}\frac{(V_w' - V_i')|V_w' - V_i'|}{t_i'}\right] A_i' + \beta_1 \frac{1}{F^2}\frac{A_0}{A_w}\left[\frac{\partial (A_i' \sigma' t_i')}{\partial x'} - \beta_2 \frac{L}{B}\sigma' t_i'\right]$$

in which: Froude number $F = V_0 / \sqrt{g Y_0}$; $A_w = Y_0 B$; β_1, β_2 are two constants:

[A-7] $$\beta_1 = \frac{1}{2}\tan^2\left(\frac{\pi}{4} + \frac{\phi}{2}\right)(1 - s_i)$$

[A-8] $$\beta_2 = 2K_{xy}\tan\phi$$

Therefore, there are four non-dimensional parameters: Froude number F, $L/(Y_0 C_*^2)$, A_0/A_w, and L/B. L is a length scale for the x-direction which represents the length of the reach of interest; Y_0 is a depth scale which represents the normal depth of the unperturbed flow; the velocity scale, V_0, could be the mean velocity of the unperturbed flow; A_0 and A_w are area scales, which could be the total ice volume and channel storage per unit width respectively.

The second group of parameters is related to ice jam properties, including the internal friction angle ϕ, seepage flow coefficient λ, maximum allowable ice concentration N_{max},

and a jam strength coefficient μ, which lumps together several parameters since each these parameters are very difficult to be determined individually.

$$[\text{A-9}] \quad \mu = K_{xy} \tan\phi \tan^2\left(\frac{\pi}{4} + \frac{\phi}{2}\right) N$$

There are also several parameters used in the model, which are basically determined based on the modeler's experience. They may be able to be calibrated towards field or experimental data. This group of parameters include the dispersion parameter α used in the ice mass conservation equation:

$$[\text{A-10}] \quad \frac{\partial A_i}{\partial t} + \frac{\partial Q_i}{\partial x} = (\alpha V_i)\frac{\partial^2 A_i}{\partial x^2}$$

and the time scale T, the constant m in the proposed constitutive model:

$$[\text{A-11}] \quad \sigma = (T)^{1/m} P(\dot{\varepsilon})^{1/m} - P$$

A.3 Sensitivity Analysis

The default value of each variable for the baseline test is listed in Table A-1. Totally 810,000 m^3 of ice was carried by the constant ambient flow, and formed an approximately 3300-m-long ice jam with its toe at station 5 km, where no ice is allowed to pass. The computed final ice jam profile of the baseline test is shown in Figure A-1. The continuous time-series variables (water level, ice thickness, water discharge, and ice discharge) at two representative stations (station 2 km and 4 km) are shown in Figure A-2 through A-4. It can be seen that all these variables show significant unsteadiness during the ice jam formation process even the ambient flow is steady.

In order to quantify the effects of parameter variation, each parameter was varied ±10% from the default value, and the variations in output are also expressed as percentage and are listed in Table A-2. Note that the dispersion parameter α was not varied ±10% since its default value is zero. A value of 1 had been used for α to do the sensitivity analysis. For the time-series continuous variables, the percentage difference is calculated at the time when the maximum variation from the baseline test happens; while for the final stable ice jam profile, the percentage difference is calculated as:

$$[\text{A-12}]\quad \varepsilon(\%) = \frac{\sum\left(Nt_i - (Nt_i)_B\right)}{\sum (Nt_i)_B}$$

in which: the subscript "B" denotes the results obtained from the baseline test; $\sum$ is done for all the computational nodes within the hypothetical channel. Model output using different values of parameters are shown in Figure A-5 through A-48. Model output from the baseline test is also correspondingly shown as dotted line in each figure for comparison.

It can be seen from Table A-2 and Figures A-5 through A-48 that the proposed model is not sensitive to the seepage velocity λ, the time scale T, and the dispersion parameter α, with non-discernible changes of outputs in comparison with the baseline outputs (marked in each figure). The model is also not particularly sensitive to the internal friction angle ϕ, jam strength parameter μ, $L/(Y_0 C_*^2)$, the constants m. The percentage difference is around ±5%, but is much bigger near the upstream end of the ice jam. This bigger variation can be seen from the figures showing the final ice jam profiles, and also those showing the time-series ice thickness variation at station 2 km. The big number of percentage

difference at this station is partly because of the relatively small ice thickness here. The proposed model is found to be more sensitive to the maximum allowable ice concentration N_{max}, Froude number F, length and width ratio L/B, and A_0/A_w. With the ±10% variation of these parameters, three to four items of the model output varied more than ±10% (Table A-2).

According to the sensitivity analysis, here are some useful information for implementing the proposed model:

1. It is recommended to use the default values (Table A-1) for the time scale T, the power law constant m, and the dispersion parameter α. These values are built in the *River1-D: ice jam* model.

2. Since the seepage velocity λ, jam strength parameter μ, internal friction angle ϕ are difficult to accurately determine, and the proposed model is not particularly sensitive to these input parameters, the default values (Table A-1) can be used unless a different reliable value for any of them is available.

3. It is desirable, although sometime might be extremely difficult, to have a reliable knowledge of the flow condition and ice condition, since the model is more sensitive to the Froude number F, length and width ratio L/B, the composite roughness of the channel with ice, how much ice is available A_0/A_w, and the maximum allowable ice concentration N_{max}.

Table A-1 List of baseline parameters for sensitivity analysis.

Parameter	Value	Description
L	5000 m	Channel length between the jam toe and the upstream boundary
B	200 m	Channel width
S_0	0.0005	Channel slope
Q	400 m^3/s	Carrier discharge
F	0.375	Froude number
L/B	25	Ratio of length and width
A_0/A_w	0.568	Ratio of incoming ice volume and channel storage volume
$L/(Y_0C_*^2)$	60	
n_b	0.020	Manning's roughness coefficient for bed
n_i	0.050	Manning's roughness coefficient for ice
ϕ	45°	Internal friction angle of ice
μ	1.0	Jam strength parameter: $\mu = K_p K_{xy} \tan\Phi N$
λ	1.50 m/s	Seepage coefficient
N_{max}	80%	Maximum allowable ice concentration
m	7	Constant in the power law
α	0 m	Dispersion parameter
T	1 s	Time scale

Table A-2 Percentage difference of model output for varying each parameter ±10%.

Parameter		ϕ	μ	λ	N_{max}	F	L/B
Final jam profile		± 3.0%	± 3.8%	± 0.2%	± 10.1%	± 5.3%	± 3.8%
Final water surface		± 0.3%	± 0.4%	± 0.1%	± 0.4%	± 1.8%	± 0.4%
Time-series variables							
2 km	H	± 0.3%	± 0.3%	± 0.1%	± 0.7%	± 0.6%	± 0.3%
	t_i	± 44.8%	± 25.9%	± 1.7%	± 75.1%	± 36.0%	± 36.9%
	Q_w	-	-	-	± 1.7%	± 12.4%	± 10.6%
	Q_i	-	-	-	± 5.4%	± 5.1%	± 14.5%
4 km	H	± 0.5%	± 0.9%	± 0.1%	± 0.1%	± 2.8%	± 1.0%
	t_i	± 1.5%	± 2.6%	-	± 3.8%	± 3.3%	± 2.5%
	Q_w	-	-	-	± 3.8%	± 13.9%	± 10.3%
	Q_i	-	-	-	± 9.3%	± 1.4%	± 17.8%

Parameter		A_0/A_w	$L/(Y_0C_*^2)$	m	T	$^*\alpha$
Final jam profile		± 10.1%	± 1.5%	± 1.4%	± 0.1%	-
Final water surface		± 0.8%	± 0.5%	± 0.2%	± 0.1%	-
Time-series variables						
2 km	H	± 1.4%	± 0.7%	± 0.2%	-	-
	t_i	± 83.5%	± 13.2%	± 15.8%	±1.0%	-
	Q_w	± 4.2%	-	-	-	-
	Q_i	± 4.8%	-	-	-	-
4 km	H	± 0.4%	± 0.7%	± 0.5%	-	-
	t_i	± 3.1%	± 1.0%	± 1.0%	± 0.1%	-
	Q_w	± 6.1%	-	-	-	-
	Q_i	± 0.5%	-	-	-	-

- variation is not discernible

* this parameter was not varied by ±10% since its default value was zero.

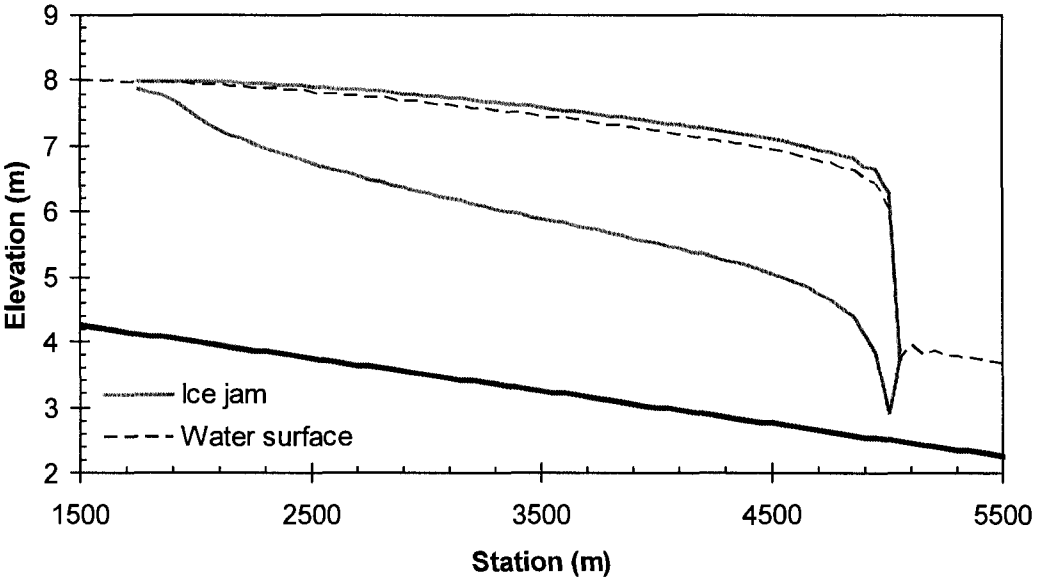

Figure A-1 Computed final ice jam configuration for the baseline test.

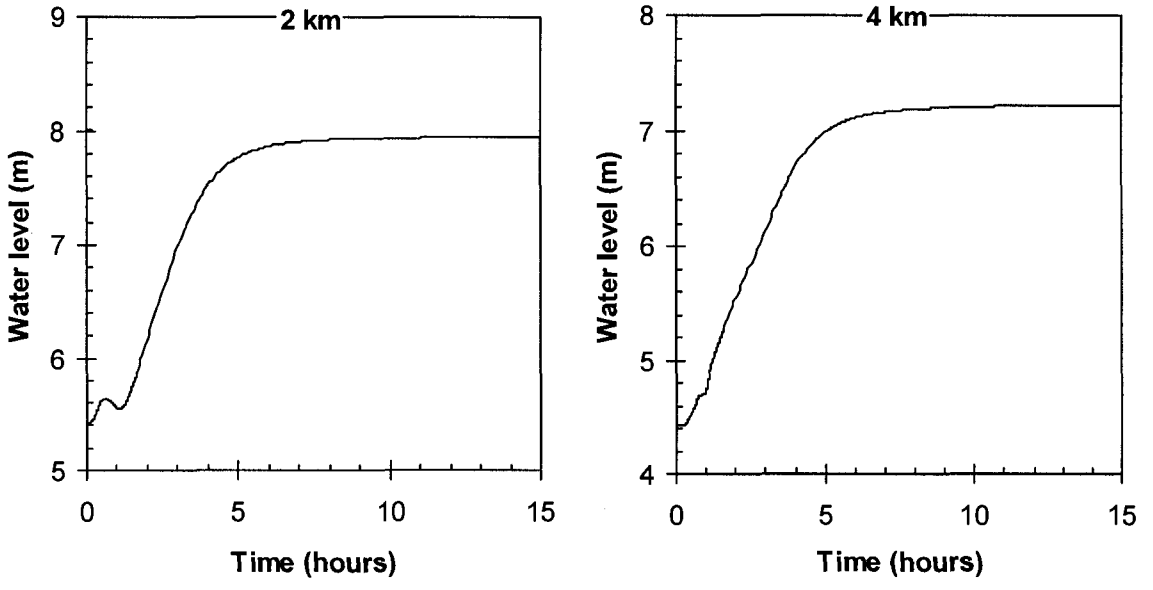

Figure A-2 Computed continuous time-series water level at station 2 km and 4 km for the baseline test.

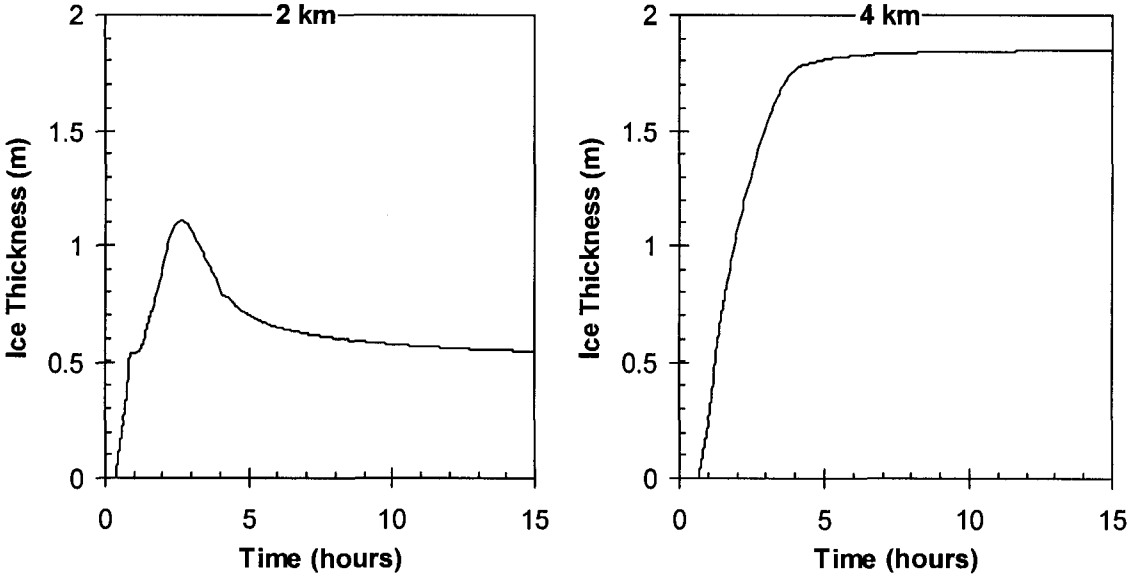

Figure A-3 Computed continuous time-series ice thickness at station 2 km and 4 km for the baseline test.

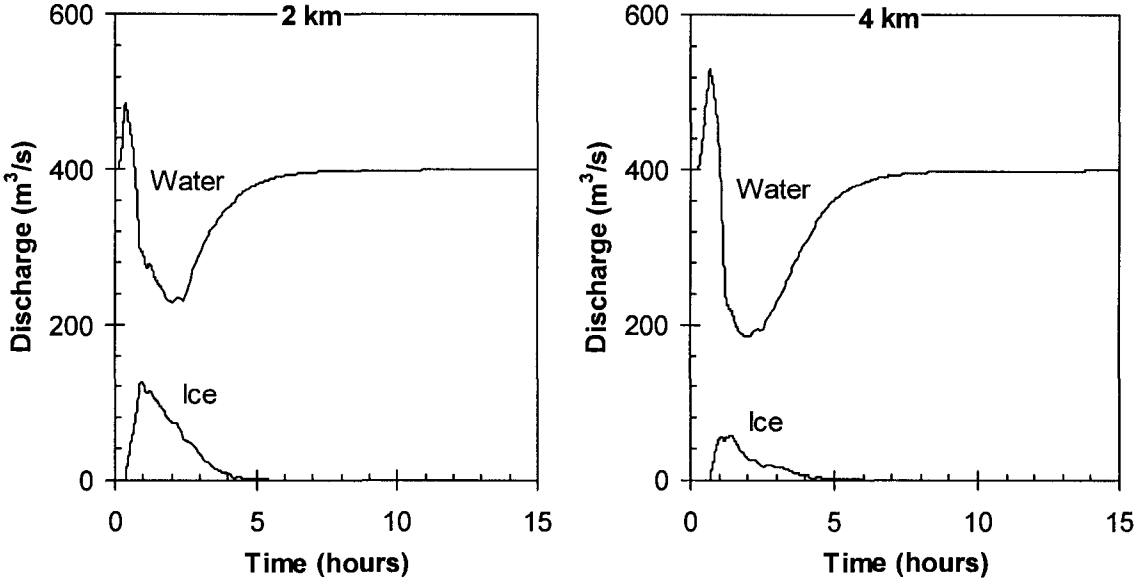

Figure A-4 Computed continuous time-series water and ice discharge at station 2 km and 4 km for the baseline test.

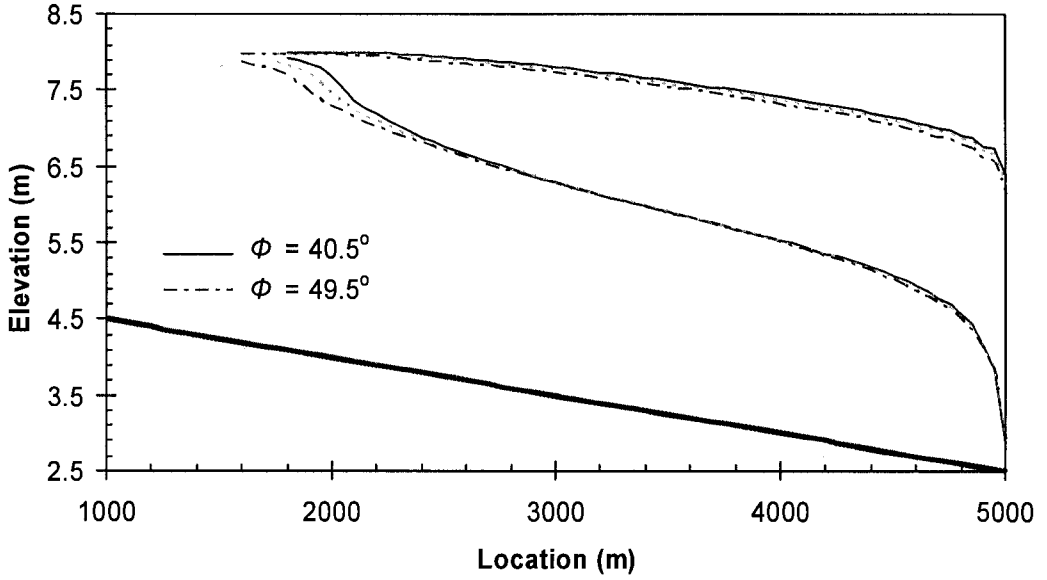

Figure A-5 Sensitivity of *River1-D*: ice jam model profiles to the internal friction angle ϕ.

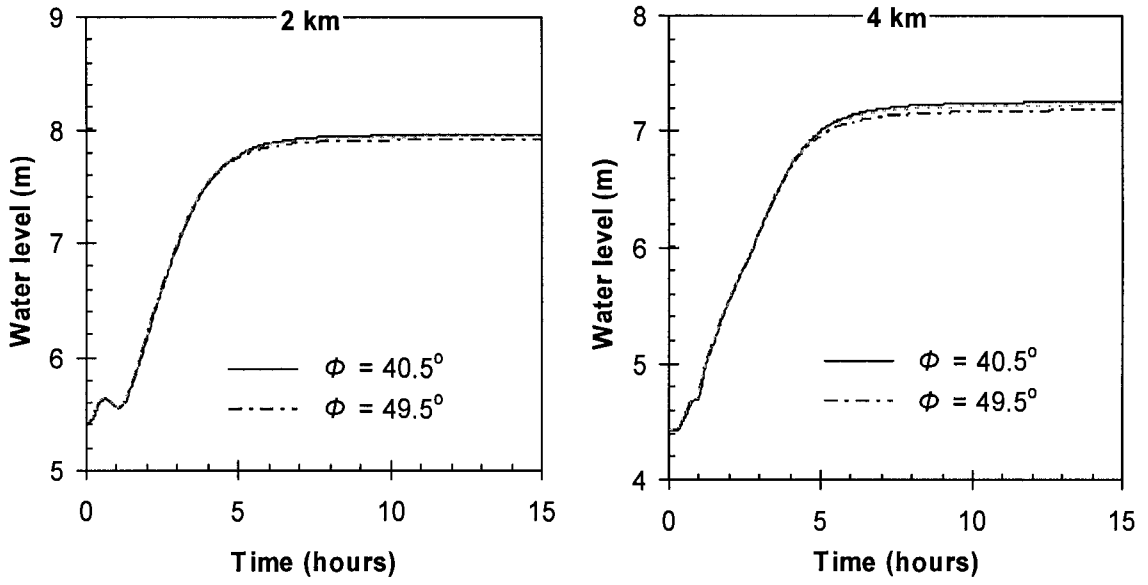

Figure A-6 Sensitivity of *River1-D*: ice jam modeled water level variation at station 2 km and 4 km to the internal friction angle ϕ.

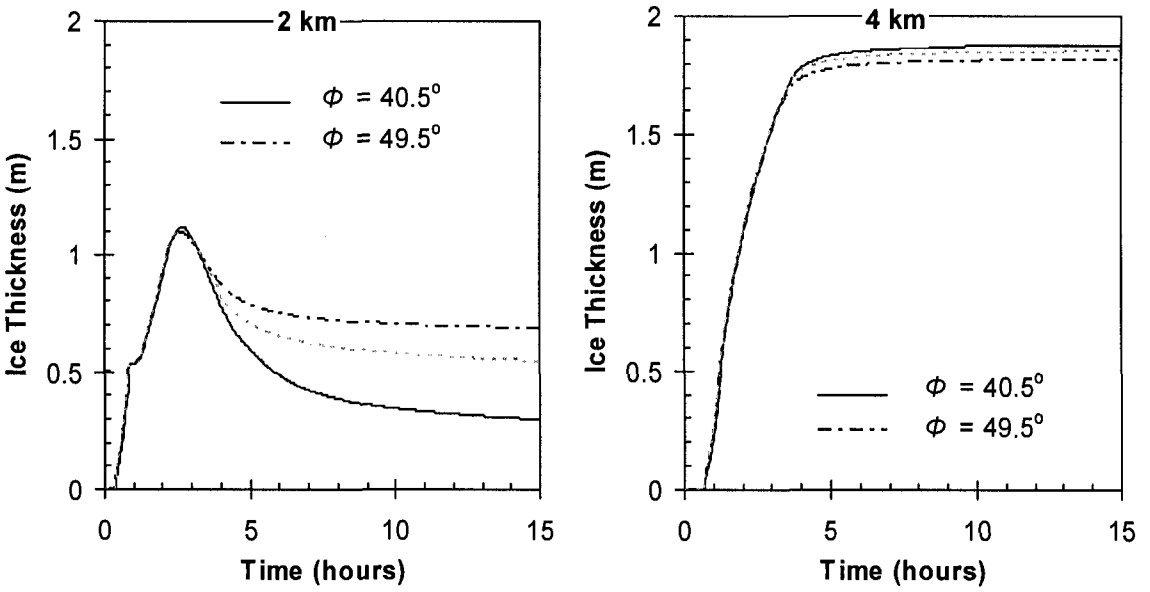

Figure A-7 Sensitivity of *River1-D*: ice jam modeled ice thickness variation at station 2 km and 4 km to the internal friction angle ϕ.

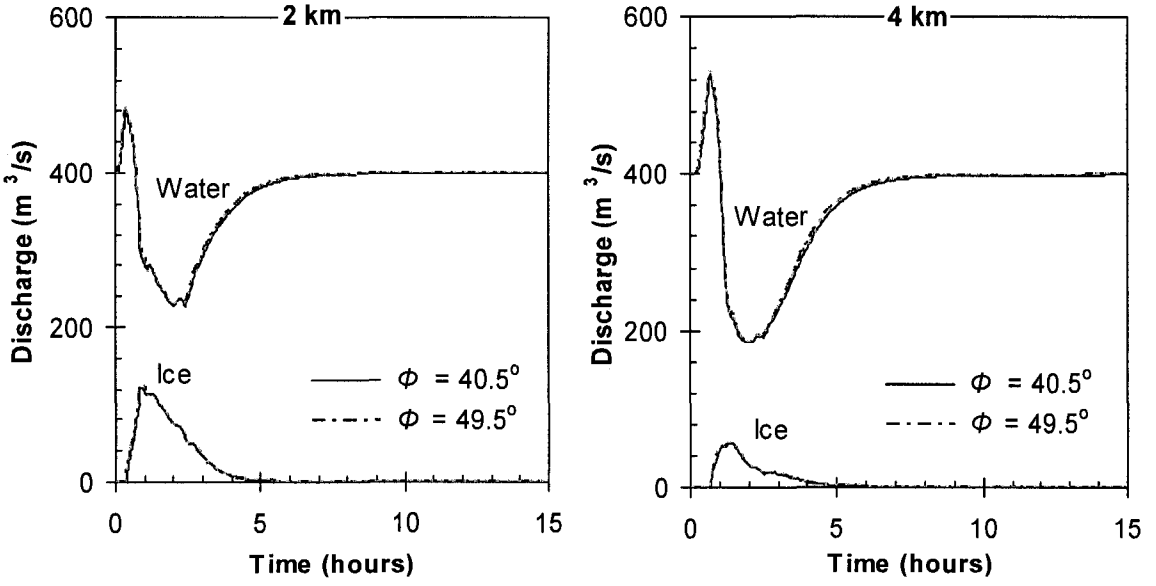

Figure A-8 Sensitivity of *River1-D*: ice jam modeled water discharge and ice discharge variation at station 2 km and 4 km to the internal friction angle ϕ.

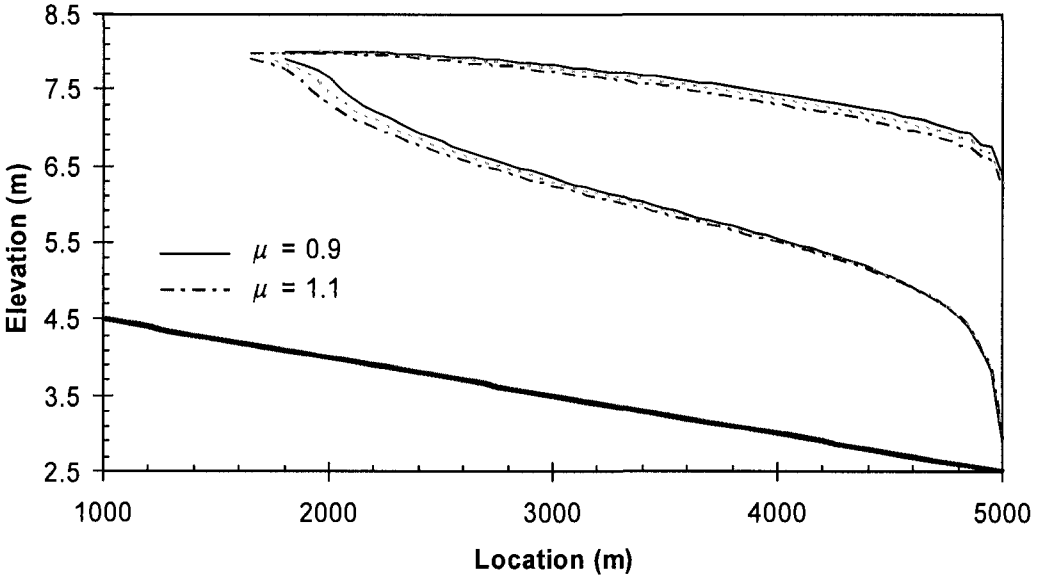

Figure A-9 Sensitivity of *River1-D*: ice jam model profiles to the combined ice jam strength coefficient μ.

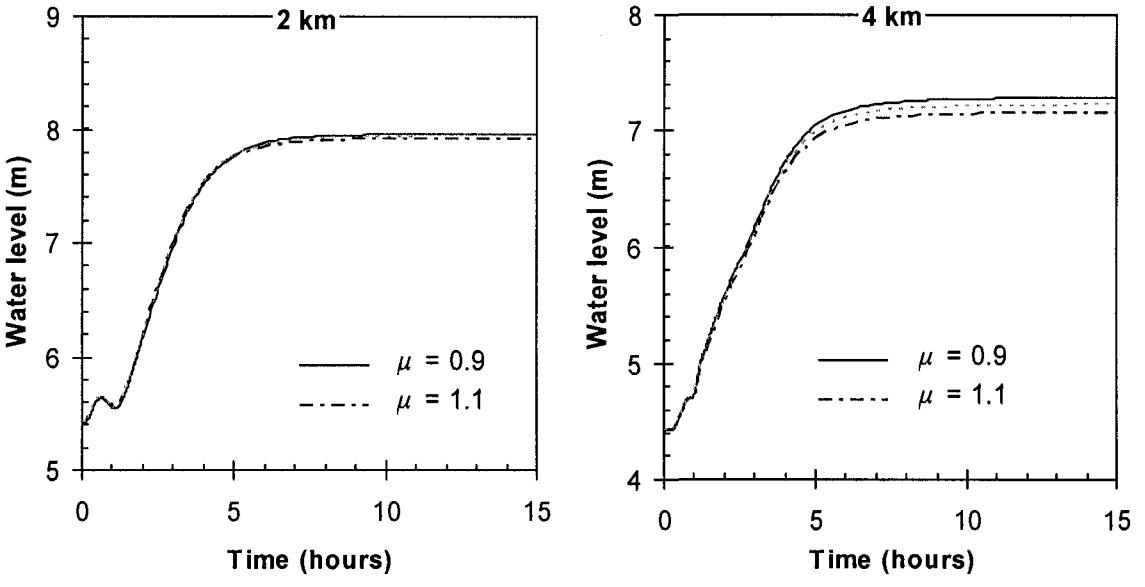

Figure A-10 Sensitivity of *River1-D*: ice jam modeled water level variation at station 2 km and 4 km to the combined ice jam strength coefficient μ.

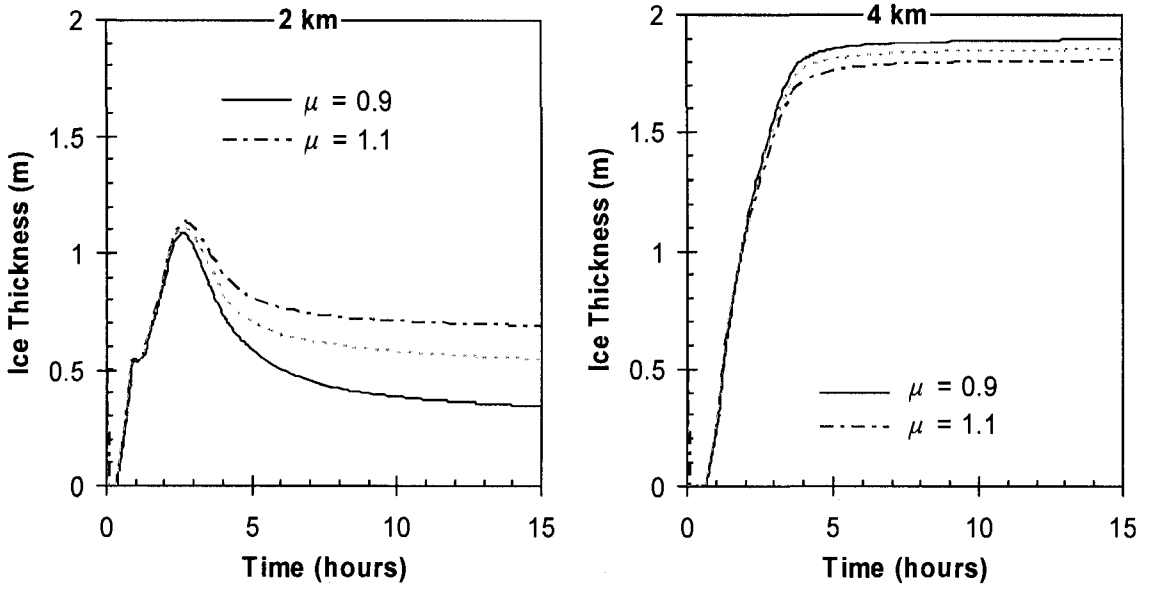

Figure A-11 Sensitivity of *River1-D*: ice jam modeled ice thickness variation at station 2 km and 4 km to the combined ice jam strength coefficient μ.

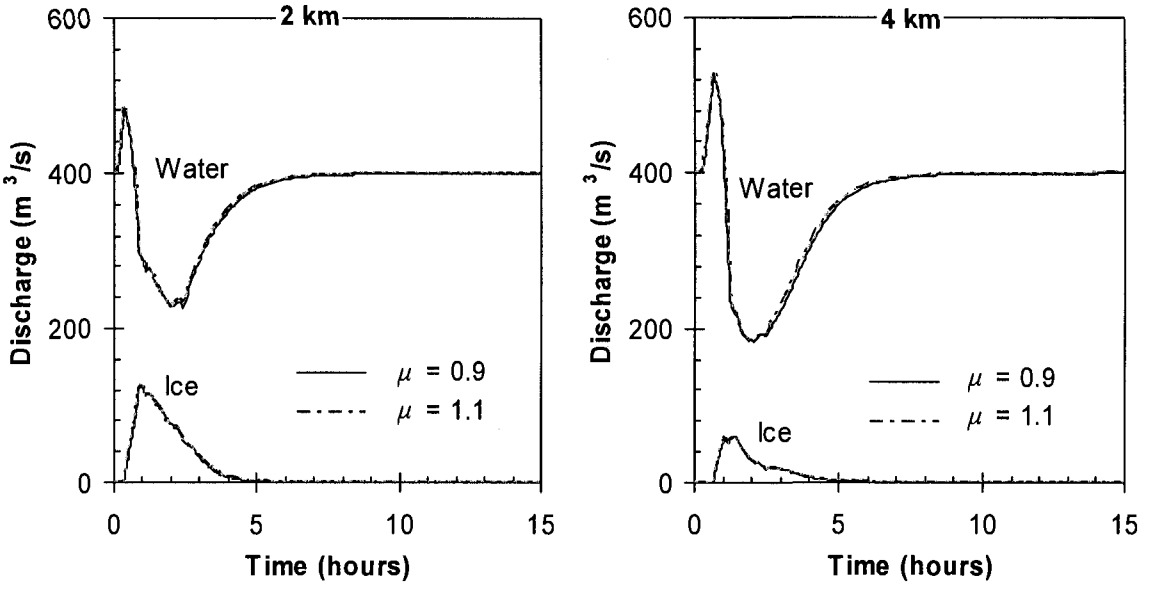

Figure A-12 Sensitivity of *River1-D*: ice jam modeled water discharge and ice discharge variation at station 2 km and 4 km to the combined ice jam strength coefficient μ.

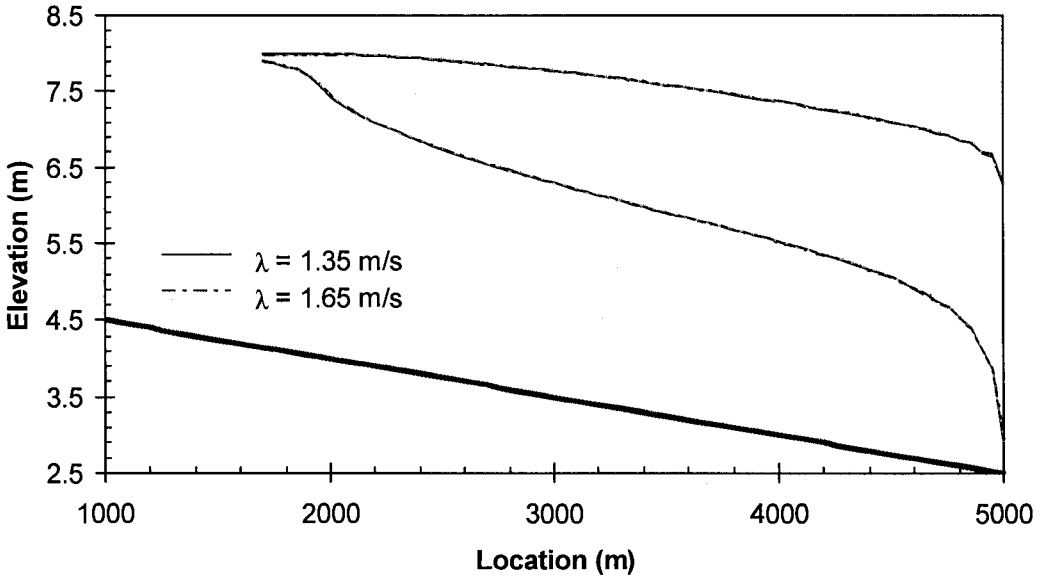

Figure A-13 Sensitivity of *River1-D*: ice jam model profiles to the seepage coefficient of the ice accumulation (λ).

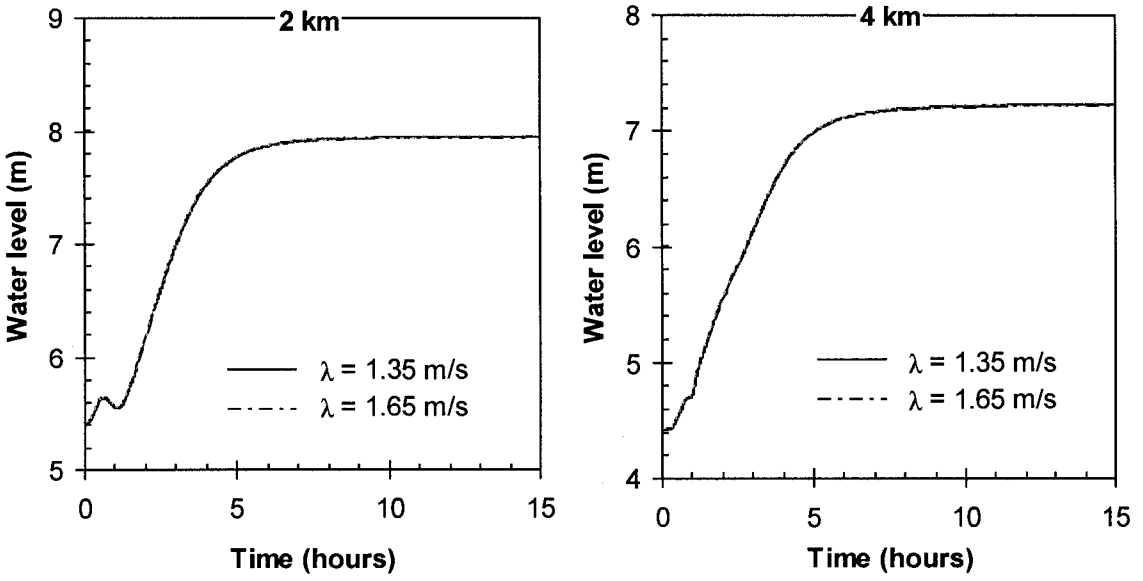

Figure A-14 Sensitivity of *River1-D*: ice jam modeled water level variation at station 2 km and 4 km to the seepage coefficient λ.

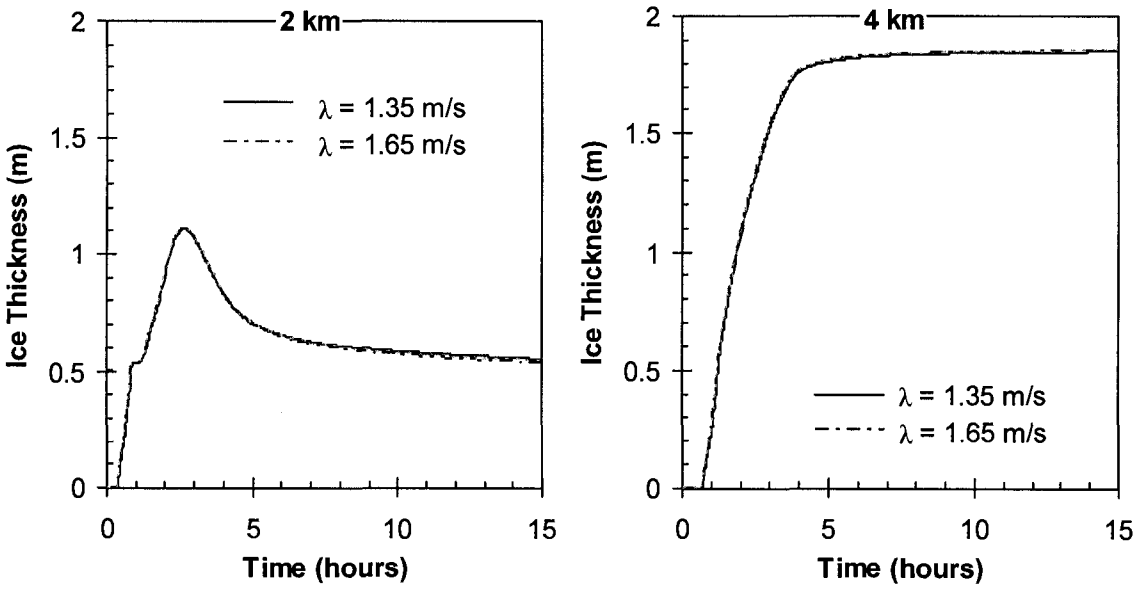

Figure A-15 Sensitivity of *River1-D*: ice jam modeled ice thickness variation at station 2 km and 4 km to the seepage coefficient λ.

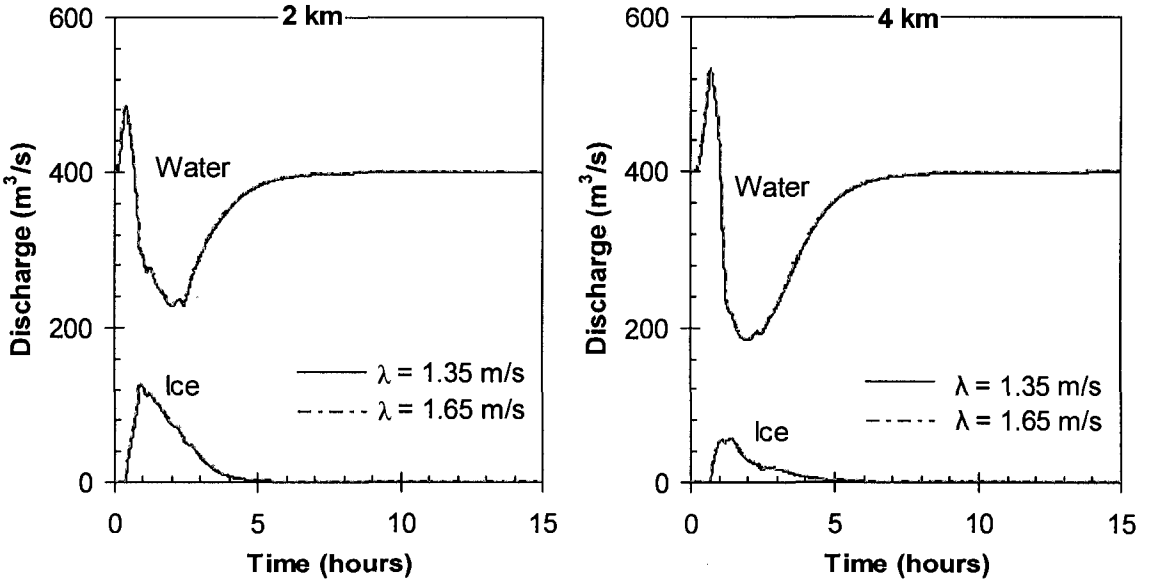

Figure A-16 Sensitivity of *River1-D*: ice jam modeled water discharge and ice discharge variation at station 2 km and 4 km to the seepage coefficient λ.

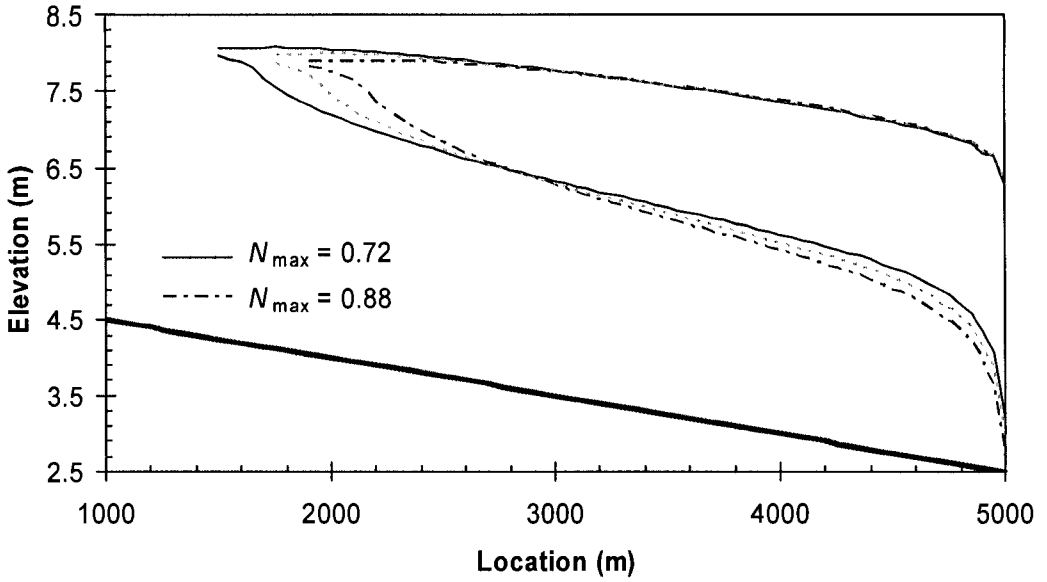

Figure A-17 Sensitivity of *River1-D*: ice jam model profiles to the maximum allowable ice concentration N_{max}.

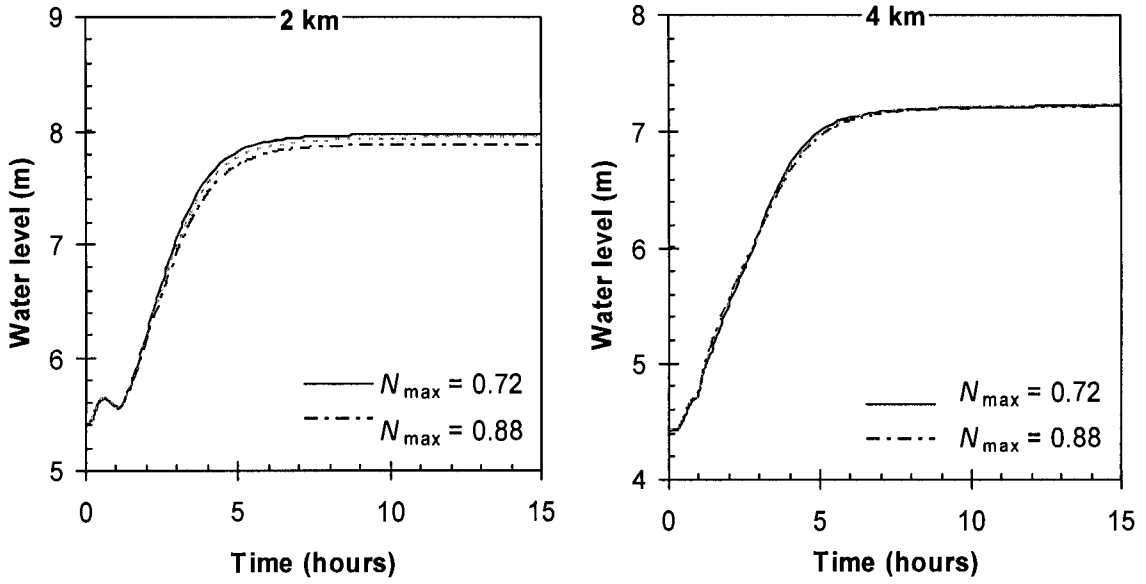

Figure A-18 Sensitivity of *River1-D*: ice jam modeled water level variation at station 2 km and 4 km to the maximum allowable ice concentration N_{max}.

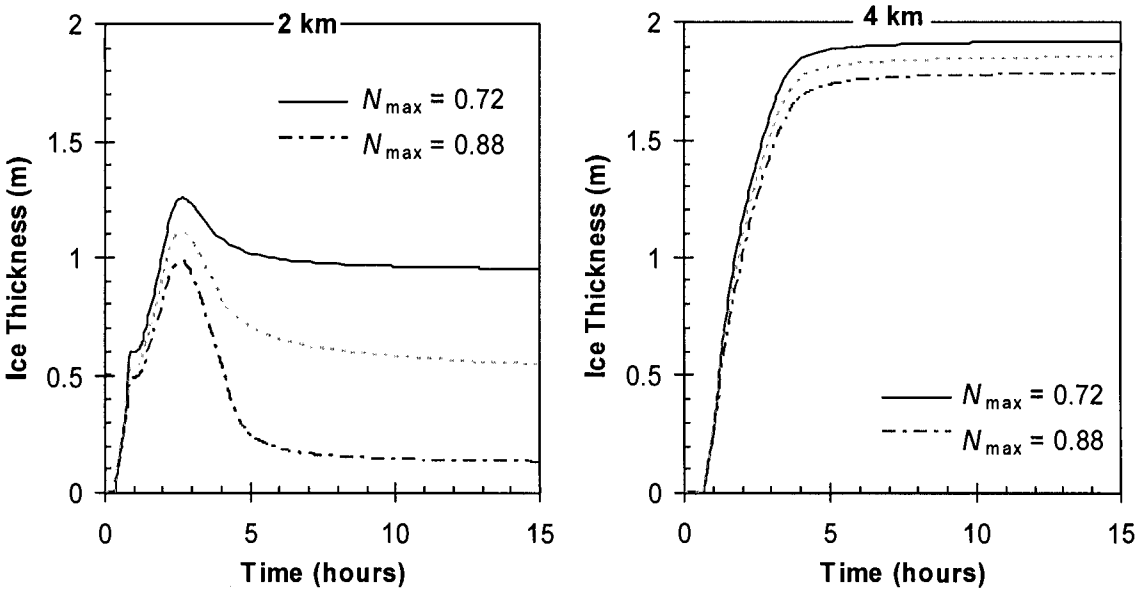

Figure A-19 Sensitivity of *River1-D*: ice jam modeled ice thickness variation at station 2 km and 4 km to the maximum allowable ice concentration N_{max}.

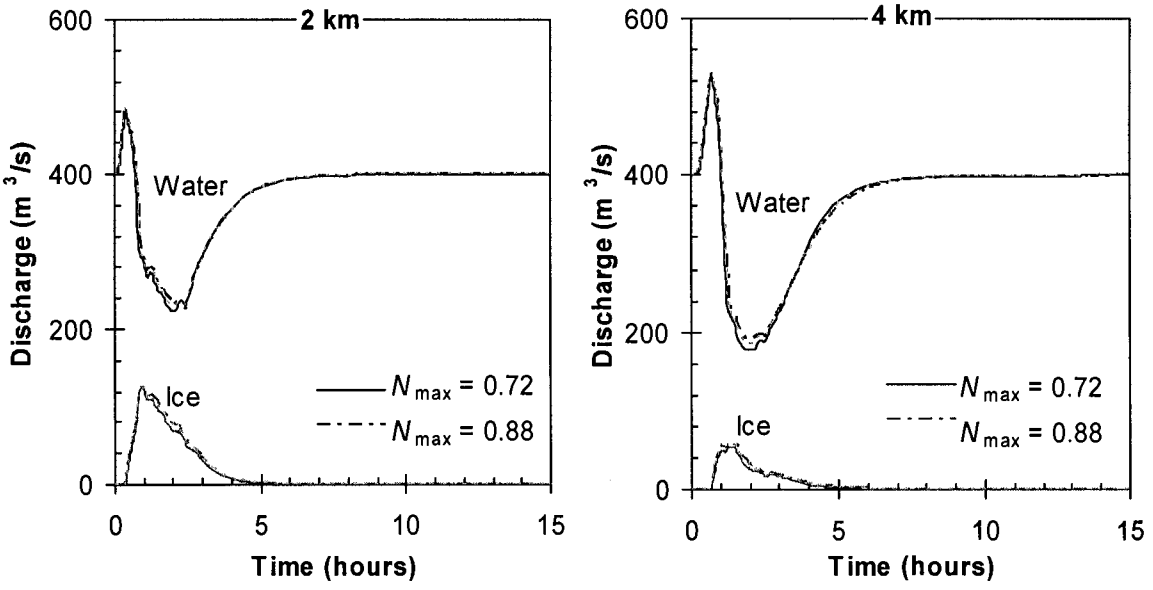

Figure A-20 Sensitivity of *River1-D*: ice jam modeled water discharge and ice discharge at station 2 km and 4 km to the maximum allowable ice concentration N_{max}.

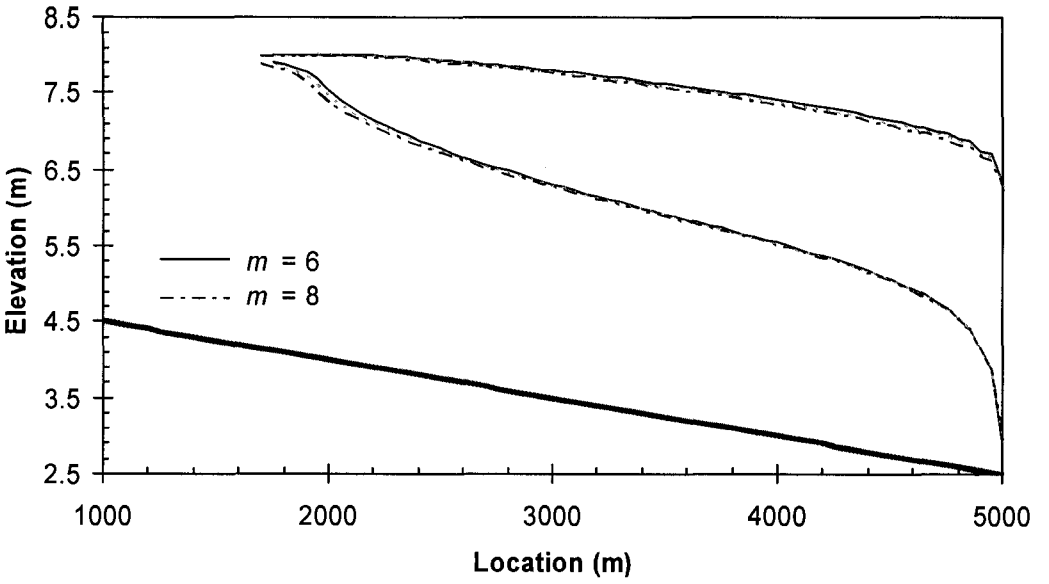

Figure A-21 Sensitivity of *River1-D*: ice jam model profiles to m (one-m^{th} power law) in the constitutive model.

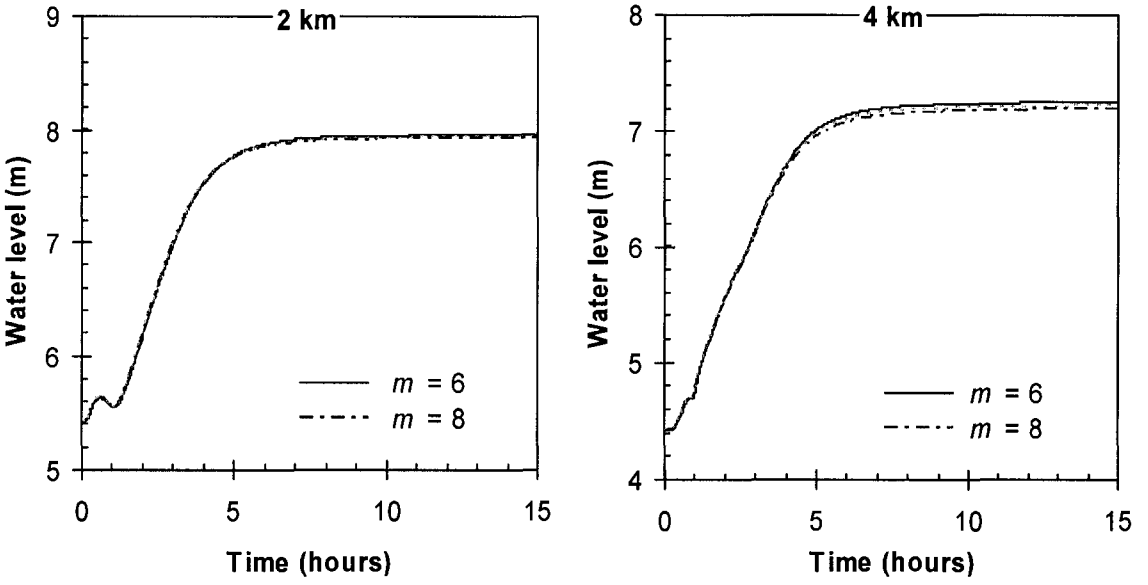

Figure A-22 Sensitivity of *River1-D*: ice jam modeled water level variation at station 2 km and 4 km to m (one-m^{th} power law) in the constitutive model.

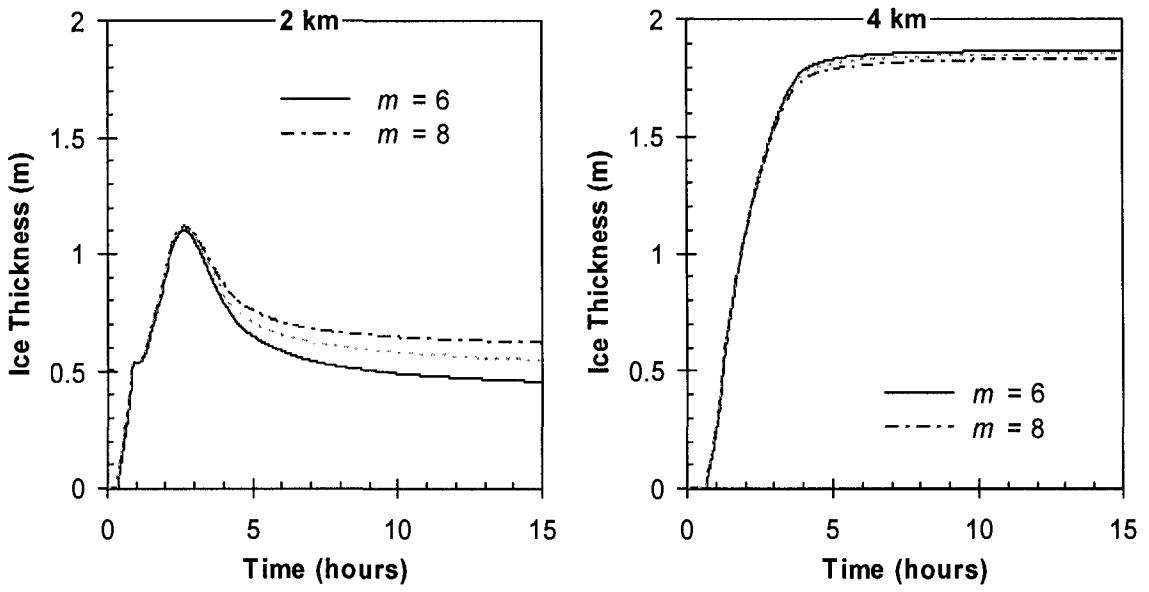

Figure A-23 Sensitivity of *River1-D*: ice jam modeled ice thickness variation at station 2 km and 4 km to m (one-m^{th} power law) in the constitutive model.

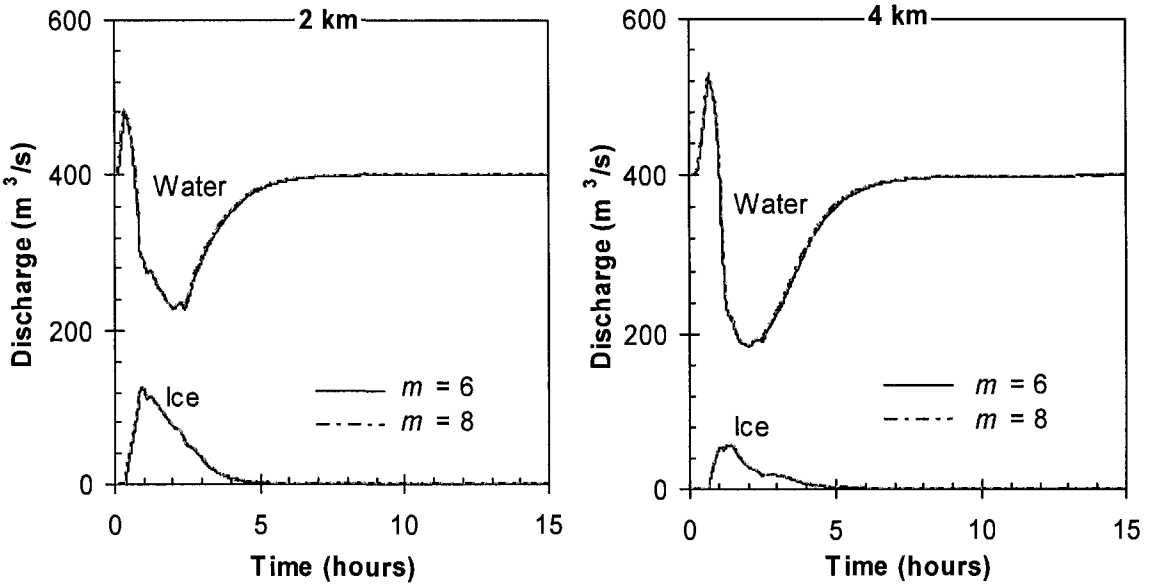

Figure A-24 Sensitivity of *River1-D*: ice jam modeled water discharge and ice discharge variation at station 2 km and 4 km to m (one-m^{th} power law) in the constitutive model.

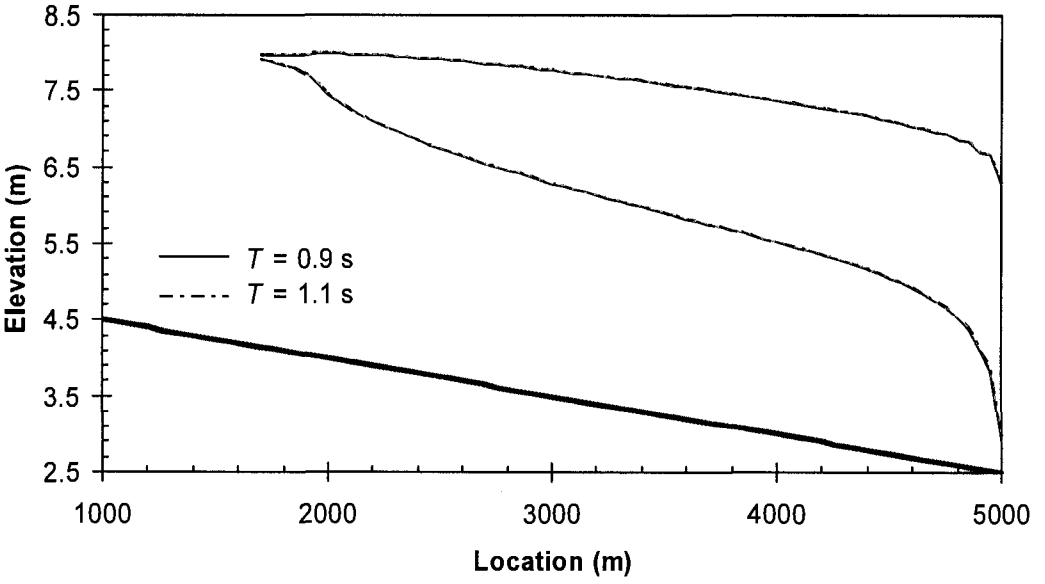

Figure A-25 Sensitivity of *River1-D*: ice jam model profiles to the time scale parameter *T*.

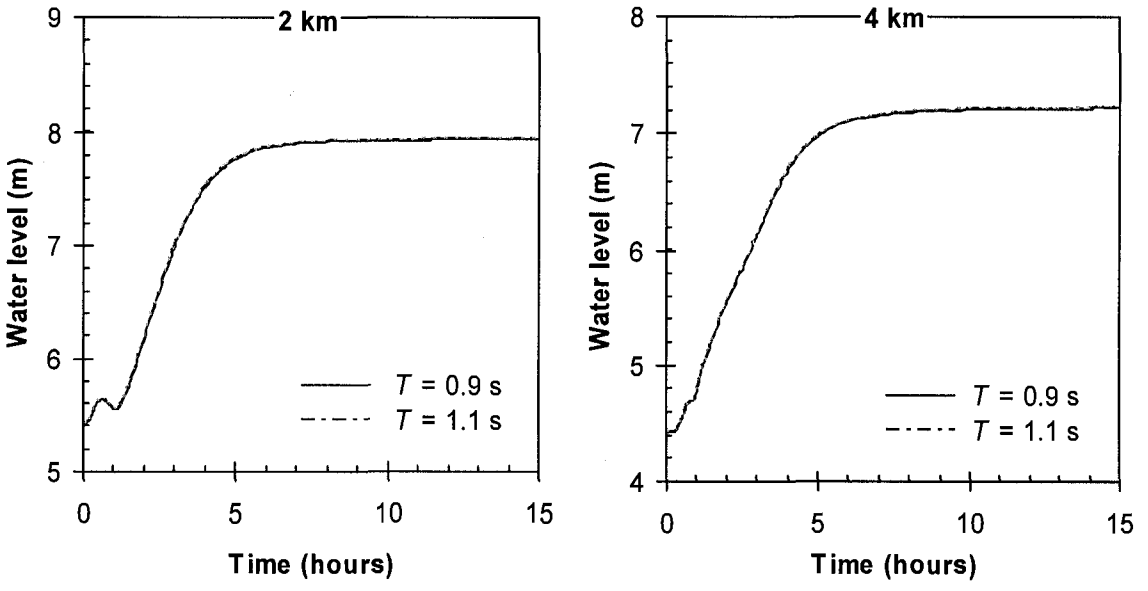

Figure A-26 Sensitivity of *River1-D*: ice jam modeled water level variation at station 2 km and 4 km to the time scale parameter *T*.

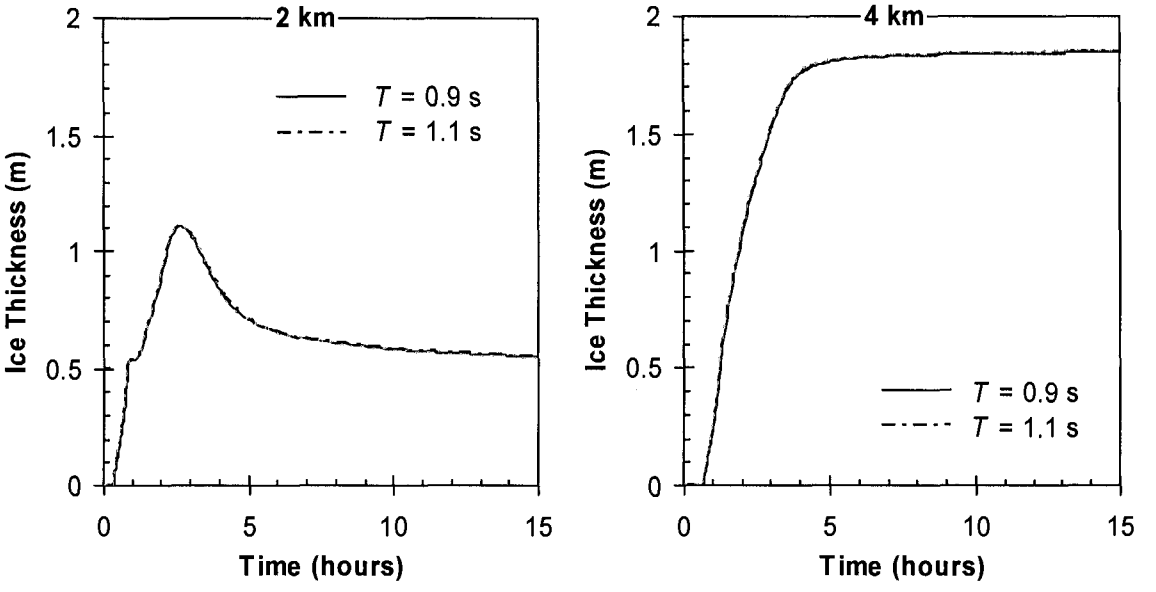

Figure A-27 Sensitivity of *River1-D*: ice jam modeled ice thickness variation at station 2 km and 4 km to the time scale parameter T.

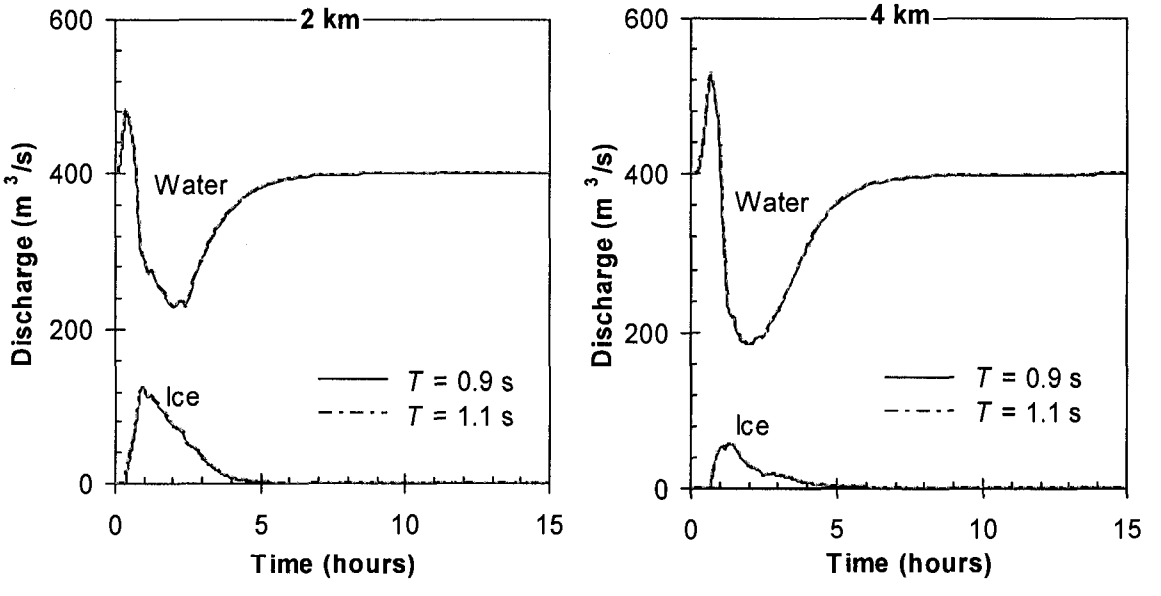

Figure A-28 Sensitivity of *River1-D*: ice jam modeled water discharge and ice discharge variation at station 2 km and 4 km to the time scale parameter T.

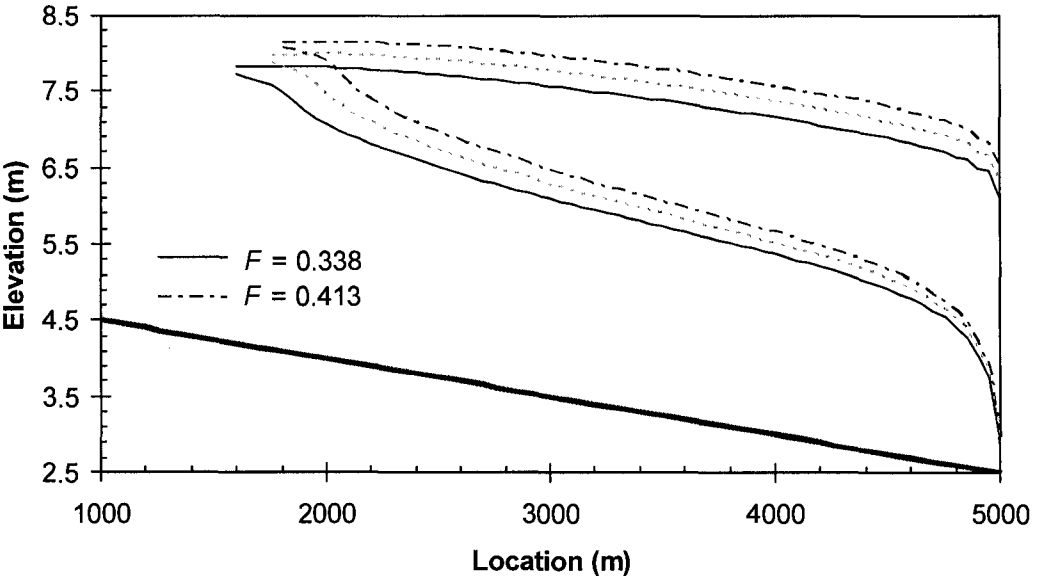

Figure A-29 Sensitivity of *River1-D*: ice jam model profiles to the Froude number *F*.

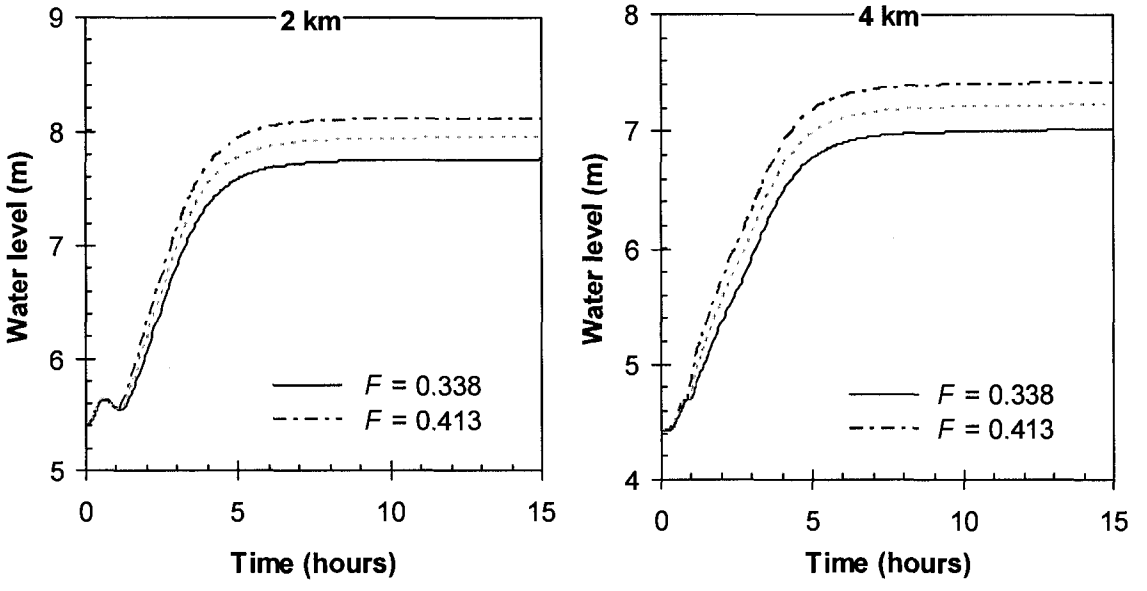

Figure A-30 Sensitivity of *River1-D*: ice jam modeled water level variation at station 2 km and 4 km to the Froude number *F*.

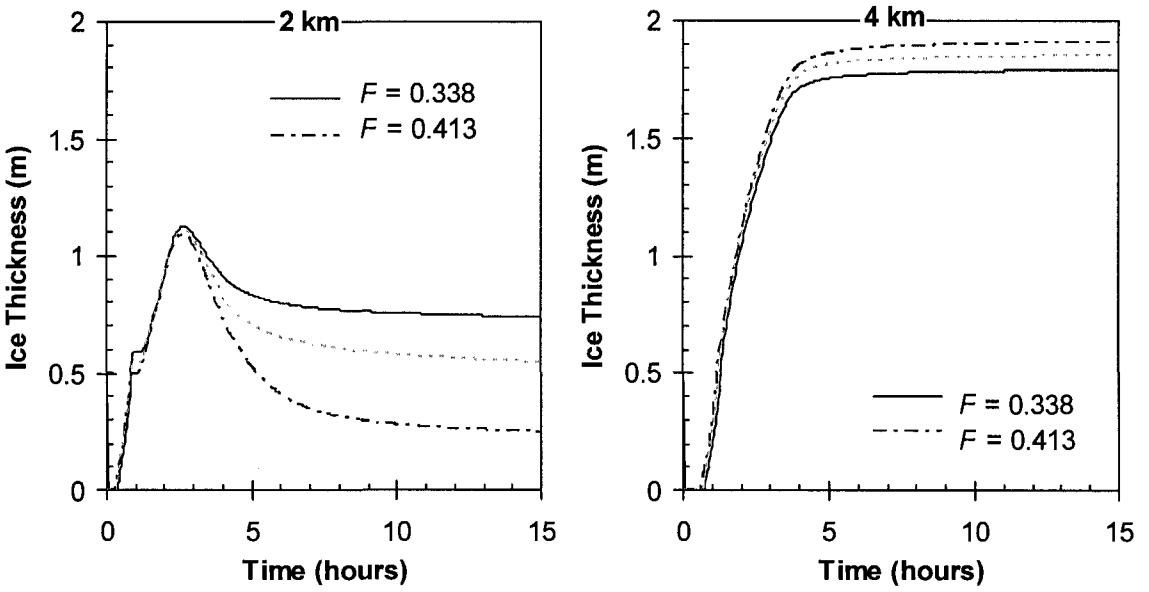

Figure A-31 Sensitivity of *River1-D*: ice jam modeled ice thickness variation at station 2 km and 4 km to the Froude number *F*.

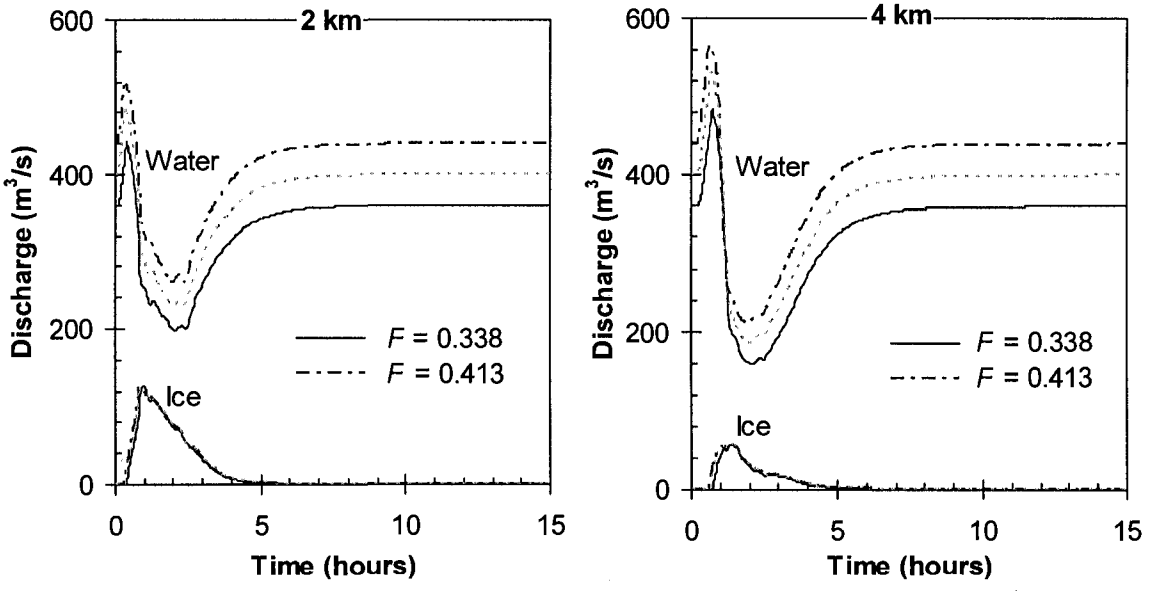

Figure A-32 Sensitivity of *River1-D: ice jam* modeled water discharge and ice discharge variation at station 2 km and 4 km to the Froude number *F*.

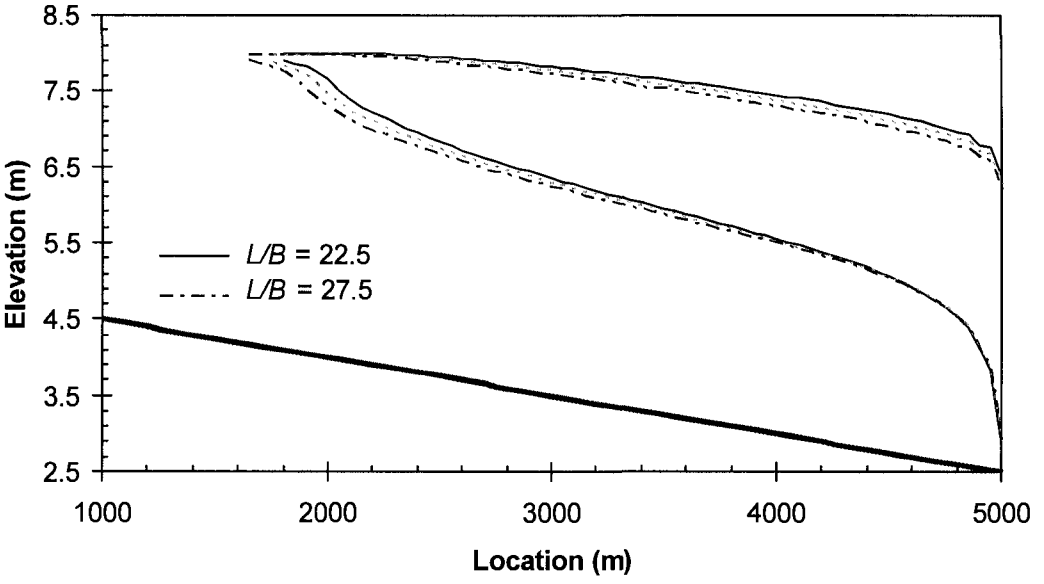

Figure A-33 Sensitivity of *River1-D*: ice jam model profiles to the *L/B* ratio.

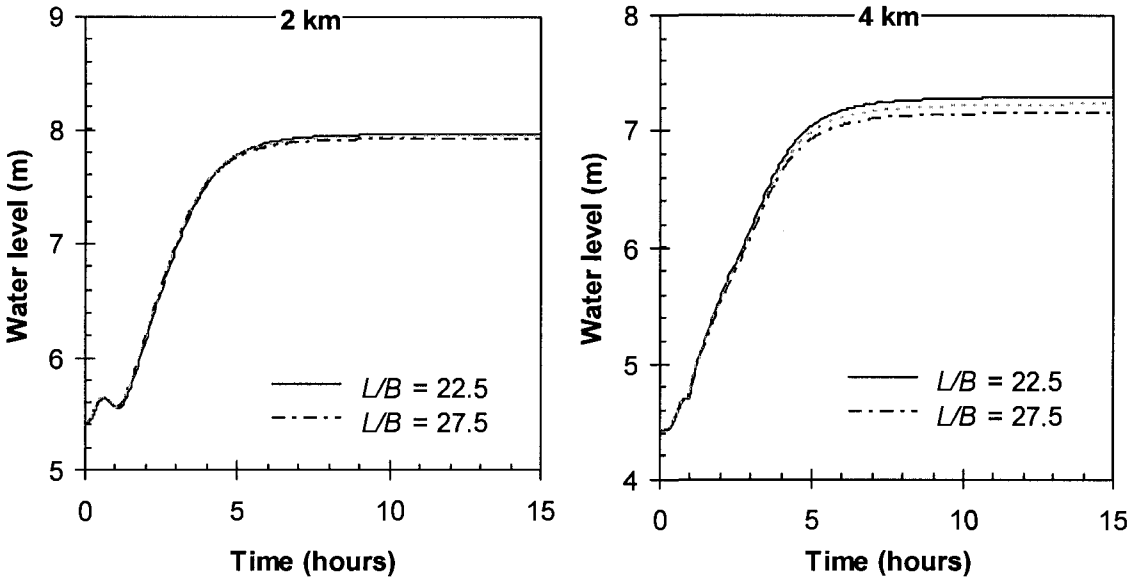

Figure A-34 Sensitivity of *River1-D*: ice jam modeled water level variation at station 2 km and 4 km to the *L/B* ratio.

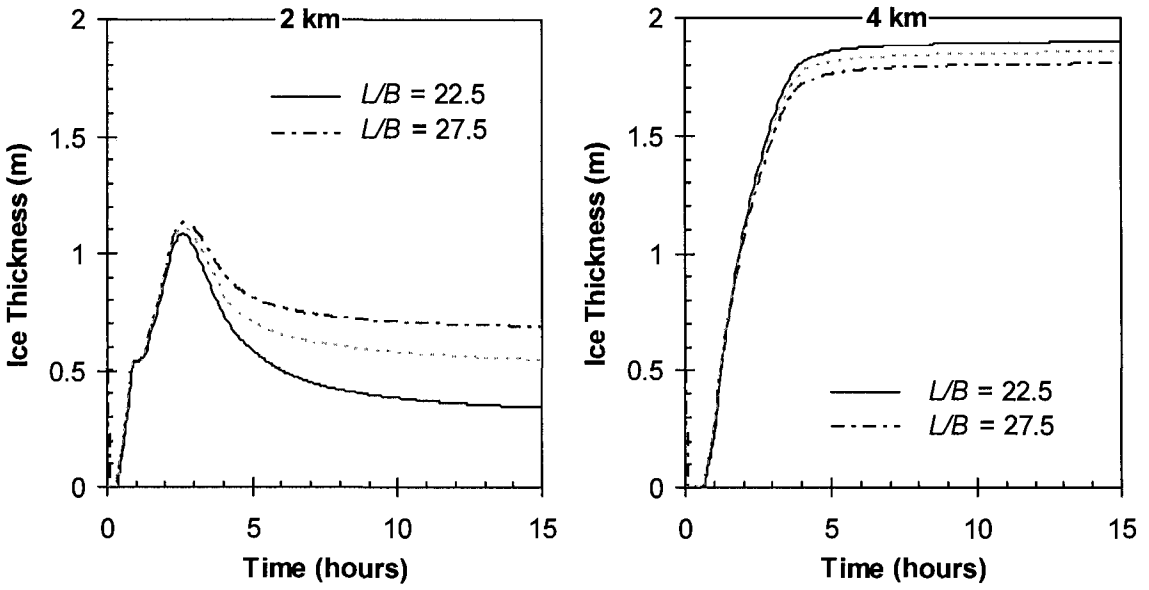

Figure A-35 Sensitivity of *River1-D*: ice jam modeled ice thickness variation at station 2 km and 4 km to the *L/B* ratio.

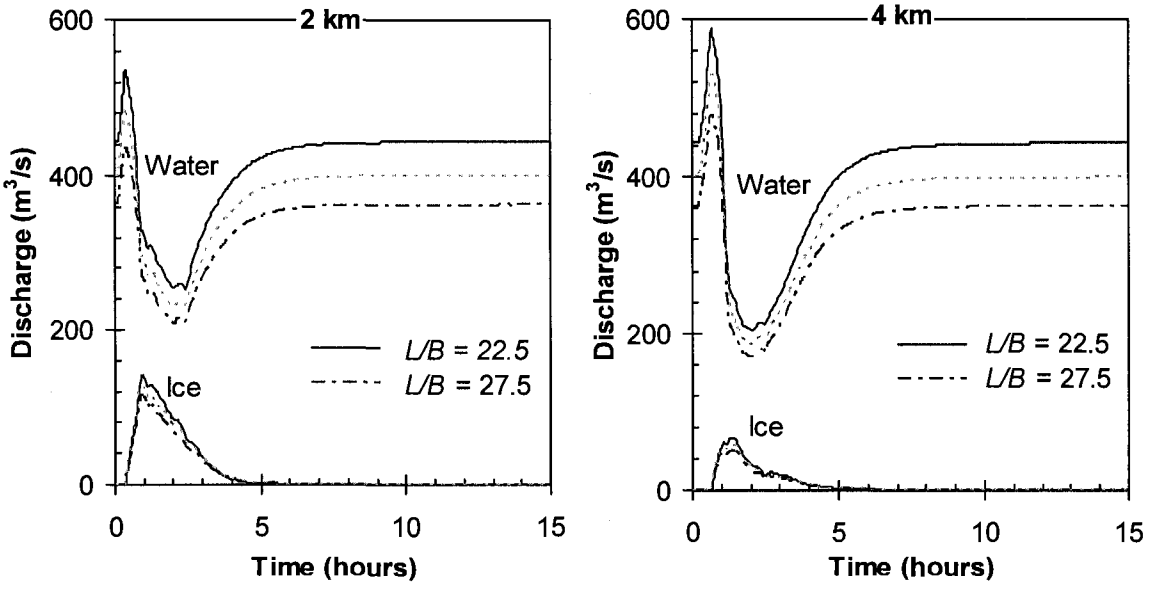

Figure A-36 Sensitivity of *River1-D*: ice jam modeled water discharge and ice discharge variation at station 2 km and 4 km to the *L/B* ratio.

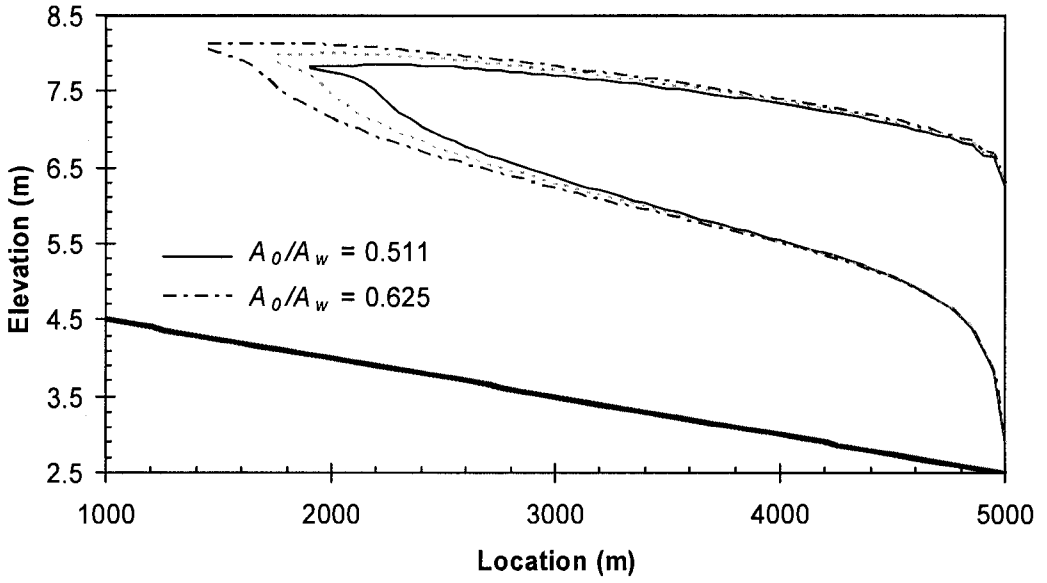

Figure A-37 Sensitivity of *River1-D*: ice jam model profiles to the ratio of ice volume and channel storage A_0/A_w.

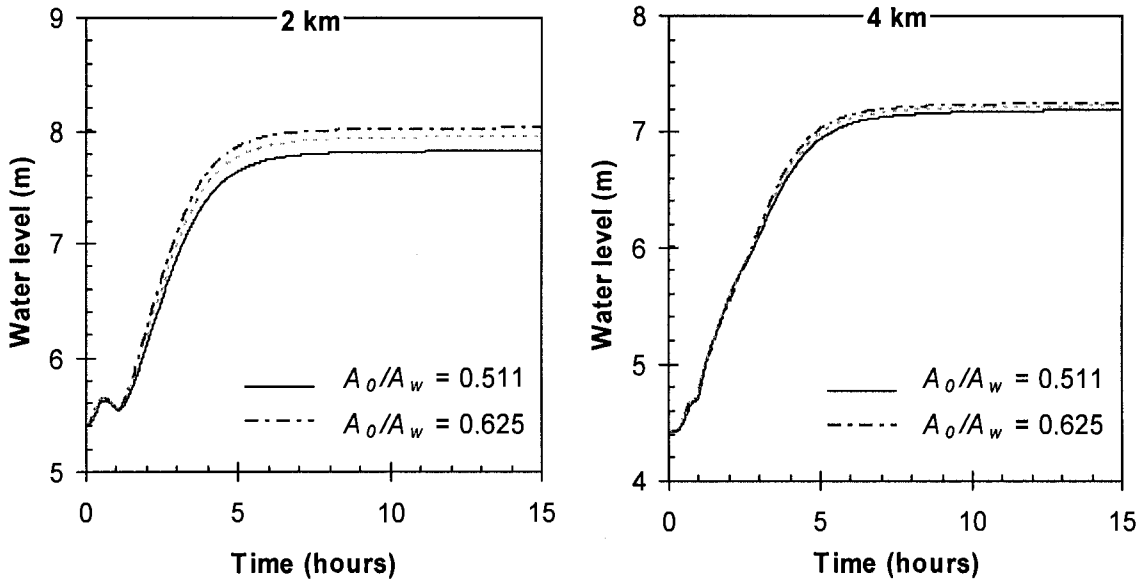

Figure A-38 Sensitivity of *River1-D*: ice jam modeled water level variation at station 2 km and 4 km to the ratio of ice volume and channel storage A_0/A_w.

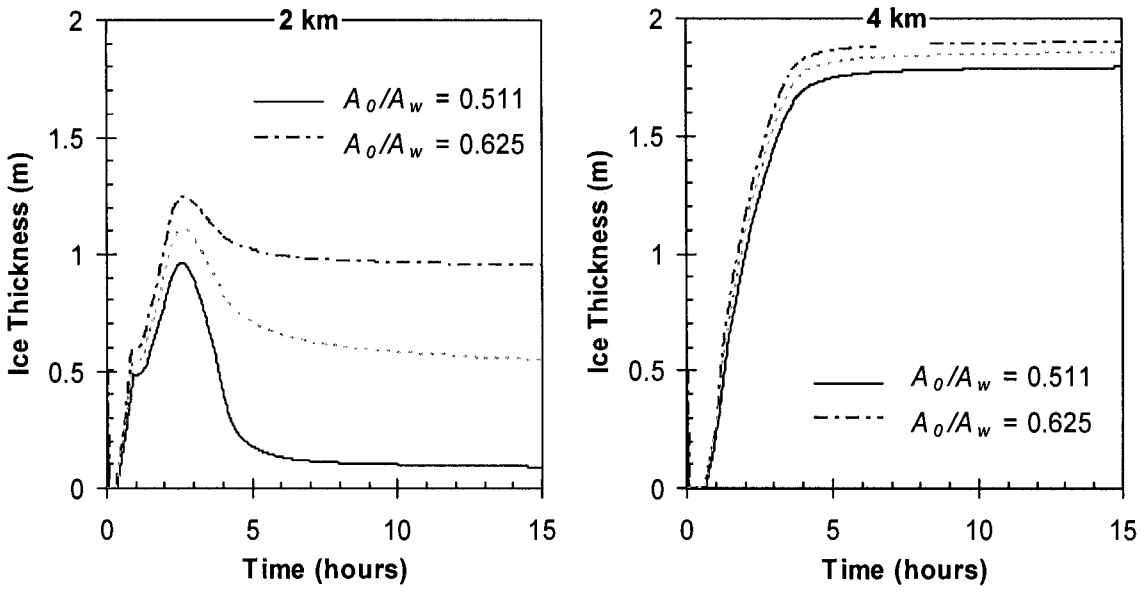

Figure A-39 Sensitivity of *River1-D*: ice jam modeled ice thickness variation at station 2 km and 4 km to the ratio of ice volume and channel storage A_0/A_w.

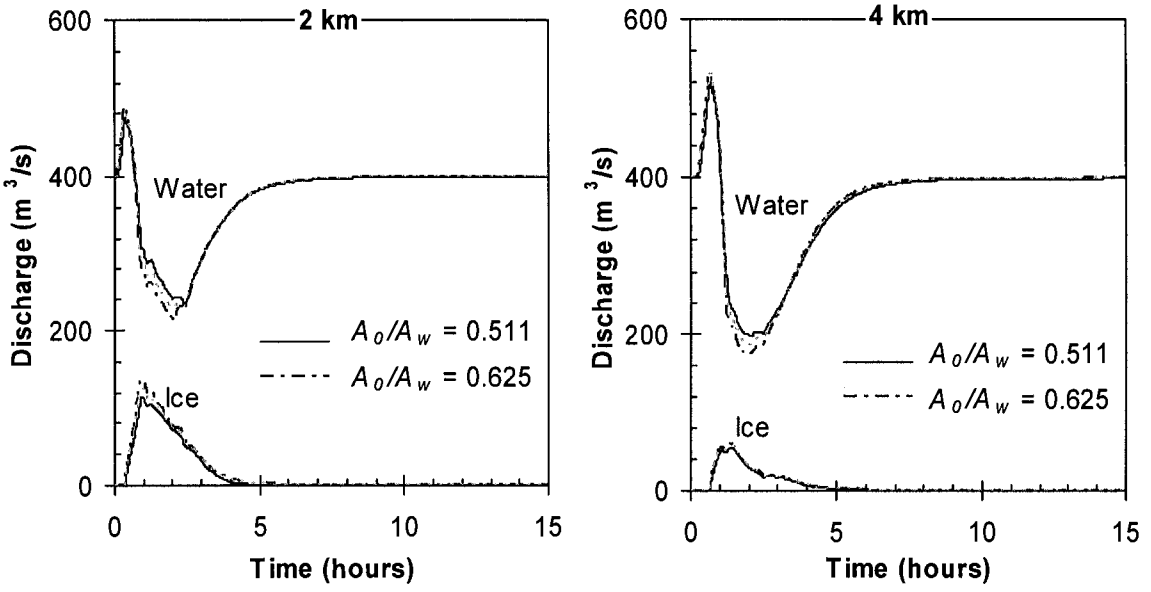

Figure A-40 Sensitivity of *River1-D*: ice jam modeled water discharge and ice discharge variation at station 2 km and 4 km to the ratio of ice volume and channel storage A_0/A_w.

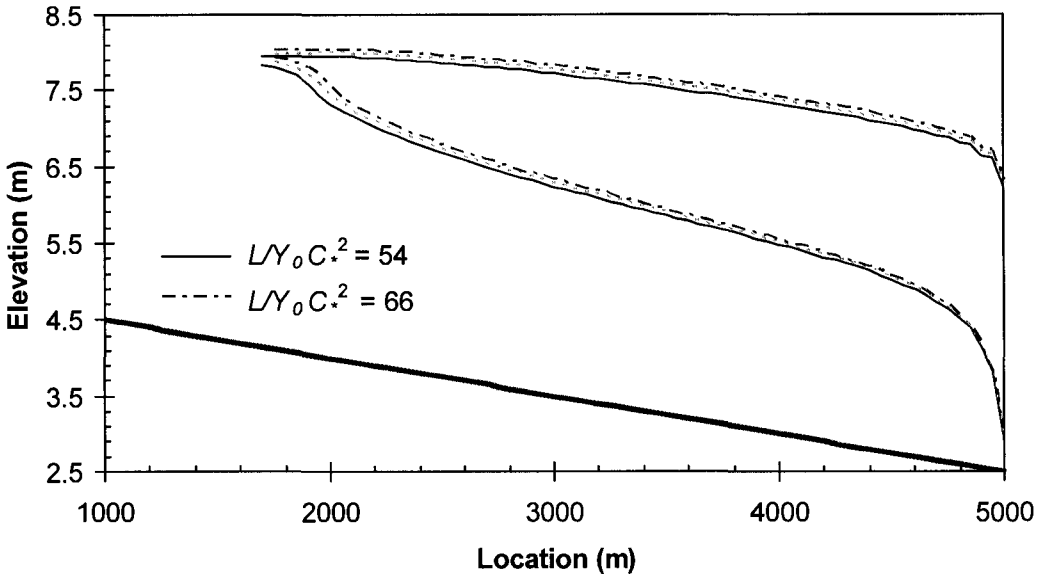

Figure A-41 Sensitivity of *River1-D*: ice jam model profiles to the parameter $L/Y_0C_*^2$.

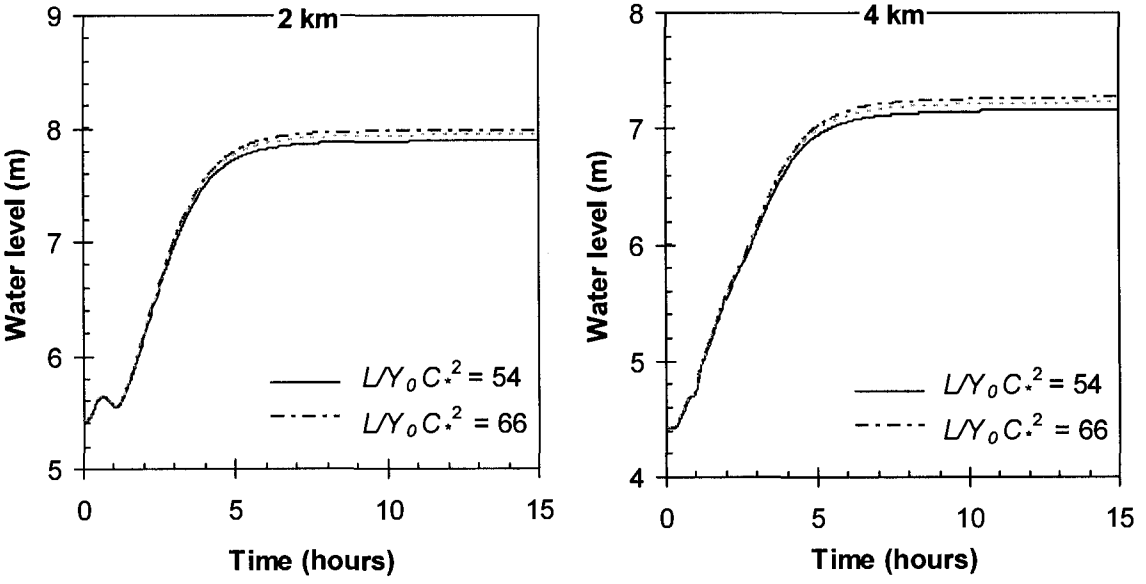

Figure A-42 Sensitivity of *River1-D*: ice jam modeled water level variation at station 2 km and 4 km to the parameter $L/Y_0C_*^2$.

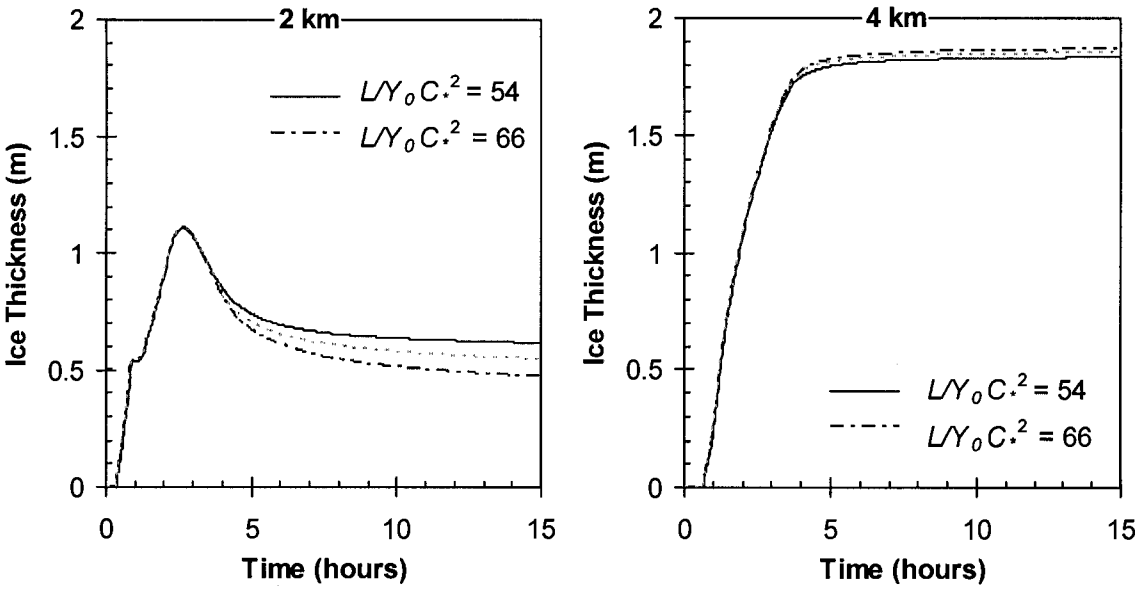

Figure A-43 Sensitivity of *River1-D*: ice jam modeled ice thickness variation at station 2 km and 4 km to the parameter $L/Y_0C_*^2$.

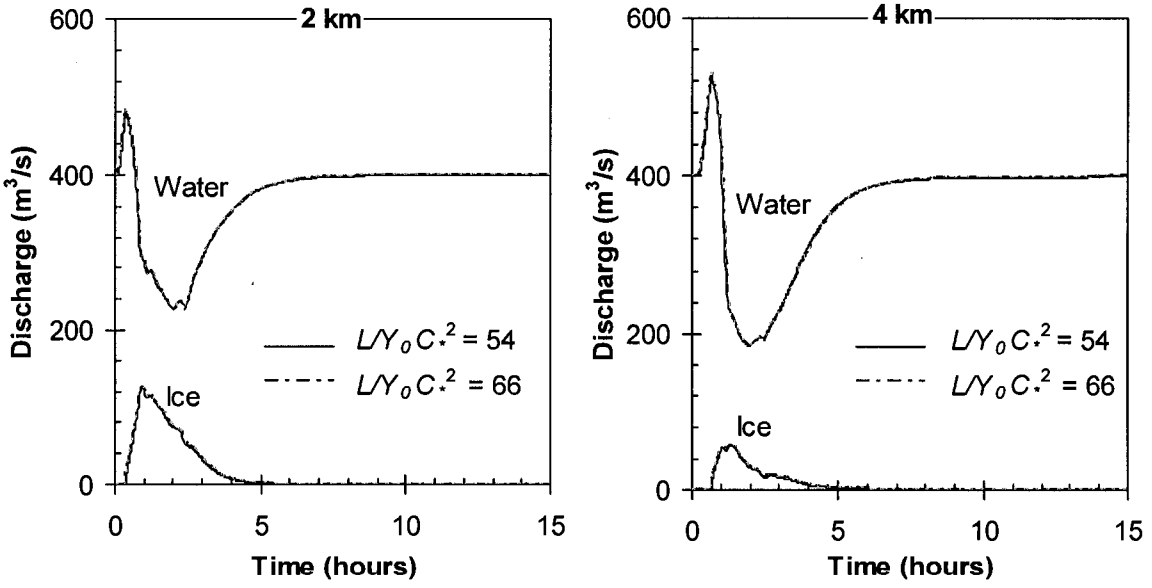

Figure A-44 Sensitivity of *River1-D*: ice jam modeled water discharge and ice discharge variation at station 2 km and 4 km to the parameter $L/Y_0C_*^2$.

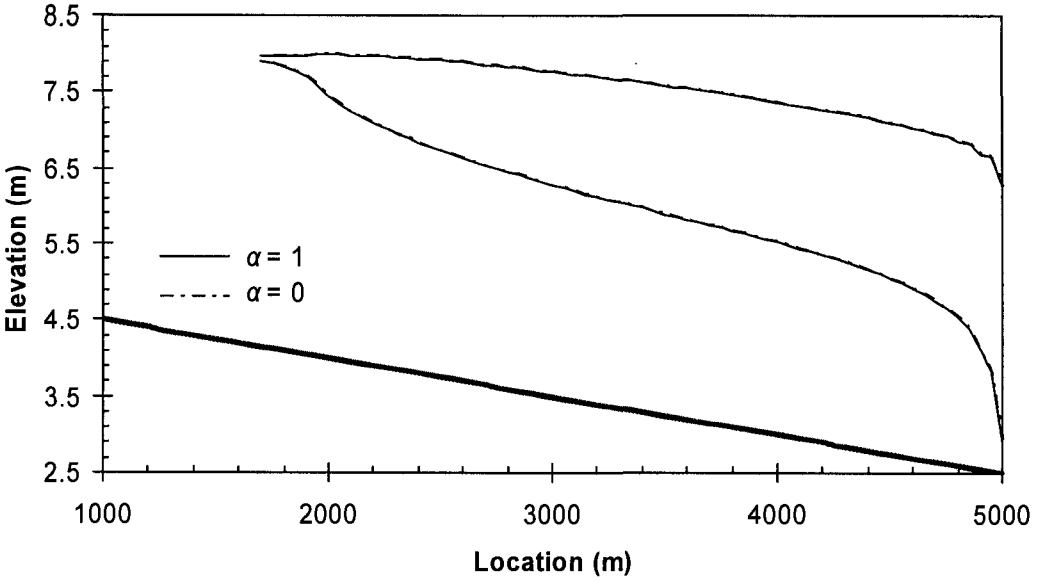

Figure A-45 Sensitivity of *River1-D*: ice jam model profiles to the dispersion parameter α.

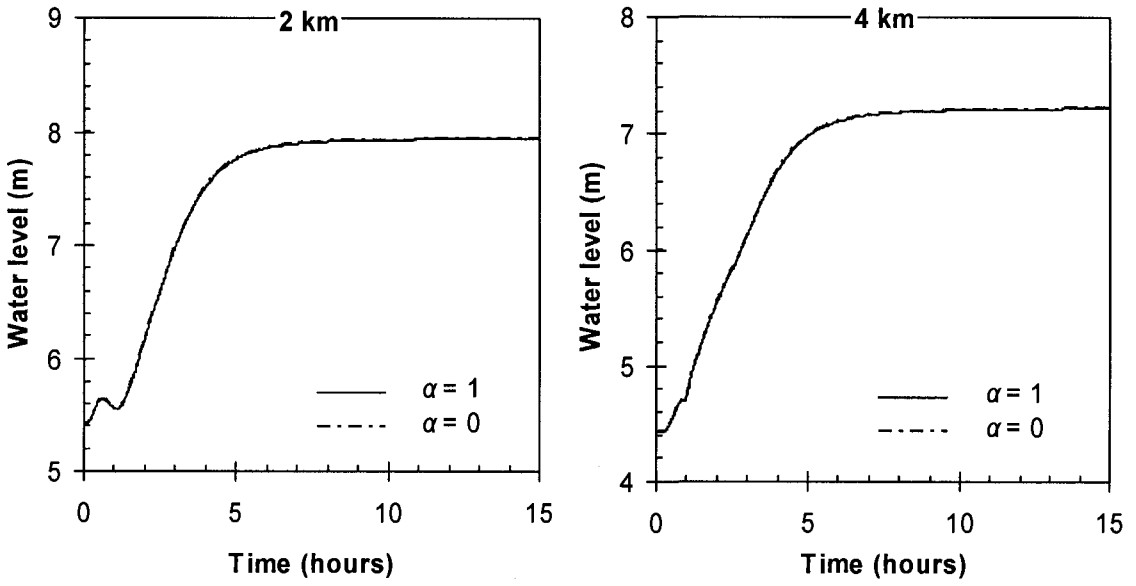

Figure A-46 Sensitivity of *River1-D*: ice jam modeled water level variation at station 2 km and 4 km to the dispersion parameter α.

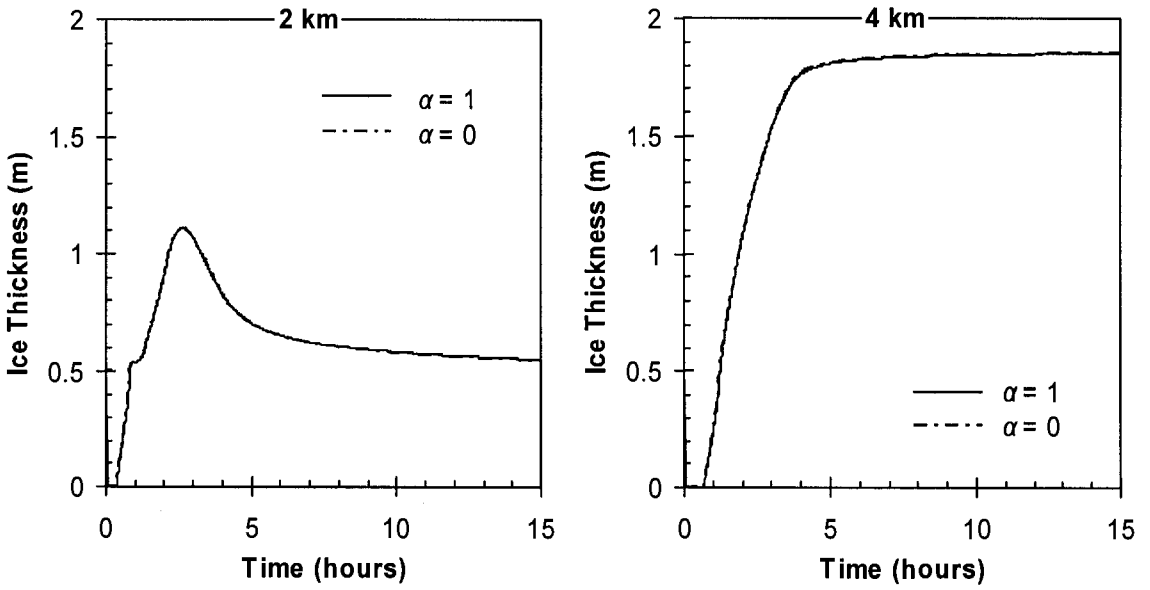

Figure A-47 Sensitivity of *River1-D*: ice jam modeled ice thickness variation at station 2 km and 4 km to the dispersion parameter α.

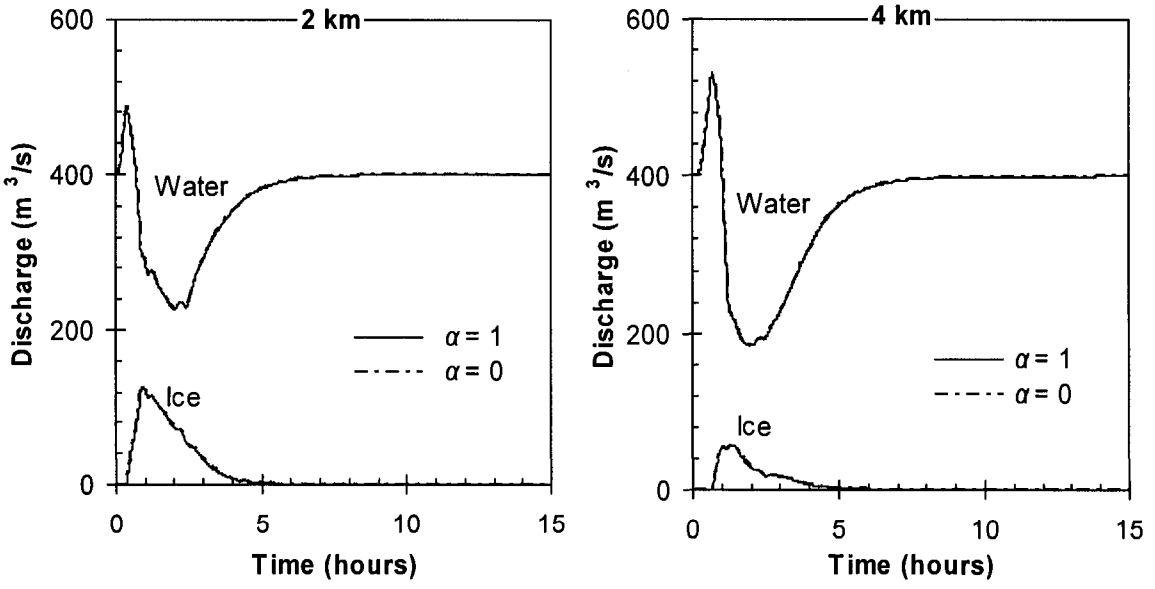

Figure A-48 Sensitivity of *River1-D*: ice jam modeled water and ice discharge variation at station 2 km and 4 km to the dispersion parameter α.

Appendix B – Effects of Unsteadiness and Ice Motion on River Ice Jam Profiles[5]

B.1 Introduction

The high water levels associated with breakup ice jams in rivers often pose a significant flood threat to public safety. A number of computational tools are available for predicting water surface and ice profiles associated with river ice jam occurrence; most are based on static ice jam stability theory (e.g. Pariset et al. 1966, Uzuner and Kennedy, 1976) combined with a steady gradually varied flow approximation (e.g. RIVJAM: Beltaos and Wong 1986, ICEJAM: Flato and Gerard 1986, and HEC-RAS: Daly and Vuyovich 2003). These models can provide information on the expected thickness and water surface profiles of stable ice jams. However, inherent in their use are the assumptions that streamflow is steady and jam strength is deformation-independent. Even if one neglects the obvious unsteady aspects of ice jam formation and focuses on the final ice jam profile as the characteristic of interest, the question remains as to whether the final "stable" ice jam profile predicted by such models is applicable under dynamic ambient flow conditions, such as might be expected during hydro-peaking events on regulated rivers.

Steady ice jam profile models have been extensively tested using field data on water level and/or ice thickness data obtained on stable ice jams (e.g. Beltaos 1993, Healy and Hicks 1999) and credible predictions of ice jam configuration have been achieved by choosing appropriate model parameters. Unfortunately, it is difficult to assess the validity of steady

[5] This appendix was accepted for publishing in the Proceeding of the 19th IAHR International Symposium on Ice, Vancouver, Canada. The paper will also be presented by the first author at this conference in July 2008.

ice jam profile models for ice jams formed under unsteady flow conditions, because of the logistical difficulties associated with measuring discharge and ice accumulation thickness variations during ice jam formation in the field. Fortunately, some success has been achieved in measuring such processes the laboratory. Zufelt (1990, 1992) qualitatively observed that the final ice jam profile was influenced by unsteady flow conditions, noting that the consolidation process could be interrupted and resumed by discharge fluctuations. Healy and Hicks (2006, 2007) measured ice jam formation and shoving events under steady and unsteady ambient flows. They found that reasonable profiles describing the final ice jam configurations could be obtained using steady ice jam profile models for ice jams formed under both steady carrier discharge conditions, and for ice jams consolidated by rapid discharge increases. These two flow conditions bracket the practical range of flow scenarios; with flow conditions during actual ice jam formation events are typically somewhere in between.

This paper utilizes the University of Alberta's *River1-D* model's new ice jam component to further explore the applicability of steady ice jam profile models, by studying the effects of unsteady flow on ice jam profile shape. This new version of the *River1-D* model employs a purely Eulerian frame of reference for both the hydrodynamic and ice dynamics components. A new one-seventh power law formulation for the constitutive law (She et al., submitted) is used for determining the internal ice resistance of the moving ice accumulation. This new model has already been validated with analytical and experimental test cases of ice jam consolidation (She et al., submitted). Here, profiles of ice jams formed during three experimental consolidation events are modeled using *River1-D*'s new ice jam component model, and compared to calculated profiles obtained

using the RIVJAM model formulation (Beltaos and Wong 1986). Comparison of the model results, together with the measured jam thickness, provides some ideas on when the unsteadiness and ice motion effects should be taken into account for predicting flood potential of river ice jams. The influences of inflow hydrographs (peaking time and peak duration) on the final jam configuration are also examined.

B.2 Computational Models

B.2.1 River1-D: ice jam model

The *River1-D: ice jam* model solves the mass and momentum conservation equations for the water and for the ice in an uncoupled sequence, using the Characteristic-Dissipative-Galerkin (CDG) finite element method (Hicks and Steffler 1992). Assuming a floating ice accumulation, the mass and momentum conservation equation for water flow can be written as:

$$\text{[B-1]} \quad \frac{\partial A_w}{\partial t} + \frac{\partial Q_w}{\partial x} = -\frac{\partial}{\partial t}\left[(1-N)\frac{s_i A_i}{N}\right] - \frac{\partial Q_u}{\partial x}$$

$$\text{[B-2]} \quad \frac{\partial Q_w}{\partial t} + \frac{\partial (Q_w V_w)}{\partial x} + gA_w \frac{\partial H_w}{\partial x} = gA_w\left(S_o - \frac{\partial s_i t_i}{\partial x}\right) - \left[\frac{n_b^2 |V_w| V_w (B+2H_w)}{R_b^{4/3}} + \frac{n_i^2 |V_w - V_i|(V_w - V_i) NB}{R_i^{4/3}}\right]$$

where: A_w and Q_w are the area and discharge of flow under the ice layer; N is the surface concentration of ice; s_i is the specific gravity of ice; A_i the ice volume per unit length of channel, (defined as $A_i = NBt_i$); B is the channel width; and t_i is the ice thickness. V_w and

H_w are the velocity and the depth of flow below the ice layer, respectively; S_o is the bed slope; n_b and n_i are the Manning's roughness coefficients for the bed and the ice, respectively; R_b and R_i are the hydraulic radius of the bed-affected, and ice-affected areas, respectively; and Q_u is the water seepage discharge within the ice layer, which is calculated in a similar way as in Shen et al. (2000).

The mass and momentum conservation equations for the floating ice layer are:

[B-3] $$\frac{\partial A_i}{\partial t}+\frac{\partial(V_i A_i)}{\partial x}=0$$

[B-4] $$A_i\left(\frac{\partial V_i}{\partial t}+V_i\frac{\partial V_i}{\partial x}\right)+gA_i\frac{\partial(s_i t_i)}{\partial x} = gA_i\left(S_o-\frac{\partial H_w}{\partial x}\right)+\frac{1}{\rho_i}\frac{\partial(A_i\sigma)}{\partial x}-\frac{2A_iK_{xy}\tan\phi}{\rho_i B}\sigma+\frac{n_i^2|V_w-V_i|(V_w-V_i)NB}{s_i R_i^{1/3}}$$

in which: ρ_i is the density of ice; K_{xy} is a lateral thrust coefficient; and ϕ is the internal friction angle. Here, σ is the internal resistance of the ice accumulation, which is determined using a one-seventh power law constitutive relationship (She et al., submitted):

[B-5] $$\sigma=(T)^{1/7}P(\dot{\varepsilon})^{1/7}-P$$

in which: T is a time scale parameter; $\dot{\varepsilon}$ is the strain rate; and the pressure term, P, is formulated as:

[B-6] $$P = \tan^2\left(45^o + \frac{\phi}{2}\right)(1-s_i)\frac{N}{N_{\max}}\frac{\rho_i g t_i}{2}$$

She et al. (submitted) provide full details of this new model's formulation and validation.

B.2.2 *RIVJAM ice jam model*

RIVJAM (Beltaos and Wong 1986), ICEJAM (Flato and Gerard 1986) and HEC-RAS (Daly and Vuyovich 2003) are probably the three most widely know steady flow ice jam profile models. They all solve an ice jam stability equation in conjunction with a steady gradually varied flow (GVF) equation. In this investigation, the RIVJAM formulation (Beltaos and Wong 1986) was selected for comparison, due to its capability of handling seepage flow through the voids of the ice accumulation.

In the RIVJAM formulation, two ordinary differential equations are solved using the Runge-Kutta method.

[B-7] $$\frac{dt_i}{dx} = \frac{s_i \rho g}{2\tan^2\left(45^o + \phi/2\right)\gamma_e}\left[\frac{f_i}{2f_o}\frac{f_o q_w^2}{4gH_w^2 s_i t_i} + \left[\frac{Q}{A_w\sqrt{\frac{4gA_w}{f_o B} + \lambda A_j}}\right]^2\right] - \frac{\tan\phi}{\tan^2\left(45^o + \phi/2\right)}\frac{t_i}{B}$$

$$[B\text{-}8] \quad \frac{dH_w}{dx} = S_o - \frac{ds_i t_i}{dx} - \left[\frac{Q}{A_w \sqrt{\frac{4gA_w}{f_o B}} + \lambda A_j} \right]^2$$

Here, γ_e is the effective unit weight of water, defined as $\gamma_e = (1 - s_i)(1 - p)\rho_i g/2$, where p is the porosity of the ice layer; q_w is the discharge under the ice layer per unit width; Q is the total discharge through and under the ice layer; and f_o and f_i are the composite and ice Darcy-Weisbach friction factor, respectively.

B.3 Analysis of an Ice Jam Consolidated by Rapid Flow Increase

Experimental ice jam consolidation events (Healy 2006, Healy and Hicks, 2007) are chosen for exploring the applicability of static ice jam profile models due to the advantage of known ice jam strength parameters (internal friction angle, porosity) and the carrier discharge. The experiments were conducted in a 32m-long, 1.22m-wide rectangular flume set to a slope of 0.00164, supplied with discharges ranging from 33 to 63L/s. Water levels at the downstream end were controlled by a weir and guide vanes. A 1.9cm-thick, 1.22m-long plywood sheet was positioned 24.5m downstream of the head tank to simulate a free-floating intact ice cover, and a wire screen was fixed to its upstream edge to facilitate initiation of an ice accumulation. Manning's n for the flume ranged from 0.020 to 0.025 under open water conditions. The specific gravity of the model ice was 0.92 and the angle of repose was found to be 46°. First, an ice accumulation was allowed to form and stabilize in the flume at a low carrier discharge. This initial ice accumulation was then collapsed by a rapid increase in discharge, shoving to a much thicker ice jam.

Manning's n of the ice was calibrated in the *River1-D: ice jam* model using:

$$[B\text{-}9] \quad n_i = n_{io}\left(t_i / t_{io}\right)^{1/3}$$

in which n_{io} is the Manning's coefficient for a single-layer of ice (t_{io} = 1cm); a value of n_{io} = 0.020 was used in the model. Manning's n for the ice ranged from 0.020 to around 0.050 for all the experimental tests. The same formulation of ice roughness was also used in the RIVJAM computations.

Although the RIVJAM computations can start at any point within an ice jam where the ice thickness and water level are known, it is important to note that the starting point must be within the reach where the ice jam stability equation applies. In the experimental test runs, ice jams were initiated by a wire mesh, providing extra resistance that is not included in the jam stability equation. Therefore, the computations should not start at a point that is too close to the wire mesh. As the ice volume is known for each experimental event, an appropriate starting point could be determined by trial and error, being chosen such that the computations give the correct ice volume.

The simulated results of three experimental ice jam consolidation events are presented in Figures B-1~B-3, representing relatively high (85%), medium (55%) and low (24%) discharge increases collapsing the initial ice accumulation. Subfigure (a) presents the measured initial ice accumulation; subfigure (b) presents the calculated final ice jam profile using the two models, along with the measurements. In all three cases, the RIVJAM profiles were calculated using the final discharge in the experiment.

Form the figures it can be seen that the *River1-D: ice jam* model consistently provides a good match to the measured final ice jam profile in all the three events. Only one slight difference occurs and that is at the upstream end of the accumulation, where the measured ice jam shows a "hook-like" shape. Healy and Hicks (2007) observed that hydraulic thickening dominated in this zone for all experiments (which is also consistent with field observations). This local hydraulic thickening effect is not considered in the current version of the *River1-D: ice jam* model.

The RIVJAM formulation was also found to also reasonably predict the profile of ice jams consolidated by high and medium increase in discharge (Figures B-1b and B-2b), again with the exception of the hydraulic thickening effect at the head of the jam (for the same reasons). However, it was found that the RIVJAM formulation could not match the profile of the ice jam consolidated by lowest increase in discharge (Figure B-3b). This is an interesting result, given that the discharge increase in this case was relatively low compare to the other two events; therefore, flow unsteadiness is unlikely to be the reason for this discrepancy. This would suggest that the means by which the ice internal resistance is quantified is the issue. This hypothesis was explored next.

Steady ice jam profile models use Rankine's passive pressure and the Mohr-Coulomb failure criterion to quantify the internal resistance of the ice accumulation, thus neglecting the effects of ice motion on the internal resistance of the ice accumulation. In contrast, the *River1-D: ice jam* model uses a one-seventh power law constitutive relationship which relates the internal resistance of the ice accumulation to the ice motion (She et al. submitted). To facilitate a direct comparison between the two approaches for the unsteady flow case, the *River1-D: ice jam* model was modified to include Rankine's passive

pressure and the Mohr-Coulomb criterion as an option. This provided three modeling alternatives for simulating the final ice jam profile created by the low (24%) increase in discharge: (1) a steady model employing the Mohr-Coulomb criteria (i.e. the RIVJAM formulation); (2) an unsteady model employing the Mohr-Coulomb criteria; and (3) an unsteady model with a one-seventh power law constitutive relationship (i.e. the new *River1-D: ice jam* model). The final ice jam profiles obtained using these three modeling approaches are shown in Figure B-4, along with the measured jam-thickness profile for comparison. As can be seen from the figure, the unsteady model employing the Mohr-Coulomb criterion gives very similar results to those obtained with the (steady) RIVJAM formulation; and entirely different from the *River1-D: ice jam* model results. It appears that including the effects of ice motion on the internal strength of the ice accumulation (e.g. as in the new *River1-D: ice jam* model) provides a better representation of the observed ice jam thickness profile, for this case where a small discharge increase produced relatively small deformations. The fact that the steady and unsteady models using the Mohr-Coulomb criterion produce very close results, confirms the hypothesis that flow unsteadiness is not the issue here.

B.4 Analysis of Effects of Inflow Hydrograph Shape on Final Ice Jam Profile

The question remains as to why it is important to include the effects of ice motion on the internal strength of the consolidating ice accumulation in some cases and not others. The fact that it appears to be more important for mild increases in discharge, combined with the observed shape of the final ice thickness profile for this case, suggests that the discharge change is sufficient to initiate a consolidation but is inadequate to complete it. This is consistent with the qualitative observations of Zufelt (1990, 1992) as well. If true,

then it is not just the magnitude of the increase in discharge that should be important, but possibly also the gradient and duration of the flow increase, as well. If so, this would be significant form a practical perspective, since the ambient flow would be expected to involve a slow increase in discharge due to snowmelt runoff caused by gradual warming, or a peak ambient flow of relatively short duration if caused by upstream ice jam releases or hydro-power operations. To investigate these effects, several runs were conducted with the *River1-D: ice jam* model to evaluate the impact of inflow hydrograph shape on the final stable ice jam profile. The experimental test case involving the high (85%) increase in discharge was used for this analysis (i.e. discharge increase from 33.5 to 61.9L/s).

The effect of varying the time to peak was examined first, and Figure B-5 presents the inflow hydrographs input to the *River1-D: ice jam* model for this series of tests. In the figure, t_p is the time for the discharge to increase from 33.5 to 61.9L/s; values of 13 seconds (i.e. the same as in the experiment), 1 minute, 3 minutes, and 6 minutes were tried. It can be seen from the model results presented in Figure B-6 that for ice jams formed under the four inflow conditions, the simulated final thickness profiles are exactly the same. Moreover, they all agree well with the thickness profile computed using the RIVJAM formulation (again calculated for the final discharge of 61.9L/s).

The effect of varying the duration of peak discharge was examined next. Keeping the same inflow rise rate (from 33.5 to 61.9 L/s in 13 seconds, as in the experiment), four different inflow hydrographs with 0, 1, 5, and infinite minutes of peak duration, as depicted in Figure B-7, were input to the *River1-D: ice jam* model. Figure B-8 illustrates the results, which suggest that the duration of the peak inflow appears to be a very important factor influencing the final jam configuration. Specifically, the longer the peak

flow is sustained, the shorter and thicker the final ice jam configuration. Comparing these result to the ice jam thickness profile calculated using the RIVJAM formulation (again using the peak discharge), also shown in Figure B-8, it is seen that the resulting profile is consistent only with sustained flow changes.

B.5 Summary and Conclusions

The standard in ice jam profile computation that has evolved in the past few decades involves a number of approximations, the two foremost being the applicability of a steady flow approximation, and the suitability of the Mohr-Coulomb failure criterion to quantify the internal resistance of the ice accumulation. The development of new unsteady ice jam formation models, with consideration of the effects of ice motion on the strength of the developing accumulation raise the potential for examining not only the ultimate (stable) ice jam profiles, but also for studying the influences of unsteady flow on the evolution of an ice jam.

In this study, the new ice jam component in the *River1-D* one-dimensional unsteady ice dynamics model has facilitated an investigation of ice jam dynamics under unsteady ambient flow conditions, enabling an assessment of the validity of conventional steady ice jam profile models. It has also facilitated an investigation of the effects of varying rates and durations of discharge increase on final ice jam profile shape. Based on these investigations, it has been found that the unsteadiness caused by very rapid increase in discharge (i.e. the passage of a highly dynamic wave) does not appear to have a significant effect on the ultimate stable jam-thickness profile for large discharge increases. However, for ice accumulations experiencing relatively small discharge increases and

deformations, steady ice jam profile calculation may underestimate the ultimate ice jam thickness profile. Further research, both experimental and numerical, is needed to explore the bounds of relevance and ranges of applicability of these steady flow approximations.

The new model has also been used to examine the importance of the rate and duration of discharge increases on ultimate (stable) ice jam thickness profiles. Preliminary results suggest that the ultimate ice jam profile is relatively insensitive to wave steepness (i.e. the rate of change of discharge, or 'time to peak'). In contrast, it seems that the duration of peak flow can significantly influence the final configuration and that steady ice jam profile models predict ice thickness profiles consistent with sustained flow changes. This importance of peak flow duration on the final ice jam configuration may have important implications for the design of stable ice covers on river subject to hydro-peaking.

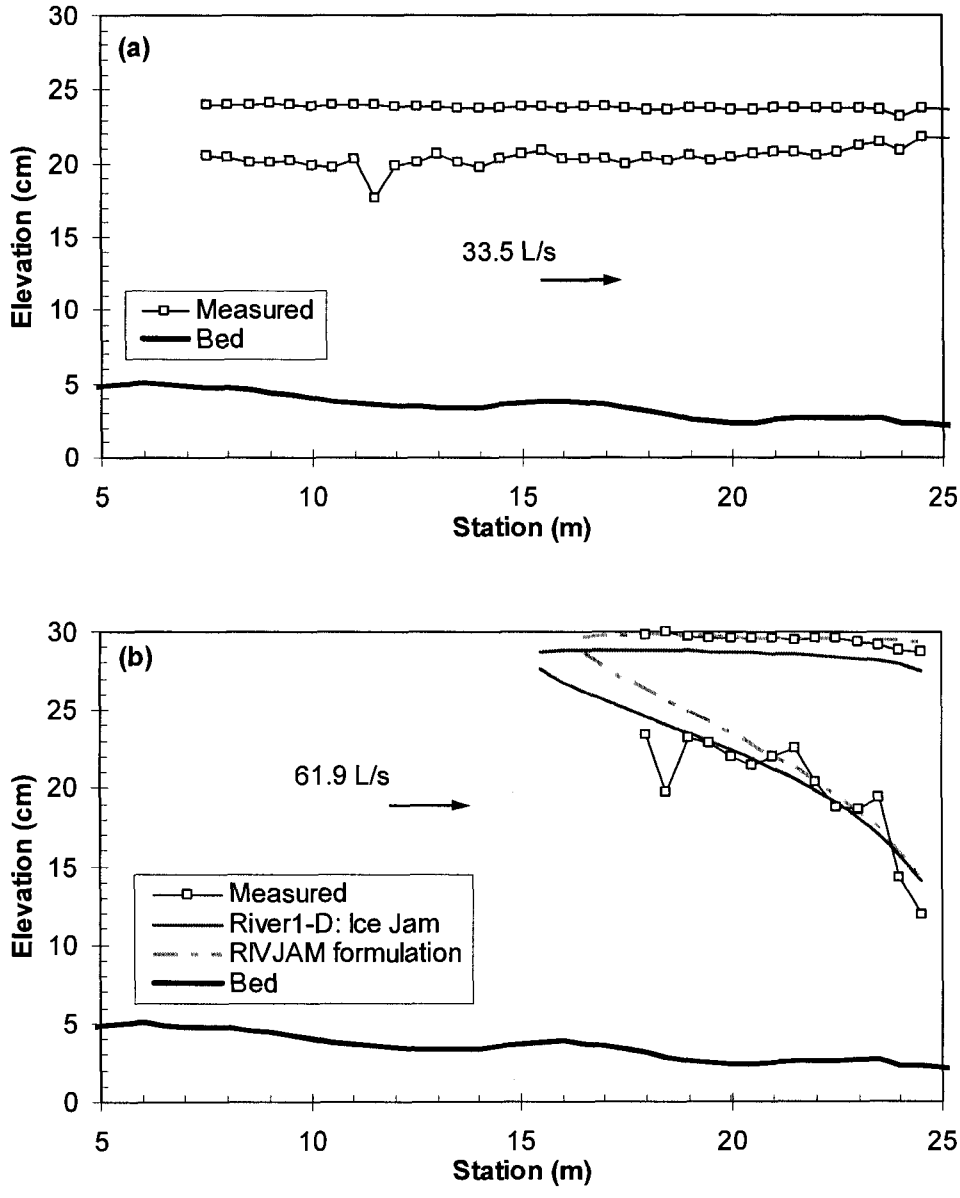

Figure B-1. *River1-D* ice jam and RIVJAM model profiles in comparison with measurements of final ice jam consolidated by 85% increase in discharge: (a) initial; (b) final ice accumulation.

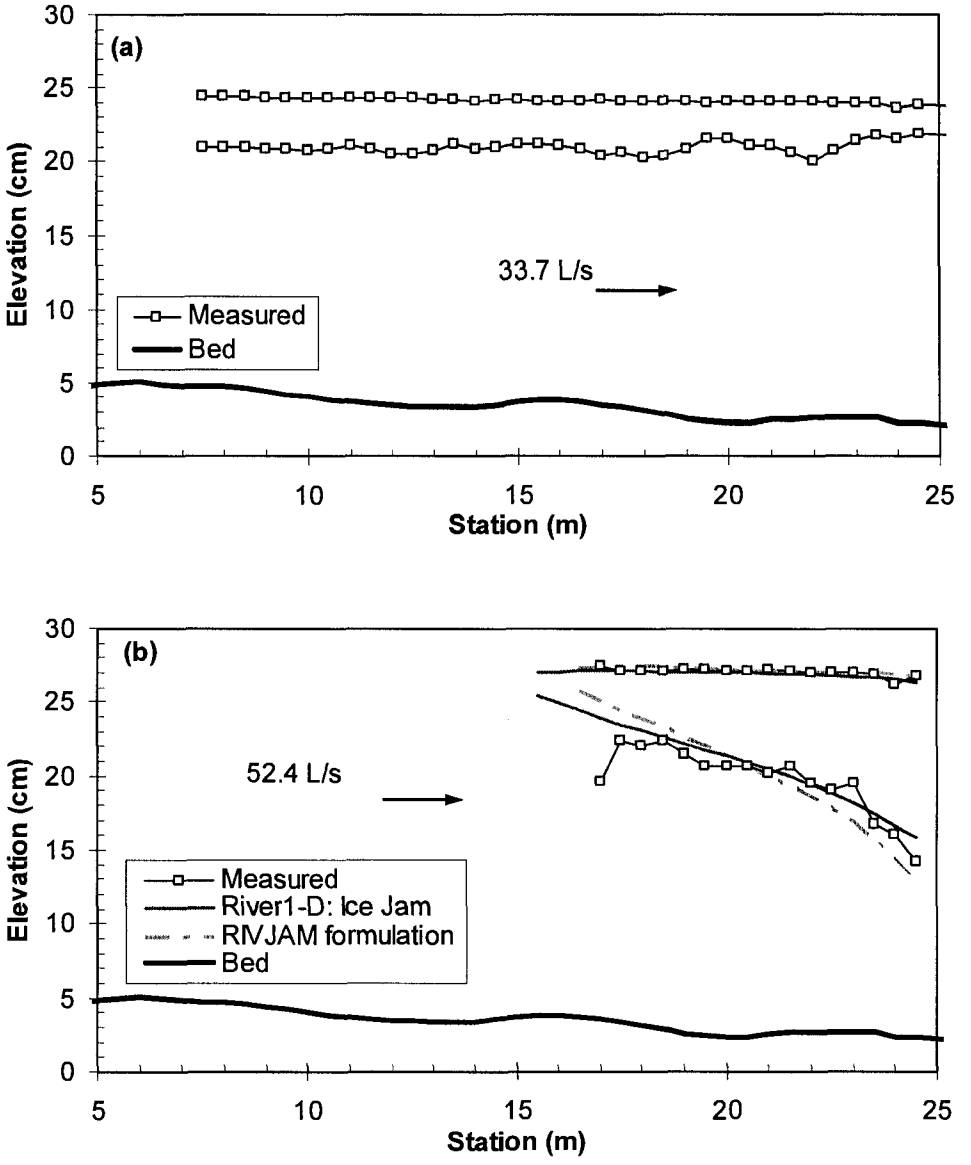

Figure B-2. *River1-D* ice jam and RIVJAM model profiles in comparison with measurements of final ice jam consolidated by 55% increase in discharge: (a) initial; (b) final ice accumulation.

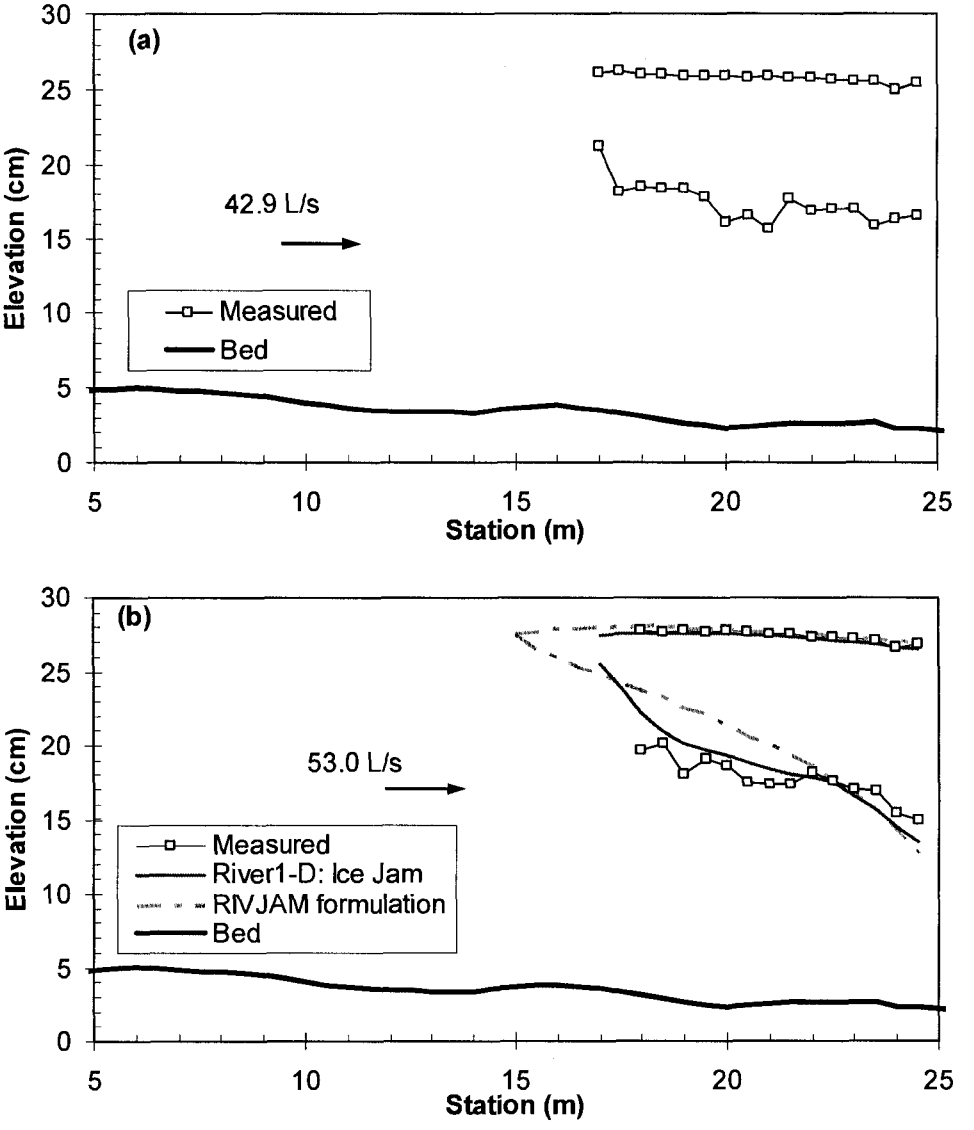

Figure B-3. *River1-D* ice jam and RIVJAM model profiles in comparison with measurements of final ice jam consolidated by 24% increase in discharge: (a) initial; (b) final ice accumulation.

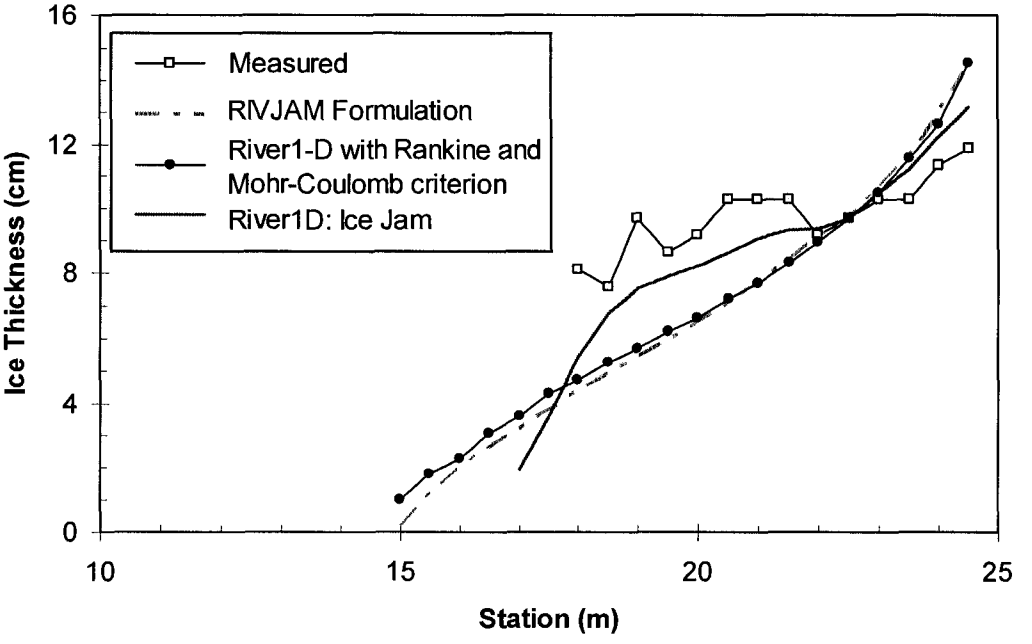

Figure B-4. Comparison of final ice jam thickness profiles computed using different methods to quantify internal resistance of the ice accumulation for a 24% increase in discharge.

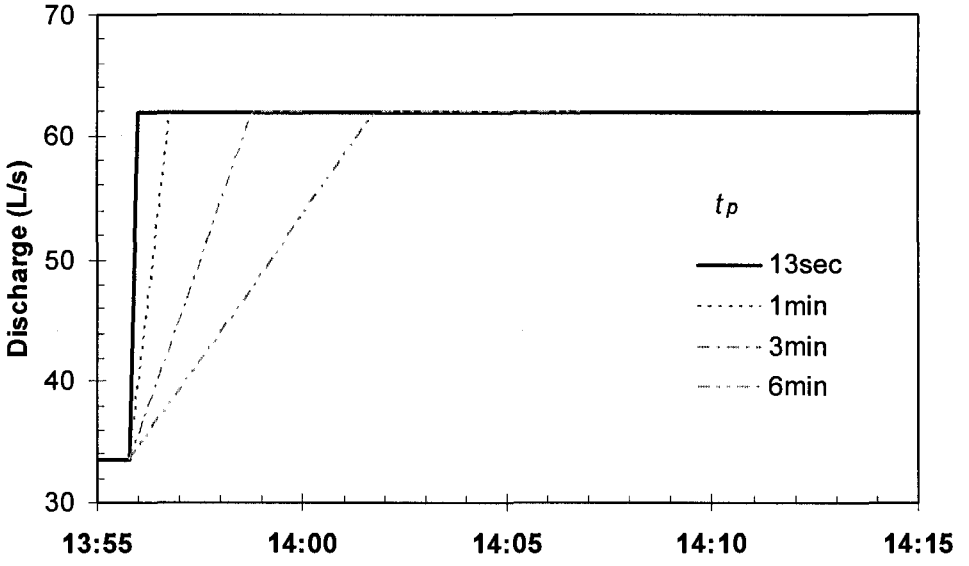

Figure B-5. River1-D inflow hydrographs for various times to peak.

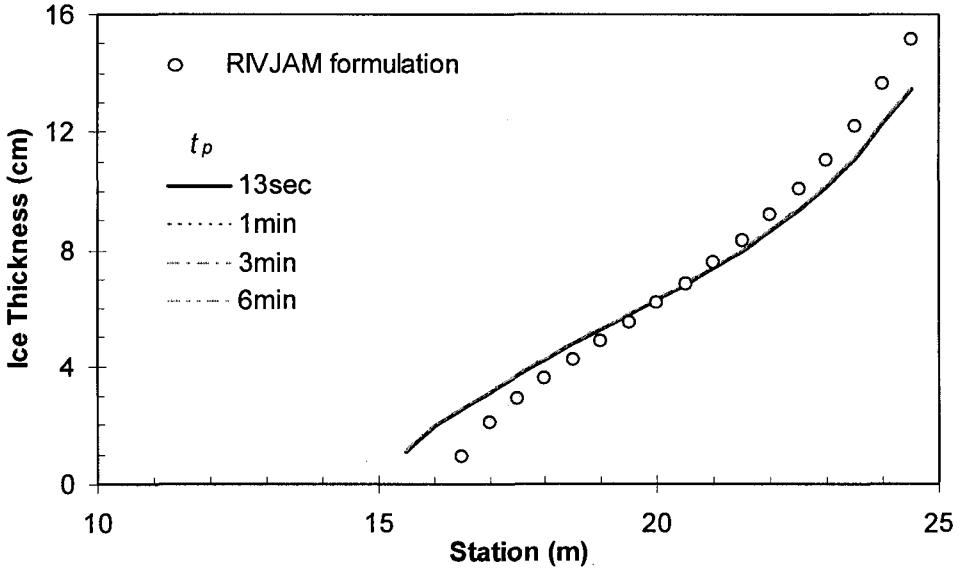

Figure B-6 Simulated ice jam profiles using *River1-D* ice jam model and RIVJAM model formulation for various times to peak.

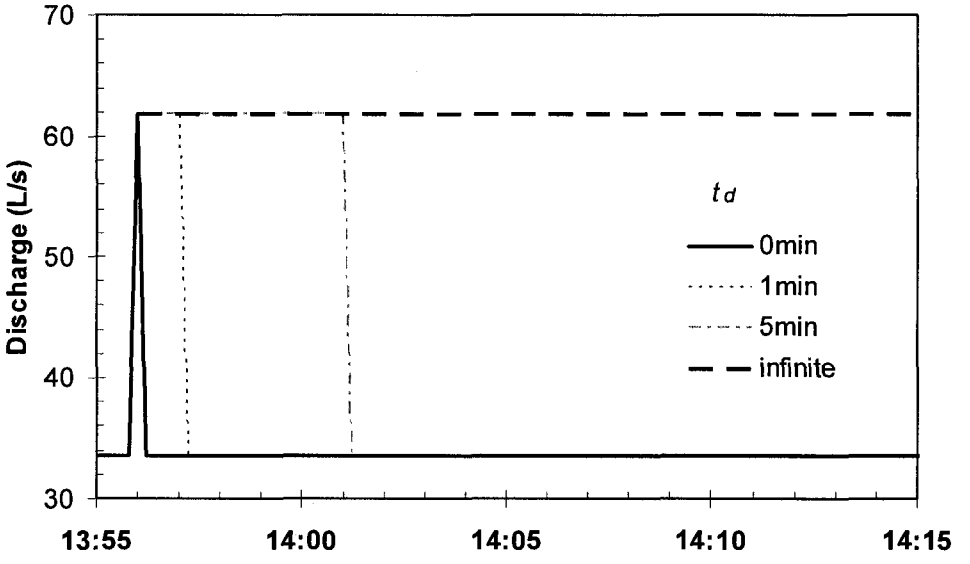

Figure B-7 *River1-D* inflow hydrographs for using various peak durations.

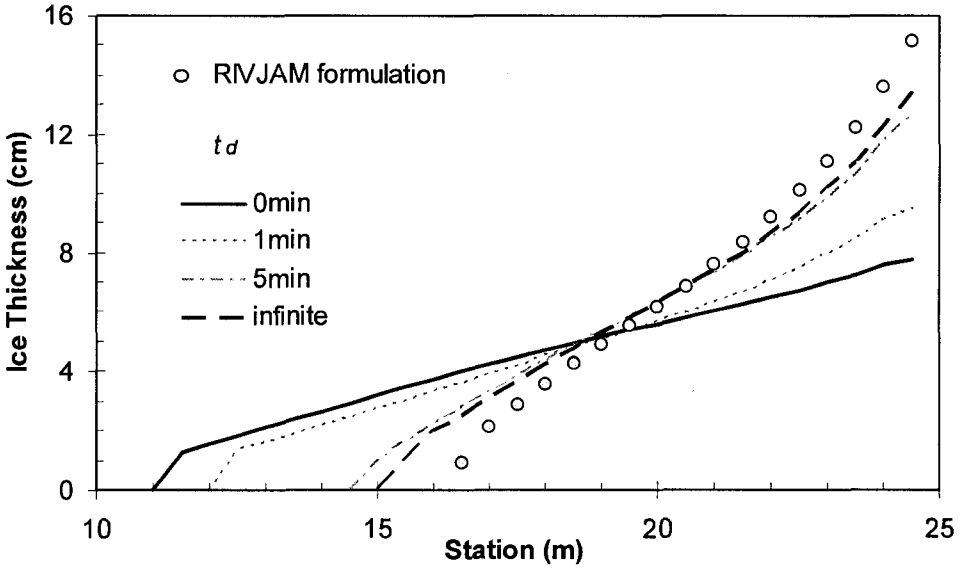

Figure B-8 Simulated ice jam profiles using *River1-D* ice jam model and RIVJAM model formulation for various peak flow durations.

B.6 References

Beltaos, S. and Wong, J. (1986). Downstream Transition of River Ice Jams. ASCE Journal of Hydraulic Engineering, 112(2): 91-110.

Beltaos, S. (1993). Numerical Computation of River Ice Jams. Canadian Journal of Civil Engineering, 20(1): 88-99.

Daly, S. F., and Vuyovich, C. M. (2003). Modeling River Ice with HEC-RAS. Proc., 12th Workshop on River Ice, Canadian Geophysical Union–Hydrology Section, Calgary, Canada, 280-290.

Flato, G., and Gerard, R. (1986). Calculation of Ice Jam Thickness Profiles. Proc., 4th Workshop on Hydraulics of River Ice, Subcommittee of Hydraulics of Ice Covered Rivers, National Research Council of Canada, Montreal.

Healy, D. and Hicks, F. (1999). Comparison of the ICEJAM and RIVJAM ice jam profile models. ASCE Journal of Cold Regions Engineering, 13(4): 180-198.

Healy, D. (2006). Experimental Observations on River Ice Accumulations. PhD Thesis, Department of Civil and Environmental Engineering, University of Alberta, Edmonton, AB, 380 pp.

Healy, D. and F. Hicks, F.E. (2006). Experimental Study of Ice Jam Formation Dynamics, ASCE Journal of Cold Regions Eng., 20(4): 117-139.

Healy, D. and Hicks, F.E. (2007). Experimental Study of Ice Jam Thickening Under Dynamic Flow Conditions. ASCE Journal of Cold Regions Engineering, 21(3): 72-91.

Hicks, F.E. and Steffler, P.M. (1992). A Characteristic-Dissipative-Galerkin scheme for open channel flow. ASCE Journal of Hydraulic Engineering, 118(2): 337-352.

Pariset, E., Hausser, R. and Gagon, A. (1966). Formation of Ice Covers and Ice Jams in Rivers. Journal of Hydraulics Division, Proc. of the American Society of Civil Engineers, 92(HY6): 1-23.

She, Y., Hicks, F., Steffler, P. and Healy, D. (2008). Constitutive Model for Internal Resistance of Moving Ice Accumulations and Eulerian Implementation for River Ice Jam Formation. Submitted to the ASCE Journal of Cold Regions Science and Technology.

Uzuner, M.S. and Kennedy, J.F. (1976). Theoretical Model of River Ice Jams. ASCE Journal of Hydraulic Engineering, 102(9): 1365-1383.

Zufelt, J.E. (1990). Experimental Observations of Shoving and Thickening - Comparison to Equilibrium Thickness Theory. Proc., 10th IAHR Symposium on Ice, Helsinki, Finland, 500-510.

Zufelt, J.E. (1992). Modes of Ice Cover Failure During Shoving and Thickening. Proceedings of the 11th IAHR Symposium, Banff, Canada, 1507-1514.

Appendix C – Summary of all Test Results for Chapter 5

The proposed model results of more experimental tests (Healy and Hicks 2001, 2007; Healy 2006) are summarized in this appendix and they compliment the model validation presented in Chapter 5. The proposed model results were compared to experimental measurements, including initial and final steady-state ice jam profiles; and the continuous time-series data at station 20 m during ice jam consolidation. 10 experimental tests that had been simulated using the proposed model *River1-D*: *ice jam* are sorted into three groups for presentation here, each representing low (< 30% increase), medium (30~70%) and high (> 70%) increase in discharge that led to the consolidation of the initial ice accumulation.

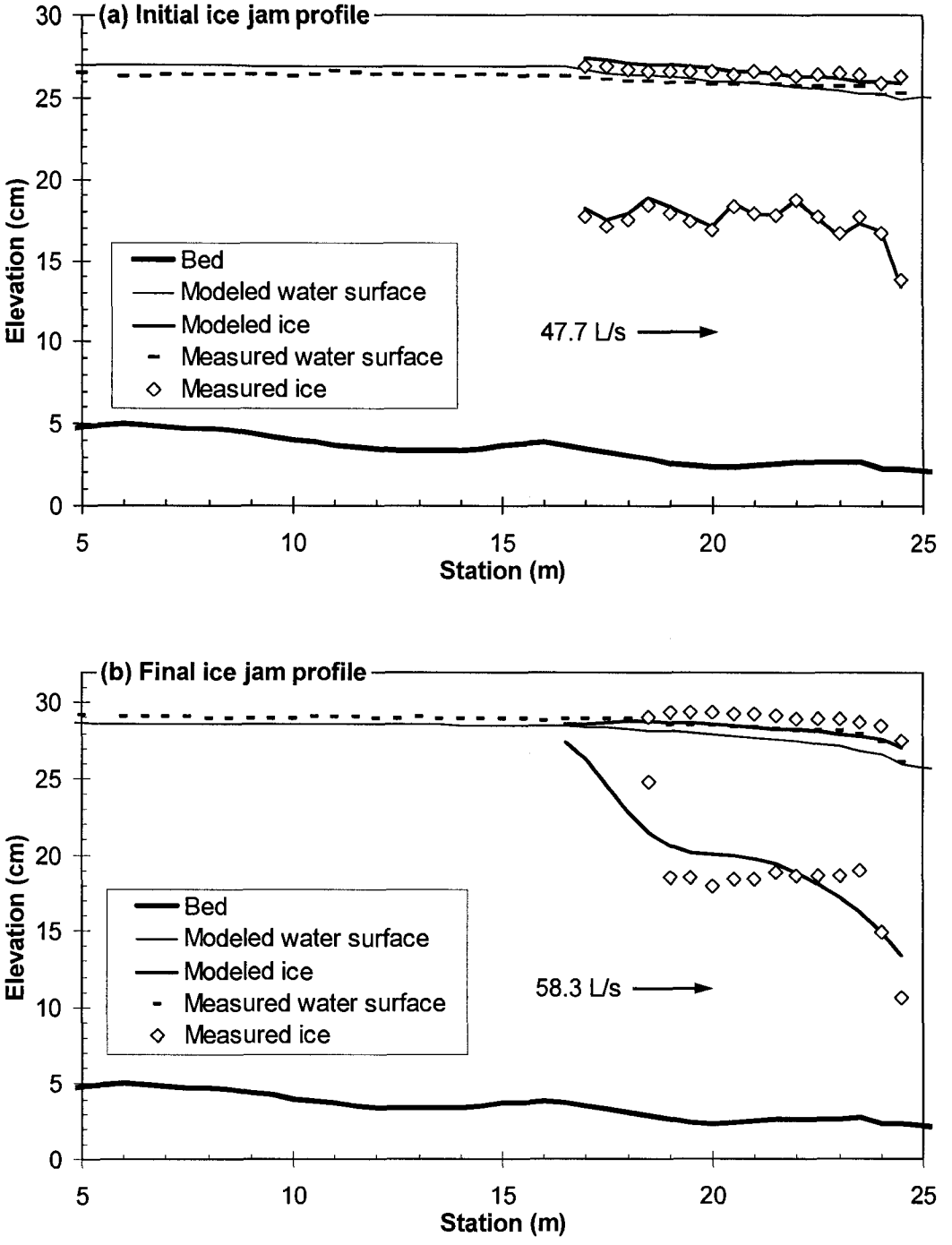

Figure C-1 Comparison of proposed model results to experimental measurements for low increase in discharge – 28-Jun-2001 test: (a) initial ice jam profile (ice thickness input to model, water surface profile computed), and (b) final ice jam profile (both ice thickness and water surface profile computed).

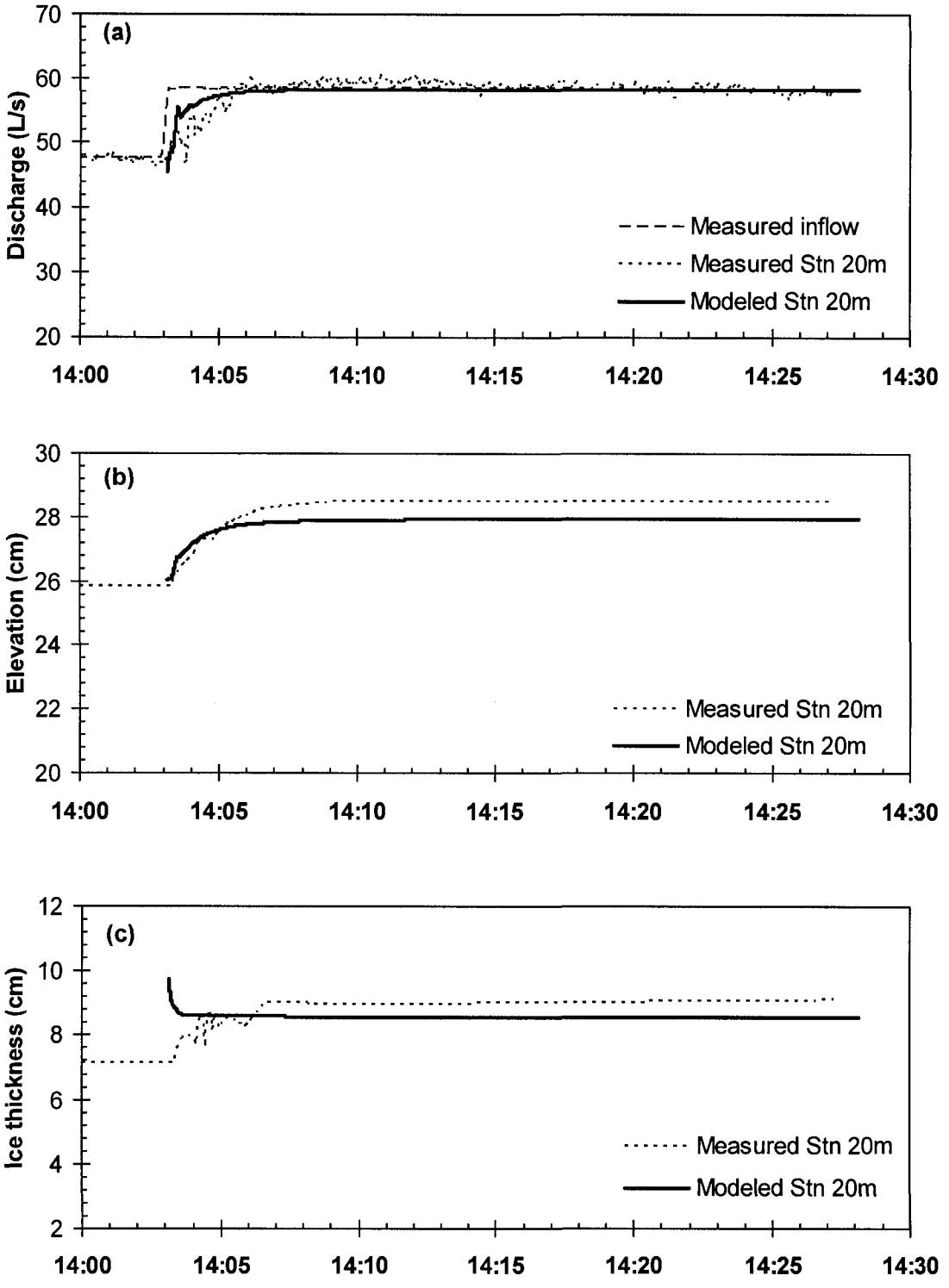

Figure C-2 Comparison of proposed model results with continuous observations of (a) discharge; (b) water level; (c) ice thickness at station 20 m for low increase in discharge – 28-Jun-2001 test.

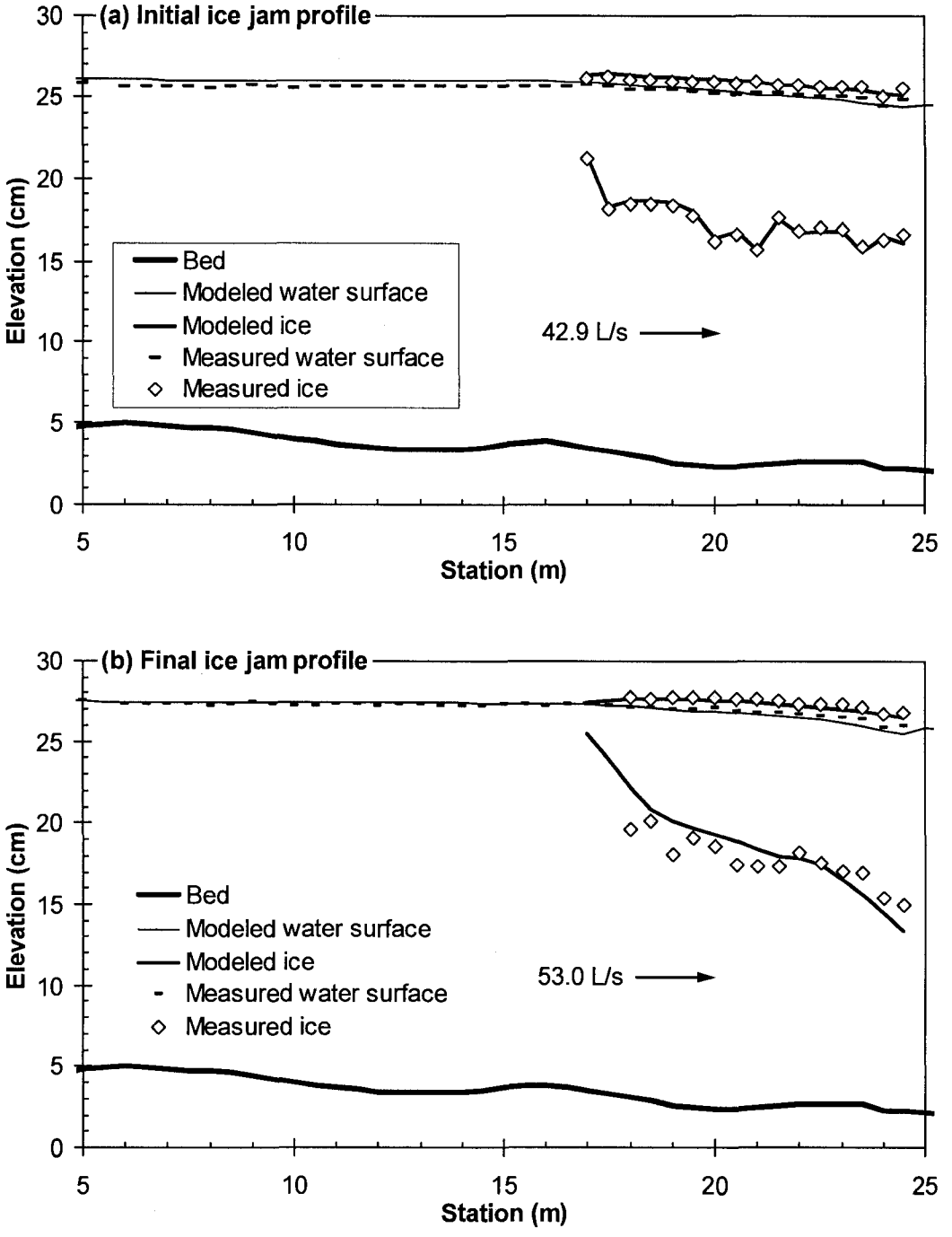

Figure C-3 Comparison of proposed model results to experimental measurements for low increase in discharge – 19-Jul-2001 test: (a) initial ice jam profile (ice thickness input to model, water surface profile computed), and (b) final ice jam profile (both ice thickness and water surface profile computed).

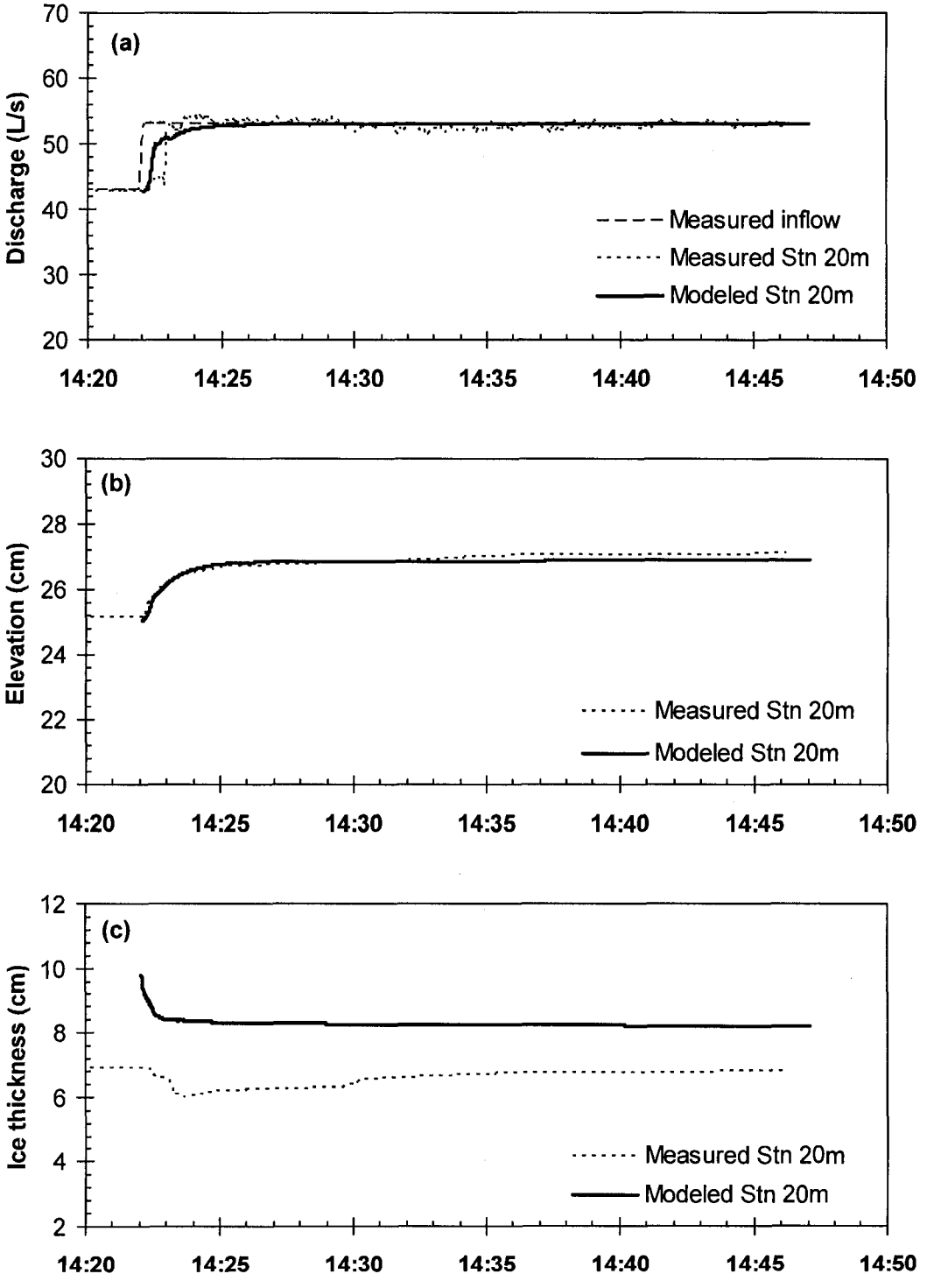

Figure C-4 Comparison of proposed model results with continuous observations of (a) discharge; (b) water level; (c) ice thickness at station 20 m for low increase in discharge – 19-Jul-2001 test.

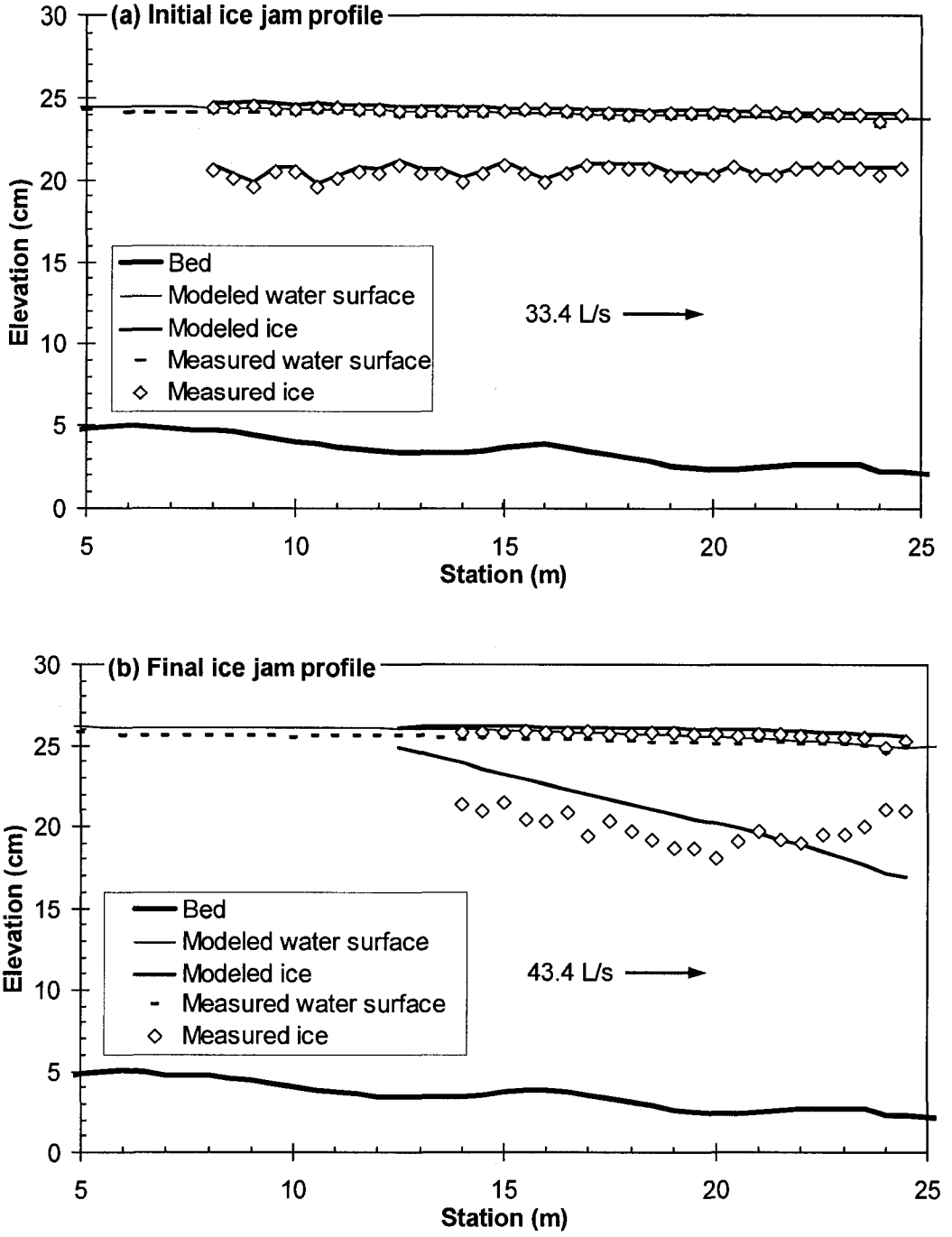

Figure C-5 Comparison of proposed model results to experimental measurements for low increase in discharge – 30-Jul-2001 test: (a) initial ice jam profile (ice thickness input to model, water surface profile computed), and (b) final ice jam profile (both ice thickness and water surface profile computed)

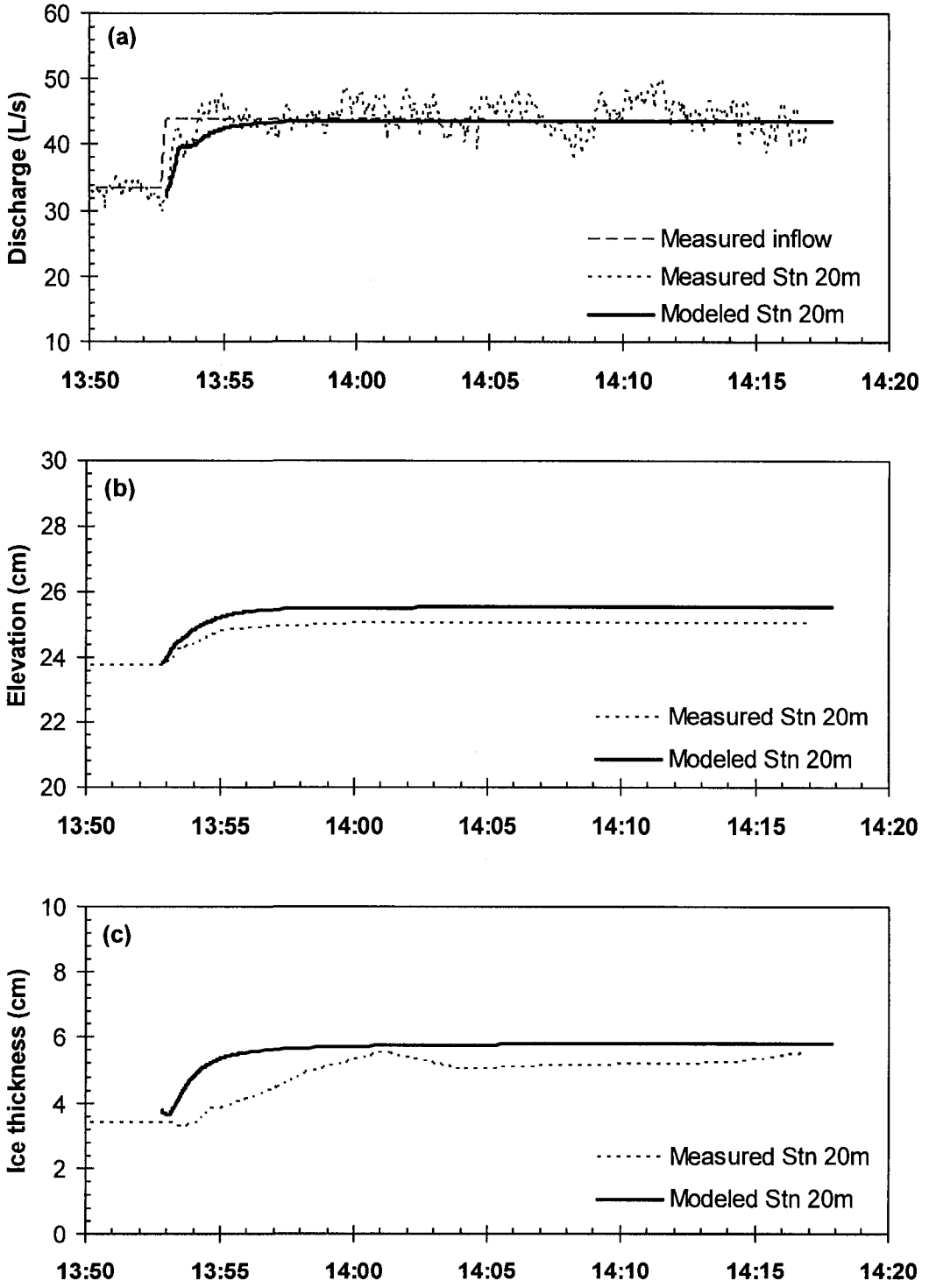

Figure C-6 Comparison of proposed model results with continuous observations of (a) discharge; (b) water level; (c) ice thickness at station 20 m for low increase in discharge – test 30-Jul-2001.

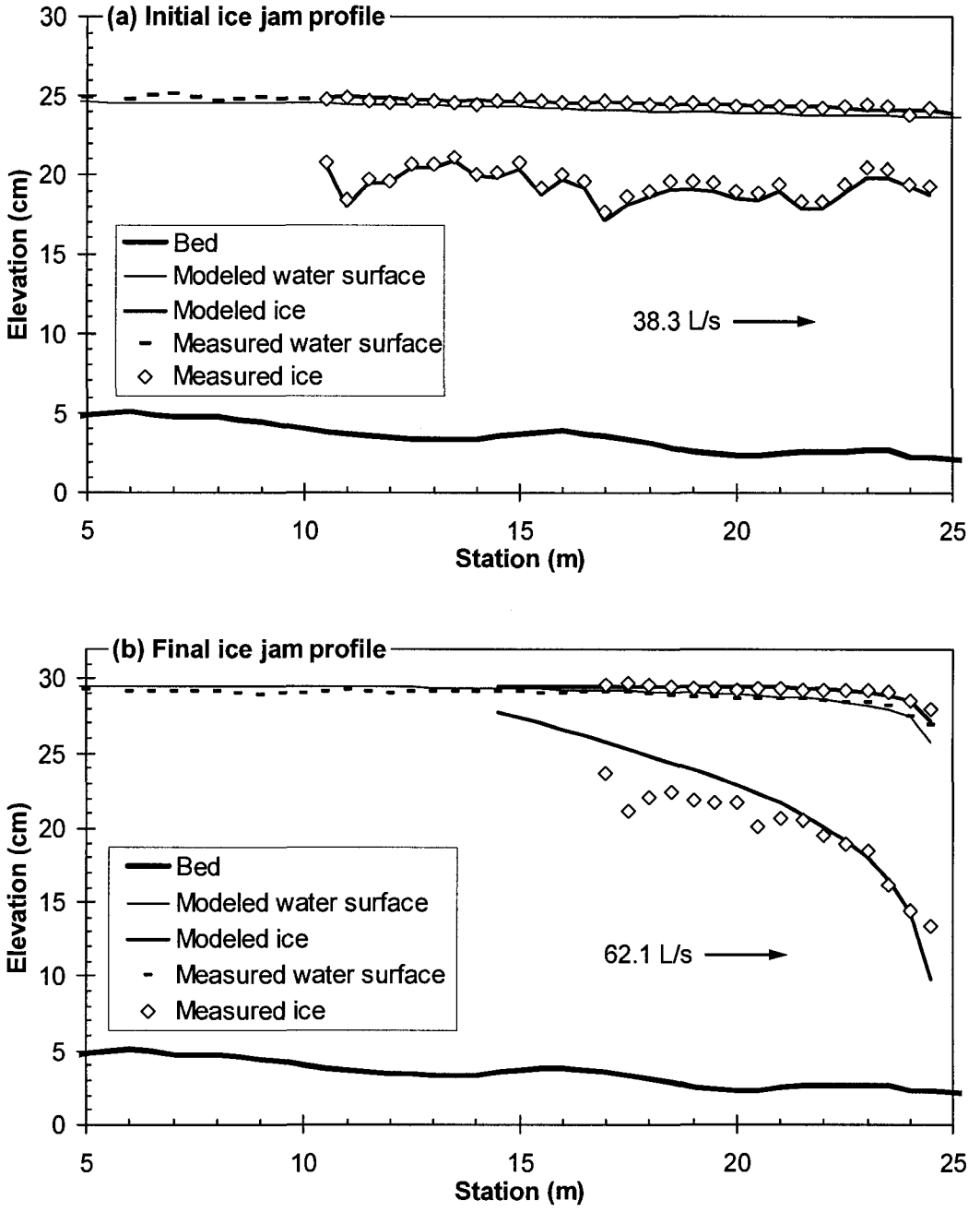

Figure C-7 Comparison of proposed model results to experimental measurements for medium increase in discharge – 21-Jun-2001 test: (a) initial ice jam profile (ice thickness input to model, water surface profile computed), and (b) final ice jam profile (both ice thickness and water surface profile computed).

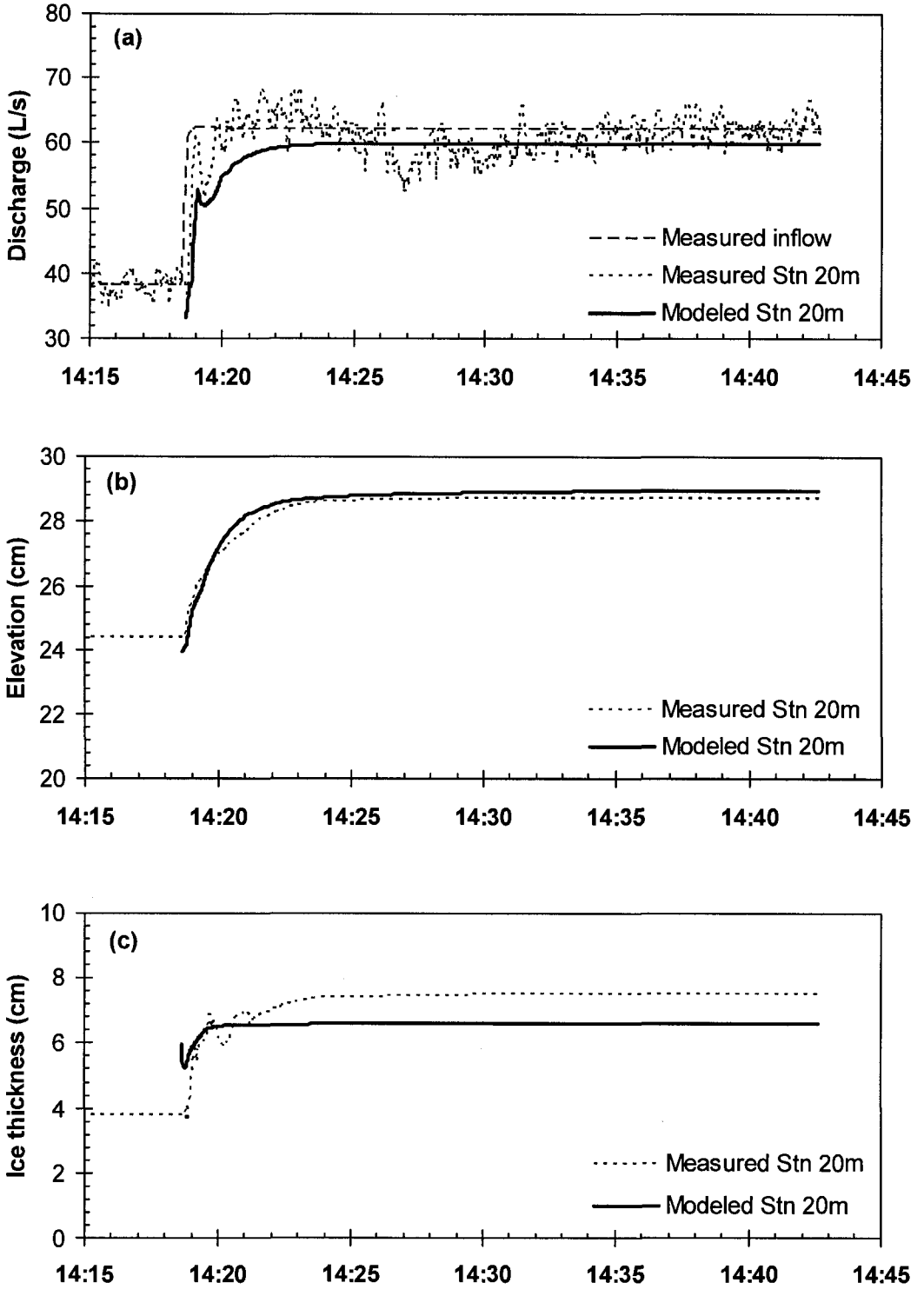

Figure C-8 Comparison of proposed model results with continuous observations of (a) discharge; (b) water level; (c) ice thickness at station 20 m for medium increase in discharge – test 21-Jun-2001.

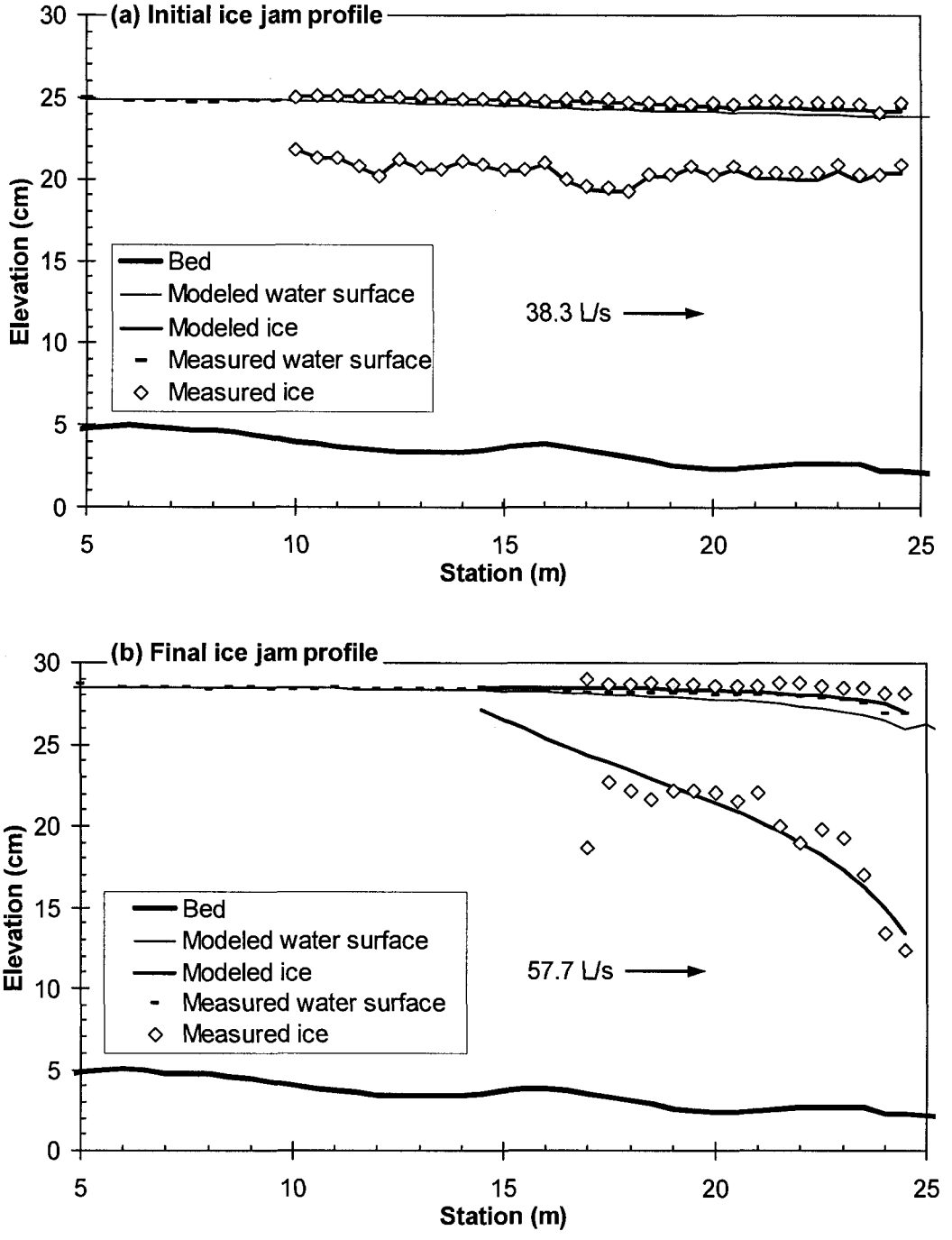

Figure C-9 Comparison of proposed model results to experimental measurements for medium increase in discharge – 20-Jul-2001 test: (a) initial ice jam profile (ice thickness input to model, water surface profile computed), and (b) final ice jam profile (both ice thickness and water surface profile computed).

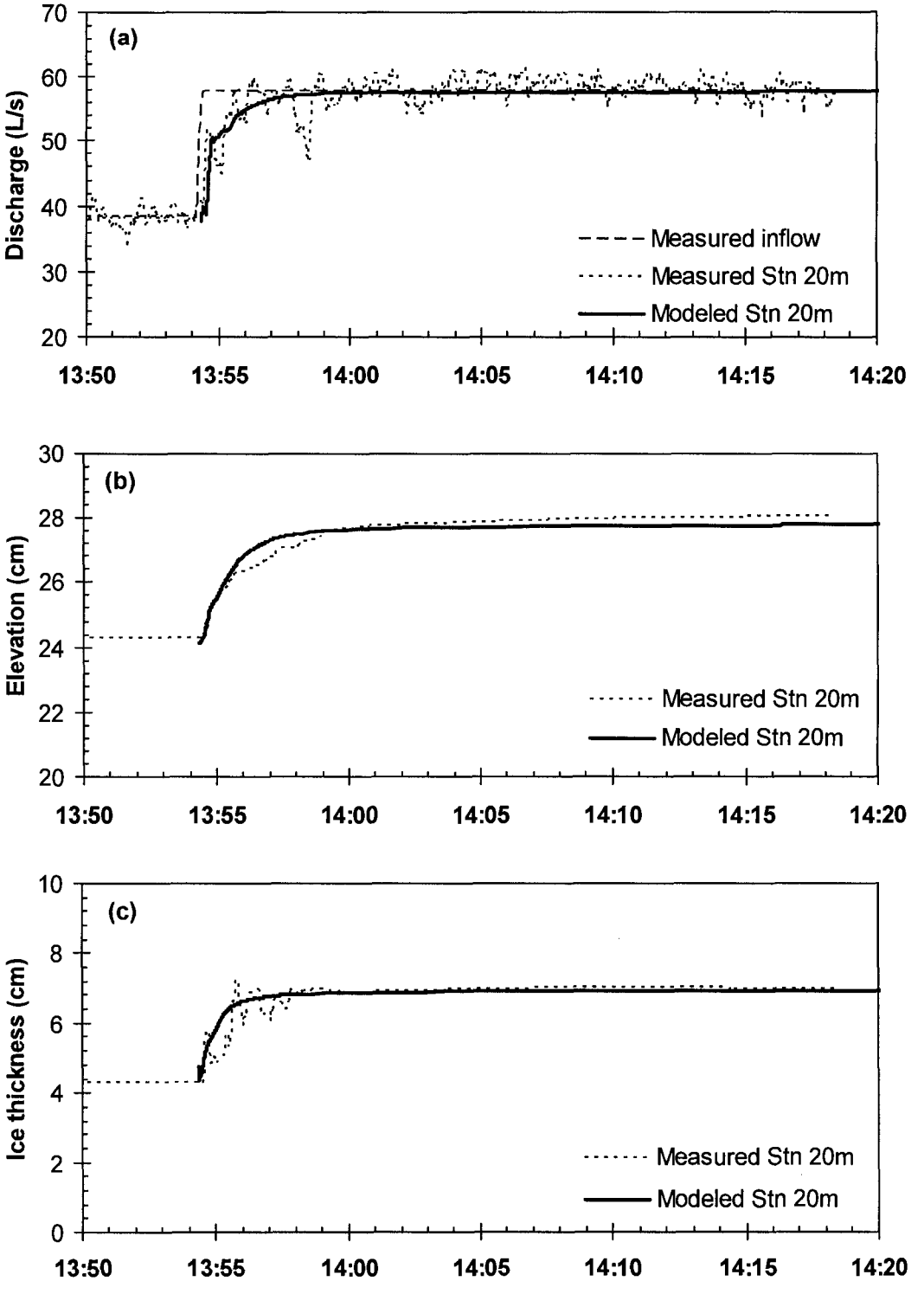

Figure C-10 Comparison of proposed model results with continuous observations of (a) discharge; (b) water level; (c) ice thickness at station 20 m for medium increase in discharge – test 20-Jul-2001.

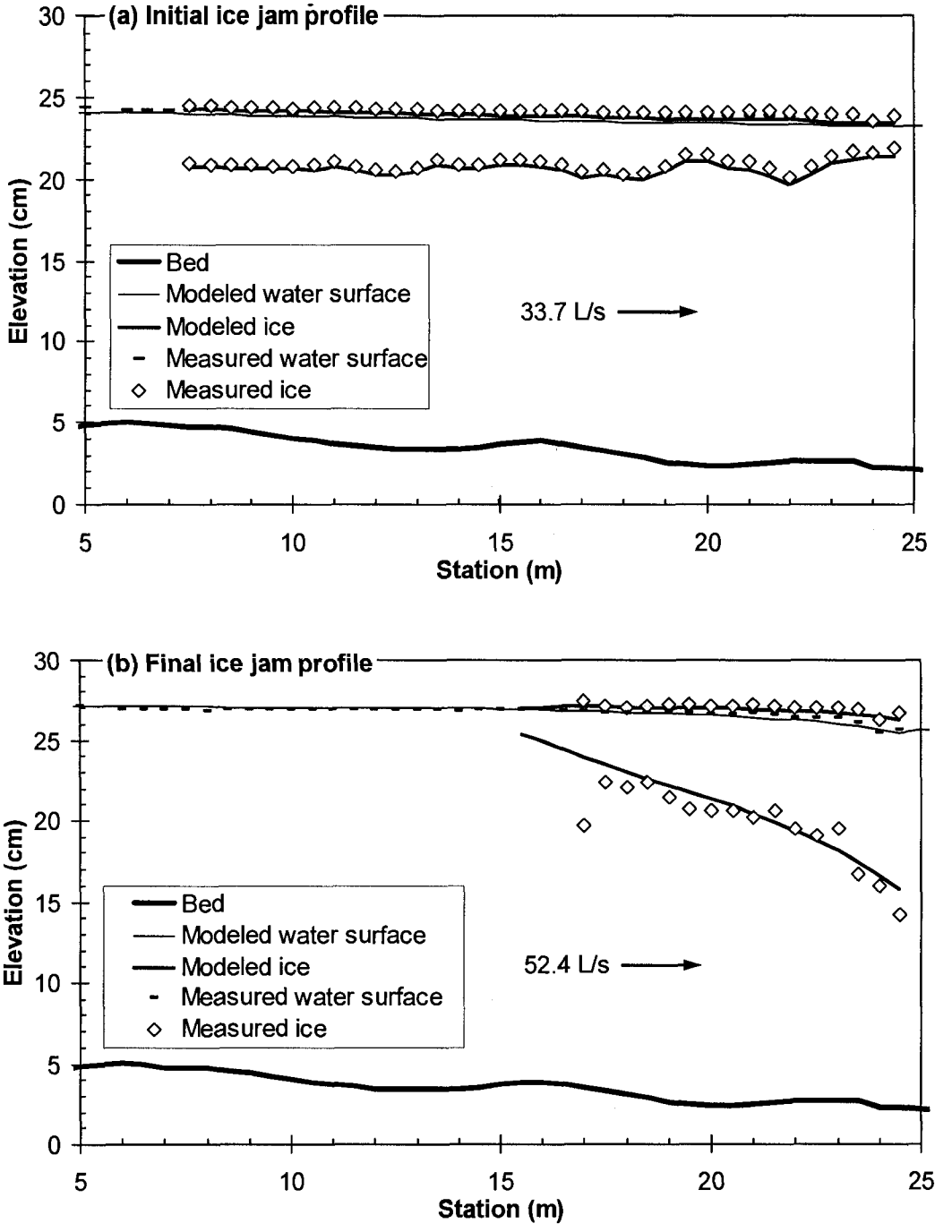

Figure C-11 Comparison of proposed model results to experimental measurements for medium increase in discharge – 31-Jul-2001 test: (a) initial ice jam profile (ice thickness input to model, water surface profile computed), and (b) final ice jam profile (both ice thickness and water surface profile computed).

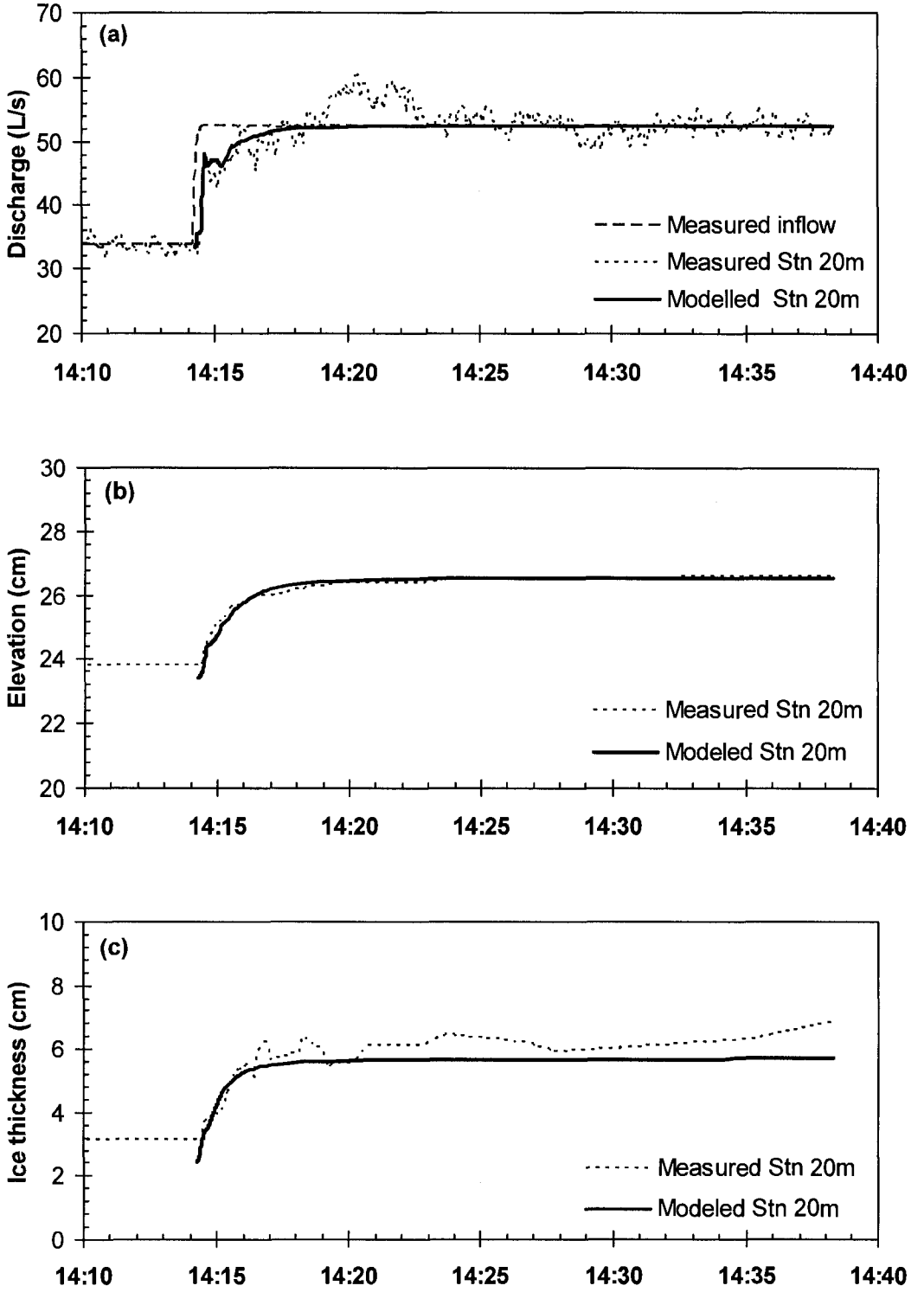

Figure C-12 Comparison of proposed model results with continuous observations of (a) discharge; (b) water level; (c) ice thickness at station 20 m for medium increase in discharge – 31-Jul-2001 test.

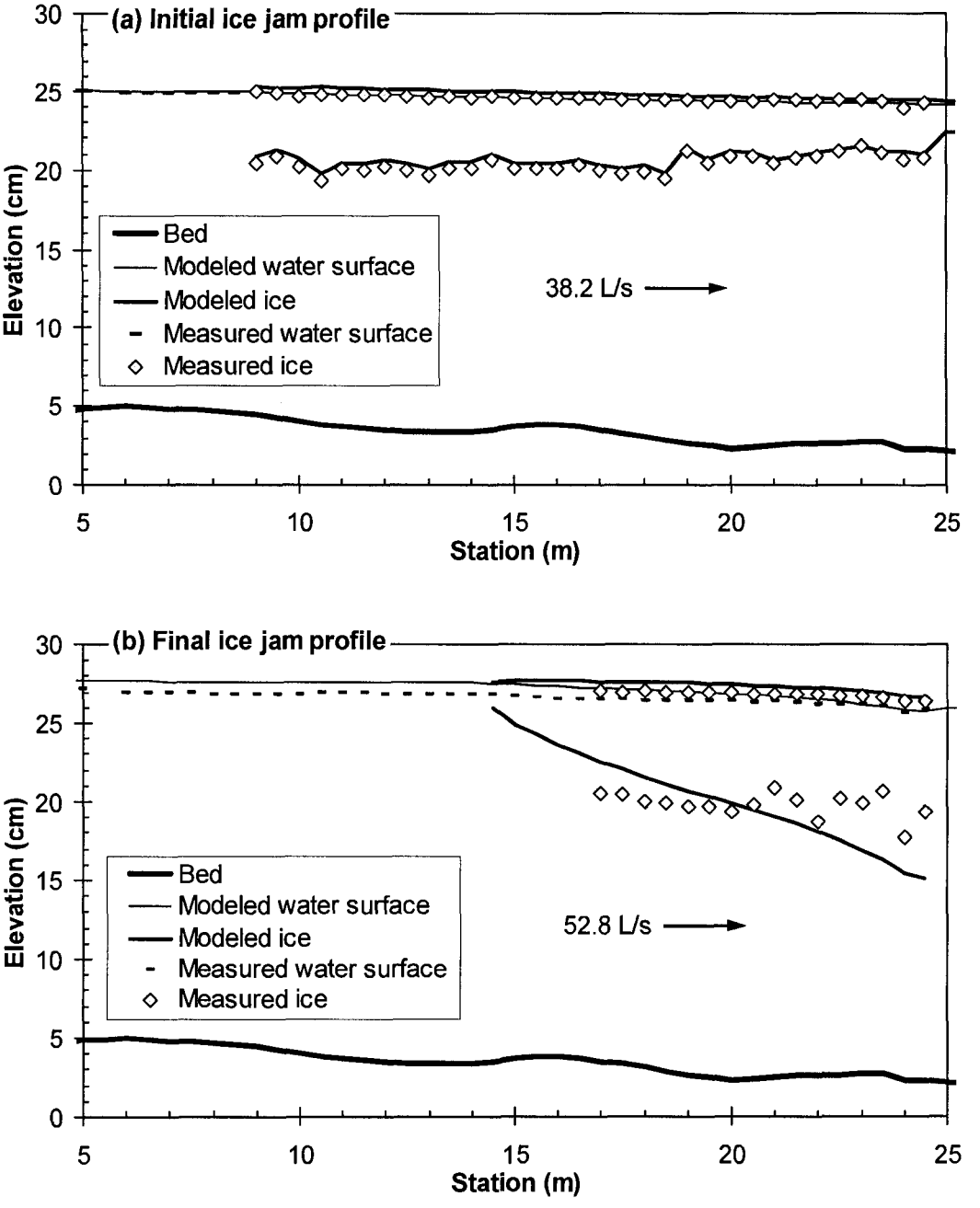

Figure C-13 Comparison of proposed model results to experimental measurements for medium increase in discharge – 07-Aug-2001 test: (a) initial ice jam profile (ice thickness input to model, water surface profile computed), and (b) final ice jam profile (both ice thickness and water surface profile computed).

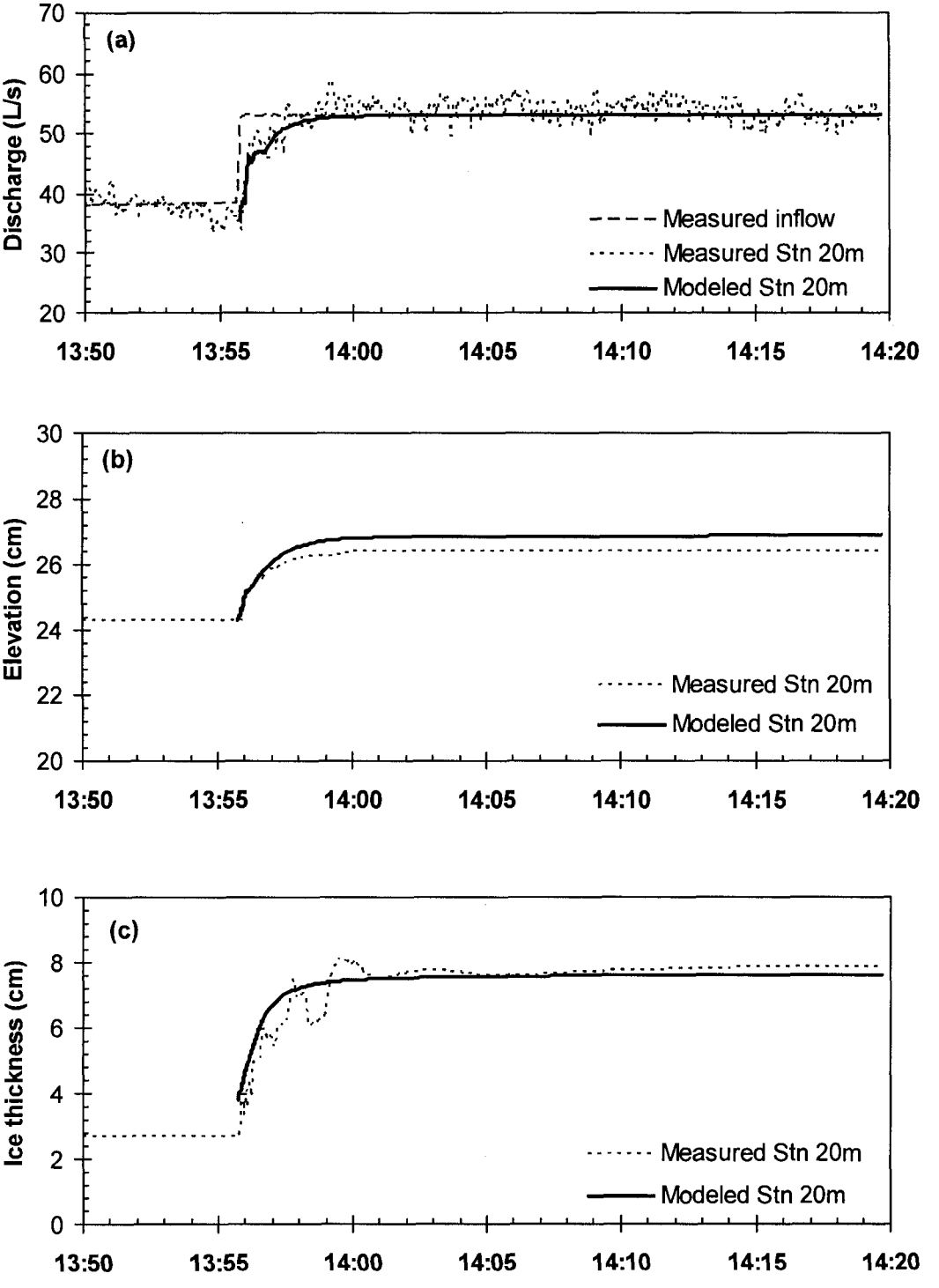

Figure C-14 Comparison of proposed model results with continuous observations of (a) discharge; (b) water level; (c) ice thickness at station 20 m for medium increase in discharge – 07-Aug-2001 test.

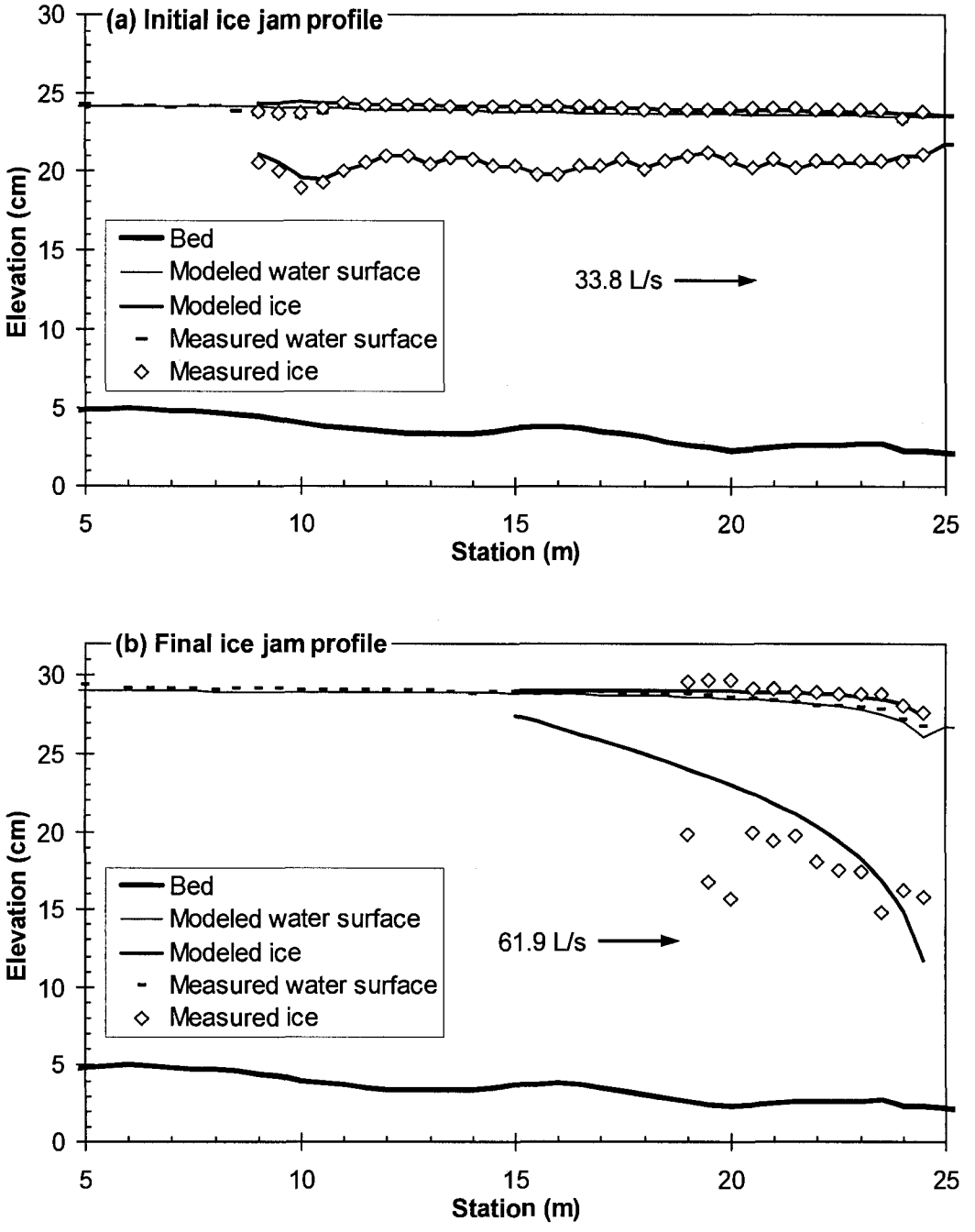

Figure C-15 Comparison of proposed model results to experimental measurements for high increase in discharge – 12-Jul-2001 test: (a) initial ice jam profile (ice thickness input to model, water surface profile computed), and (b) final ice jam profile (both ice thickness and water surface profile computed).

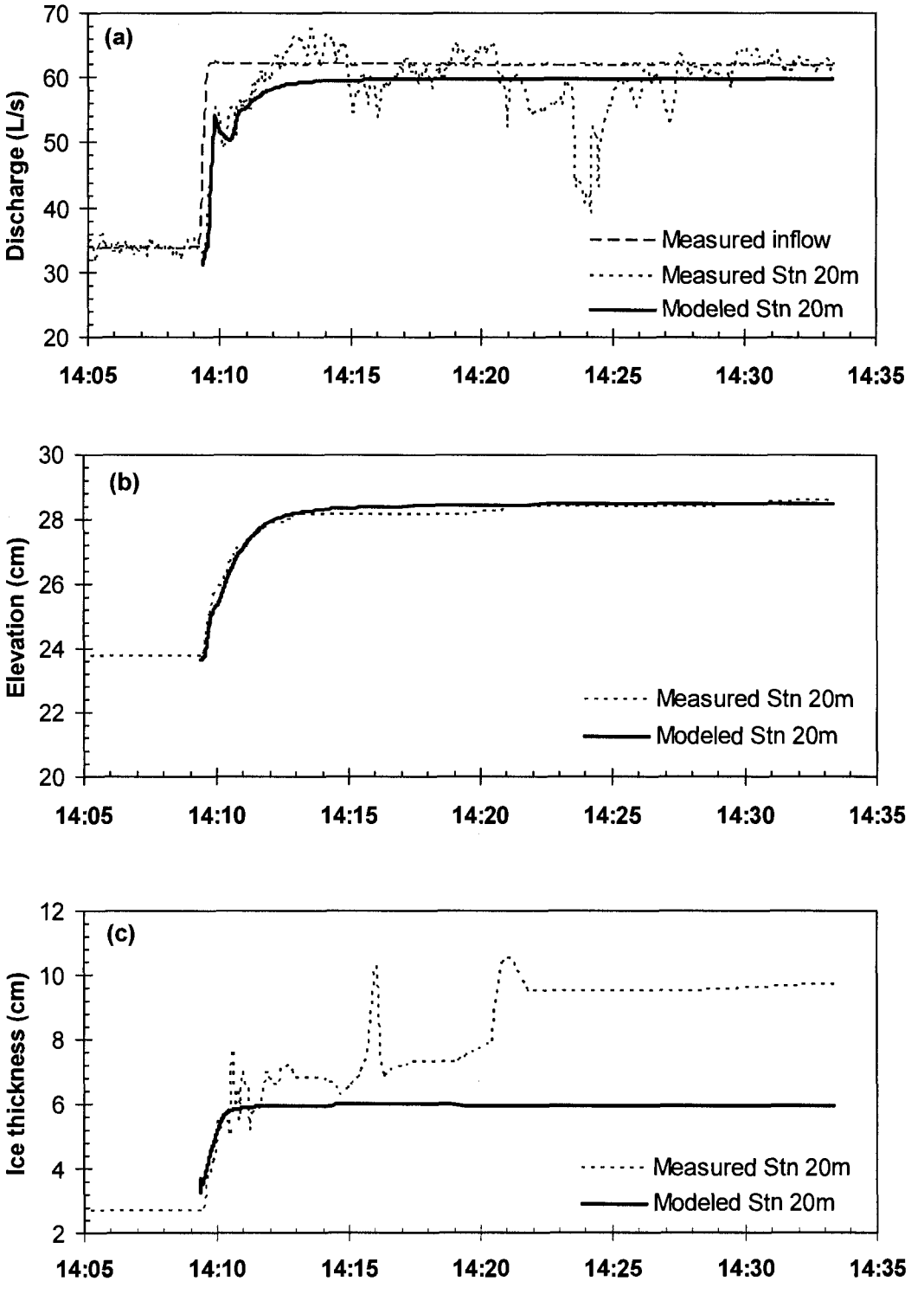

Figure C-16 Comparison of proposed model results with continuous observations of (a) discharge; (b) water level; (c) ice thickness at station 20 m for high increase in discharge – 12-Jul-2001 test.

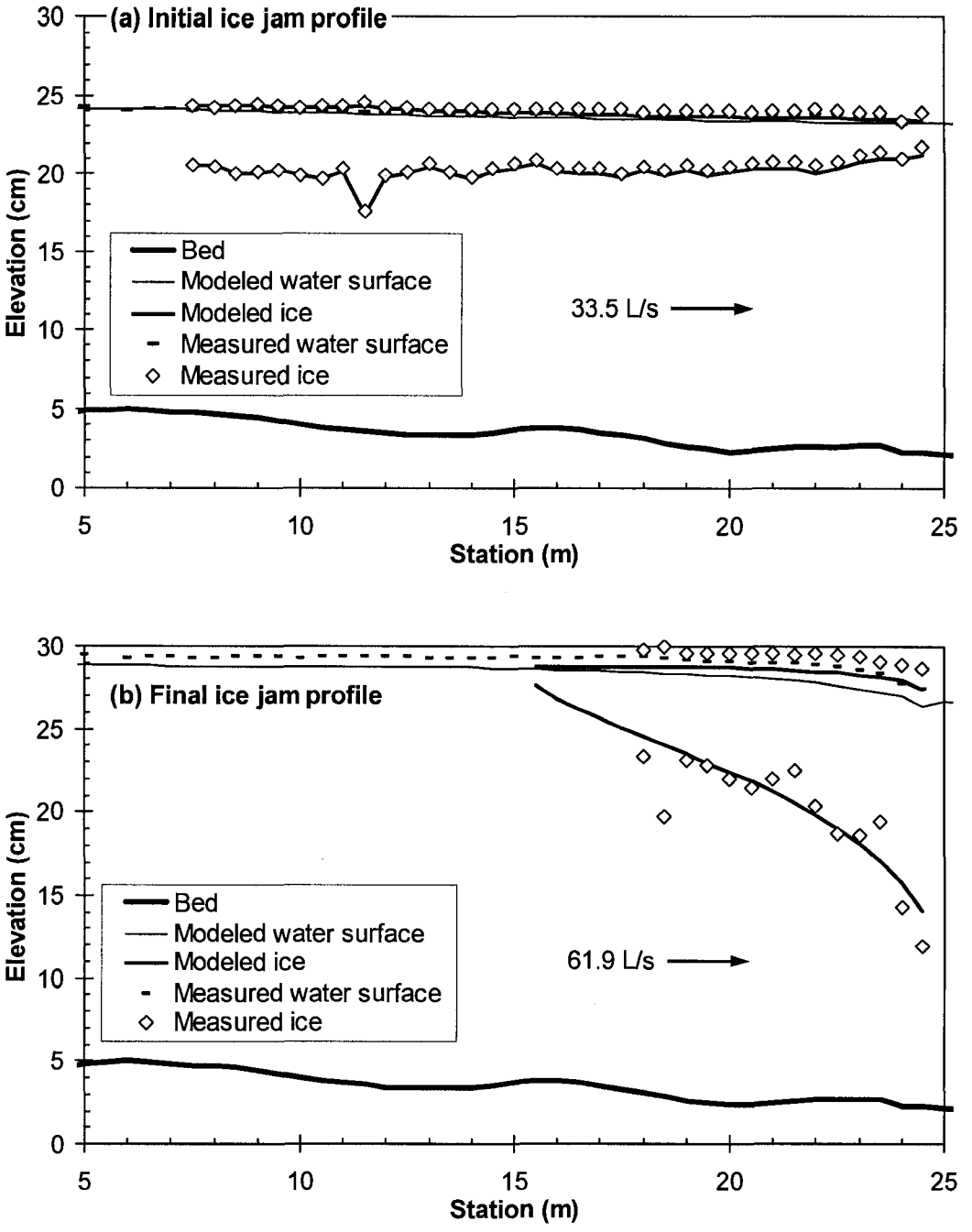

Figure C-17 Comparison of proposed model results to experimental measurements for high increase in discharge – 01-Aug-2001 test: (a) initial ice jam profile (ice thickness input to model, water surface profile computed), and (b) final ice jam profile (both ice thickness and water surface profile computed).

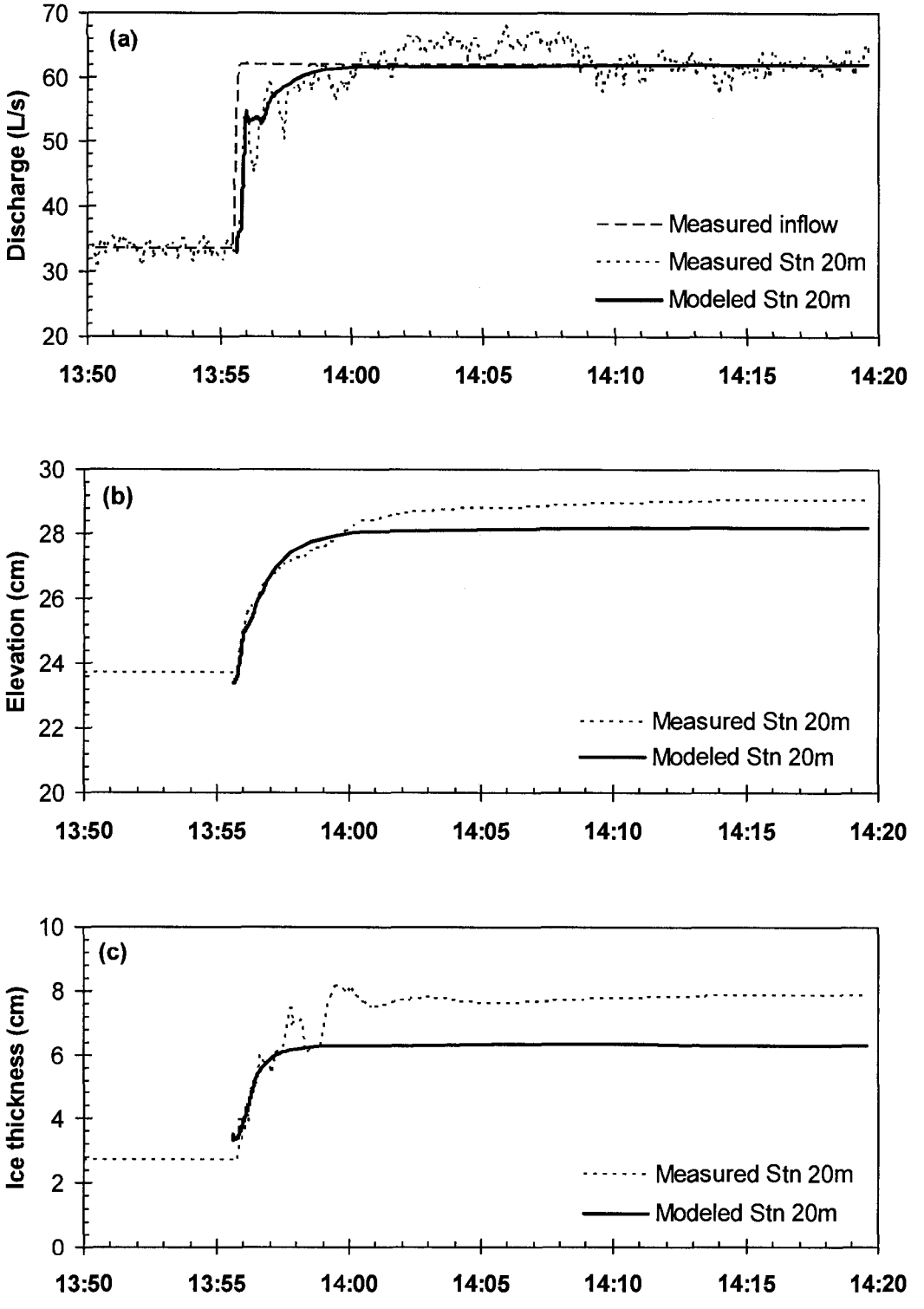

Figure C-18 Comparison of proposed model results with continuous observations of (a) discharge; (b) water level; (c) ice thickness at station 20 m for high increase in discharge – 01-Aug-2001 test.

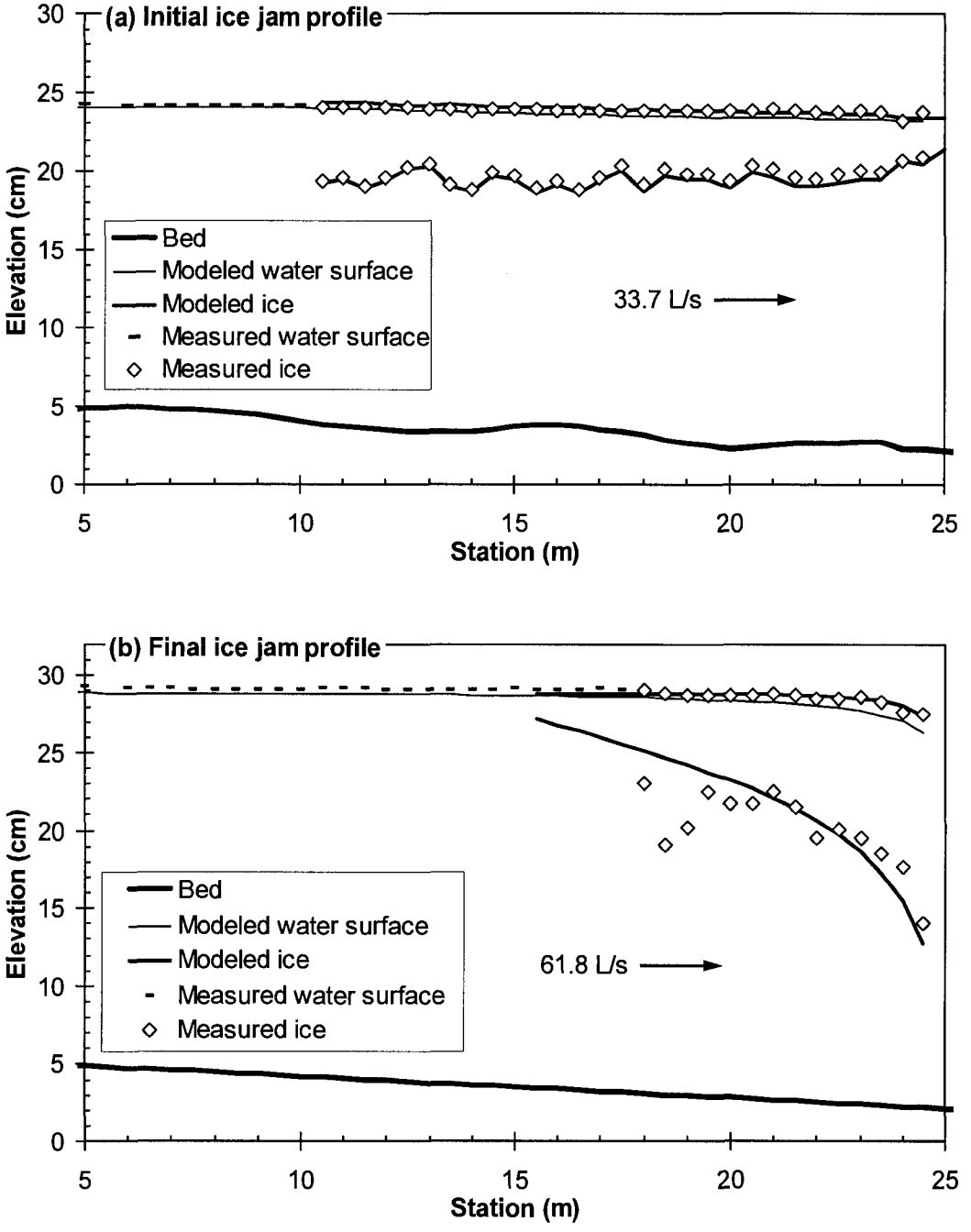

Figure C-19 Comparison of proposed model results to experimental measurements for high increase in discharge – 15-Aug-2001 test: (a) initial ice jam profile (ice thickness input to model, water surface profile computed), and (b) final ice jam profile (both ice thickness and water surface profile computed).

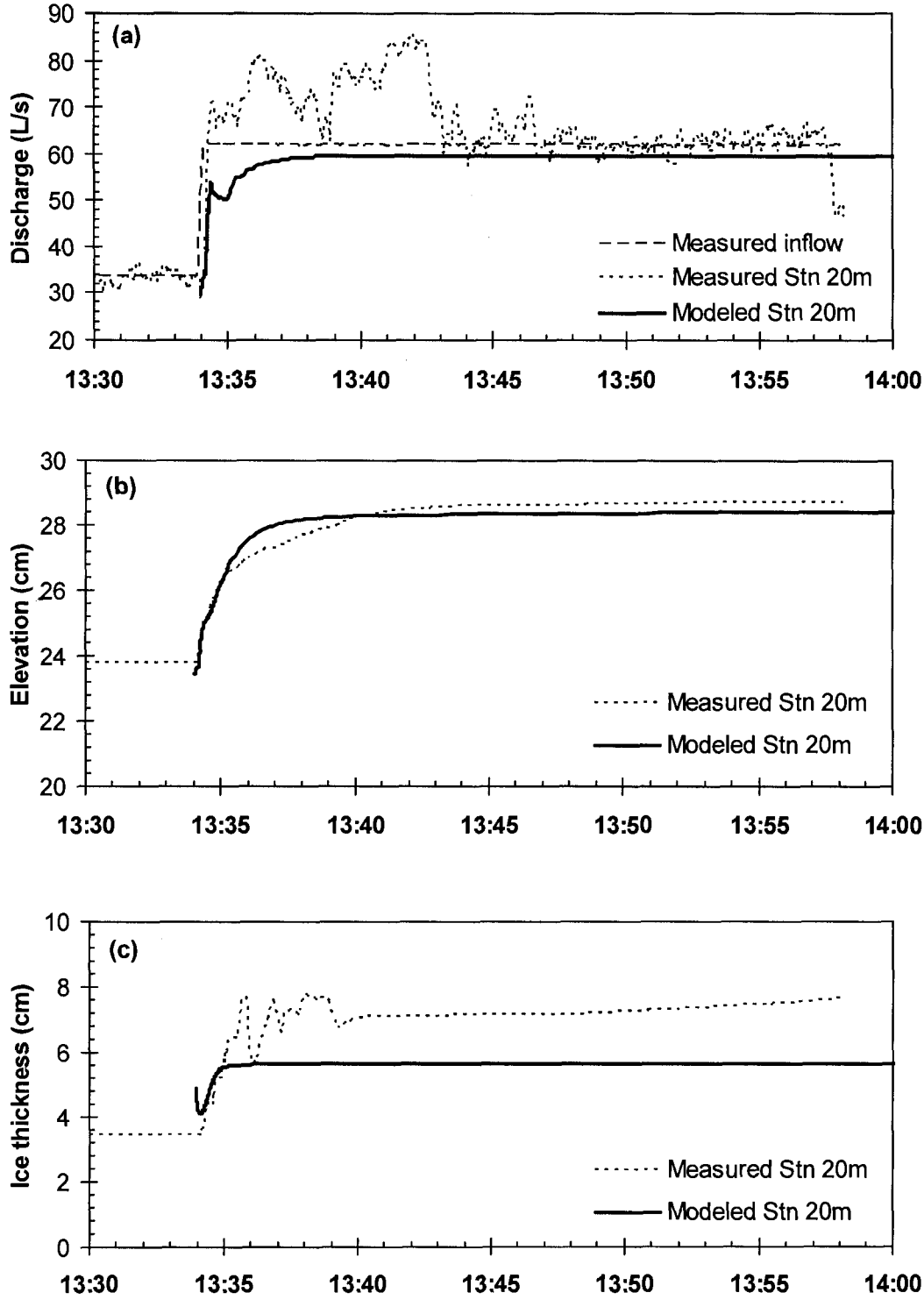

Figure C-20 Comparison of proposed model results with continuous observations of (a) discharge; (b) water level; (c) ice thickness at station 20 m for high increase in discharge – 15-Aug-2001 test.